UILU-ENG-72-2021

CIVIL ENGINEERING STUDIES
STRUCTURAL RESEARCH SERIES NO. 394

A FINITE ELEMENT APPROACH TO THE DYNAMIC ANALYSIS OF CONTINUOUS HIGHWAY BRIDGES

By
A. C. EBERHARDT
and
W. H. WALKER

Department of Civil Engineering
UNIVERSITY OF ILLINOIS
at URBANA-CHAMPAIGN
URBANA, ILLINOIS
DECEMBER 1972

UILU-ENG-72-2021

CIVIL ENGINEERING STUDIES
STRUCTURAL RESEARCH SERIES NO. 394

A FINITE ELEMENT APPROACH TO THE DYNAMIC ANALYSIS OF CONTINUOUS HIGHWAY BRIDGES

By
A. C. EBERHARDT
and
W. H. WALKER

Department of Civil Engineering
UNIVERSITY OF ILLINOIS
at URBANA-CHAMPAIGN
URBANA, ILLINOIS
DECEMBER 1972

A FINITE ELEMENT APPROACH TO THE DYNAMIC ANALYSIS OF CONTINUOUS HIGHWAY BRIDGES

by

A. C. Eberhardt
and

W. H. Walker

Department of Civil Engineering
University of Illinois
at Urbana-Champaign
Urbana, Illinois
December 1972

ACKNOWLEDGMENTS

This report was prepared as a doctoral dissertation under the general direction of W. H. Walker. The information and suggestions provided by Professor L. A. Lopez pertaining to the efficient use of the IBM 360-75 computer system is gratefully acknowledged.

The authors greatly appreciate the financial support which was received from the National Science Foundation. The computer funds which were furnished by the University of Illinois Research Board are also gratefully acknowledged.

The first author also wishes to thank his wife, Joy, for her assistance in this effort.

TABLE OF CONTENTS

Page

APPENDIX

LIST OF TABLES

LIST OF FIGURES

LIST OF FIGURES (Continued)

LIST OF FIGURES (Continued)

LIST OF FIGURES (Continued)

1. INTRODUCTION

1.1 General

Short to medium-span slab and girder bridges are an ubiquitous part of the national highway system. Their consequential economic and design significance make it desirable to continue to search for new analytical methods that yield more detailed predictions of the dynamic response of bridge structures to the effects of moving vehicles.

Highway bridges that are subjected to a high volume of heavy truck traffic experience a great number of stress cycles. This repeated loading and unloading of the structural members affects the fatigue life of the structure to a degree dependent upon the magnitude and time history of the stresses induced in the structure as well as the expected number of stress events.

New and improved structural materials, design concepts, and construction methods continue to be developed. High strength steel and concrete and prestressed and precast concrete construction techniques are being used more frequently. These developments help to produce more efficient bridge structures which have lower dead loads in comparison to total load capacity. At the same time, the live load carried by these structures becomes a greater percentage of the total load capacity, and thus the stress cycles that occur during loading and unloading have an increased range. This increase in the range of stress within each cycle in turn alters the fatique life of the structure.

The behavior of a bridge structure that is acted upon by a moving vehicle is not described adequately by its static response alone. The

actual transient vehicle forces and bridge inertia forces produce a strain-time history which may be visualized as an oscillating dynamic component or dynamic increment superimposed upon the static influence line. The dynamic component is seen to contribute substantially to the total range of live load stress induced by moving vehicles. The importance of this dynamic increment of strain has made it desirable to obtain strain-time histories at as many critical locations as possible in order to permit a more comprehensive study of the probable incidence of fatigue.

In addition to the prediction of strains or stresses required for design against fatigue, dynamic deflections and accelerations are needed to study the sensitivity of the user to the dynamic response of the bridge. Of course, this problem is of significance only when pedestrians or stopped vehicles are present on the structure concurrently with moving traffic. In the present specifications,[1] constraints are placed on live-load deflections and span-to-depth ratios--neither of which is directly related to user psychological of physiological reaction. Recent studies[2] have shown that the limitation of deck accelerations is a more rational approach. In any case, predictions of dynamic deflections and accelerations are needed to establish more rational design criteria.

Studies are also needed to determine the manner in which variations in structural type and proportions alter the dynamic response of highway bridges. Design parameter studies are especially helpful in determining the extent to which new methods of construction affect bridge behavior. Stress-time histories can be obtained directly from field tests, but the parameters associated with each testing program can be varied to

only a limited degree. The need to extend field-test predictions beyond their limited range by means of parameter studies emphasizes the desirability of developing more refined analytical methods.

1.2 Background

Mathematical models that represent a bridge structure as a one, two, or three-span continuous beam having no transverse dimensions have often been used to study the dynamic response of highway bridges subjected to heavy vehicles.[3,4,5,6] These models introduce the idealization that all points on any transverse section deflect alike. Furthermore, the actual mass and damping properties of the structure are lumped into a series of point masses and dashpots spaced at equal intervals within each span of the continuous-beam model. Consistent with these bridge idealizations, a vehicle model was developed which represents the flexibility of the tire-suspension system as a series of springs and frictional damping devices.[7] It has been shown that the initial phase of the vertical oscillation of the vehicle, the phase difference between the motions of the individual axles, and the initial values of interleaf friction in the suspension system as well as axle spacing and vehicle speed are quite significant. The amplitude of the initial oscillations of the vehicle and other effects of roadway roughness have also been studied.[8] The larger the initial amplitudes of variation of the interacting forces between the tires and the bridge deck, the greater will be the dynamic response of the bridge.

In early analytical studies of bridge response, the inability to handle a mathematical model which predicted the transverse distribution of strain hampered attempts to correctly represent the complex behavior

of slab and girder bridge structures. However, with improved computational facilities, techniques which incorporate such analytical tools as Fourier series approximations, finite difference analogs, orthotropic plate models, and Rayleigh-Ritz energy procedures have been used to obtain analytical results for two-dimensional stress problems.[9,10,11] However, the applicability of these techniques is often limited because of the difficulty in handling multiple spans, skewed bridge decks, and unusual boundary conditions. Generally, a new deflection function, which is usually expressed as a series expansion, must be assumed each time the number of spans is increased or the boundary conditions are altered. Because of these restrictions, such solution techniques have been used to solve only one or two-span bridge problems with conventional boundary conditions.

Studies have also been made in which a series of beams, assembled in a closely-spaced grid, have been employed to simulate the behavior of slab and girder highway bridges. The more rigorous schemes have employed diagonal members in order to represent the properties of the bridge deck more completely.[12,13] While these grid models yield results which appear to be within an average of ten percent of test results, there is no direct way to determine the magnitude of internal stresses at any points other than at the intersections of the beam elements.

Another approach which incorporates a lattice structure composed of linear elastic members has been developed by Benard[14] to simulate both plate and shell structures. The lattice analogy can be applied to a wide range of continuous structures since it is not limited to one

particular lattice arrangement. However, the generality of the approach is accompanied by the somewhat tedious process of calculating the geometry of the lattice analogue.

Since the early 1960's, the finite element approach has been recognized to be a powerful tool for analysis. It has given the researcher the ability to analyze two and three-dimensional stress problems accurately and efficiently. Results, which have compared well with other analytical techniques, have been obtained from equations that were developed on the basis of energy principles. The magnitude of internal stresses in an element of the structure can be obtained directly in the analysis. The method also provides for the efficient handling of a wide variety of boundary conditions with a minimum amount of difficulty. Skewed quadrilateral elements have been developed which further increase the flexibility of the method.

The use of the finite element approach in the area of structural dynamics is also the object of much study. It has been shown to be well suited to the problem of determining the natural frequencies and mode shapes of two-dimensional stress models. It is not so obvious as to whether or not such a technique can be used efficiently to solve problems that involve time-dependent relationships and numerical integration procedures.

1.3 Object and Scope

The object of this investigation is to develop a finite element method for the analysis of the dynamic response of highway bridges in the elastic range of deformation when subjected to the action of moving vehicles.

The bridge deck is divided into a number of finite plate elements, and the bridge girders and transverse stiffeners are treated as eccentric stiffeners. The vehicle is represented as a multi-axle sprung load. The load-deformation diagram of each tire-suspension assembly is idealized as a bilinear, hysteretic relationship.

The primary objectives of the study reported herein are as follows:

(a) The formulation of a finite element method of analysis for dynamic bridge problems,
(b) The development of computer programs which may be required in the application of the method, and
(c) The study of the merit of the approach relative to its accuracy and usefullness.

In Chapter 2, descriptions of the bridge and vehicle models are presented. The equations of motion, the integration procedure, and the reduced stiffness matrix approach are described in Chapter 3. Chapter 4 is devoted to a discussion of the three computer programs developed in conjunction with this study. In Chapter 5, results of several finite-element solutions are compared with theoretical data from earlier studies and experimental data from laboratory tests and field measurements. Chapter 6 contains a summary of the work accomplished, conclusions, and recommendations for further study. In Appendix A, a method of assembling a structural stiffness matrix is presented. Appendix B is devoted to a derivation of the equations of motion for the vehicle model.

1.4 Notation

The symbols used in this study are defined when they are first introduced in the text. For convenient reference, frequently used symbols are summarized below:

A_i	ith generalized coordinate for the plate bending displacement function
A_{pi}	ith generalized coordinate for the in-plane deformation function
A_s	cross-sectional area of a stiffener element
a_1	ratio of the horizontal distance between the center of gravity of the tractor and its rear axle to the axle spacing of the tractor, as shown in Fig. 15
a_2	$1-a_1$
a_3	ratio of the horizontal distance between the center of gravity of the trailer and its rear axle to the horizontal distance between that axle and the "fifth wheel pivot," as shown in Fig. 15
a_4	$1-a_3$
a_5	ratio of the "fifth wheel" offset to the axle spacing of the tractor, as shown in Fig. 15
B_f, B_p, B_s	matrices relating the generalized coordinates to strains for the f, p, and s elements, respectively
C	viscous damping matrix for the assembled structure
c	viscous damping matrix for the vehicle tire-suspension systems
C_f, C_p, C_s	matrices which relate the generalized coordinates to nodal displacements for the f, p, and s elements, respectively
C_r	viscous damping matrix for the reduced stiffness formulation of the equations of motion for the bridge model

C_1, C_{1v}	vectors defined by Eq. (3.19) for the bridge and vehicle models, respectively
C_2, C_{2v}	vectors defined by Eq. (3.20) for the bridge and vehicle models, respectively
C_{1r}, C_{2r}	reduced forms of the matrices C_1 and C_2, respectively
D_f, D_p, D_s	rigidity matrices relating strains to forces in the f, p, and s elements, respectively
[D], [E], [F]	matrices defined by Eqs. (3.22)
$[D_r]$, $[E_r]$, $[F_r]$	reduced forms of the matrices D , E , and F
E	modulus of elasticity for the plate material
E_s	modulus of elasticity for the stiffener material
f	subscript denoting plate bending element
f_b	fundamental bridge frequency
f_h	frequency of the highest mode of vibration of the bridge model
F_f, F_p, F_s	equivalent nodal force vectors corresponding to the f, p, and s elements, respectively
F_{ij}	equivalent nodal force at the ith node corresponding to the jth degree of freedom
F_i'	break-away value of $F_{s,i}$
$F_{s,i}$	frictional force at time t_s in the leaf springs of the ith suspension system
$f_{t,i}$	pseudo-frequency of the ith tire-suspension system when the tire spring acts alone
$f_{ts,i}$	pseudo-frequency of the ith tire-suspension system when the tire spring and the suspension spring act in series
G	shear modulus of the stiffener material
[G]	matrix defined by Eq. (3.25a)
g	acceleration of gravity

G_f	transformation matrix relating ψ to ψ'
G_p	transformation matrix relating ε to ε'
$[G_r]$	reduced form of the matrix G
[H]	matrix for transforming interacting forces into the corresponding set of joint forces and moments
h	transformation matrix for vehicle forces given in Fig. 18
$[H_r]$	transformation matrix defined by Eq. (3.42)
I_x	moment of inertia of the stiffener element with respect to the midplane of the bridge deck
i_{1x}, i_{1y}, i_{2x}, i_{2y}	dynamic indices of the vehicle mass defined by Eqs. (2.63)
J	St. Venant's torsional stiffness constant for the cross-section of the stiffener element
[J]	matrix defined by Eq. (3.25b)
K	stiffness matrix for the assembled structure
K_f, K_p, K_s	element stiffness matrices for the f, p, and s elements
K_r	reduced stiffness matrix for the bridge model
k_s, k_{s+1}	effective stiffness in a tire-suspension assembly at times t_s and t_{s+1}, respectively
$k_{t,i}$	effective stiffness of the ith tire spring
$k_{ts,i}$	effective stiffness of the ith tire-suspension assembly when the suspension spring and the tire spring act in series
k_v	stiffness matrix of the assembled tire-suspension assemblies of the vehicle model
L	length of the eccentric stiffener element
L_b	total length of the bridge
L_t	total length of the vehicle

L_1, L_2	axle spacings, as shown in Fig. 15a
L_3	$L_2 + a_5 L_1$, as shown in Fig. 15a
ℓ	total length of a single-span bridge, one half of the total length of a two-span bridge with equal spans, or the length of the center span of a three-span bridge
M	mass matrix for the assembled bridge structure
m	mass matrix for the vehicle model
M_{es}	bending moment in the stiffener element
M_f	mass matrix for the plate bending element
M_p	vector containing the plate moments $M_{x'}$, $M_{y'}$, and $M_{x'y'}$
M_r	reduced mass matrix containing only the vertical inertia properties of the bridge model
M_s	mass matrix for the stiffener element
$M_{x'}$, $M_{y'}$, $M_{x'y'}$	plate moments in the x' and y' directions and the twisting moment, respectively
{N}	vector containing the plate forces $N_{x'}$, $N_{y'}$, and $N_{x'y'}$
[N]	matrix defined by Eq. (3.25c)
N_{cr}	number of integration steps required for the vehicle to travel the length of the bridge
N_{es}	axial force in the stiffener element
$N_{x'}$, $N_{y'}$, $N_{x'y'}$	in-plane forces in the x' and y' directions and the shear force in the x'y' plane, respectively
p	subscript denoting the plane-stress plate element
{p}	nodal load vector

P_d	vector of disturbing forces applied at the support points of the vehicle mass
P_i	vector of forces interacting between the vehicle tires and the bridge deck
$P_{i,s}$	value of P_i at time t_s
$P_{st,i}$	static reaction in the ith vehicle tire
P_w	vector of tire reactions resulting from bridge displacements and bridge roughness
p_1, p_2, p_3	bridge loading vectors containing nodal vertical forces, nodal moments in the x direction, and nodal moments in the y direction, respectively
q	displacement coordinate representing the displacement of a vehicle mass support point or a nodal point in the bridge model
R_s	transformation matrix defined by Eq. (2.47)
$\bar{R}_s$	matrix transforming nodal displacements from skewed coordinates to rectangular coordinates
r_{1x}, r_{1y}	radii of gyration of the tractor mass about axes passing through the center of gravity of the tractor mass parallel to the x' and y' axes, respectively
r_{2x}, r_{2y}	radii of gyration of the trailer mass about axes passing through the center of gravity of the trailer mass parallel to the x' and y' axes, respectively
s	subscript denoting an eccentric stiffener element
S_x	first moment of the stiffener area with respect to the midplane of the bridge deck
S_1, S_2, S_3	distances between wheels for axles, 1, 2, and 3, respectively
t	thickness of the plate elements

T_i	torsional moment at the ith end of the stiffener element
t_s	time after s number of integration steps
u, v, w	components of the displacement vector for the reference surface in the x, y, and z directions, respectively
u_f, u_p, u_s	nodal displacement vectors for the f, p, and s elements, respectively
$u_{i,s}$	deformation in the ith tire-suspension assembly at time t_s
v	velocity of the vehicle
$\{w\}, \{\dot{w}\}, \{\ddot{w}\}$	vectors containing the dynamic deflections, velocities, and accelerations of the nodal points in the bridge model
$\bar{w}$	assumed displacement function for the plate bending element
W_e, W_i	external and internal work, respectively
w_i	weight of the ith tire-suspension assembly
w_p	vector of vehicle wheel displacements resulting from dynamic deflections of the bridge deck
W_1, W_2	weights of the tractor and trailer bodies, respectively
$\{w_1\}$, $\{w_2\}$, $\{w_3\}$, $\{w_4\}$, $\{w_5\}$	nodal bridge deformation vectors containing vertical deflections, rotations about the y axis, rotations about the x axis, in-plane deformations in the x direction, and in-plane deformations in the y direction, respectively
x, y, z	skewed coordinates axes
x', y', z	rectangular coordinate axes
x_3, x_4	plate dimensions in the x direction as shown in Fig. 1
y_1	plate dimension in the y direction as shown in Fig. 1

$\{z\}$, $\{\dot{z}\}$, $\{\ddot{z}\}$	vectors containing dynamic displacements, velocities, and accelerations of the support points of the vehicle mass
Z_f, Z_p, Z_s	row vectors relating the generalized coordinates to the deflection function for the f, p, and s elements
α	skew angle between the axes of the skewed coordinate system as shown in Fig. 1; also the quantity given by $v/2\ell f_b$, referred to as the speed parameter
β	a dimensionless parameter used in the numerical integration procedure to describe the assumed variation of acceleration within the time interval Δt
β_i	the ith generalized coordinate for the eccentric stiffener element
Δt	length of time interval between times t_s and t_{s+1}
ε, ε'	strain vectors in skew and rectangular coordinates, respectively
θ_x, $\theta_{x'}$	rotation about the x and x' axes, respectively
θ_y, $\theta_{y'}$	rotation about the y and y' axes, respectively
ν	Poisson's ratio for the plate material
ρ_f, ρ_s	mass per unit volume of the plate and stiffener materials, respectively
ψ, ψ'	curvature vectors for the plate bending element in skewed and rectangular coordinates, respectively
ξ	x / L_b where x is the distance along the x axis from the far left support abutment to the drive axle of the vehicle

2. IDEALIZATION OF BRIDGE AND VEHICLE

2.1 Finite-Element Bridge Model

2.1.1 General. In 1961, Oran[9] used a concentrically stiffened plate to simulate the behavior of a single-span bridge. An orthotropic plate has also been used to represent a slab and girder bridge structure.[15] But, in order to apply either of these two methods, the stiffness of the slab or girders was increased to approximate the effects of composite action between the slab and girders. To eliminate this problem, Gustafson[16] and Mehrain[17] independently developed a method through which slab and beam elements are described as separate structural elements and made to interact in such a way as to represent varying degrees of composite action.

The structural elements developed in this study incorporate much of the theory and observations which were presented by Gustafson and Mehrain in their separate studies. Therefore, a discussion of energy principles and two-dimensional stress analysis is not presented.

2.1.2 Plate Elements in Flexure. In order to provide some degree of flexibility, a trapezoidal element is chosen as shown in Fig. 1. The configuration of the element is described in terms of the four nodal points i, j, k, and l. The middle plane of the slab is assumed to coincide with the xy plane. Also, it is assumed that the behavior of a plate in bending is adequately described by the displacement w and the rotations θ_y and θ_x at each of the four nodes.

Having established a twelve degree-of-freedom system, it becomes necessary to choose an expression that describes the displacement of a

plate element at any point (x,y) as a function of at least twelve generalized coordinates. The following displacement function, as used by Adini and Clough[18], incorporates all but two terms of a fourth-order polynomial:

$$w(x,y) = [1,x,y,x^2,xy,y^2,x^3,x^2y,xy^2,y^3,x^3y,xy^3] \begin{Bmatrix} A_1 \\ A_2 \\ \cdot \\ \cdot \\ \cdot \\ \cdot \\ A_{11} \\ A_{12} \end{Bmatrix} = Z_f A \qquad (2.1)$$

Eq. (2.1) is employed often, for it is simple to use and satisfies all of the following requirements for acceptable displacement functions except number 4:

1. All rigid-body displacements are included.
2. Uniform strain states are included.
3. The function is continuous and differentiable within each element and is defined in terms of nodal displacements.
4. Continuity of displacements across interfaces of all adjoining elements is satisfied.

5. The chosen function is either completely or intrinsically related to the geometry of the element.

Along any line that has x or y as a constant, the displacement w will vary as a cubic. If the boundaries or interfaces of the element are composed of such lines, the values of slope and displacement at each end of the boundaries will define the displacement along the boundaries uniquely since a cubic is uniquely defined by four constants. Therefore, continuity of w will be satisfied along any interface since adjacent elements share a common set of end-values of slope and displacement. However, this is not, in general, the case in Gustafson's work.[16] Continuity was not satisfied since his skewed element does not have element interfaces which are composed of y = constant lines unless a skew angle of 90 degrees is used.

Even if the above requirement is satisfied, Eq. (2.1) is a non-conforming shape function. The gradient of w normal to any boundary varies along the boundary in a parabolic manner. However, the parabola is not specified uniquely since only two values of normal slope are defined on such lines, and a discontinuity of normal slope occurs along the element interfaces.

Argyris[19] in 1965 proposed a shape function which is obtained by consideration of the "natural modes" of deflection of the element. These modes are obtained by taking a parabolic or cubic displacement variation on two opposite edges of the element and connecting these by anti-symmetric modes. Finally, uniform twist and rigid body modes are added.

Compatibility of normal slope between adjacent elements is provided at the mid-point as well as the end points of each interface. None the less, the approach was not employed since the complexity of the displacement function nearly eliminates any benefit derived from the small improvement in slope compatibility.

While a triangular element such as that used by Zienkiewicz[20] may have some theoretical advantage, the force and displacement transformations are considerably more difficult to deal with and the use of a comparable grid size requires twice the number of elements used in a quadrilateral system. This in turn somewhat penalizes the efficiency of the approach. Nevertheless, the relative merit of the triangular element is worthy of investigation.

The generalized displacements at each node of the quadrilateral element can be written in the form:

$$u_i = \begin{Bmatrix} w_i \\ \theta_{yi} \\ \theta_{xi} \end{Bmatrix} = \begin{Bmatrix} w \\ w_{,x} \\ -w_{,y} \end{Bmatrix} (x_i, y_i) \qquad (2.2)$$

Hence, the vector defining the nodal displacements for the element in Fig. 1 becomes:

$$u_f = \begin{Bmatrix} u_i \\ u_j \\ u_k \\ u_l \end{Bmatrix} = C_f \; A \qquad (2.3)$$

where C_f is a 12 x 12 matrix as given in Fig. 2. Solving for the vector A, Eq. (2.3) becomes:

$$A = C_f^{-1} u_f \tag{2.4}$$

The matrix C_f^{-1} is given in Fig. 3. The curvature vector in rectangular coordinates (x',y') is:

$$\psi_{(x',y')} = \begin{Bmatrix} -w,_{x'x'} \\ -w,_{y'y'} \\ 2w,_{x'y'} \end{Bmatrix} \tag{2.5}$$

The relationship between the rectangular coordinates (x',y') and the skew coordinates (x,y) may be written as:

$$\begin{Bmatrix} x \\ y \end{Bmatrix} = \begin{bmatrix} 1 & -c \\ 0 & s \end{bmatrix} \begin{Bmatrix} x' \\ y' \end{Bmatrix} \tag{2.6}$$

where $s = 1/\sin \alpha$, and $c = \cos \alpha / \sin \alpha$. The skew angle α is shown in Fig. 1. The corresponding curvature transformation is found by successive differentiation to be:

$$\begin{Bmatrix} -w,_{x'x'} \\ -w,_{y'y'} \\ 2w,_{x'y'} \end{Bmatrix} = \begin{bmatrix} 1 & 0 & 0 \\ c^2 & s^2 & sc \\ 2c & 0 & s \end{bmatrix} \begin{Bmatrix} -w,_{xx} \\ -w,_{yy} \\ 2w,_{xy} \end{Bmatrix} = G \; \psi_{(x,y)} \tag{2.7}$$

If the indicated differentiation is performed, Eq. (2.7) yields:

$$\psi_{(x',y')} = G \; B_{f(x,y)} \; A \tag{2.8}$$

The 3 x 12 matrix, B_f, is as follows:

$$\left[\begin{array}{ccc|cccccccccc} 0 & 0 & 0 & -2 & 0 & 0 & -6x & -2y & 0 & 0 & -6xy & 0 \\ 0 & 0 & 0 & 0 & 0 & -2 & 0 & 0 & -2x & -6y & 0 & -6xy \\ 0 & 0 & 0 & 0 & 2 & 0 & 0 & 4x & 4y & 0 & 6x^2 & 6y^2 \end{array}\right]$$

where x and y are the skew coordinates of the point under consideration. It can be seen from examination of the matrix B_f in Eq. (2.8) that the first three generalized displacements, A_1, A_2, and A_3, do not contribute to the determination of the curvature vector ψ since neither a rigid body displacement nore a linear displacement in the x or y direction will affect curvature in the plate element. Therefore, only zeros are contained in the first three columns of the B_f matrix. Later, it will be seen that the three void columns allow the final expression for the stiffness matrix of the flexural element to be simplified.

The internal force-displacement relations from the classical theory of plates[21] are written with the axes of orthotropy coinciding with the rectangular x' and y' coordinates as follows:

$$M_p = \left\{\begin{array}{c} M_{x'} \\ M_{y'} \\ M_{x'y'} \end{array}\right\} = \left[\begin{array}{ccc} D_x & D_1 & 0 \\ D_1 & D_y & 0 \\ 0 & 0 & D_{xy} \end{array}\right] \left\{\begin{array}{c} -w_{,x'x'} \\ -w_{,y'y'} \\ 2w_{,x'y'} \end{array}\right\} \tag{2.9}$$

$$M_p = D_f \psi = D_f G_f B_f A \tag{2.10}$$

For an isotropic material, D_f is expressed as follows:

$$D_f = \frac{E t^3}{12 (1 - \nu^2)} \begin{bmatrix} 1 & \nu & 0 \\ \nu & 1 & 0 \\ 0 & 0 & (1-\nu)/2 \end{bmatrix} \tag{2.11}$$

where E is the elastic modulus, t the thickness, and ν Poisson's ratio. The nodal force vector is represented by

$$F_f = \{F_{i1}, F_{i2}, F_{i3}, F_{j1}, F_{j2}, \ldots, F_{\ell 1}, F_{\ell 2}, F_{\ell 3}\} \tag{2.12}$$

where F_{i1}, F_{i2}, and F_{i3} correspond to the nodal shear and the nodal moments about the y and x axes, respectively, at the ith node of the element.

The stiffness matrix can now be established by applying, successively, virtual unit displacements at each nodal point. The external work, which is produced by the nodal forces while moving through this set of unit displacements, is given by

$$\delta W_e = (\delta u_f)^T F_f \tag{2.13}$$

The internal work, which is done by the internal stresses moving through their corresponding virtual strains, is given by

$$\delta W_i = - \int \int (\delta \psi)^T \{M_p\} \, dx'dy' \tag{2.14}$$

where

$$\{\delta\Psi\} = [G_f]\ [B_f]\ \{\delta A\} = [G_f]\ [B_f]\ [C_f]^{-1}\ \{\delta u_f\} \tag{2.15}$$

Equating the sum of the internal work, Eq. (2.14), and the external work, Eq. (2.13), to zero and rearranging terms yields the following stiffness equation:

$$\left\{F_f\right\} = \left[C_f^{-1}\right]^T \left[\bar{K}_f\right] \left[C_f^{-1}\right] \left\{u_f\right\} \tag{2.16}$$

$\bar{K}_f$, which is the stiffness matrix in terms of the generalized coordinates can be written as

$$\bar{K}_f = \int_{area} B_f^T\ G_f^T\ D_f\ G_f\ B_f\ dx'dy' \tag{2.17}$$

$$\bar{K}_f = \int_0^{y_1 \sin\alpha} \int_0^{ky + x_3} B_f^T\ G_f^T\ D_f\ G_f\ B_f\ dxdy \tag{2.18}$$

where $k = (x_4 - x_3) / y_1$. The quantities x_3, x_4, y_1, and α are shown in Fig. 1. Finally, Eq. (2.16) can be written in the form

$$F_f = K_f\ u_f \tag{2.19}$$

in which K_f is the stiffness matrix for the flexure plate element in terms of the nodal forces and nodal displacements. Prior to performing the integration indicated in Eq. (2.18), it becomes advantageous to place an additional restriction on the geometry of the element. By requiring two sides of the element to be parallel to the x axis, it becomes possible to define the limits of integration on y independent of the variable x.

This in turn allows the integration of Eq. (2.18) to be performed in a straight-forward manner. The matrix $\bar{K}$ is given in Fig. 4 in its integrated form.

As pointed out in the discussion following Eq. (2.8), the first three columns of the matrix B_f contain only zeros. This implies that the K_f matrix is not affected by the first three elements of the generalized displacement vector A. Therefore, the first three columns of the B_f matrix and the first three rows of the C_f^{-1} matrix can be dropped without affecting the resulting K_f matrix. The matrix B_f becomes a 3 x 9 matrix, and C_f^{-1} becomes a 9 x 12 matrix. These modifications also apply to B_f^T in Eq. (2.18) and $C_f^{-1\,T}$ in Eq. (2.16). Finally, the original 12 x 12 $\bar{K}_f$ matrix in Eq. (2.18) is reduced to a 9 x 9 matrix. These modifications are demonstrated by dotted lines in Fig. 3 and Fig. 4.

Since the operations indicated in Eq. (2.16) are easily performed by computer, no attempt was made to find the explicit form of the resulting 12 x 12 K_f matrix of Eq. (2.19).

2.1.3 Plane Stress Elements. The behavior of the element when acted on by in-plane forces is assumed to be adequately described by u and v displacements in the x and y directions, respectively, at each of the four corner nodes. A displacement function in the form of a polynomial is assumed as follows:

$$\begin{Bmatrix} u \\ v \end{Bmatrix} = \begin{bmatrix} 1 & x & y & xy & 0 & 0 & 0 & 0 \\ 0 & 0 & 0 & 0 & 1 & x & y & xy \end{bmatrix} \begin{Bmatrix} A_{p1} \\ A_{p2} \\ \cdot \\ \cdot \\ \cdot \\ \cdot \\ A_{p7} \\ A_{p8} \end{Bmatrix} = Z_p A_p \qquad (2.20)$$

This function, which was used by Clough[27] in 1965, satisfies all of the requirements of Art. 2.1.2. The formulation proceeds from this point in a manner similar to that of the previous section. The nodal displacements, when expressed in terms of the generalized coordinate vector A_p, are:

$$u_p = \begin{Bmatrix} u_i \\ v_i \\ u_j \\ v_j \\ u_k \\ v_k \\ u_l \\ v_l \end{Bmatrix} = \begin{bmatrix} C \\ p \end{bmatrix} \begin{Bmatrix} A \\ p \end{Bmatrix} \qquad (2.21)$$

When premultiplied by C_p^{-1}, Eq. (2.21) becomes

$$A_p = C_p^{-1} u_p \tag{2.22}$$

The matrix C_p and its inverse are shown in Fig. 5. The strain vector in rectangular coordinates (x',y') is

$$\varepsilon'_{(x',y')} = \begin{Bmatrix} u'_{,x'} \\ v'_{,y'} \\ u'_{,y'} + v'_{,x'} \end{Bmatrix} \tag{2.23}$$

Subscripts are used to indicate differentiation with respect to x' or y'.

The transformation matrix, which relates the rectangular displacements u' and v' to the skew displacements u and v, is

$$\begin{Bmatrix} u \\ v \end{Bmatrix} = \begin{bmatrix} 1 & 0 \\ \cos\alpha & \sin\alpha \end{bmatrix} \begin{Bmatrix} u' \\ v' \end{Bmatrix} \tag{2.24}$$

The corresponding transformation matrix for strains is

$$\{\varepsilon'\} = \begin{Bmatrix} u'_{,x'} \\ v'_{,y'} \\ u'_{,y'} + v'_{,x'} \end{Bmatrix} = \begin{bmatrix} 1 & 0 & 0 \\ c^2 & s^2 & -sc \\ -2c & 0 & s \end{bmatrix} \begin{Bmatrix} u_{,x} \\ v_{,y} \\ u_{,y} + v_{,x} \end{Bmatrix} = G_p \varepsilon \tag{2.25}$$

where $s = 1/\sin\alpha$, and $c = \cos\alpha / \sin\alpha$. The strain vector ε' can now be related to the generalized coordinates as follows:

$$\{\varepsilon'\} = [G_p] \begin{bmatrix} 0 & 1 & 0 & y & 0 & 0 & 0 & 0 \\ 0 & 0 & 0 & 0 & 0 & 0 & 1 & x \\ 0 & 0 & 1 & x & 0 & 1 & 0 & y \end{bmatrix} \{A_p\} = G_p \; B_p \; A_p \qquad (2.26)$$

The first and fifth columns of B_p contain only zeros. Therefore, it is evident that the strain vector ε' is not a function of the generalized coordinates A_{p1} and A_{p5}, which represent rigid body movements. A similar observation made it possible to reduce the size of the matrix B_f in Eq. (2.8) by elimination of the first three generalized coordinates of the flexural element. The third and sixth columns of B_p are seen to be identical. This indicates that the strain vector is related to A_{p3} and A_{p6} in exactly the same manner. With these two observations at hand, several simplifications can be made. Let A^* be as follows:

$$\{A^*\} = \begin{Bmatrix} A_2 \\ A_4 \\ A_3 + A_6 \\ A_7 \\ A_8 \end{Bmatrix} = [C^*_p]^{-1} \{u_p\} \qquad (2.27)$$

The matrix $C^{*\,-1}_p$ is shown in Fig. 6. Eq. (2.26) can now be written as follows:

$$\{\varepsilon'\} = [G_p] \begin{bmatrix} 1 & y & 0 & 0 & 0 \\ 0 & 0 & 0 & 1 & x \\ 0 & x & 1 & 0 & y \end{bmatrix} \quad \{A^*\} = G_p \quad B_p^* \quad A^* \tag{2.28}$$

The force-displacement relations for the in-plane forces are

$$N = \begin{Bmatrix} N_x \\ N_y \\ N_{xy} \end{Bmatrix} = \begin{bmatrix} D_x & D_1 & 0 \\ D_1 & D_y & 0 \\ 0 & 0 & D_{xy} \end{bmatrix} \begin{Bmatrix} u'_{,x'} \\ v'_{,y'} \\ u'_{,y'} + v'_{,x'} \end{Bmatrix} = D_p \; G_p \; B_p^* \; A^* \tag{2.29}$$

where D_p for the plane stress case with an isotropic material is

$$D_p = \frac{E\,t}{1-\nu^2} \begin{bmatrix} 1 & \nu & 0 \\ \nu & 1 & 0 \\ 0 & 0 & (1-\nu)/2 \end{bmatrix} \tag{2.30}$$

The stiffness matrix for in-plane forces can now be written in terms of the generalized coordinates as follows:

$$\bar{K}_p = \int_{area} B_p^{*\,T} \; G_p^{\,T} \; D_p \; G_p \; B_p^* \; dx'dy'$$

$$= \int_0^{y_1 \sin\alpha} \int_0^{ky+x_3} B_p^{*\,T} \; G_p^{\,T} \; D_p \; G_p \; B_p^* \; dxdy \tag{2.31}$$

where $k = (x_4 - x_3) / y_1$. The quantities x_3, x_4, y_1 and α are shown in Fig. 1. The matrix $\bar{K}_p$ is given explicitly in Fig. 7. The stiffness matrix which relates nodal displacements to nodal forces is found by using Eq. (2.21) and can be written as follows:

$$\left[K_p\right] = \left[C_p^*\right]^{-1^T} \left[\bar{K}_p\right] \left[C_p^*\right]^{-1} \tag{2.32}$$

Finally, the stiffness equation for in-plane forces becomes

$$F_p = K_p u_p \tag{2.33}$$

in which F_p is the nodal force vector as given below.

$$F_p = \{F_{i1}, F_{i2}, F_{j1}, F_{j2}, F_{k1}, F_{k2}, F_{l1}, F_{l2}\} \tag{2.34}$$

where F_{i1} and F_{i2} correspond to the in-plane forces in the x and y directions, respectively, at the ith node of the element.

The two stiffness matrices K_f and K_p are combined to form one stiffness matrix for both in-plane and flexural forces.

2.1.4 Eccentric Stiffener Elements. Initially, the stiffness matrix for a beam element is derived in rectangular coordinates as shown in Fig. 8. The longitudinal direction of the beam will be denoted by the x axis. Later, transformation matrices for beams along both the x and y axes will be presented to transform the expressions into global skew coordinates.

Nodal displacements are defined in terms of the four quantities w, θ_y, θ_x, and u. The torsional deformation θ_x is assumed to be independent of the other nodal displacements. Therefore, only flexural and axial deformations are considered initially.

The u, w displacement vector is assumed to be a function of six generalized coordinates as follows:

$$\begin{Bmatrix} u \\ w \end{Bmatrix} = \begin{bmatrix} 1 & x & 0 & 0 & 0 & 0 \\ 0 & 0 & 1 & x & x^2 & x^3 \end{bmatrix} \begin{Bmatrix} \beta_{s1} \\ \beta_{s2} \\ \beta_{s3} \\ \beta_{s4} \\ \beta_{s5} \\ \beta_{s6} \end{Bmatrix} = Z_s \quad \beta_s \qquad (2.35)$$

Taking $\theta_y = w,_x$, the nodal displacement vector is found to be

$$u_s = \begin{Bmatrix} w_1 \\ \theta_{y1} \\ u_1 \\ w_2 \\ \theta_{y2} \\ u_2 \end{Bmatrix} = C_s \quad \beta_s \qquad (2.36)$$

When premultiplied by C_s^{-1}, Eq. (2.36) becomes

$$\beta_s = C_s^{-1} \quad u_s \qquad (2.37)$$

The matrix C_s and its inverse are given explicitly in Fig. 9. The axial strain and curvature vector may be written as follows:

$$\begin{Bmatrix} u,_x \\ -w,_{xx} \end{Bmatrix} = \begin{bmatrix} 0 & 1 & 0 & 0 & 0 & 0 \\ 0 & 0 & 0 & 0 & -2 & -6x \end{bmatrix} \{\beta_s\} = B_s \quad C_s^{-1} \quad u_s \qquad (2.38)$$

The force displacement equations are written as

$$\begin{Bmatrix} N_{es} \\ M_{es} \end{Bmatrix} = [D_s] \begin{Bmatrix} u,_x \\ -w,_{xx} \end{Bmatrix} \qquad (2.39)$$

where D_s is defined as

$$[D_s] = E_s \begin{bmatrix} A_s & S_x \\ S_x & I_x \end{bmatrix} \qquad (2.40)$$

in which A_s is the cross-sectional area of the stiffener, S_x is the first moment of the stiffener area with respect to the reference surface, and I_x is the moment of inertia of the stiffener with respect to the reference surface (see Fig. 8).

As in previous sections, the stiffness matrix for the beam element may be written as follows:

$$\bar{K}_s' = C_s^{-1^T} \left\{ \int_0^L B_s^T \quad D_s \quad B_s \quad dx \right\} \quad C_s^{-1} \qquad (2.41)$$

Torsional deformation is assumed to vary linearly along the length of the stiffener element. This assumption enables the torsional moment at the ends of the element to be defined solely by the end

rotations θ_{x1} and θ_{x2} as follows:

$$\begin{Bmatrix} T_1 \\ T_2 \end{Bmatrix} = \begin{bmatrix} JG/L & -JG/L \\ -JG/L & JG/L \end{bmatrix} \begin{Bmatrix} \theta_{x1} \\ \theta_{x2} \end{Bmatrix} \tag{2.42}$$

where J is St. Venant's torsional stiffness constant, G is the shear modulus, and L is the length of the element. Eq. (2.42) is valid only when warping effects can be ignored. Such a simplification is warranted for most wide flange steel shapes used in bridge design since these sections exhibit extremely low values of torsional stiffness compared to the torsional stiffness of the bridge deck. However, if a closed section, such as a box girder, supports the bridge, Eq. (2.42) may not accurately represent the torsional behavior of the eccentric stiffener. The torsional stiffness matrix in Eq. (2.42) and the stiffness matrix which is given by Eq. (2.41) may now be combined to form a total stiffness equation of the form

$$F_s = \bar{K}_s u_s \tag{2.43}$$

Eq. (2.43) is given explicitly in Fig. 10.

2.1.5 Transformation of Beam Elements from Local to Skew Coordinates. The stiffness matrix in Eq. (2.43) was derived for a beam element which was assumed to have its longitudinal axis coincident with the x axis of a rectangular coordinate system. Transformation matrices must now be employed in order to establish the stiffness of the element in relation to global forces and displacements.

The relationship between displacements relative to the rectangular

coordinates (x',y') and displacements in global skew coordinates (x,y) for a beam parallel to the x axis may be written as follows:

$$\begin{Bmatrix} w' \\ \theta_{y'} \\ \theta_{x'} \\ u' \end{Bmatrix} = \begin{bmatrix} 1 & 0 & 0 & 0 & 0 \\ 0 & 1 & 0 & 0 & 0 \\ 0 & c & s & 0 & 0 \\ 0 & 0 & 0 & 1 & 0 \end{bmatrix} \begin{Bmatrix} w \\ \theta_y \\ \theta_x \\ u \\ v \end{Bmatrix} = \bar{R}_s \quad u_s \qquad (2.44)$$

For a beam parallel to the y axis, the transformation is written as

$$\begin{Bmatrix} w' \\ \theta'_y \\ \theta'_x \\ u' \end{Bmatrix} = \begin{bmatrix} 1 & 0 & 0 & 0 & 0 \\ 0 & 0 & -1 & 0 & 0 \\ 0 & s & c & 0 & 0 \\ 0 & 0 & 0 & 0 & 1 \end{bmatrix} \begin{Bmatrix} w \\ \theta_y \\ \theta_x \\ u \\ v \end{Bmatrix} = \bar{R}_s \quad u_s \qquad (2.45)$$

where, as previously stated, $s = 1/\sin \alpha$, and $c = \cos \alpha / \sin \alpha$. The stiffness matrix in skew coordinates is then found to be

$$K_s = R_s^T \quad \bar{K}_s \quad R_s \qquad (2.46)$$

where

$$R_s = \left[\begin{array}{c|c} \bar{R}_s & 0 \\ \hline 0 & \bar{R}_s \end{array}\right] \qquad (2.47)$$

2.1.6 Assembly of the Structural Elements. The static analysis of a bridge structure can be obtained by solving the following matrix equation:

$$\{p\} = [K] \{w\} \tag{2.48}$$

where p is the nodal load vector, K is the $5N \times 5N$ stiffness matrix for the assembled structure, w is the nodal displacement vector, and N is the total number of nodes in the structure. As will be seen later, the matrix K is also required in the solution of dynamic problems.

The matrix K can be generated either through a series of logical operations[23] or through the use of localizing matrices[16]. The approach which was employed in this study is presented in Appendix A together with some suggestions which relate to computational efficiency.

2.1.7 Implementation of Boundary Conditions. One of the most significant advantages of the finite element approach to analysis is its adaptability to the variety of boundary conditions which can occur in plate and shell structures. Unlike a finite difference approach, it permits a variety of boundary conditions to be easily imposed upon the equilibrium equations.

The most common types of boundary conditions are achieved simply by imposing prescribed support displacements such as zero vertical, horizontal, or rotational displacements. However, since prescribed displacements are not always zero, the problem can not always be solved simply by omitting the equilibrium equation which corresponds to the known displacement. This procedure is undesirable because it usually requires extensive reorganization of matrices which are in secondary computer storage.

A second more popular approach is to replace all stiffness quantities in the row corresponding to the prescribed displacement with zero except for the element on the diagonal which is given the value of unity. The corresponding term in the force vector is then replaced by the magnitude of the known displacement. When the equilibrium equations are solved, the magnitude of the displacement becomes identical to the value contained in the force vector. This method also was not the best approach because the equilibrium equations become unsymmetrical when the off-diagonal elements of the rows which correspond to prescribed displacements are set equal to zero.

An approach which is used by Zienkiewicz[20] was found to be most suitable. The off-diagonal elements which were set equal to zero in the previous method are left unchanged, thus preserving the symmetry of the equilibrium equations. Instead, the term on the diagonal is multiplied by a large number, say 10^{12}. This essentially has the same effect as setting the off-diagonal terms to zero since their magnitudes become relatively insignificant. The corresponding term in the force vector is at the same time replaced by this newly-formed diagonal term multiplied by the magnitude of the prescribed displacement, δ. When the equilibrium equations are solved, the modified row will essentially be as follows:

$$K_{ii} \cdot 10^{12} \cdot x_i = K_{ii} \cdot 10^{12} \cdot \delta \qquad (2.49)$$

which in turn reduces to the form $x_i = \delta$. It should be pointed out, however, that the off-diagonal terms will cause the resulting displacements to be slightly different from the prescribed values.

After all boundary conditions have been imposed, the equilibrium equations may be solved. The method used in this study to solve static problems is a modified Gauss elimination process. This method, which has been used by Zienkiewicz,[20] is designed specifically for solving problems which are characterized by a banded stiffness matrix. Dynamic problems, however, were not so easily handled. As will be seen later, a reduced stiffness matrix approach was required which in turn caused the resulting equations to be completely unbanded.

2.1.8 Plate Element Mass Matrix. As in the case of the plate element stiffness matrix, the mass matrix for the total plate element can be derived in two parts. However, because of certain assumptions which will be discussed later, it is necessary to develop only the mass matrix which corresponds to the flexural plate element. The derivation of the mass matrix for the plane-stress element follows the same general procedure and will not be presented in this study.

The inertial forces for the flexural plate element can be defined in terms of the vertical and rotational accelerations $\ddot{w}$, $\ddot{\theta}_y$, and $\ddot{\theta}_x$ as follows:

$$\left\{F_f\right\} = \left[M_f\right] \begin{Bmatrix} \ddot{w}_1 \\ \ddot{\theta}_{y1} \\ \ddot{\theta}_{x1} \\ \cdot \\ \cdot \\ \cdot \\ \cdot \\ \ddot{w}_4 \\ \ddot{\theta}_{y4} \\ \ddot{\theta}_{x4} \end{Bmatrix} \tag{2.50}$$

where F_f is defined in Eq. (2.21), and M_f can be written as:

$$M_f = \rho_f \, t \, C_f^{-1\,T} \left\{ \int_0^{y_1 \sin \alpha} \int_0^{ky + x_3} Z_f^{\,T} \, Z_f \, dxdy \right\} C_f^{-1} \tag{2.51}$$

where ρ_f is the mass per unit volume, t is the slab thickness, C_f^{-1} is defined in Fig. 3, and k is equal to $(x_4 - x_3)/ y_1$. The terms x_3, x_4, y_1, and α are shown in Fig. 1. The row vector Z_f is given in Eq. (2.1). The quantity enclosed in braces is given in its expanded form in Fig. 11.

2.1.9 Mass Matrix for Eccentric Stiffeners. If a rectangular coordinate system is initially assumed, the mass matrix $\bar{M}_s$ for an eccentric stiffener may be found from the expression which follows:

$$\bar{M}_s = \int_0^L \rho_s \, A_s \, Z_m^T \, Z_m \, dx \tag{2.52}$$

where ρ_s is the mass per unit volume of the stiffener, A_s is the area of the cross-section, and L is the length of the stiffener element. The matrix Z_m as used by Przemieniecki[24] relates the local displacement coordinates u_x, u_y, and u_z to the nodal displacement vector as follows:

$$\begin{Bmatrix} u_x \\ u_y \\ u_z \end{Bmatrix} = [Z_m] \begin{Bmatrix} w_1 \\ \theta_{y1} \\ \theta_{x1} \\ u_1 \\ w_2 \\ \theta_{y2} \\ \theta_{x2} \\ u_2 \end{Bmatrix} \tag{2.53}$$

The matrix Z_m^T is given explicitly in Fig. 12.

The mass matrix may be transformed to skew coordinates as follows:

$$M_s = R_s^T \, \bar{M}_s \, R_s \tag{2.54}$$

where R_s is the transformation matrix developed in Art. 2.1.5, and $\bar{M}_s$ is the matrix established by Eq. (2.52). The matrix $\bar{M}_s$ is given explicitly in Fig. 13.

The procedure for assembling the mass matrix for the entire structure is identical to the procedure outlined in Art. 2.1.6 for the structural stiffness matrix.

2.1.10 Viscous Damping Matrix. Damping in the bridge model is provided for through the application of viscous damping forces which are assumed to act at the nodal points in the structural model. The damping matrix C is defined as follows:

$$C = \zeta C_c \tag{2.55}$$

where ζ is an input parameter which is referred to as the damping ratio. The critical damping matrix C_c is approximated by the following expression:

$$C_c = 4 \pi f_b M \tag{2.56}$$

where M is the mass matrix for the assembled structure, and f_b is the fundamental natural frequency of the bridge model in cycles per second.

2.1.11 Concentrated Vehicle Wheel Loads. Each vehicle wheel load is treated as a concentrated load. When a wheel load is located within the boundaries of a bridge deck element, the force exerted by the tire is transformed into an equivalent set of moments and forces which act at the four nodes of the deck element. This transformation process

is similar to that which is used to find the fixed-end moments and shears associated with a set of member loads in a frame analysis problem. Since in-plane forces are neglected in a fixed-end plate element subjected to vertical loads only, the notation introduced in Art. 2.1.2 is used in the equations that are presented in this section.

The work that is performed by the nodal forces when the nodes are each given a unit displacement is found to be

$$\delta W_p = \{\delta u_f\}^T \{F_f\} \tag{2.57}$$

The work produced by a single concentrated vertical load is

$$\delta W_q = (\delta \bar{w})^T_{x_1, y_1} P_i \tag{2.58}$$

where P_i is the magnitude of the concentrated force which interacts between the vehicle tire and the bridge deck. The coordinates x_1 and y_1 give the location of the concentrated force relative to the plate element on which it acts. From Eqs. (2.1) and (2.4), the expression for the deflection of the plate element can be rewritten as follows:

$$\bar{w}(x,y) = \{Z_f\} [C_f]^{-1} \{u_f\} \tag{2.59}$$

If Eq. (2.59) is substituted into Eq. (2.58), the expression for W_q becomes

$$\delta W_q = \{\delta u_f\}^T [C_f]^{-1\,T} \{Z_f\}^T P_i \tag{2.60}$$

The above expressions for δW_p and δW_q are now equated as follows:

$$\{\delta u_f\}^T \{F_f\} = \{\delta u_f\}^T [C_f]^{-1\,T} \{Z_f\}^T P_i \tag{2.61}$$

It can be shown that the above equation may be simplified to yield the following expression for the equivalent set of nodal forces associated with the interacting force P_i:

$$\left\{F_f\right\} = \left[C_f^{-1}\right]^T \left\{Z_f\right\}^T P_i \qquad (2.62)$$

As shown in Fig. 14, the values of x and y used to evaluate the terms in Z_f are the distances to the concentrated wheel load from the origin of the element on which the load is located.

Gustafson[16] has shown that each wheel load may instead be distributed over some small arbitrary contact area. Even though it yields a more reasonable representation of the vehicle load, Gustafson's approach was not utilized since such a refinement is detectable only if the magnitudes of stresses and strains in the bridge deck in the immediate vicinity of a vehicle load are investigated.

2.2 The Vehicle Model

In previous bridge-vehicle interaction studies, the vehicle model has been assumed to act in a single plane.[3,7] In this study, the vehicle model is given a third dimension, consistent with the bridge idealization, in order to better predict the transverse behavior of the bridge. This modification also permits the effects of rolling to be considered.

The tractor-trailer vehicle model consists of two interconnected rigid bodies which are supported by a series of springs and dashpots as shown in Fig. 15. The quantity W_1 represents the weight of the tractor mounted on its suspension system. The quantities i_{1x} and i_{1y} are

required to describe the rotational moments of inertia of the weight W_1 about the x and y axes, respectively, and are referred to as the dynamic indices of the tractor. The point masses with the weights w_1, w_2, w_3, and w_4 represent the mass of each tire plus one half of the mass of the corresponding axle and suspension system. The quantities W_2, i_{2x}, i_{2y}, w_5, and w_6 refer to the trailer and have the same definitions as the corresponding tractor quantities. The quantities i_{1x}, i_{1y}, i_{2x}, and i_{2y} may be expressed mathematically as follows:

$$i_{1x} = 1/4\,(r_{1x}/S_1)^2 \qquad i_{1y} = (r_{1y}/L_1)^2 / (a_1 a_2)$$

$$i_{2x} = 1/4\,(r_{2x}/S_3)^2 \qquad i_{2y} = (r_{2y}/L_3)^2 / (a_3 a_4) \qquad (2.63)$$

where r_{1x} and r_{1y} are the radii of gyration of the tractor mass W_1 about axes which pass through the center of gravity of W_1 in the directions of the x and y axes, respectively; the quantities r_{2x} and r_{2y} are the corresponding quantities for the trailer mass W_2. The quantities S_1, L_1, S_3, and L_3 are indicated in Fig. 15.

The weights $\bar{w}_1$, $\bar{w}_2$, $\bar{w}_3$, $\bar{w}_4$, $\bar{w}_5$, and $\bar{w}_6$ are also indicated in Fig. 15. These weights are "unsprung" in that they move with the bridge deck and are not affected by deformations in the tire or suspension springs; the mass of an unsprung weight experiences an acceleration, velocity, and displacement which are identical to the acceleration, velocity, and displacement of the bridge deck at the location of the vehicle load. The unsprung masses were introduced to permit better correlation of the theoretical solutions with the behavior of a laboratory vehicle model in which a solid (unsprung) wheel was used.

The relationship between load and deformation in each tire-suspension assembly is idealized as a bilinear, hysteretic function. The bilinear function is used to represent the stiffness of a tire-suspension assembly which changes when the limiting value of interleaf friction in its suspension system is exceeded. This effect is produced by two linearly elastic springs in series and a frictional damping device which acts in parallel with the upper spring. The lower spring represents the stiffness of the tire in the assembly. The upper spring and frictional device account for the effects of interleaf friction in the leaf springs of the suspension system.

The value of the frictional force developed at any particular time t_s is designated by F_s, and the force at which the frictional damping device breaks down or "unlocks" is F'. As long as $-F' < F_s < F'$ in a particular tire-suspension assembly, the damper is assumed to act as a rigid link; and the suspension spring remains inactive. However, if F_s reaches the value of $\pm F'$, the damper unlocks and the suspension spring begins to act in series with the tire spring. At that instant, the effective stiffness of the assembly changes from k_t to k_{ts}, where

$$\frac{1}{k_{ts}} = \frac{1}{k_t} + \frac{1}{k_s} \tag{2.64}$$

The quantity k_s denotes the stiffness of the suspension spring; k_t is the stiffness of the tire, and k_{ts} is the combined stiffness of the tire spring and suspension spring acting in series. For the ith tire-suspension assembly, the quantities $k_{t,i}$ and $k_{ts,i}$ are

often defined in terms of $f_{t,i}$ and $f_{ts,i}$, respectively. The quantity $f_{t,i}$ denotes the pseudo-frequency of the ith assembly when only the tire spring is active, and $f_{ts,i}$ represents the pseudo-frequency of the ith assembly when the tire spring and the suspension spring act in series. The quantities $k_{t,i}$ and $k_{ts,i}$ may be calculated from the following equations:

$$k_{t,i} = 4\pi^2(f_{t,i})^2 P_{st,i} / g \tag{2.65}$$

and

$$k_{ts,i} = 4\pi^2(f_{ts,i})^2 P_{st,i} / g \tag{2.66}$$

where $P_{st,i}$ is the reaction in the ith tire when the vehicle is in a position of static equilibrium, and g is the gravitational acceleration.

The model described above was chosen because it is simple, straightforward, and yet able to exhibit many characteristics that are significant to the dynamic response of heavy highway vehicles. However, a recent study has shown that the response of the vehicle model can be improved by using a more detailed representation of the suspension system.[25] Based on this work, one possible modification is the placement of a portion of the mass of the suspension system between the tire spring and the suspension spring. An additional degree of freedom is then required to determine the deflection and acceleration of the suspension system mass. This mass is often referred to as "unsprung mass" since its inertia properties are related only to deformations in the vehicle tires.

The vehicle model can also be improved by replacing the single suspension spring and friction device with several sets of suspension springs and friction devices acting in parallel. It is then possible to produce a more realistic leaf-spring model by allowing each frictional device to unlock at different values of friction force, thus creating a multi-linear load-deformation function for the tire-suspension system. More detailed discussions of the behavior of tire-suspension systems on heavy vehicles are presented in Refs. 3, 7, and 25.

3. METHOD OF ANALYSIS

3.1 Equations of Motion

3.1.1 Displacement Coordinates. The coordinate vector $\{w_r\}$ denotes the displacements of the rth node of the bridge model. This vector includes two in-plane displacements, two rotations, and one displacement in the vertical direction, all of which are measured from the static equilibrium position of the bridge structure when it is acted upon by the dead weight of the bridge alone. The positive sense of each element of the vector is shown in Fig. 1. The configuration of the surface of the bridge deck when the structure is subject to its own weight is specified by the function $d_i(x)$, where the subscript 'i' refers to the ith wheel path. This function represents the deviation of the deck surface from a horizontal line which passes through the point on the deck surface where the ith wheel path crosses the left abutment and continues along the ith wheel path. This deviation is the result of a combination of factors which include dead-load deflection, initial camber and roadway unevenness. Since the only effects these deviations have on the bridge-vehicle system are the distorsions they cause in the tires of the vehicle, only deviations along each wheel path are considered.

The coordinate z_i specifies the vertical displacement of the point of attachment of the ith tire-suspension assembly to the vehicle mass. This displacement, which is taken to be positive when downward, is measured from the static equilibrium position of the ith support point when the vehicle is located on a horizontal plane which passes through the left abutment.

The forces which are exerted on the bridge deck by the tires of the vehicle will be referred to as the interacting forces. These interacting forces will be considered to be positive when they act downward on the bridge deck and produce compressive forces in the tire-suspension systems of the vehicle. Negative interacting forces are permitted although it is assumed that the vehicle tire remain in contact with the bridge deck at all times.

3.1.2 Equations of Motion for the Bridge Model. The equations of motion for the finite element bridge model may be expressed in matrix form as follows:

$$[M]\left\{\ddot{w}\right\} + [C]\left\{\dot{w}\right\} + [K]\left\{w\right\} = [H]\left\{P_i\right\} \qquad (3.1)$$

where w is a vector containing one nodal bridge displacement for each degree of freedom in the bridge model. A dot superscript denotes one differentiation with respect to time. The matrices M and C are the mass and damping matrices, respectively. The vector P_i denotes the interacting force between the bridge surface and the vehicle tires. The matrix H is a matrix of load coefficients and represents the forces at the bridge joints which are induced by a unit vector of interacting forces. The matrix H transforms each interacting force in the vector P_i into a corresponding vector of fixed-end shears and moments at each node of the element on which each wheel load is located. The non-zero elements of each column in H are taken from the column vector which results from the product $\left[C_f^{-1}\right]^T \left\{Z_f\right\}^T$ in Eq. (2.62).

3.1.3 Equations of Motion for the Vehicle. Using matrix notation, the equations of motion for the vehicle can be stated as follows:

$$[m]\left\{\ddot{z}\right\} + [k_v]\left\{z\right\} = [h]\left\{P_w\right\} \tag{3.2}$$

where $\ddot{z}$ and z are vectors in which the acceleration and displacement of each support point of the vehicle mass are contained, respectively. Each term in the vector P_w represents that part of the reaction in one of the vehicle tires which cannot be expressed as a function of the corresponding displacement coordinate in the vector z. The derivation of Eq. (3.2) is presented in Appendix B; and the matrices m, k_v, and h are given explicitly in Figs. 16, 17, and 18, respectively.

Eq. (3.2) can be easily modified to include absolute viscous damping in the suspension system of the vehicle as follows:

$$[m]\left\{\ddot{z}\right\} + [c]\left\{\dot{z}\right\} + [k_v]\left\{z\right\} = [h]\left\{P_w\right\} \tag{3.3}$$

The procedure presented in Art. 2.1.10 for bridge damping is also used to specify viscous damping in the vehicle model. Eq. (3.3) has been developed for heavy highway vehicles with leaf spring suspension systems and will require modification if another system, such as the air bag suspension system, is to be represented accurately. Also, it should be noted that relative damping in the tires is ignored in Eq. (3.3).

3.2 Numerical Integration Procedure

3.2.1 General. The equations of motion for the bridge-vehicle system are solved numerically through the use of a step-by-step integration procedure. The time required for the vehicle to cross the bridge is first divided into a number of short intervals. Then, at the end of each interval of time, the equations of motion are solved to determine the values of acceleration, velocity, and displacement for each coordinate in the system.

3.2.2 Evaluation of Interacting Forces. In order to solve the equations of motion for the bridge-vehicle system, it is necessary to determine the magnitude of the interacting forces at the end of each time interval. If one assumes that the interacting forces are determined by a constant force function or some mathematical expression that is solely a function of time, the procedure is greatly simplified since the vehicle model and the equations that define its behavior are eliminated from the solution. However if a vehicle model, such as the one used in this study, is employed, the reaction force in a given tire becomes a function of the effective stiffness of its tire-suspension spring assembly and the deformation that is applied to the spring assembly.

The procedure described below was first presented by Huang.[7] The terms $P_{i,s}$ and $P_{i,s+1}$ shall represent the magnitude of a single interacting force at time t_s and t_{s+1}, respectively. Furthermore, it is assumed that all quantities corresponding to time t_s have been evaluated.

In order to determine the value of $P_{i,s+1}$, it is initially assumed that the effective stiffness of the corresponding tire-suspension spring assembly remains constant between times t_s and t_{s+1} even though this may later prove to be false. This assumption establishes the validity of the following equation:

$$P_{i,s+1} = P_{i,s} + \Delta P_i = P_{i,s} + k_{s+1}\,(u_{i,s+1}-u_{i,s}) \qquad (3.4)$$

where k_{s+1} is either k_{ts} or k_t depending upon whether or not the limiting value of interleaf friction was developed in the suspension system at time t_s. The quantities $u_{i,s}$ and $u_{i,s+1}$ denote the deformation in the tire-suspension spring assembly at times t_s and t_{s+1}, respectively.

If k_{s+1} in Eq. (3.4) is equal to k_t, the friction force, F_{s+1}, in the leaf springs of the suspension system at time t_{s+1} may be calculated as follows:

$$F_{s+1} = F_s + \Delta P_i \qquad (3.5)$$

However, if k_{s+1} is equal to k_{ts}, Eq. (3.5) does not yield a valid result. The following relationship must instead be true:

$$|F_{s+1}| = |F_s| = F' \qquad (3.6)$$

since the effective stiffness of the tire-suspension spring assembly will equal k_{ts} only as long as the absolute value of the friction force in the leaf springs remains equal to F'. Therefore, if k_{s+1} is assumed to be equal to k_{ts}, Eqs. (3.4) and (3.6) will yield valid results only if it is proved that the leaf springs remain unlocked between times t_s and t_{s+1}. In this study, the leaf springs are considered to remain

unlocked only if the absolute value of F_{s+1}, as given by Eq. (3.5), is greater than F'. If this condition is not satisfied, the leaf springs are considered to become inactive immediately after time t_s, and the stiffness of the spring assembly is assumed to equal k_t over the entire time interval. Since the original assumption that k_{s+1} is equal to k_{ts} has been proven to be false, $P_{i,s+1}$ must be recalculated using Eq. (3.4) with k_{s+1} equal to k_t. Also, F_{s+1} is re-evaluated using Eq. (3.5).

One last possibility must be considered. The effective stiffness of the tire-suspension spring assembly may change from k_t to k_{ts} between times t_s and t_{s+1}. The interacting force $P_{i,s+1}$ is first calculated by Eq. (3.4) with k_{s+1} equal to k_t since k_{s+1} is initially assumed to remain constant over the time interval. Next, Eq. (3.5) is used to calculate F_{s+1}. The effective stiffness of the spring assembly will remain equal to k_t only as long as the absolute value of F_{s+1} remains less than F'. If the absolute value of F_{s+1} as given by Eq. (3.5) exceeds F', the original assumption that the effective stiffness of the spring assembly remains constant is again proven to be false. The amount of deformation, u_e, which exists in the spring assembly when the leaf springs engage, is found as follows:

$$u_e = \frac{F_{s+1} \pm F'}{k_t} \tag{3.7}$$

where F_{s+1} is the frictional force as given by Eq. (3.5). If F_{s+1} is positive, then the negative sign is used in Eq. (3.7). The value of $P_{i,s+1}$ is now corrected as follows:

$$P_{i,s+1} = P_{i,s+1} + (k_{ts} - k_t)(u_{i,s+1} - u_e) \tag{3.8}$$

The friction force F_{s+1} is corrected simply by setting it equal to $\pm F'$ depending upon the sign of F_{s+1} as given by Eq. (3.5).

3.2.3 Deformation in Tire-Suspension System. The amount of deformation in the springs of the tire-suspension system at time t_{s+1} is:

$$\left\{u\right\}_{s+1} = \left\{z\right\}_{s+1} + \left\{d_p\right\} - \left\{w_p\right\}_{s+1} \tag{3.9}$$

A positive value term in the vector u_{s+1} indicates a shortening of the springs in the corresponding tire-suspension assembly. The vector z contains a displacement coordinate for each of the support points of the vehicle mass. The ordinates which describe the bridge deck profile are given in d_p, and the vector $w_{p,s+1}$ denotes the deflection of the deck under each of the vehicle tires as a result of the static and dynamic vehicle loading and the inertia forces of the bridge mass at time t_{s+1}.

The value of each term in the vector $w_{p,\,s+1}$ can be found from Eq. (2.59). The coordinates x and y specify the location of the tire reaction P_i relative to the origin of the panel on which the tire is located. Eq. (3.9) may also be written as follows:

$$\left\{u\right\}_{s+1} = \left\{z\right\}_{s+1} + \left\{d_p\right\} - [H]^T \left\{w\right\}_{s+1} \tag{3.10}$$

The matrix H^T relates the displacements of the bridge deck under each wheel load to the vector of nodal bridge displacements w_{s+1}. The non-zero elements of each row in the matrix H^T are taken from the row vector which results from the product of $(z_f)\,[C_f]^{-1}$ in Eq. (2.59). The matrix H was first introduced in Eq. (3.1). Eq. (3.10) is now

substituted into Eq. (3.4) as follows:

$$\{P_i\}_{s+1} = \{P_i\}_s + [k]_{s+1}\{z\}_{s+1} - [k]_{s+1}[H]^T\{w\}_{s+1} + [k]_{s+1}\{d_p\} - \{u\}_s \qquad (3.11)$$

The matrix k_{s+1} is a symmetric matrix since all non-zero terms are located on the diagonal. The term $k_{i,i}$ is the effective stiffness of the ith tire-suspension spring assembly at time t_{s+1}. If the vector P_i in Eq. (3.1) is now replaced by its equivalent as given by Eq. (3.11), the equations of motion for the bridge model at time t_{s+1} are modified as follows:

$$[M]\{\ddot{w}\}_{s+1} + [C]\{\dot{w}\}_{s+1} + [K]\{w\}_{s+1} + [H][k]_{s+1}[H]^T\{w\}_{s+1} - [H][k]_{s+1}\{z\}_{s+1}$$
$$= [H]\{P_i\}_s + [k]_{s+1}(\{d_p\} - \{u\}_s) \qquad (3.12)$$

It is also desirable to use Eq. (3.11) to modify the equations of motion for the vehicle model. However, Eq. (3.11) cannot be incorporated directly into Eq. (3.3) since the behavior of the vehicle has been expressed in terms of the disturbing forces P_d instead of the total interacting forces P_i. The vector P_d is defined in Appendix B as follows:

$$\{P_d\}_{s+1} = [k]_{s+1}\{z\}_{s+1} - \{P_w\}_{s+1} \qquad (3.13)$$

The matrix k_{s+1} is the same diagonal matrix that appears in Eq. (3.11). The vector P_d may also be defined in terms of P_i as

$$\{P_d\}_{s+1} = \{P_i\}_{s+1} - \{P_{st}\} \qquad (3.14)$$

Each term in the vector P_{st} represents the reaction in one of the vehicle tires when the vehicle is in a position of static equilibrium. Substitution of Eq. (3.11) into the above equation yields

$$\left\{P_d\right\}_{s+1} = \left\{P_i\right\}_s - \left\{P_{st}\right\} + [k]_{s+1} \left\{z\right\}_{s+1} - [k]_{s+1} [H]^T \left\{w\right\}_{s+1} + [k]_{s+1} \left(\left\{\begin{matrix} d \\ p \end{matrix}\right\} - \left\{u\right\}_s\right) \tag{3.15}$$

By comparing Eqs. (3.13) and (3.15), it becomes apparent that P_w is defined by the following equation:

$$\left\{P_w\right\}_{s+1} = \left\{P_{st}\right\} - \left\{P_i\right\}_s + [k]_{s+1} \left(\left\{u\right\}_s - \left\{\begin{matrix} d \\ p \end{matrix}\right\}\right) + [k]_{s+1} [H]^T \left\{w\right\}_{s+1} \tag{3.16}$$

Eq. (3.16) may now be substituted into Eq. (3.3) as follows:

$$-[h]\,[k]_{s+1}\,[H]^T \left\{w\right\}_{s+1} + [m] \left\{\ddot{z}\right\}_{s+1} + [c] \left\{\dot{z}\right\}_{s+1} + [k_v]_{s+1} \left\{z\right\}_{s+1} = [h] \left(\left\{P_{st}\right\} - \left\{P_i\right\}_s + [k]_{s+1} \left\{u\right\}_s - [k]_{s+1} \left\{\begin{matrix} d \\ p \end{matrix}\right\}\right) \tag{3.17}$$

3.2.4 Integration of the Equations of Motion. The equations of motion for the bridge-vehicle system are solved through the use of a numerical integration procedure which was developed by Newmark.[26] Based on some assumed variation of acceleration within the time interval Δt, the velocity and displacement at time t_{s+1} are expressed in terms of the unknown acceleration at time t_{s+1} and the known acceleration, velocity, and displacement at time t_s as follows:

$$\dot{q}_{s+1} = \dot{q}_s + \tfrac{1}{2} \Delta t\, \ddot{q}_s + \tfrac{1}{2} \Delta t\, \ddot{q}_{s+1} \tag{3.18a}$$

$$q_{s+1} = q_s + \Delta t\, \dot{q}_s + (\tfrac{1}{2} - \beta)(\Delta t)^2\, \ddot{q}_s + \beta (\Delta t)^2\, \ddot{q}_{s+1} \tag{3.18b}$$

where β is a dimensionless parameter which specifies the variation of the acceleration within the time interval. The vector q represents the displacement of the coordinates of the bridge or vehicle, and a dot superscript indicates one differentiation with respect to time. All vectors are related to time by either the subscript s or $s+1$. For most of the results presented in this study, β was given the value $1/6$ which corresponds to a linear variation of acceleration within the time interval.

Eq. (3.18b) may be rearranged to produce the following expression for the acceleration at time t_{s+1}:

$$\{\ddot{q}\}_{s+1} = \frac{1}{\beta(\Delta t)^2}\{q\}_{s+1} - \frac{1}{\beta(\Delta t)^2}\{q\}_s - \frac{1}{\beta\Delta t}\{\dot{q}\}_s - \left(\frac{1}{2\beta} - 1\right)\{\ddot{q}\}_s$$

$$= \frac{1}{\beta(\Delta t)^2}\{q\}_{s+1} - \{C_1\} \qquad (3.19)$$

In order to simplify the above equation, all known vectors have been combined into one vector called C_1. By substituting Eq. (3.19) into Eq. (3.18a), the velocity at time t_{s+1} is redefined as follows:

$$\{\dot{q}\}_{s+1} = \frac{1}{2\beta\Delta t}\{q\}_{s+1} - \frac{1}{2\beta\Delta t}\{q\}_s - \left(\frac{1}{2\beta} - 1\right)\{\dot{q}\}_s - \Delta t\left(\frac{1}{4\beta} - 1\right)\{\ddot{q}\}_s$$

$$= \frac{1}{2\beta\Delta t}\{q\}_{s+1} - \{C_2\} \qquad (3.20)$$

where $\{C_2\}$ is a vector which is used to represent all known vectors in the above equation.

If the vector $\{\dot{w}\}_{s+1}$ is replaced by its equivalent as given by Eq. (3.19) and if the vector $\{\ddot{w}\}_{s+1}$ is similarly replaced by Eq. (3.20), then the equation of motion for the bridge model, as given by Eq. (3.12), may be rewritten as follows:

$$\left[\frac{1}{\beta(\Delta t)^2}[M] + \frac{1}{2\beta\Delta t}[C] + [K] + [H]\,[k]_{s+1}[H]^T\right]\{w\}_{s+1} - [H]\,[k]_{s+1}\{z\}_{s+1}$$

$$= [H]\left(\{P_i\}_s + [k]_{s+1}(\{d_p\} - \{u\}_s)\right) + [M]\{C_1\} + [C]\{C_2\} \qquad (3.21)$$

The number of unknown vectors in the equations of motion for the bridge model has now been reduced to two, namely the vectors $\{w\}_{s+1}$ and $\{z\}_{s+1}$. Let the matrices D, E, and F be defined as follows:

$$[D] = \frac{1}{\beta(\Delta t)^2}[M] + \frac{1}{2\beta\Delta t}[C] + [K] + [H]\,[k]_{s+1}[H]^T \qquad (3.22a)$$

$$[E] = -[H]\,[k]_{s+1}$$

$$\{F\} = [H]\,\{P_i\}_s + [k]_{s+1}(\{d_p\} - \{u\}_s) + [M]\{C_1\} + [C]\{C_2\} \qquad (3.22c)$$

If Eqs. (3.22) are substituted into Eq. (3.21), the equations of motion for the bridge model may be written as follows:

$$[D]\,\{w\}_{s+1} + [E]\,\{z\}_{s+1} = \{F\} \qquad (3.23)$$

Eqs. (3.19) and (3.20) are also substituted for the vectors $\{\ddot{z}\}_{s+1}$ and $\{\dot{z}\}_{s+1}$, respectively, in Eq. (3.17) to modify the equations of motion for the vehicle model as follows:

$$- [h]\ [k]_{s+1}\ [H]^T \{w\}_{s+1} + \left[\frac{1}{\beta(\Delta t)^2} [m] + \frac{1}{2\beta\Delta t} [c] + [k]_{s+1} \right] \{z\}_{s+1}$$

$$= [h] \left(\{P_{st}\} - \{P_i\}_s + [k]_{s+1} (\{u\}_s - \{d_p\}) \right) + [m]\{C_1\} + [c]\{C_2\} \quad (3.24)$$

As was the case in Eq. (3.21), the only unknown terms in Eq. (3.24) are the vectors $\{w\}_{s+1}$ and $\{z\}_{s+1}$. The matrices G, J, and N are now defined as follows:

$$[G] = - [h]\ [k]_{s+1}\ [H]^T \quad (3.25a)$$

$$[J] = \frac{1}{\beta(\Delta t)^2} [m] + \frac{1}{2\beta\Delta t} [c] + [k]_{s+1} \quad (3.25b)$$

$$\{N\} = [h] \left(\{P_{st}\} - \{P_i\}_s + [k]_{s+1} (\{u\}_s - \{d_p\}) \right) + [m]\{C_1\} + [c]\{C_2\} \quad (3.25c)$$

Substitution of Eqs. (3.25) into Eq. (3.24) yields the following expression:

$$[G]\ \{w\}_{s+1} + [J]\ \{z\}_{s+1} = \{N\} \quad (3.26)$$

Eqs. (3.23) and (3.26) are now combined to form a set of simultaneous linear equations in which the number of unknowns is equal to the number of equations. These equations are written in matrix form as follows:

$$\left[\begin{array}{c|c} D & E \\ \hline G & J \end{array}\right] \left\{\begin{array}{c} w \\ \hline z \end{array}\right\}_{s+1} = \left\{\begin{array}{c} F \\ \hline N \end{array}\right\} \quad (3.27)$$

3.3 Reduced Stiffness Matrix Approach

3.3.1 General. The application of the finite element method to dynamics problems usually involves the solution of a large number of equations. While it is not unusual to solve two or three hundred equations for a problem involving static analysis, it is common practice to reduce the number of dynamic degrees of freedom when a numerical integration procedure is used to obtain a dynamic solution. This is accomplished by considering only those degrees of freedom that are related to vertical displacements of the bridge mass. Also, the rotational inertia forces and in-plane inertia forces are ignored. It is generally acknowledged that such a simplification can be made without substantially affecting the dynamic response of the structure. However, such an assumption is not applied relative to the forces which result from the stiffness of the bridge model. A reduced stiffness approach is adopted instead, since each component of the stiffness matrix is required to suitably define the configuration of the structural model.

3.3.2 Development of a Reduced Stiffness Matrix. As previously stated, static solutions for the given bridge model can be obtained through the solution of Eq. (2.48). The matrices in Eq. (2.48) may be reorganized into a number of submatrices as follows:

$$\begin{Bmatrix} p_1 \\ p_2 \\ p_3 \\ 0 \\ 0 \end{Bmatrix} = \begin{bmatrix} K_{11} & K_{12} & K_{13} & K_{14} & K_{15} \\ K_{21} & K_{22} & K_{23} & K_{24} & K_{25} \\ K_{31} & K_{32} & K_{33} & K_{34} & K_{35} \\ K_{41} & K_{42} & K_{43} & K_{44} & K_{45} \\ K_{51} & K_{52} & K_{53} & K_{54} & K_{55} \end{bmatrix} \begin{Bmatrix} w_1 \\ w_2 \\ w_3 \\ w_4 \\ w_5 \end{Bmatrix} \tag{3.28}$$

The vectors p and w have each been grouped into five subvectors. The subvectors p_1 and w_1 contain the vertical forces and displacements at each joint, respectively. In a similar manner, p_2 and w_2 contain moments and rotations about the y axis; p_3 and w_3 contain moments and rotations about the x axis; w_4 and w_5 contain in-plane displacements in the x and y directions, respectively. The subvectors p_4 and p_5 are replaced by zeros since it is assumed that the equivalent nodal force vector which results from a vehicle wheel load does not include in-plane forces in the x or y direction. The fifth row of Eq. (3.28) may be rearranged to form the equation

$$\begin{aligned} \{w_5\} &= -[K_{55}]^{-1}[K_{51}]\{w_1\} - [K_{55}]^{-1}[K_{52}]\{w_2\} \\ &\quad -[K_{55}]^{-1}[K_{53}]\{w_3\} - [K_{55}]^{-1}[K_{54}]\{w_4\} \\ &= -[K_{r11}]\{w_1\} - [K_{r12}]\{w_2\} - [K_{r13}]\{w_3\} - [K_{r14}]\{w_4\} \end{aligned} \tag{3.29}$$

The terms containing an 'r' subscript are introduced to simplify the above expression and to indicate that the matrices which they represent are to be retained for use in the back-substitution phase of the

solution procedure. The remaining four rows of Eq. (3.28) may also be written as four separate matrix equations. Through the substitution of Eq. (3.29), the vector w_5 is eliminated from each equation as follows:

$$\{p_1\} = \left[[K_{11}] - [K_{15}][K_{r11}]\right]\{w_1\} + \left[[K_{12}] - [K_{15}][K_{r12}]\right]\{w_2\} + \left[[K_{13}] - [K_{15}][K_{r13}]\right]\{w_3\} + \left[[K_{14}] - [K_{15}][K_{r12}]\right]\{w_4\} \quad (3.30a)$$

$$\{p_2\} = \left[[K_{21}] - [K_{25}][K_{r11}]\right]\{w_1\} + \left[[K_{22}] - [K_{25}][K_{r12}]\right]\{w_2\} + \left[[K_{23}] - [K_{25}][K_{r13}]\right]\{w_3\} + \left[[K_{24}] - [K_{25}][K_{r14}]\right]\{w_4\} \quad (3.30b)$$

$$\{p_3\} = \left[[K_{31}] - [K_{35}][K_{r11}]\right]\{w_1\} + \left[[K_{32}] - [K_{35}][K_{r12}]\right]\{w_2\} + \left[[K_{33}] - [K_{35}][K_{r13}]\right]\{w_3\} + \left[[K_{34}] - [K_{35}][K_{r14}]\right]\{w_4\} \quad (3.30c)$$

$$\{0\} = \left[[K_{41}] - [K_{45}][K_{r11}]\right]\{w_1\} + \left[[K_{42}] - [K_{45}][K_{r12}]\right]\{w_2\} + \left[[K_{43}] - [K_{45}][K_{r13}]\right]\{w_3\} + \left[[K_{44}] - [K_{45}][K_{r14}]\right]\{w_4\} \quad (3.30d)$$

If prime terms are introduced, Eqs. (3.30) may be written in matrix form as

$$\begin{Bmatrix} p_1 \\ p_2 \\ p_3 \\ 0 \end{Bmatrix} = \begin{bmatrix} K'_{11} & K'_{12} & K'_{13} & K'_{14} \\ K'_{21} & K'_{22} & K'_{23} & K'_{24} \\ K'_{31} & K'_{32} & K'_{33} & K'_{34} \\ K'_{41} & K'_{42} & K'_{43} & K'_{44} \end{bmatrix} \begin{Bmatrix} w_1 \\ w_2 \\ w_3 \\ w_4 \end{Bmatrix} \quad (3.31)$$

An expression for w_4 is obtained by rearranging the fourth row of Eq. (3.31) into the form

$$\{w_4\} = -[K'_{44}]^{-1}[K'_{41}]\{w_1\} - [K'_{44}]^{-1}[K'_{42}]\{w_2\} - [K'_{44}]^{-1}[K'_{43}]\{w_3\}$$

$$= -[K_{r8}]\{w_1\} - [K_{r9}]\{w_2\} - [K_{r10}]\{w_3\} \qquad (3.32)$$

As in Eq. (3.29), K_r terms are introduced primarily in order to simplify the above expression. Through the substitution of Eq. (3.32), the subvector w_4 is eliminated from the first three rows of Eq. (3.31). These three rows, as modified by Eq. (3.32), may be written as three separate equations in the form

$$\{p_1\} = \left[[K'_{11}] - [K'_{14}][K_{r8}]\right]\{w_1\} + \left[[K'_{12}] - [K'_{14}][K_{r9}]\right]\{w_2\}$$

$$+ \left[[K'_{13}] - [K'_{14}][K_{r10}]\right]\{w_3\} \qquad (3.33a)$$

$$\{p_2\} = \left[[K'_{21}] - [K'_{24}][K_{r8}]\right]\{w_1\} + \left[[K'_{22}] - [K'_{24}][K_{r9}]\right]\{w_2\}$$

$$+ \left[[K'_{23}] - [K'_{24}][K_{r10}]\right]\{w_3\} \qquad (3.33b)$$

$$\{p_3\} = \left[[K'_{31}] - [K'_{34}][K_{r8}]\right]\{w_1\} + \left[[K'_{32}] - [K'_{34}][K_{r9}]\right]\{w_2\}$$

$$+ \left[[K'_{33}] - [K'_{34}][K_{r10}]\right]\{w_3\} \qquad (3.33c)$$

Double prime terms are now introduced to simplify the expression of Eqs. (3.33) in matrix form as follows:

$$\begin{Bmatrix} p_1 \\ p_2 \\ p_3 \end{Bmatrix} = \begin{bmatrix} K'''_{11} & K'''_{12} & K'''_{13} \\ K'''_{21} & K'''_{22} & K'''_{23} \\ K'''_{31} & K'''_{32} & K'''_{33} \end{bmatrix} \begin{Bmatrix} w_1 \\ w_2 \\ w_3 \end{Bmatrix} \tag{3.34}$$

Continuing the above procedure, the third row of Eq. (3.34) is rearranged to obtain the following expression for w_3:

$$\begin{aligned} \{w_3\} &= \left[K'''_{33}\right]^{-1}\{p_3\} - \left[K'''_{33}\right]^{-1}\left[K'''_{31}\right]\{w_1\} - \left[K'''_{33}\right]^{-1}\left[K'''_{32}\right]\{w_2\} \\ &= \left[K'''_{33}\right]^{-1}\{p_3\} - \left[K_{r6}\right]\{w_1\} - \left[K_{r7}\right]\{w_2\} \end{aligned} \tag{3.35}$$

Substitution of Eq. (3.35) for w_3 in the first two rows of Eq. (3.34) yields the equation

$$\left\{\begin{array}{c} p_1 - K'''_{13}K'''^{-1}_{33}\,p_3 \\ \hline p_2 - K'''_{23}\,K'''^{-1}_{33}\,p_3 \end{array}\right\} = \left[\begin{array}{cc|cc} K'''_{11} & -K'''_{13}\,K_{r6} & K'''_{12} & -K'''_{13}\,K_{r7} \\ \hline K'''_{21} & -K'''_{23}\,K_{r6} & K'''_{22} & -K'''_{23}\,K_{r7} \end{array}\right] \left\{\begin{array}{c} w_1 \\ \hline w_2 \end{array}\right\} \tag{3.36}$$

And with the introduction of triple prime terms, Eq. (3.36) is written

$$\begin{Bmatrix} p_1 - K'''_{13}\,K'''^{-1}_{33}\,p_3 \\ p_2 - K'''_{23}\,K'''^{-1}_{33}\,p_3 \end{Bmatrix} = \begin{bmatrix} K''''_{11} & K''''_{12} \\ K''''_{21} & K''''_{22} \end{bmatrix} \begin{Bmatrix} w_1 \\ w_2 \end{Bmatrix} \tag{3.37}$$

Next, the second row of Eq. (3.37) is premultiplied by the inverse of K''''_{22} in order to obtain an expression for w_2 in the form

$$\{w_2\} = \left[K'''_{22}\right]^{-1}\{p_2\} - \left[K'''_{22}\right]^{-1}\left[K'''_{23}\right]\left[K'''_{33}\right]^{-1}\{p_3\} - \left[K'''_{22}\right]^{-1}\left[K'''_{21}\right]\{w_1\}$$

$$= \left[K'''_{22}\right]^{-1}\{p_2\} - \left[K_{r4}\right]\{p_3\} - \left[K_{r5}\right]\{w_1\} \qquad (3.38)$$

Eq. (3.38) is now substituted for w_2, and the first row of Eq. (3.34) becomes

$$\{p_1\} - \left[K'''_{12}\right]\left[K'''_{22}\right]^{-1}\{p_2\} - \left[\left[K'''_{13}\right]\left[K'''_{33}\right]^{-1} - \left[K'''_{12}\right]\left[K_{r4}\right]\right]\{p_3\}$$

$$= \left[\left[K'''_{11}\right] - \left[K'''_{12}\right]\left[K_{r5}\right]\right]\{w_1\} \qquad (3.39)$$

Finally, additional 'r' subscripted terms are introduced to simplify Eq. (3.39) as follows:

$$\{p_1\} - \left[K_{r2}\right]\{p_2\} - \left[K_{r3}\right]\{p_3\} = \left[K_r\right]\{w_1\} \qquad (3.40)$$

where K_r is the reduced stiffness matrix which relates the unknown vertical bridge displacements w_1 to the vertical nodal forces p_1, the nodal moments about the y axis p_2, and the nodal moments about the x axis p_3, all of which are known quantities. Once w_1 has been calculated from Eq. (3.40), the remainder of the unknown bridge displacements, namely the two rotational displacement vectors, w_2 and w_3, and the two in-plane displacement vectors, w_4 and w_5, may be calculated by employing Eqs. (3.38), (3.35), (3.32), and (3.29), respectively.

Eq. (3.21) can now be modified to incorporate the concept of the reduced stiffness matrix as follows:

$$\left[\frac{1}{\beta(\Delta t)^2}[M_r]+\frac{1}{2\beta\Delta t}[C_r]+[K_r]+[H_r][k]_{s+1}[H_r]^T\right]\{w_1\}_{s+1}-[H_r][k]_{s+1}\{z\}_{s+1}$$

$$=[H_r]\left(\{P_i\}_s+[k]_{s+1}(\{d_p\}-\{u\}_s)\right)+[M_r]\{C_1\}+[C_r]\{C_2\} \quad (3.41)$$

In the equation above, several matrices have been reduced in order to employ the reduced stiffness matrix, K_r. The matrix M has been modified to include only that part of the mass which experiences vertical accelerations. The remaining elements of the original equivalent mass matrix, which experience rotational accelerations or accelerations in the plane of the bridge deck, have been eliminated since it has been assumed that the effects of the inertia forces that these elements contribute are small compared to the effects of mass elements that have been retained. In a similar manner, only those elements in the damping matrix, C, that are functions of the velocities of the bridge joints in the vertical direction are retained in the matrix C_r. The vectors C_1 and C_2 are reduced to include only those terms that are directly related to w_1.

In order to evaluate the matrix H_r in Eq. (3.41), it is necessary to reorganize the matrix H, which was first introduced in Eq. (3.1), into the three submatrices H_{r1}, H_{r2}, and H_{r3}. The matrix H_{r1} contains those elements of H that determine the vector of vertical joint forces, p_1, which results from the interacting forces $P_{i,s+1}$. The matrix H_{r2} determines the vector of joint moments about the y axis, p_2, which result from $P_{i,s+1}$, and H_{r3} is the matrix that determines the vector of joint moments about the x axis, p_3, from $P_{i,s+1}$. The matrix H_r, as used in Eq. (3.41), can then be calculated from the equation

$$[H_r] = [H_{r1}] - [K_{r2}]\ [H_{r2}] - [K_{r3}]\ [H_{r3}] \qquad (3.42)$$

The matrices K_{r2} and K_{r3} were introduced in Eq. (3.40). The remaining terms in Eq. (3.41) are taken directly from Eq. (3.21) with no modification.

If 'r' subscripts are also used to indicate the effects of the modifications described in the paragraph above on the matrices D, E, and F defined by Eqs. (3.22), then Eq. (3.41) can be rewritten as follows:

$$[D_r]\ \{w_1\}_{s+1} + [E_r]\ \{z\}_{s+1} = \{F_r\} \qquad (3.43)$$

In order to make the equations of motion for the vehicle model compatible with the above reduced equations of motion for the bridge model, the matrix H^T is replaced with H_r^T and the vector w_{s+1} is reduced to $w_{1,s+1}$ in Eq. (3.24). The equations of motion for the vehicle model are then written as follows:

$$-[h]\ [k]_{s+1}\ [H_r]^T \{w_1\}_{s+1} + \left[\frac{1}{\beta(\Delta t)^2}[m] + \frac{1}{2\beta\Delta t}[c] + [k]_{s+1}\right]\{z\}_{s+1}$$

$$= [h]\left(\{P_{st}\} - \{P_i\}_s + [k]_{s+1}\left(\{u\}_s - \{d_p\}\right)\right) + [m]\{C_1\} + [c]\{C_2\} \qquad (3.44)$$

All terms in the above equation other than H_r^T and $w_{1,s+1}$ are taken directly from Eq. (3.24). Eq. (3.26) may now be rewritten in the form

$$[G_r]\ \{w_1\}_{s+1} + [J]\ \{z\}_{s+1} = \{N\} \qquad (3.45)$$

Only the matrix G is given an r subscript since the matrix J and the vector N remain as defined by Eqs. (3.25). Finally, Eq. (3.27), when

modified for the reduced stiffness approach, may be written as follows:

$$\left[\begin{array}{c|c} D_r & E_r \\ \hline G_r & J \end{array}\right] \left\{\begin{array}{c} w_1 \\ \hline z \end{array}\right\}_{s+1} = \left\{\begin{array}{c} F_r \\ \hline N \end{array}\right\} \tag{3.46}$$

The total number of times that the equations of motion must be solved is normally dictated by specific criteria which in most cases guarantee that the numerical integration procedure will yield results which are stable, convergent, and accurate. The number of integration steps that is required to satisfy these criteria is in most cases more than three times the number of steps that is needed to adequately describe the behavior of the bridge-vehicle system. For this reason, only Eqs. (3.46), (3.20), and (3.19) must be solved after each time interval since they determine the vectors $w_{1,s+1}$, $\dot{w}_{1,s+1}$, and $\ddot{w}_{1,s+1}$, respectively. The remaining bridge displacements are assumed to have negligible inertia forces associated with them. Therefore, these displacements, which are represented by the vectors w_2, w_3, w_4, and w_5, are evaluated perhaps after every third to sixth time interval depending upon how often a full print-out of the configuration of the bridge-vehicle system is required. In order to implement this simplification, any information concerning the velocities and accelerations that are associated with the displacement vectors w_2 through w_5 has been sacrificed. The above mentioned criteria, which insure stability and convergence, are discussed in more detail in Art. 3.3.3.

3.3.3 Maximum Time Interval of Integration. As demonstrated below, the reduced stiffness approach has one other major advantage. When employing a numerical integration procedure such as the one used

in this study, it is necessary to determine approximately the amount of time that may elapse between the points in time when the equations of motion must be satisfied.

As previously stated, an assumption has to be made as to the variation of acceleration within the time interval Δt if Eqs. (3.19) and (3.20) are to be used to determine the accelerations and velocities at time t_{s+1}. For example, a value of β equal to 1/6 corresponds to a linear variation of acceleration within the time interval.

The total number of integration steps N_{cr} may be defined by the equation

$$N_{cr} = \frac{L_b + L_t}{v \, \Delta t} \tag{3.47}$$

where L_b is the total length of the bridge, L_t is the total length of the vehicle, and v is the velocity of the vehicle. The relationship between N_{cr} and Δt is clearly defined by Eq. (3.47).

Based on stability and convergence criteria developed by Newmark [26], the following equation was devised to establish a minimum value for N_{cr}:

$$N_{cr} \geq 3 \pi \sqrt{\beta} \; f_h (L_b + L_t)/v \qquad (\beta \geq 1/8) \tag{3.48}$$

where f_h is the highest natural frequency of the unloaded bridge. The frequency of each mode of vibration is easily obtained from an Eigenvalue solution. Note that Eq. (3.48) is valid only for values of β that are equal to or greater than 1/8.

Once a suitable value of N_{cr} has been determined, Eq. (3.47) is rearranged to provide the following expression for Δt:

$$\Delta t = \frac{L_b + L_t}{v\, N_{cr}} \tag{3.49}$$

Eq. (3.49), when used in conjunction with Eq. (3.48), will yield values of Δt which are approximately 67 percent of the values established by Newmark[26]. The shorter time interval is used in order to provide greater accuracy.

As indicated by Eq. (3.48), the frequency of the highest mode of vibration, f_h, directly affects the time and cost of solving a given problem. Elimination of all in-plane and rotational modes of vibration through the reduced stiffness approach makes it permissible to choose a value of f_h equal to the frequency of the highest vertical mode of vibration. As a result, f_h will be much lower than it would have been if all modes of vibration that correspond to the five-degree-of-freedom system were considered.

3.4 Initial Conditions

In order to start the integration procedure, it is necessary to describe the initial configuration of the bridge-vehicle system. The bridge structure is assumed to be in a state of static equilibrium. Therefore, both the acceleration and velocity of each node in the bridge model are set equal to zero. The situation where the bridge is in a state of free vibration due to the prior passage of a vehicle is not considered.

On the other hand, it is not reasonable to assume that moving vehicles are in a state of static equilibrium as they enter onto a bridge deck. Some amount of vehicle oscillation will always be present as a

result of approach pavement roughness and differential settlement at the pavement-bridge interface.

Four equations are required to calculate the initial values of force, displacement, velocity, and acceleration for each tire-suspension assembly in the vehicle. For convenience in defining the vehicle initial conditions prior to the time of entrance onto the bridge, the interacting force variations are assumed to be sinusoidal. Thus the initial conditions can be expressed in terms of phase angles and dynamic amplitudes. An alternative, not explored in this study, involves the computation of the response of the vehicle to the effect of a known or specified roughness on the approach pavement to determine values of initial conditions for direct input to the bridge-vehicle solution. The magnitude of interacting force is given by the equation

$$P_o = P_{st} + \Delta P \cos (\omega_o t - \varphi) \tag{3.50}$$

where ΔP is the amplitude of a sinusoidal function which describes the assumed variation in interacting force, ω_o is the circular natural frequency of the tire-suspension system at time t_o, and φ is an arbitrary phase angle. The initial deformation in the tire-suspension system is

$$u_o = \Delta P \cos (\omega_o t - \varphi)/k_o \tag{3.51}$$

where k_o is the stiffness of the tire-suspension system at time t_o. The quantities ω_o and k_o are determined by examining the initial value of friction in the leaf springs of the suspension system, F_o. If $|F_o| \geq F'$, then the leaf springs are assumed to be unlocked and $\omega_o = 2 \pi f_{ts}$ and $k_o = k_{ts}$. On the other hand, if the leaf springs

are locked then $\omega_o = 2\pi f_t$ and $k_o = k_t$.

The initial velocity of the tire-suspension system is given by:

$$\dot{u}_o = -\omega_o \Delta P \sin(\omega_o t - \phi)/k_o \tag{3.52}$$

Finally, the acceleration is as follows:

$$\ddot{u}_o = -\omega_o^2 \Delta P \cos(\omega_o t - \phi)/k_o$$

$$= -g\,\Delta P \cos(\omega_o t - \phi)/P_{st} \tag{3.53}$$

4. COMPUTER PROGRAMS

4.1 GENERAL

The procedures developed in this study were programmed in accordance with the capabilities of the University of Illinois' IBM 360-75 computer system. The programs that were written can be grouped relative to their three basic functions. Because it was found to be convenient, economical, and less complicated, the practice of separating the solution into three distinct programs was maintained throughout the entire study. The first program generates the mass and stiffness matrices, reduces the stiffness matrix, and finds the corresponding Eigenvalues and Eigenvectors for a given problem. The function of the second program is to determine the dynamic response of the combined bridge-vehicle system. The third program allows the option of performing either a constant force solution or a crawl curve analysis. A constant force solution is one in which damping, springing, and inertial properties of the vehicle are ignored. The vehicle tire loads then may be treated as forces of constant magnitude equal to the static wheel reactions when the vehicle is at rest. A crawl curve analysis receives its name from the assumption that the vehicle speed is reduced to the point when damping and inertial forces in both the vehicle and the bridge vanish. In other words, the solution procedure is reduced to that of generating static influence lines for deflections, moments, and strains.

The programs have been designed to solve structures having up to three spans, five longitudinal girders, and 65 joints. Two-span bridges must be symmetrical about the center pier and three-span bridges

must have equal side spans. Also, it is assumed that the bridge deck behaves as an isotropic plate. Skewed bridges may not be analyzed since all transformation matrices have been omitted from the solution procedure. The vehicle model may have one, two, or three axles. These limitations were implemented because they simplified computer programming and reduced execution time on the computer without violating the requirements of the problems presented in Chapter 5; they are arbitrary restrictions which can be made less severe to permit the solution of more complex problems.

The computer programs are briefly discussed below. Input and output data are described. Also, the computational process for each program is presented.

4.2 Determination of Stiffness and Mass Matrices

4.2.1 Input Data. The following geometrical and physical properties of the bridge structure constitute the input data for Program 1:

1. The number of spans.
2. The length of each span in feet.
3. The total width of the bridge deck in feet.
4. The total number of panels in the transverse direction; this number is usually one less than the number of girders.
5. The number of panels in the transverse direction between two adjacent girders - usually the girders will be spaced one panel width apart.

6. The number of panels in the longitudinal direction in each span.
7. The number of girder property data cards - one data card is required for each set of girder properties.
8. The properties of each set of girders which include the area A, the torsional stiffness J, the moment of inertia about the centroid of the section I, the total depth of the girder section in inches, and the weight per unit length of the section in kips per foot; the set of girders which has these properties is located by specifying the starting and ending longitudinal joint lines, the number of joint lines between consecutive girders in the transverse direction, and the transverse joint lines on which each string of girders start and end.
9. The properties for each curb-handrail assembly which include A, J, I, the effective depth in inches, and the weight per unit length in kips per foot; the left and right curb-handrail assemblies are individually described; and both are assumed to extend the entire length of the structure.
10. The properties of those transverse stiffeners which are located at the support points of the bridge deck; these properties include A, I, and the effective depth in inches; a code is used to indicate whether

or not such stiffeners are to be included in the analysis.

11. The properties of intermediate transverse stiffeners which include A, I, and the effective depth in inches, and the transverse joint lines on which such stiffeners are located; the effective depth of each type of member described under items 8, 9, 10, and 11 is needed to include the effects of the eccentricity of each member relative to the mid-plane of the bridge deck; the properties A, J, and I are given in inch units.
12. The thickness of the bridge deck.
13. The strength of the bridge deck in kips per square inch; this is an optional means of computing the modulus of elasticity which is to be used only if the deck material is concrete.
14. Poisson's ratio for the deck material.
15. The composite action factor which may vary between 0 and 100 percent.
16. The unit weight of the deck material in kips per square foot.
17. The modulus of elasticity of the girders and stiffeners in KSI.
18. Poisson's ratio for the girder material to be used to calculate the shear modulus G.
19. The modulus of elasticity of the deck material, optional.

20. The modular ratio between the deck and girder materials, optional; items 13, 19, and 20 are inter-related; only one of these items should be used for each problem.

4.2.2 Output Data. The following data are generated by Program 1:

1. The stiffness submatrices K_r, K_{r2}, K_{r3}, K_{r4}, K_{r5}, K_{r6}, K_{r7}, K_{r8}, K_{r9}, K_{r10}, K_{r11}, K_{r12}, K_{r13}, K_{r14}, K'^{-1}_{22}, and K'^{-1}_{33}; these matrices are defined in Eqs. (3.29), (3.32), (3.34), (3.35), (3.37), (3.38), and (3.40).
2. The mass matrix M_r.
3. The total weight of the bridge.
4. The Eigenvalues and Eigenvectors which correspond to M_r and K_r.

Items 3 and 4 are output directly as printed data. Items 1 and 2 along with the input data described in Art. 4.2.1 are placed in a permanent data set on disk storage to be used by Programs 2 and 3. A general flow diagram for Program 1 is shown in Fig. 19.

4.3 Dynamic Response of a Combined Bridge-Vehicle System

4.3.1 Input Data. The following items constitute the input data for Program 2:

1. The static reactions in the first, third, and fifth vehicle tires which result from the sprung vehicle loads only, P_{st1}, P_{st3}, and P_{st5}, respectively; the tire reactions P_{st2}, P_{st4}, and P_{st6} are assumed to be equal to P_{st1}, P_{st3}, and P_{st5}, respectively.

2. The initial x coordinates for axles 1, 2, and 3 relative to the first abutment, in inches; the x coordinate for each axle that is located off the bridge to the left of the first abutment will have a negative value; and the x coordinate of the first axle will normally be zero since the first axle is usually placed directly over the abutment at the start of a solution.
3. The y coordinates of tires 1 and 2 relative to joint line 1, in inches; the y coordinate for tires 3 and 5 is assumed to equal the y coordinate of tire 1; and the y coordinate for tires 4 and 6 is assumed to equal the y coordinate of tire 2. The y coordinate of tire 2 will always be greater than the y coordinate of tire 1, and it is arbitrarily assumed that the y coordinate of each tire remains constant throughout the entire solution.
4. The velocity of the vehicle in miles per hour; this velocity is later printed out in the units of inches per second.
5. The total number of integration steps required for the vehicle to cross the bridge.
6. The total number of steps to be carried out in the solution; item 6 may be set less than, equal to, or greater than item 5.
7. The number of steps that are to transpire between the times at which the configuration of the bridge-vehicle system is to be printed and plotted.

8. The ratio of the initial tire reactions to their corresponding static values.
9. The phase angle, in degrees; used in Eqs. (3.50) through (3.53) to describe the initial oscillation of each tire-suspension assembly.
10. The ratio of the friction force in the leaf springs of the vehicle to the static reactions in their corresponding tires.
11. The title to be used to identify graphic and printed results.
12. The total number of axles on the vehicle.
13. The total number of bridge-roughness coefficients per wheel path to be input from data cards; the maximum number of coefficients that may be input was arbitrarily set at 500 per wheel path.
14. The total number of half sine waves of bridge roughness per span; this information is required only if bridge roughness is to be idealized as a series of sine waves.
15. The ratio of the maximum amplitude of the bridge-roughness sine-wave function to the average dead-load deflection of the bridge deck at midspan; this input item was developed in order to facilitate the use of a half sine wave to represent dead-load deflection in a single-span bridge problem.

16. The maximum amplitude of the bridge-roughness sine-wave function, in inches; this input item is ignored if item 15 is input as a nonzero quantity.
17. The weight of each sprung vehicle mass excluding the weight of all tire-suspension assemblies.
18. The sprung weight of each tire-suspension assembly; the sum of items 17 and 18 should equal the sum of all static tire reactions as given in item 1.
19. The unsprung weight of each tire-suspension assembly.
20. The ratio of the limiting value of friction in each leaf spring to the static reaction in the corresponding tire.
21. The dynamic indices as defined by Eqs. (2.63) for the vehicle masses described in item 17.
22. The damping ratio for viscous damping in the tire-suspension systems of the vehicle; this is the ratio in percent of actual damping to critical damping.
23. The frequency of each tire-suspension system when the tire spring alone is active, $f_{t,i}$.
24. The frequency of each tire-suspension system when the suspension spring and the tire spring both act in series, $f_{ts,i}$.
25. Five scaling parameters for plotted results.
26. The speed parameter, α; if α is input as a nonzero value, the velocity of the vehicle given in item 4 will be re-evaluated using the equation $v = 2\alpha\ell f_b$ where

ℓ is the total length of a single-span bridge, one half of the total length of a two-span bridge with equal spans, or the length of the center span of a three-span bridge; the term f_b denotes the fundamental frequency of the bridge.

27. The value of β that is to be used in the numerical integration procedure.
28. The fundamental frequency of the bridge model, f_b, as determined by an Eigenvalue solution.
29. The frequency of the highest mode of vibration of the bridge model, f_h, as determined by an Eigenvalue solution.
30. The damping ratio in percent for viscous damping in the bridge model; the ratio of actual damping to the value of critical damping that corresponds to the fundamental mode of vibration.

All other information required to perform the solution has been generated and stored by Program 1. Therefore, this information may be input from permanent disk storage as often as necessary. This arrangement becomes extremely useful whenever several problems involve a particular bridge model with a constant set of mass and stiffness properties.

4.3.2 Description of Solution Procedure. The solution procedure consists of the following basic operations:

1. Read in problem parameters.
2. Read in bridge properties from data set created by

Program 1.

3. Initialize counters, define initial conditions for bridge and vehicle, and determine time interval Δt.
4. Print echo check of input data.
5. Calculate stiffness properties of vehicle tire-suspension assemblies.
6. Form the mass matrix for the vehicle model.
7. Begin the numerical integration procedure at time t_{s+1}.
8. Locate vehicle at time t_{s+1}.
9. Set joint load vector equal to zero.
10. Determine roughness ordinate under each vehicle tire.
11. Determine deformations in suspension systems and changes in tire reactions resulting from bridge roughness.
12. For each tire that is situated on the bridge deck, determine the plate element on which it is located and its position relative to the local coordinate system of the plate element.
13. Find the fixed-end moment and shear coefficients that relate tire reaction to joint moments and forces, and define the load vector which results from the quantity $P_{i,s}-k_{s+1}u_s$.
14. Set up and solve Eq. (3.46).
15. Determine the accelerations and velocities of the bridge and vehicle models at time t_{s+1} using Eqs. (3.19) and (3.20).

16. Determine the amount of deformation in each tire-suspension assembly at time t_{s+1}.
17. Determine the magnitude of friction in the leaf springs of the vehicle; and if one or more leaf springs become activated or deactivated, change the stiffness of the corresponding tire-suspension system or systems.
18. Find the total reaction in the vehicle tires at time t_{s+1}.
19. Find the joint loads and moments that result from the total tire reactions.
20. If data from this integration step is not to be printed or plotted, skip to Step 23.
21. Solve Eqs. (3.38), (3.35), (3.32), and (3.29).
22. Calculate all deflections, moments, shears, and reactions that are to be printed or plotted.
23. Evaluate the vectors C_1 and C_2 which are to be used in the next integration step in Eq. (3.41); these vectors were first introduced in Eqs. (3.19) and (3.20), respectively, in which the vector q is used to represent the bridge displacement vector w_1.
24. Evaluate the vectors C_{v1} and C_{v2} which are to be used in the next integration step to solve Eq. (3.44); these vectors are also defined using Eqs. (3.19) and (3.20), respectively, but the vector q in this case

represents the vehicle displacement vector z.

25. If data from this integration step is not to be printed or plotted, go to Step 27.
26. Print and store on disk the required output data obtained during this integration step.
27. Increment the time variable using the equation $t_{s+1} = t_{s+1} + \Delta t$.
28. If another integration step is to be performed, return to Step 8, otherwise proceed to Step 29.
29. Plot output data if required.
30. If another problem is to be solved, return to Step 1, otherwise stop.

Deflections, accelerations, moments, and shears at all pertinent locations in the bridge structure are printed and plotted. Strains in the bottom flange of the bridge girders and interacting forces between the bridge deck and vehicle tires are also obtained.

4.4 Constant Force and Crawl Curve Analysis Program.

4.4.1 General. Program 3 has a dual purpose in that it can be used to perform either a constant force solution or a crawl curve analysis and differs from Program 2 mainly because the vehicle model is no longer a required part of the solution procedure. In both the constant force solution and the crawl curve analysis, the reaction in each tire of the vehicle is assumed to equal the reaction that occurs when the vehicle is in a position of static equilibrium. This assumption makes it possible to represent the vehicle as a set of constant forces moving along the

bridge at some known velocity. Since all inertial effects in the vehicle are ignored, the equations of motion for the vehicle are no longer required. Also, the equations of motion for the bridge model are simplified since the interacting forces are determinate. The equations of motion for the bridge model in Program 3 are obtained by simplifying Eq. (3.41) as follows:

$$\left(\frac{1}{\beta(\Delta t)^2}[M_r] + \frac{1}{2\beta\Delta t}[C_r]+[K_r]\right)\{w_1\}_{s+1} = [H_r]\{P_i\} + [M_r]\{C_1\} + [C_r]\{C_2\} \quad (4.1)$$

in which P_i is the vector of interacting force which remain constant throughout the solution. All other bridge equations used in the solution procedure remain as given in Eqs. (3.19), (3.20), (3.29), (3.32), (3.35), and (3.38).

A crawl curve analysis is obtained simply by further eliminating all inertia and damping effects in the bridge from the equations of motion. Thus, Eq. (4.1) is reduced to the form

$$[K_r]\ \{w_1\}_{s+1} = [H_r]\ \{P_i\} \quad (4.2)$$

which is the static equilibrium equation for the bridge model. Eqs. (3.29), (3.32), (3.35), and (3.38) remain unchanged since they contain no inertia or damping effects in their original form, whereas Eqs. (3.19) and (3.20) are no longer required since accelerations and velocities are assumed to vanish in the crawl curve analysis.

4.4.2 Input Data and Solution Procedure. As a result of the differences described above, the input data for Program 3 is limited to items 1 through 7, 11, 12, 25, 27, 28, and 30 as listed in Art. 4.3.1. Also, a code is entered to indicate whether a constant force or crawl

curve analysis is to be performed.

The solution procedure consists of the following basic operations:

1. Read in problem parameters.
2. Read in bridge properties from data set created by Program 1.
3. Initialize counters, define initial conditions for bridge model, and determine time interval Δt.
4. Print each check of input data.
5. Set inertia and damping coefficients in Eq. (4.1) to zero if a crawl curve analysis is to be performed.
6. Begin numerical integration procedure at time $t_{s+1} = \Delta t$.
7. Locate vehicle loads at time t_{s+1}.
8. Set joint load vector equal to zero.
9. For each tire force that is situated on the bridge deck, determine the plate element on which it is located and its position relative to the local coordinate system of the plate element.
10. Find the fixed-end joint moments and shears that result from each tire load.
11. Set up and solve Eq. (4.1).
12. If a constant force solution is being performed, determine the accelerations and velocities of the joints in the bridge model using Eqs. (3.19) and (3.20), respectively.

13. If data from this integration step is not to be printed or plotted, skip to Step 16.
14. Solve Eqs. (3.38), (3.35), (3.32), and (3.29).
15. Calculate all deflections, moments, shears, and reactions that are to be printed or plotted.
16. If a constant force solution is being performed, evaluate the vectors C_1 and C_2 which are to be used in the next integration step to solve Eq. (4.1); these vectors were first introduced in Eqs. (3.19) and (3.20), respectively.
17. If data from this integration step is not to be printed or plotted, go to Step 19.
18. Print and store on disk the required output data obtained during this integration step.
19. Increment the time variable using the equation $t_{s+1} = t_{s+1} + \Delta t$.
20. If another integration step is to be performed, return to Step 7, otherwise proceed to Step 21.
21. Plot output data if required.
22. If another problem is to be solved, return to Step 1, otherwise stop.

The printing and plotting capabilities of Program 3 are identical to those of Program 2. However, interacting forces are not printed or plotted as output data since they are constant throughout the entire solution.

5. DISCUSSION AND EVALUATION OF NUMERICAL RESULTS

5.1 General

To evaluate the performance of the theory developed in this study, a number of solutions were generated for comparison with results from available theoretical, laboratory, and field studies. The structures considered include single-beam and multi-beam bridges of one, two, and three spans. A number of comparisons are presented and discussed below to demonstrate the versatility, usefullness, and accuracy of the finite element bridge analysis when applied to both static and dynamic problems.

It should be noted that the solutions for the single-beam idealization of the bridge were obtained using theory and computer programs developed in the course of an investigation entitled Impact in Highway Bridges conducted at the University of Illinois at Urbana-Champaign as part of the Illinois Cooperative Highway Research program. These solutions have been verified by comparisons with both laboratory studies and field measurements. In particular, the results obtained using the Huang theory[6,7] were verified by extensive comparisons with the results of the AASHO Road Test bridge studies.[27] These latter tests also were used to validate the assumption and importance of frictional damping in the vehicle suspension.

The work done by Oran[9] on the behavior of a multigirder simple-span bridge was verified by means of comparisons with a laboratory model study also conducted at the University of Illinois. However, further validations of the Oran theory by means of comparisons with the results of field tests could not be made at the time because computer capabilities

had not advanced to the point where frictional damping and the three-dimensional nature of the vehicle could be handled. The results presented herein include a first attempt to test a three-dimensional bridge-vehicle dynamic response theory by means of comparisons with the results of field studies. The comparisons are presented to validate in a equalitative way the theory which has been developed; to limit the study to a reasonable scope, no attempt was made to include extensive parametric variations to optimize the comparison of theory with field results. The uncertainties in finding the initial conditions of the bridge-vehicle system in the field are very great. For example, the initial motions of the vehicle as it enters the bridge and the mechanisims of the structural behavior of the bridge with respect to composite action are very significant but very difficult to measure under field conditions. Several such difficulties will be discussed in the sections which follow.

5.2 The Single-Span, Single-Beam Bridge

The finite element theory developed herein was first tested by considering a bridge in simplest terms, i.e. as a simple-supported prismatic beam. To establish equivalents between the finite-element solutions and available single-beam solutions by Huang,[6,7] the finite-element model was specialized to include a symmetrical pair of beams and a connecting deck element loaded such that the two beams and the connecting deck element acted as a single unit. The vehicle was represented as a two-dimensional plane model with appropriate vehicle characteristics, including multiple, sprung axles with interleaf frictional damping. With this simple case, the numerical solution technique and bookkeeping scheme for handling

frictional forces in the vehicle suspension facilitated the evaluation of the effects of bridge-deck roughness and the initial oscillation of the vehicle.

A total of 14 comparisons were made considering a number of typical combinations of parameters; the specific parameters considered are summarized in Table 1. The input parameters are presented using the notation of Ref. (4) and include the speed parameter, vehicle-bridge weight ratio, the vehicle-bridge frequency ratio when the vehicle vibrates on the tires only, the corresponding frequency ratio when the tires and vehicle suspension system act together, the ratio of the maximum or limiting value of the interleaf friction force to the static axle reaction in each tire-suspension assembly, the ratio of the initial amplitude of the interacting force to the corresponding static value, the camber in the bridge profile expressed in terms of the amplitude of the dead load deflection of the structure, the maximum amplitude of bridge roughness assuming that roughness is taken as a sine-wave function, the total number of half sine waves in the bridge deck roughness function, and the coefficient of viscous damping for the bridge. Also indicated in Table 1 are the value of β in the numerical integration procedure, the total number of integration steps, the total number of joints in the finite-element idealization, and the cost of the finite-element solution.

Results of the comparisons are presented in two forms. Time-history curves for moments, deflections, and interacting forces are presented in Figs. 20 through 25 to illustrate two of the least favorable comparisons. Results for all 14 solutions are compared on the basis of selected data points in tabular form in Table 2. It should be emphasized

that the differences tabulated in Table 2 are best explained in light of the appearance of the time histories illustrated in Figs. 20 through 25.

As shown in Figs. 20 and 23, differences between the vehicle interacting forces predicted by the two theoretical methods are most significant when the vehicle approaches midspan; this discrepancy is believed to be the key to the explanation of all major inconsistancies between the two methods of analysis.

In the early stages of the present finite-element study, the deflected shape of the bridge deck was approximated by straight-line segments between the joints in the bridge idealization. This approximation greatly simplified the procedure for determining distortions in the suspension system of the vehicle by eliminating the need for computing curvature in the deck plate elements of the bridge model. The significance of this approximation did not become evident until comparisons with results from laboratory model tests were made. During this later work, which is reported in Art. 5.3, it was determined that the straight-line approximation for bridge deck deflection in many cases introduced a considerable error. In particular, errors were most noticeable in regions of high curvature near midspan. It is believed that this straight-line approximation is primarily responsible for the discrepancies between interacting forces which in turn caused the differences in the moment and deflection curves shown in Figs. 21, 22, 24, and 25; however, for reasons of economy, these comparisons were not rerun after the solution procedure was modified to calculate the curvature of the deck elements in an exact way.

In spite of the differences in solution technique, it is interesting to note that in both a qualitative and quantitative sense the

comparisons between the beam theory and the finite-element theory are close and appear satisfactory from the response curves shown in Figs. 20 through 25. This is to be expected since other studies[6] have shown that moderate differences in interacting force do not produce large differences in moment and deflection induced in the structure. The agreement in phase between the two theories is reasonably close. From the appearance of the time histories, however, it can be seen that while the differences between total response ordinates are small, larger relative differences may be expected in the dynamic increments predicted by the two theories; that is, larger differences will occur when the common crawl or static influence is subtracted.

Turning to the comparison of results shown in Table 2, from the first column it is seen that the difference between the maximum dynamic deflections determined by each theory in every case is less than 5 percent. The difference between maximum dynamic moments in all comparisons was less than 3 percent. However, the dynamic increments of moment that correspond to the maximum dynamic moments predicted by the two theories differ in some cases by more than 20 percent, illustrating the comment made above. Small phase shifts also affect comparisons of the dynamic increments. The difference between maximum values of the interacting forces, shown in the fourth column, are in all instances less than 3 percent.

In Table 2, cases 4 and 5 demonstrate that, given an equal number of integration steps, the values predicted on the basis of β equal to 1/6 produces better agreement than the value of β equals a 1/4; this is to be expected since the Huang results were computed using β equal to 1/6. Similarly, cases 7 and 8 demonstrate that agreement between the two methods

improves when the number of joints used in the idealization is increased from five to seven. Finally, cases 9 and 10 demonstrate that the agreement will improve as the number of integration steps is increased. It should be noted that the results based on Huang's theory were obtained using 600 integration steps. In the present study it was felt that the 600 step solutions were an uneconomic luxury; with a need to conserve computer time and money, the accuracy obtained by a lesser number of steps, a difference of less than 2 percent, was accepted.

5.3 The Single-Span, Multigirder Bridge

Response predictions using the finite-element model were next compared with theoretical and experimental studies of the behavior of an all-aluminum, five-girder, I-beam bridge model. The characteristics of the bridge and vehicle models and the test procedures are described in Ref. (28), and the results of the laboratory tests are presented in Refs. (29) and (30).

Theoretical predictions of the dynamic behavior of the test model using the theory developed by Oran have been compared previously[9] with the experimental data. In Oran's doctoral study, the bridge is analyzed as a plate continuous over flexible beams through the application of a combination of the Levy method of analysis for rectangular plates simply supported along two opposite edges and the Rayleigh-Ritz energy procedure in which the deflection of the bridge structure is expressed as a series of trigonometric functions.

The bridge and vehicle parameters used to obtain theoretical predictions from the finite-element model are presented in Table 3; the

finite-element model is pictured in Fig. 26. The history curves for total dynamic deflection at midspan of beams A, B, and C produced by a single wheel load moving over beam C are given in Fig. 27. The corresponding curves for dynamic increment of deflection are shown in Fig. 28.

One special adjustment in the finite-element model was made when the geometric properties of the laboratory test bridge were represented. Under normal circumstances, the width of each deck element is assumed to equal the center-to-center spacing between the corresponding beam elements; but since the rectangular beam elements were unusually wide, the center-to-center plate width yielded a low transverse stiffness. More accurate results were achieved when the bridge deck was represented by a series of plate elements having a width equal to the clear span between beams; each remaining portion of the deck was assumed to act as an integral part of the beam directly below. This assumption was reasonable since full composite action existed between the beams and the deck of the laboratory test model. A similar adjustment is recommended whenever a wide beam section is used instead of a narrow I-shaped section. This adjustment for wide beams was required only in the aluminum bridge model; otherwise, the narrow-beam assumption was satisfactory in this study.

As shown in Fig. 27, both theoretical solutions yield total deflection response curves which are in reasonable agreement with the experimental data. The dynamic increment of deflection, shown in Fig. 28, indicated less favorable agreement between the theoretical and experimental data. However, the peak responses at midspan are still reasonably close and phase agreement is maintained until the static deflection is considerably reduced. The experimental curves for beams D and E are included

in Fig. 28 to demonstrate that, although the structure and the loading are presumably symmetric with respect to the longitudinal center line of the bridge, the experimental results for the responses of the symmetric beams are not identical. These differences demonstrate the degree to which the experimental results are influenced by inconsistencies in the properties of the system.

Some discrepancies between the two theoretical solutions are to be expected since the torsional properties and the composite behavior of the bridge deck and beams are not treated identically in the two theories. In Oran's approach, the neutral axis of the cross-section of each individual beam is assumed to coincide with the midplane of the bridge deck. Torsional and flexural stiffness resulting from composite action between the bridge deck and the eccentric beam elements are input approximately as part of the stiffness of the beam; to demonstrate the comparison between the analytical techniques without the influence of this difference, the problem was rerun using the same input data except that torsion, composite action, and bridge roughness were eliminated. As shown in Figs. 29, 30, and 32, the predicted displacements and interacting forces were nearly identical for the two procedures. The predicted moments for beams A and B, which are presented in Fig. 31, were also in very close agreement; but Oran's solution failed to show any evidence of a peak in the moment in beam C. This discrepancy occurs because the ordinary theory of flexure of slabs does not apply in the immediate vicinity of a concentrated load.[31] Therefore, Oran's method predicted moments accurately at all locations except when the load approached the point on beam C where the moment was being calculated.

5.4 The Two-Span, Multigirder Bridge

Theoretical or laboratory studies of the dynamic response of two-span, multibeam highway bridges subjected to moving vehicles are not available in the literature. Thus the present results will be compared and evaluated with respect to data obtained from field tests on the Shaffer Creek Bridge[32] which is a two-span continuous, steel multibeam highway bridge. The Shaffer Creek Bridge study is part of a reseach program entitled Dynamic Stresses in Highway Bridges conducted at the University of Illinois at Urbana-Champaign.

The characteristics of the bridge, and the conditions, test procedures, and results of the field tests are presented in Ref. (32). The parameters used to define the finite element model for the theoretical solutions are presented in Table 3; the finite element model is pictured in Fig. 33. Fig. 34 shows the transverse position of the vehicle on the bridge deck and the roughness profiles for the two corresponding wheel paths. Theoretical history curves for static and dynamic deflections are presented in Fig. 35. The experimental and theoretical curves for dynamic strain in the lower flanges of the bridge girders are compared in Fig. 36. Two major discrepancies are apparent. The experimental data indicate that the peak response occured when the driving axle of the vehicle was over the center pier of the bridge while the theoretical analysis predicts maximum response when the driving axle is closer to the midpoint of the first span. Secondly, the experimental measurements indicate that the higher modes of vibration do not significantly influence the dynamic behavior of the structure, whereas the theoretical response shows a considerable amount of high frequency variation especially as the vehicle moves across the second span

of the bridge.

Theoretical and experimental static deflections are compared in Fig. 37. The finite element model provided reasonably good results when the vehicle was near the point at which displacements were measured. However, theoretical displacements differ markedly from measured displacements as the vehicle moves across the second span. The theoretical and experimental static strains shown in Fig. 38 compare more favorably, but some difference is noted in the transverse distribution of strain. In the theoretical analysis, the maximum strain in beam C is greater than the experimental value whereas the maximum strains in beams A and E are smaller than those obtained in the field tests.

The discrepancies between field test results and theoretical predictions are the result of several factors. Theoretical solutions were derived in accordance with the assumption that the degree of composite action, which exists between the steel girders and the concrete bridge deck, is constant. However, test data indicate that the degree of composite action in the actual bridge varies with the longitudinal position of the vehicle and thus by inference on the magnitude of the shear force at the girder-deck interface. This force is developed by friction since shear connectors are not used in the structure.

It is believed, but not confirmed by direct measurements of slip, that the shear force between the bridge deck and steel girders reaches a limiting value during the vehicle crossing and slippage at the interface reduces the degree of composite action. Whenever the degree of composite action is reduced, the moment of inertia of the deck and girder combination is also reduced. This phenomenon can greatly affect the behavior of the

structure. In theory, when the bridge is unloaded, neglecting previous loading history, all five girder-deck cross-sections will exhibit fully composite action. However, as the load moves across the span, the beam or beams directly below the load carry a major portion of the bending moment and thus develop much greater stresses than those further removed from the load. At some limiting condition, the moment of inertia of the highly loaded beam decreases because of a breakdown in composite action, and some of its moment is redistributed to the adjacent beams which have not experienced as great or perhaps any reduction in moment of inertia. As the load approaches the center of the span, the lightly loaded beams absorb a greater proportion of the load; and once the load passes the center of the span, the process tends to reverse. Thus the transverse distribution of moment constantly changes as the load travels along the structure. Also, the effective stiffness of the structure is directly related to the composite moment of inertia of the beams; and in turn, the stiffness directly affects the natural frequencies of the structure.

Further discrepancies undoubtedly arose as a result of the unavailability of accurate data defining the initial conditions in the vehicle as it entered onto the bridge deck. If further analysis had been possible, it would have been desirable to approximate the vehicle's initial conditions by subjecting the vehicle model to a displacement function that is equivalent to the surface profile of the approach pavement. At least, such a method would provide more rational information on the effects of initial oscillations in the vehicle model.

After studying the results presented in Figs. 35 through 38, the reader should bear in mind that no attempt has been made, nor was it

possible at the time, to explore more thoroughly the data available from the field tests. It is felt that the results used for the static case, shown in Figs. 37 and 38, are reliable. It has been observed qualitatively in the field test data that some test vehicle crossings produce more evidence of dynamic components having the fundamental frequency and a larger residual free vibration than others. A thorough study of the correlation between theory and field data obviously is needed; the results herein are presented primarily to show the capabilities of the theory and to suggest the possibility that fruitful comparisons may be made in the future. Also, as has been suggested in the above paragraphs, partial composite action has a complex influence on structural response and may not be fully understood in the dynamic loading situation.

Fourier Series analyses were performed on all time histories. Typical results of these analyses are shown in Figs. 39 through 42. The Fourier coefficients have been connected with straight-line segments for visual clarity. As expected, these results indicate that the peak dynamic response occurs at a frequency of approximately 6.6 cycles per second which is the undamped natural frequency of the bridge model as shown in Fig. 43. The undamped natural frequencies shown in Fig. 43 were obtained from an Eigenvalue analysis of the reduced mass and stiffness matrices of the bridge model. As shown in Appendix C, 50 percent composite action was assumed to develop between the slab and girders. The undamped natural frequencies shown in Fig. 43 correspond to the thirty vertical dynamic degrees of freedom of the bridge model. The mode shapes or Eigenvectors associated with the four lowest frequencies are illustrated in Figs. 44 and 45.

The Fourier Series coefficients shown in Figs. 39 and 40 indicate that deflections and moments are mainly influenced by those modes of vibration that correspond to frequencies of less than 20 cps. As shown in Fig. 43, only the first six natural modes of vibration correspond to frequencies of less than 20 cps. This implies that a meaningful modal solution can be obtained by considering only those six modes of vibration. On the other hand, Figs. 41 and 42 indicate that higher modes of vibration have a substantial influence on accelerations and can not be so easily neglected when accelerations are of prime interest.

5.5 The Three-Span, Single-Beam Bridge

Single-beam finite element solutions of three-span bridges were obtained by loading a symmetrical pair of beams and a connecting deck element in such a way that the two beams and the deck element acted as a single unit. Analytical results were then compared with results from a three-span, single-beam theory and computer code developed by Huang.(7) The results of three different solutions are presented to demonstrate the nearly perfect agreement between the two models. The bridge and vehicle parameters for the three solutions are given in non-dimensional form in Table 3. The actual input parameters for cases a, b, and c are presented in Appendix C.

Case a is a so-called smoothly-moving vehicle solution in which the vehicle is assumed to have no initial oscillation and the bridge exhibits no surface roughness. Results from the two theories are presented in Figs. 46 through 50. Case b demonstrates bridge-vehicle response to a sine-wave roughness function with a wave length of 48 feet and an amplitude

of 0.3 inches. The results for this problem are shown in Figs. 51 through 55. Case c considers the effects of initial conditions in a single axle vehicle. Each tire force is assumed to have an initial value of 1.5 times its static value, and initial interleaf friction forces are such that both suspension systems on the two-wheel, single-axle vehicle are initially unlocked. The results for Case c are presented in Figs. 56 through 60. In all three cases, the Huang beam idealization and the finite element solution produce results that are nearly identical.

5.6 The Three-Span, Multigirder Bridge

The final structure to be modeled was a three-span, five girder bridge designated as the Salt Fork River Bridge. The bridge, tested as part of the investigation entitled Dynamic Stresses in Highway Bridges, was instrumented and its response to a simulated AASHO HS20-44 vehicle was recorded.[32] The parameters used to define the finite element model are presented in Table 3; the finite element model is pictured in Fig. 61.

During preliminary numerical studies, it was established that a dynamic solution for the 65 joint bridge idealization would cost a minimum of $240; it was decided that sufficient computer funds were not available to develop and test a dynamic analysis of the three-span, multigirder bridge. The cost of a dynamic analysis could have been lowered by reducing the number of degrees of freedom in the bridge model, but further simplification of the model would greatly reduce the probability of achieving meaningful results from the analysis.

However, it was feasible to use the finite element model for generating static influence lines for comparison with "crawl curve" data from the field test studies. The input parameters for the crawl curve

analysis are presented in Table 3 . Influence lines for deflections and strains at midspan of the center span are shown in Figs. 62 and 63, respectively. The experimental curves for beams D and E are included in Figs. 62 and 63 to demonstrate that, although the structure and the loading are presumably symmetric with respect to the longitudinal center line of the bridge, the experimental results for the responses of the symmetrical beams are not identical. These differences demonstrate the degree to which the experimental results are influenced by inconsistencies in the properties of the system. Uncertainties about the properties and structural characterists of the bridge deck, curbs, and handrails also made it difficult to accurately model the bridge structure. However, many of the discrepancies between field test results and theoretical results are believed to have been caused by the effects of partial composite action. In any case more extensive parametric studies using the finite element model would be required to define the influence of the various parameters just cited.

A corresponding theoretical and experimental influence lines for deflections and strains in an exterior span were not available. However, theoretical results for the midpoint are shown in Figs. 64 and 66 and field measurements, recorded at a distance of forty-two one hundreths of the exterior span length from the exterior abutment are presented in Figs. 65 and 67. While the time-history data from the two locations, of course, are not identical, the qualitative similarity in behavior demonstrated by the two sets of curves is apparent.

5.7 Some Observations on Behavior of the Finite Element Bridge Model

During the course of the invesigation, it became apparent that the multigirder finite element bridge model was sensitive to moderate

variations of certain bridge parameters as well as the placement of vehicle loads. Numerous observations of this sensitivity have suggested the following hypotheses:

1. The transverse distribtuion of stresses is greatly affected by the torsional stiffness of beams and concrete curbs along the free edges of the structure.
2. The behavior of the bridge deck becomes more critical as the vehicle loads move away from the direct support of the longitudinal girders.
3. When a vehicle load first comes into contact with the bridge deck, the stiffness of transverse stiffeners over the bridge abutments significantly affects the response of the structure if the vehicle loads are not directly over the main bridge girders.
4. Comparisons of analytical results with measured response data from field tests indicate a need for more sophisticated modeling techniques.

The above comments are based on conjecture resulting from study of the numerical results primarily in the form of time histories of moments and deflections obtained during the development of the computer programs. It is difficult to select specific numerical examples from the voluminous data accumulated. Thus only a qualitative discussion is presented in this section. Frankly, to present meaningful results, a systematic numerical study is required of the phenomena indicated herein, and such is suggested as a topic for further research.

All of the above opinions suggest that the behavior of the finite element bridge model is heavily dependent upon the interaction of the plate and beam elements. Earlier in the text, it was pointed out that compatibility of slope between plate elements was not satisfied along the entire interface of adjacent elements. A similar lack of compatibility also exists between the plate and beam elements with the effect that torsional distortions in the beam elements are not compatible with the corresponding deformations in the plate elements at any points other than at the ends of the beam elements. Originally, this lack of compatibility was not too objectionable. The effects of these errors on the behavior of the model were negligible since the torsional stiffness of a steel I-shaped girder is quite low. However, comparisons of analytical results with field test data later indicated that the torsional properties of curbs, median strips, and other large concentrations of material have a substantial influence on the behavior of the structure when such elements are cast as an integral part of the bridge deck. Problems then arose because such projections from the bridge deck were also treated as eccentric stiffeners. It is believed that significant errors were caused by the lack of compatibility especially when these concrete projections possessed considerable torsional stiffness. This lack of compatibility seemed to cause the most difficulty when vehicle loads were located between longitudinal girder so as to create large transverse bending moments in the deck plate elements. In such cases, slope compatibility conditions greatly influence the manner in which bending and twisting moments resulting from direct vehicle loads are transferred from the plate elements to the longitudinal girders. Therefore, it is recommended that further studies be conducted to determine

if higher order beam and plate elements, which satisfy more stringent compatibility requirements, are advantageous when both accuracy and computer costs are considered.

5.8 Observations on the Behavior of the Vehicle Model

All of the analytical and experimental results presented in this study were aimed specifically at the evaluation of the performance of various dynamic bridge models, and little attention has been given to the performance of the vehicle model. In fact, its performance was evaluated soley on the basis of comparisons of interacting force data with data from other analytical models. In a recent study[25] in which several typical heavy highway vehicles were instrumented, tests indicated a need for more sophisticated vehicle models. Some of the implications of the work described in Ref. 25 on the studies reported herein are presented in the following discussion.

Results from a study of factors that influence the response of highway vehicles to pavement roughness demonstrated that vehicle response is substantially affected by tire enveloping, suspension system mass, and wheel rotation excitation. Tire enveloping is defined as the ability of a tire to conform to road irregularities thus enabling the tire to absorb sharp changes in road profile without equally sharp changes in vehicle response. When tire enveloping is ignored, dynamic loads that result from pavement roughness are consistantly too high.

In order to properly calculate the inertia forces resulting from the mass of vehicle tires, axles, and suspension system, an additional degree of freedom is required. This additional degree of freedom, which is

located between the tire stiffness spring and the leaf springs of the suspension system, is needed to determine the magnitude of accelerations and velocities experienced by the suspension system mass.

Wheel rotation excitation is caused by rim assembly runout, tire nonuniformity, and improper wheel balancing and alignment. A truck that is rolling on a perfectly smooth surface will experience a considerable amount of dynamic loading unless wheel rotation excitation is kept to a minimum. It was found that dynamic loads resulting from wheel rotation excitation could not be ignored in tests involving heavy highway vehicles. The magnitude of maximum dynamic loads was found to be substantially affected by tire stiffness, tire enveloping, and the mass of the suspension system. The rate of decay of dynamic loads was mainly influenced by spring stiffness, viscous damping, and the breakaway level of interleaf friction in the suspension system. In order to obtain accurate vehicle response data, the vehicle model should exhibit all characterists that significantly influence the behavior of the actual vehicle.

However, once an elaborate vehicle model has been developed, there remains the problem of measuring the significant properties associated with an actual vehicle. If the vehicle model is to be used to simulate a certain class of vehicles rather than one particular vehicle, additional considerations must be taken into account. No two vehicles will exhibit identical properties. Properties related to tire wear and wheel alignment never remain constant. Many significant vehicle properties can only be determined by approximate methods. These considerations tend to reduce the usefullness of a highly sophisticated vehicle model. In such cases, a model such as the one developed in this study may be adequate

especially if the user is concerned only with obtaining maximum loads.

5.9 Solution Time and Cost

Solution time and cost are functions of many variables some of which are the number of joints or dynamic degrees of freedom, the number of time steps, the size of in-core memory, the number of steps between two successive data print-outs, and the amount of plotted output. Therefore, no attempt was made to develop an equation for estimating run time or solution cost. Instead, it was found that the most effective estimate of run time and cost could be achieved simply by setting up a run and allowing the computer to perform about ten to fifteen time-step iterations. Since the time and cost are nearly directly proportional to the number of time steps, accurate estimates could be made simply by extrapolating data from the trial run.

The influence of the total number of joints, the size of in-core memory, the number of integration steps, and the solution time on computer cost for typical solutions on the University of Illinois' 360-75 IBM computer is summarized in Table 4 . The first four examples are actual costs for the dynamic analysis of various bridge-vehicle combinations. The fifth example pertains to a static crawl-curve analysis performed on the three-span, five-beam Salt Fork River Bridge model; and the last example gives the cost of a dynamic solution for the same three-span bridge model. The data for the dynamic analysis of the three-span model were estimated from a trial solution since a full solution was never performed.

6. SUMMARY AND CONCLUSIONS

6.1 Summary

A finite-element method of analysis has been developed to predict the dynamic response of a multigirder, multispan highway bridge under the action of a moving vehicle. The bridge structure is considered to be composed of a number of discrete plate and stiffener elements which are connected at common nodal points. Compatibility of deformations between all elements meeting at a given node is required. The final form of the assumed displacement function for each type of element is expressed in terms of nodal displacements. The principle of virtual work is then used to develop a stiffness matrix which relates nodal forces to nodal displacements. Finally, the individual stiffness matrices are assembled to form a stiffness matrix for the entire structure. In a similar manner, mass and damping matrices for the plate and beam elements are developed and assembled. The mass, damping, and stiffness matrices are then incorporated into the equations of motion for the bridge model.

Two-axle single unit or three-axle semi-trailer trucks are idealized, respectively, as one or two rigid bodies supported by four or six tire-suspension assemblies. Equilibrium equations are written to relate rotational and vertical inertia forces of the vehicle mass to the disturbing forces in the tire-suspension assemblies. The leaf springs of each suspension system are represented by a bilinear, elastic spring in parallel with a friction device. The vehicle mass inertia forces are related to the suspension system forces to yield the equations of motion for the vehicle. The deformation of each tire-suspension system is determined by

assuming that the vehicle tires remain in contact with the bridge deck at all times. This compatibility condition is then used to link the equations of motion for the bridge to the equations of motion for the vehicle. The complete set of equations describe the interactive dynamic behavior of the bridge and vehicle.

Three computer programs were developed. The first program generates the mass and stiffness matrices for the finite element bridge model; the second performs a dynamic analysis of the bridge-vehicle system; and the third performs both a constant-force solution and a crawl-curve analysis of the bridge. The programs have been written to consider one, two, or three span bridges with up to five longitudinal girders. The bridge model can be given as many as 65 nodal points and the vehicle can exhibit up to six vertical degrees of freedom.

With the aid of the computer programs, several problems are solved. These problems are divided into five categories according to bridge type:

(1) Single-span, single-beam,

(2) Single-span, multibeam,

(3) Two-span, multibeam,

(4) Three-span, single-beam, and

(5) Three-span, multibeam.

Comparisons with the three-span, single-beam bridge theory developed by Huang[6,7] were excellent. Comparisons with Huang's single-span, single-beam bridge theory and a single-span, multibeam bridge theory developed by Oran[9] showed good agreement; it is believed that comparisons with

Huang's single-span theory would have been greatly improved if curvature in the bridge deck had been calculated using an exact method rather than approximated by a series of straight-line segments.

Theoretical results were compared with selected data from field tests, but it was not possible within the scope of the present study to make a systematic parameter study to optimize the degree of agreement. Comparisons with data from the Shaffer Creek Bridge tests and the Salt Fork River Bridge tests indicated fair agreement statically. However, the dynamic increments of deflection and strain predicted by the theoretical dynamic analysis of the Shaffer Creek Bridge model differed considerably from field test results. These differences in response were attributed mainly to changes in stiffness which result from partial composite action occurring between the bridge deck and the steel girders. Such variations in stiffness affect the transverse distribution of stresses as well as the natural modes and frequencies of the bridge.

When full composite action was assured in a controlled laboratory test, theoretical predictions of dynamic response were quite satisfactory. This was demonstrated by comparisons with the measured response of a single-span, five-girder aluminum test model[28,29,30] in which the solid rectangular aluminum beams were bonded to the thin aluminum bridge deck to insure full composite action between the deck and beams.

6.2 Conclusions and Recommendations for Further Study

The finite-element model yields response predictions which compare quite satisfactorily with those obtained by other analytical techniques. The versatility of the model exceeds that of the other techniques studied, and a wide assortment of boundary conditions can be easily

implemented. The model can be modified to consider more than three spans; the size or complexity of the bridge is limited only by considerations of computer space and cost of solution.

A major source of disagreement between theoretical response predictions and experimental data is believed to result from variations in the degree of composite action between the bridge deck and the steel girders. Such variations change the stiffness of the effective T-beam sections, thus affecting both the transverse distribution of stresses and the natural frequencies of the structure. Agreement between theoretical and experimental results would be improved by developing a model that allows for time-variations in the degree of composite action.

A second source of discrepancies between theoretical and experimental data results from the inability in the field studies to accurately determine the magnitude of initial oscillations in the test vehicle as it comes into contact with the bridge deck. Initial oscillations resulting from approach pavement roughness and surface discontinuities at the junction between the approach pavement and the bridge deck substantially affect the dynamic response of the bridge-vehicle system.

During the course of the investigation, it was observed that the multigirder finite-element bridge model was sensitive to small changes in the placement of vehicle loads and moderate variations of certain bridge parameters. Therefore, further studies are recommended to determine if higher order beam and deck elements, which satisfy more stringent compatibility requirements, improve the transverse continuity of the bridge structure by an amount sufficient to justify the required additional computer time.

The measured bridge response data used herein were not selected on a statistical basis to be representative of all data collected during the field tests. A thorough study of the correlation between theory and field data obviously is needed; the results herein were presented primarily to demonstrate the capabilities of the theory and to suggest the possibility that fruitful comparisons may be made in the future.

Further study is also needed to determine if the finite-element model is capable of accurately predicting strains at interior points in the deck-plate elements. Satisfactory predictions of strains in the bottom fibers (flanges) of the bridge girders were obtained, but no attempt was made to predict strains in the deck-plate elements of the model. It is unlikely that the deck elements will yield satisfactory values of strain under all possible loading conditions since they will yield accurate results only so long as the assumption of a linearly elastic, homogeneous material is valid.

Newmark, Siess, and Penman[33] have reviewed certain other common assumptions that are also relevant to the present study. Specifically, the deck structure assumed in a theoretical analysis normally differs from actual concrete bridge decks in that the moment of inertia of the slab is not definitely known because of cracking of the slab. A lack of homogeneity is produced because cracking tends to be more severe at the centers of the panels than at the edges over the beams; such variations produce a corresponding difference in stiffness at these locations and cause the slab to act as if it were non-prismatic in the transverse direction. Cracking also introduces a difference in properties of the slab in different directions since cracking affects the moment of inertia

of the slab. Therefore, the slab is anisotropic and not isotropic (as is assumed in the formulation of the present theory). Anisotropic properties can be included in the formulation, but the pattern of cracking is so irregular that such refinements are unwarranted. Thus, it appears that the development of a non-linear plate element may not in itself insure the accurate prediction of strains in reinforced concrete bridge decks.

The method presented herein for the dynamic analysis of continuous highway bridges is very general in its formulation, and it is beyond the scope of this study to develop all the capabilities that are inherent in the method. A skewed finite plate element has been developed for the analysis of conventional skewed bridges and variable-width bridges such as those used for entrance and exit ramps on elevated freeway systems. The method can be modified to handle almost any type of slab and girder highway bridge including curved bridges.

The vehicle model also may be modified to handle special conditions. Lateral forces resulting from a curved vehicle path or non-uniform vehicle velocities caused by acceleration or braking could be included in the analysis, but the reduced stiffness formulation would have to be modified to include loadings in the plane of the bridge deck. The transverse position of the vehicle on the bridge could be varied in some prescribed manner as the vehicle crossed the bridge. Additional vehicle properties such as tire enveloping, suspension system mass, and wheel rotation excitation also could be incorporated in the vehicle model.

Bridge-vehicle interaction involves the behavior of two complex systems. Continued study is required if an adequate understanding of this dynamic interaction is to be fully realized. In view of the rather high

solution time and cost of the present method of analysis, it is believed that the development of a mode-superposition method would be a valuable extension of the present study. Solution costs could be reduced by employing a modal method which considers only the predominant modes of vibration of the bridge.

Finally, the finite element method appears to be a workable and versatile approach to the dynamic analysis of bridge response. Further study should be devoted to making the finite element method a more effective research tool, particularly in the area of computer simulation of bridge response to truck traffic.

REFERENCES

1. Standard Specification for Highway Bridges, American Association of State Highway Officials, 10th Edition, Washington, D.C., 1969.

2. Wright, R. N. and Walker, W. H., Bulletin No. 19, American Iron and Steel Institute, New York, 1971.

3. Luthe-Garcia, R., Walker, W. H., and Veletsos, A. S., "Dynamic Response of Simple-Span Highway Bridges in the Inelastic Range," Civil Engineering Studies, Structural Research Series No. 287, University of Illinois, Urbana, 1964.

4. Nieto-Ramirez, J. A., and Veletsos, A. S., "Response of Three-Span Continuous Highway Bridges to Moving Vehicles," Engineering Experiment Station Bulletin No. 489, University of Illinois, Urbana, 1966.

5. Spates, K. R. and Heins, C. P., "Analysis of a Single Curved Girder Under Various Loading and Boundary Conditions," Civil Engineering Department, University of Maryland, College Park, 1968.

6. Walker, W. H. and Veletsos, A. S., "Response of Simple-Span Highway Bridges to Moving Vehicles," Engineering Experiment Station Bulletin No. 486, University of Illinois, Urbana, 1966.

7. Huang, T. and Veletsos, A. S., "Dynamic Response of Three-Span Continuous Highway Bridges," Civil Engineering Studies, Structural Research Series No. 190, University of Illinois, Urbana, 1960.

8. Toledo-Leyva, J. and Veletsos, A. S., "Effects of Roadway Unevenness on Dynamic Response of Simple-Span Highway Bridges," Civil Engineering Studies, Structural Research Series No. 168, University of Illinois, Urbana, 1958.

9. Oran, C. and Veletsos, A. S., "Analysis of Static and Dynamic Response of Simple-Span Multigirder Highway Bridges," Civil Engineering Studies, Structural Research Series No. 221, University of Illinois, Urbana, 1961.

10. Bell, L. C. and Heins, C. P., "The Solution of Curved Bridge Systems Using the Slope-Deflection Fourier Series Method," Civil Engineering Department, University of Maryland, College Park, 1968.

11. Hails, R. L. and Heins, C. P., "The Study of a Stiffened Curved Plate Model Using the Finite Difference Technique," Civil Engineering Department, University of Maryland, College Park, 1968.

12. Yettram, A. L. and Husain, H. M., "Grid-Framework Method for Plates in Flexure," Journal of the Engineering Mechanics Division, ASCE, Vol. 91, No. EM3, Proc. Paper 4361, June 1965.

13. Yettram, A. L. and Husain, H. M., "Plane-Framework Methods for Plates in Expansion," Journal of the Engineering Mechanics Division, ASCE, Vol. 92, No. EM1, Proc. Paper 4695, February, 1966.

14. Benard, E. F., "A Study of the Relationship Between Continuous and Lattice Structures," Ph.D. Thesis, University of Illinois, Urbana, 1965.

15. Heins, C. P. and Looney, C. T. G., "Bridge Analysis Using Orthotropic Plate Theory," Journal of the Structural Division, ASCE, No. ST2, February, 1968.

16. Gustafson, W. C., "Analysis of Eccentrically Stiffened Skewed Plates," Structures," Ph.D. Thesis, University of Illinois, Urbana, 1966.

17. Mehrain, Mehrdad, "Finite Element Analysis of Skew Composite Plates," Ph.D. Thesis, University of California, Berkeley, 1967.

18. Adini, A. and Clough, R. W., "Analysis of Plate Bending by the Finite Element Method," NSF Report, Grant G7337, 1960.

19. Argyris, J. H., "Continua and Discontinua," Proc. of the Conference on Matrix Methods in Structural Mechanics, Air Force Inst. of Tech., Wright-Patterson Air Force Base, Ohio, October, 1965.

20. Zienkiewicz, O. C., "The Finite Element Method in Structural and Continuum Mechanics," McGraw-Hill, New York, 1967.

21. Timoshenko, S. and Woinowsky-Krieger, S., "Theory of Plates and Shells," McGraw-Hill, New York, 2nd ed., 1959.

22. Clough, R. W., "The Finite Element Method in Structural Mechanics," Chapter 7 of Stress Analysis, ed. O. C. Zienkiewicz and G. S. Holister, J. Wiley, New York, 1965.

23. Livesley, R. K., "Matrix Methods of Structural Analysis," Pergamon Press, London, 1964.

24. Przemieniecki, J. S., "Theory of Matrix Structural Analysis," McGraw-Hill, New York, 1968.

25. Whittemore, A. P., Wiley, J. R., Schultz, P. C., and Pollock, D. E., "Dynamic Pavement Loads of Heavy Highway Vehicles," National Cooperative Highway Research Program Report No. 105, Highway Research Board, Washington, D. C., 1970.

26. Newmark, N. M., "A Method of Computation for Structural Dynamics," ASCE Transactions, Paper No. 3384, Vol. 127, Part I, 1962.

27. Fenves, S. J., Veletsos, A. S., and Siess, C. P., "Dynamic Studies of Bridges on the AASHO Test Road," Highway Research Board Special Report 71, NAS-NRC Publication 968, Washington, D.C., 1962.

28. Prince-Alfaro, J. and Veletsos, A. S., "Dynamic Behavior of an I-Beam Bridge Model Under a Smoothly Rolling Load," Civil Engineering Studies, Structural Research Series No. 167, University of Illinois, Urbana, 1958.

29. Huang, C. L. and Walker, W. H., "Analysis of Data Obtained from Tests on a Highway Bridge Model," Part D, Tenth Progress Report, Highway Bridge Impact Investigation, University of Illinois, Urbana, 1960.

30. Walker, W. H., "Model Studies of the Dynamic Response of a Multigirder Highway Bridge," Engineering Experiment Station Bulletin No. 495, University of Illinois, Urbana, 1968.

31. Newmark, N. M. and Siess, C. P., "Moments in I-Beam Bridges," University of Illinois Engineering Experiment Station, Bulletin 336, 1942.

32. Walker, W. H. and Ruhl, J. A., "Investigation of Dynamic Stresses in Highway Bridges - an Interim Report," Department of Civil Engineering, University of Illinois, Urbana, 1971.

33. Newmark, N. M., Siess, C. P., and Penman, R. R., "Studies of Slab and Girder Highway Bridges," University of Illinois Engineering Experiment Station, Bulletin 363, 1946.

TABLE 1

INPUT PARAMETERS AND COST FOR SINGLE-BEAM, SINGLE-SPAN SOLUTIONS

RUN NO.	α	$\frac{W_v}{W_b}$	$\frac{f_t}{f_b}$	$\frac{f_{ts}}{f_b}$	μ	$\frac{P_0}{P_{st}}$	$\frac{d_c}{d_{DL}}$	b_o	m	$\frac{c}{c_{cr}}$	B	N	N.J.	Cost
1	.20	.2	.7	-	∞	1.5	0	0	0	0	1/4	200	7	3.87
2	.18	.2	.7	-	∞	1.0	0	0	0	0	1/4	200	7	3.95
3	.18	.2	.3	-	∞	1.0	0	0	0	0	1/4	200	7	3.90
4	.20	.1	1.0	4/7	.15	1.5	0	0	0	0	1/6	350	7	5.59
5	.20	.1	1.0	4/7	.15	1.5	1.0	0	0	0	1/4	350	7	5.59
6	.15	.2	.7	-	∞	1.0	1.0	0	0	0	1/6	300	7	4.97
7	.15	.2	.7	-	∞	1.0	0	0	0	0	1/6	200	7	4.30
8	.15	.2	.7	-	∞	1.0	0	0	0	0	1/6	200	5	3.13
9	.15	.2	.7	.4	.15	1.0	1.0	0	0	0	1/6	350	7	5.48
10	.15	.2	.7	.4	.15	1.0	1.0	0	0	0	1/6	300	7	4.93
11	.14	.2	.68	.39	.15	1.0	0	1/2	5	0	1/6	300	7	4.85
12	.14	.2	.68	.39	.15	1.0	0	1/2	5	.05	1/6	300	7	4.81
13	.14	.2	.68	.39	.15	1.0	0	1/4	7	0	1/6	300	7	4.96
14	.14	.2	.68	.39	.15	1.0	0	1/4	3	0	1/6	350	7	5.52

TABLE 2

COMPARISONS OF RESULTS FOR SINGLE-BEAM, SINGLE-SPAN SOLUTIONS

RUN NUMBER	PERCENT DIFFERENCES			
	TOTAL DEFLECTION	TOTAL MOMENT	DYNAMIC INCREMENT OF MOMENT	INTERACTING FORCE
1	.2	.1	.2	.3
2	.3	1.5	9.6	.1
3	.3	.2	1.3	.1
4	.9	1.6	3.2	1.2
5	1.2	2.9	5.9	2.8
6	1.0	1.7	8.9	1.3
7	.0	.0	.0	.1
8	.3	.3	2.0	2.8
9	2.8	2.5	22.3	.0
10	4.8	2.7	23.6	2.0
11	.7	.1	.3	.1
12	.7	.1	.1	.1
13	2.0	.6	1.5	.7
14	1.0	1.0	3.3	.1

TABLE 3

NON-DIMENSIONAL PARAMETERS FOR FINITE ELEMENT SOLUTIONS

NAME	NUMBER OF SPANS	NUMBER OF BEAMS		$\frac{W_v}{W_b}$	$\frac{f_t}{f_b}$	INITIAL OSCILLATION	ROUGHNESS
Aluminum Test Model	1	5	0.160	0.313	0.518	No	Yes
Shaffer Creek	2	5	.158	0.575	0.542	No	Yes
Case A	3	1	0.175	0.200	0.5	No	No
Case B	3	1	0.150	0.175	0.5	No	Yes
Case C	3	1	0.150	0.175	0.5	Yes	No
Salt Fork	3	5	N.A.	0.180	N.A.	No	No

TABLE 4

TIME-COST-SIZE COMPARISONS FOR SIX TYPICAL FINITE-ELEMENT COMPUTER SOLUTIONS
(Runs Made Between 9/70 and 11/70)

	COST, DOLLARS	NUMBER OF JOINTS	NUMBER OF TIME STEPS	SOLUTION TIME, MINUTES	CORE REGION
1 Span - 1 Beam, DA	4.81	14	300	1.00	122K
1 Span - 5 Beams, DA	9.27	25	220	1.96	134K
3 Spans - 1 Beam, DA	17.85	30	300	4.24	138K
2 Spans - 5 Beams, DA	73.75	45	644	21.75	146K
3 Spans - 5 Beams, CCA	40.67	65	156	11.08	170K
3 Spans - 5 Beams, DAE	240.00	65	1140	70.00	180K

DA = Dynamic Analysis

CCA = Crawl Curve Analysis

DAE = Dynamic Analysis, Estimated

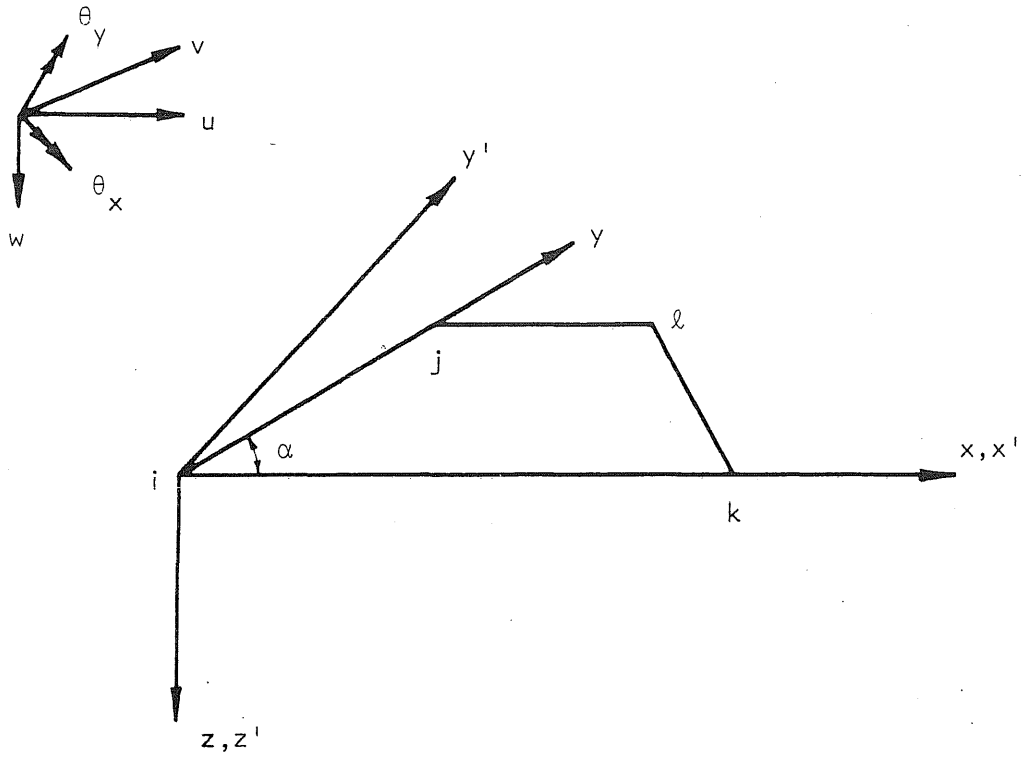

(a) Rectangular and Skew Coordinate Systems

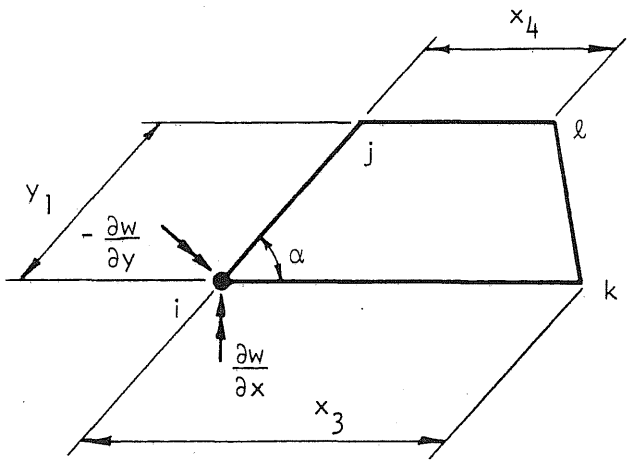

(b) Plan View in Skew Coordinate System

FIG. 1 TRAPEZOIDAL SHAPED ELEMENT

$$
\begin{bmatrix}
1 & 0 & 0 & 0 & 0 & 0 & 0 & 0 & 0 & 0 & 0 & 0 \\
0 & 1 & 0 & 0 & 0 & 0 & 0 & 0 & 0 & 0 & 0 & 0 \\
0 & 0 & -1 & 0 & 0 & 0 & 0 & 0 & 0 & 0 & 0 & 0 \\
1 & 0 & y_1 & 0 & 0 & y_1^2 & 0 & 0 & 0 & y_1^3 & 0 & 0 \\
0 & 1 & 0 & 0 & y_1 & 0 & 0 & 0 & y_1^2 & 0 & 0 & y_1^3 \\
0 & 0 & -1 & 0 & 0 & -2y_1 & 0 & 0 & 0 & -3y_1^2 & 0 & 0 \\
1 & x_3 & 0 & x_3^2 & 0 & 0 & x_3^3 & 0 & 0 & 0 & 0 & 0 \\
0 & 1 & 0 & 2x_3 & 0 & 0 & 3x_3^2 & 0 & 0 & 0 & 0 & 0 \\
0 & 0 & -1 & 0 & -x_3 & 0 & 0 & -x_3^2 & 0 & 0 & -x_3^3 & 0 \\
1 & x_4 & y_1 & x_4^2 & x_4y_1 & y_1^2 & x_4^3 & x_4^2y_1 & x_4y_1^2 & y_1^3 & x_4^3y_1 & x_4y_1^3 \\
0 & 1 & 0 & 2x_4 & y_1 & 0 & 3x_4^2 & 2x_4y_1 & y_1^2 & 0 & 3x_4^2y_1 & y_1^3 \\
0 & 0 & -1 & 0 & -x_4 & -2y_1 & 0 & -x_4^2 & -2x_4y_1 & -3y_1^2 & -x_4^3 & -3x_4y_1^2
\end{bmatrix}
$$

FIG. 2 C_f MATRIX

$$
\begin{bmatrix}
1 & 0 & 0 & 0 & 0 & 0 & 0 & 0 & 0 & 0 & 0 & 0 \\
0 & 1 & 0 & 0 & 0 & 0 & 0 & 0 & 0 & 0 & 0 & 0 \\
0 & 0 & -1 & 0 & 0 & 0 & 0 & 0 & 0 & 0 & 0 & 0 \\
\hline
-3/x_3^2 & -2/x_3 & 0 & 0 & 0 & 0 & 3/x_3^2 & -1/x_3 & 0 & 0 & 0 & 0 \\
-1/x_3y_1 & -1/y_1 & 1/x_3 & B & C & 0 & 1/x_3y_1 & 0 & -1/x_3 & -B & I & 0 \\
-3/y_1^2 & 0 & 2/y_1 & 3/y_1^2 & 0 & 1/y_1 & 0 & 0 & 0 & 0 & 0 & 0 \\
2/x_3^3 & 1/x_3^2 & 0 & 0 & 0 & 0 & -2/x_3^3 & 1/x_3^2 & 0 & 0 & 0 & 0 \\
3/x_3^2y_1 & 2/x_3y_1 & 0 & -3/x_4^2y_1 & -2/x_4y_1 & 0 & -3/x_3^2y_1 & 1/x_3y_1 & 0 & 3/x_4^2y_1 & -1/x_4y_1 & 0 \\
D & E & -2/x_3y_1 & F & 2G & -1/x_4y_1 & -D & H & 2/x_3y_1 & -F & -2I/y_1 & 1/x_4y_1 \\
2/y_1^3 & 0 & -1/y_1^2 & -2/y_1^3 & 0 & -1/y_1^2 & 0 & 0 & 0 & 0 & 0 & 0 \\
-2/x_3^3y_1 & -1/x_3^2y_1 & 0 & 2/x_4^3y_1 & 1/x_4^2y_1 & 0 & 2/x_3^3y_1 & -1/x_3^2y_1 & 0 & -2/x_4^3y_1 & 1/x_4^2y_1 & 0 \\
-J & -E/y_1 & 1/x_3y_1^2 & K & -G/y_1 & 1/x_4y_1^2 & J & -H/y_1 & -1/x_3y_1^2 & -K & I/y_1^2 & -1/x_4y_1^2
\end{bmatrix}
$$

FIG. 3 C_f^{-1} MATRIX (Continued on next page)

$$B = (3x_3/x_4^2y_1) - (2x_3^2/x_4^3y_1)$$

$$C = (2x_3/x_4y_1) - (x_3^2/x_4^2y_1)$$

$$D = (-2x_4^2/x_3^3y_1^2) + (3x_4/x_3^2y_1^2) + (2/x_3y_1^2)$$

$$E = (-x_4^2/x_3^2y_1^2) + (2x_4/x_3y_1^2) - (1/y_1^2)$$

$$F = (4x_3^2/x_4^3y_1^2) - (6x_3/x_4^2y_1^2) - (1/x_4y_1^2)$$

$$G = (x_3^2/x_4^2y_1^2) - (2x_3/x_4y_1^2) + (1/y_1^2)$$

$$H = (x_4/x_3y_1^2) - (x_4^2/x_3^2y_1^2)$$

$$I = (x_3/x_4y_1) - (x_3^2/x_4^2y_1)$$

$$J = (-2x_4^2/x_3^3y_1^3) + (3x_4/x_3^2y_1^3) + (1/x_3y_1^3)$$

$$K = (1/x_4y_1^3) + (3x_3/x_4^2y_1^3) - (2x_3^2/x_4^3y_1^3)$$

FIG. 3, Continued

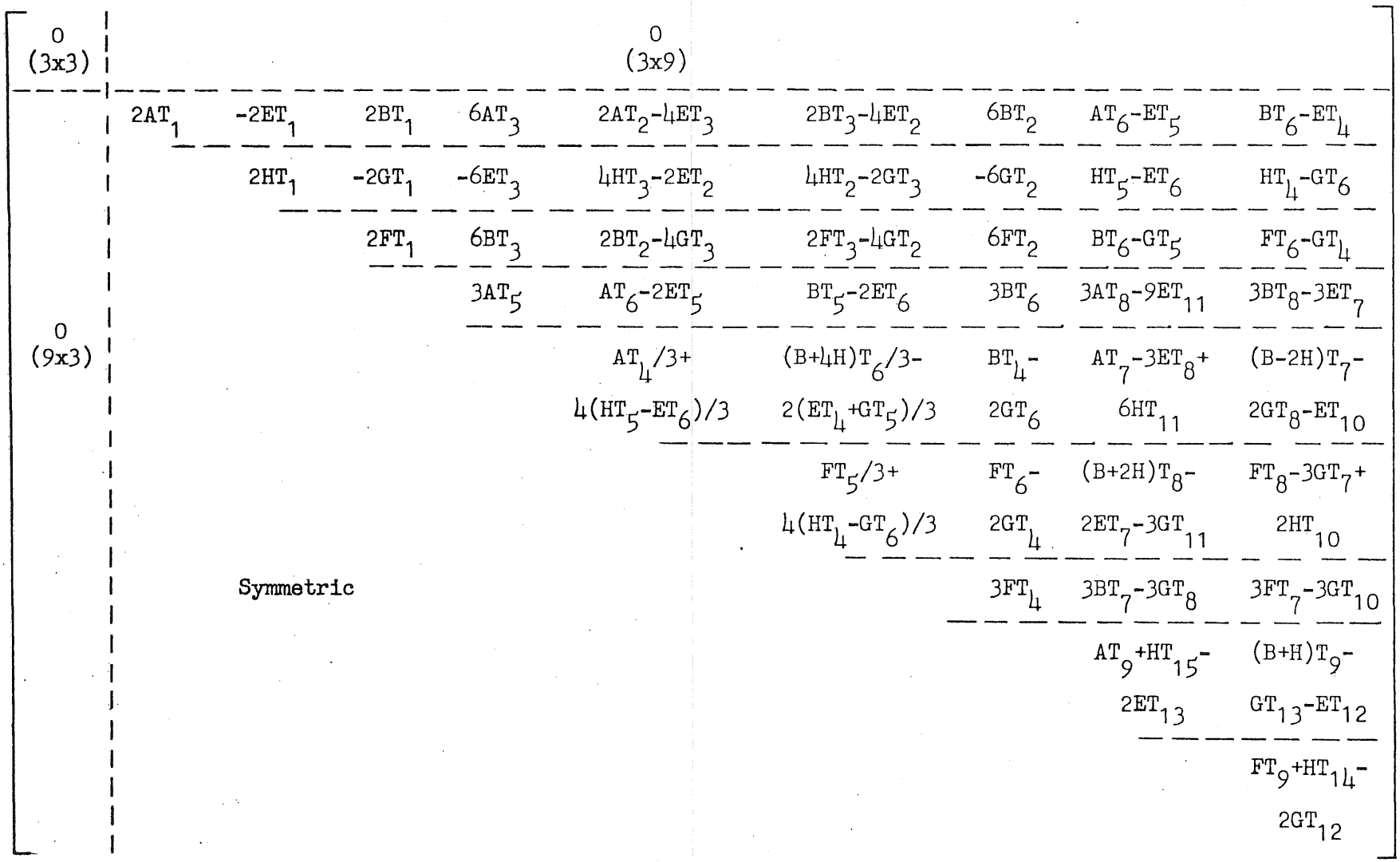

FIG. 4 $\bar{K}_f$ MATRIX (Continued on next page)

$$A = D_x + 2c^2D_1 + 4c^2D_{xy} + c^4D_y$$

$$B = s^2(D_1 + c^2D_y)$$

$$E = sc(D_1 + c^2D_y + 2D_{xy})$$

$$F = s^4D_y$$

$$G = s^3cD_y$$

$$H = s^2(c^2D_y + D_{xy})$$

$$c = \cos\alpha \,/\, \sin\alpha$$

$$s = 1 \,/\, \sin\alpha$$

$$T_1 = y_1(ky_1 + 2x_3)$$

$$T_2 = y_1^2(2ky_1/3 + x_3)$$

$$T_3 = y_1(k^2y_1^2/3 + kx_3y_1 + x_3^2)$$

$$T_4 = y_1^3(3ky_1 + 4x_3)$$

$$T_5 = y_1(k^3y_1^3 + 4k^2x_3y_1^2 + 6kx_3^2y_1 + 4x_3^3)$$

$$T_6 = y_1^2(1.5k^2y_1^2 + 4kx_3y_1 + 3x_3^2)$$

$$T_7 = y_1^3(1.2k^2y_1^2 + 3kx_3y_1 + 2x_3^2)$$

$$T_8 = y_1^2(.8k^3y_1^3 + 3k^2x_3y_1^2 + 4kx_3^2y_1 + 2x_3^3)$$

$$T_9 = y_1^3(2k^3y_1^3 + 7.2k^2x_3y_1^2 + 9kx_3^2y_1 + 4x_3^3)$$

$$T_{10} = y_1^4(2.4ky_1 + 3x_3)$$

$$T_{11} = y_1(.2k^4y_1^4 + k^3x_3y_1^3 + 2k^2x_3^2y_1^2 + 2kx_3^3y_1 + x_3^4)$$

$$T_{12} = y_1^4(3k^2y_1^2 + 7.2kx_3y_1 + 4.5x_3^2)$$

FIG. 4 (Continued on next page)

$$T_{13} = y_1^2(1.5k^4y_1^4 + 7.2k^3x_3y_1^3 + 13.5k^2x_3^2y_1^2 + 12kx_3^3y_1 + 4x_3^3)$$

$$T_{14} = y_1^5(6ky_1 + 7.2x_3)$$

$$T_{15} = y_1(1.2k^5y_1^5+7.2k^4x_3y_1^4+18k^3x_3^2y_1^3+24k^2x_3^3y_1^2+18kx_3^4y_1+7.2x_3^5)$$

$$k = (x_4 - x_3)/y_1$$

Note: D_x, D_1, D_y, and D_{xy} are given in Eq. (2.9)

FIG. 4, Continued

$$\begin{bmatrix}
1 & 0 & 0 & 0 & 0 & 0 & 0 & 0 \\
0 & 0 & 0 & 0 & 1 & 0 & 0 & 0 \\
1 & 0 & y_1 & 0 & 0 & 0 & 0 & 0 \\
0 & 0 & 0 & 0 & 1 & 0 & y_1 & 0 \\
1 & x_3 & 0 & 0 & 0 & 0 & 0 & 0 \\
0 & 0 & 0 & 0 & 1 & x_3 & 0 & 0 \\
1 & x_4 & y_1 & x_4y_1 & 0 & 0 & 0 & 0 \\
0 & 0 & 0 & 0 & 1 & x_4 & y_1 & x_4y_1
\end{bmatrix}$$

(a) C_p Matrix

$$\begin{bmatrix}
1 & 0 & 0 & 0 & 0 & 0 & 0 & 0 \\
-1/x_3 & 0 & 0 & 0 & 1/x_3 & 0 & 0 & 0 \\
-1/y_1 & 0 & 1/y_1 & 0 & 0 & 0 & 0 & 0 \\
1/(x_3y_1) & 0 & -1/(x_4y_1) & 0 & -1/(x_3y_1) & 0 & 1/(x_4y_1) & 0 \\
0 & 1 & 0 & 0 & 0 & 0 & 0 & 0 \\
0 & -1/x_3 & 0 & 0 & 0 & 1/x_3 & 0 & 0 \\
0 & -1/y_1 & 0 & 1/y_1 & 0 & 0 & 0 & 0 \\
0 & 1/(x_3y_1) & 0 & -1/(x_4y_1) & 0 & -1/(x_3y_1) & 0 & 1/(x_4y_1)
\end{bmatrix}$$

(b) C_p^{-1} Matrix

FIG. 5 C_p AND C_p^{-1} MATRICES

$$
\begin{bmatrix}
\frac{-1}{x_3} & 0 & 0 & 0 & \frac{1}{x_3} & 0 & 0 & 0 \\
\frac{1}{x_3\ y_1} & 0 & \frac{-1}{x_4 y_1} & 0 & \frac{-1}{x_3 y_1} & 0 & \frac{1}{x_4\ y_1} & 0 \\
\frac{-1}{y_1} & \frac{-1}{x_3} & \frac{1}{y_1} & 0 & 0 & \frac{1}{x_3} & 0 & 0 \\
0 & \frac{-1}{y_1} & 0 & \frac{1}{y_1} & 0 & 0 & 0 & 0 \\
0 & \frac{1}{x_3\ y_1} & 0 & \frac{-1}{x_4 y_1} & 0 & \frac{-1}{x_3 y_1} & 0 & \frac{1}{x_4\ y_1}
\end{bmatrix}
$$

FIG. 6 C_p^{-1*}

$$
\begin{bmatrix}
AT_1 & AT_2-ET_3 & -ET_1 & BT_1 & BT_3-ET_2 \\
 & AT_4-2ET_5+HT_6 & HT_3-ET_2 & BT_2-GT_3 & (B+H)T_5-ET_4-GT_6 \\
 & & HT_1 & -GT_1 & HT_2-GT_3 \\
\text{Symmetric} & & & FT_1 & FT_3-GT_2 \\
 & & & & HT_4-2GT_5+FT_6
\end{bmatrix}
$$

FIG. 7 $\bar{K}_p$ MATRIX (Continued on next page)

$$T_1 = y_1(0.5ky_1 + x_3)$$

$$T_2 = y_1^2(ky_1/3 + 0.5x_3)$$

$$T_3 = 0.5y_1(k^2y_1^2/3 + kx_3y_1 + x_3^2)$$

$$T_4 = y_1^3(0.25ky_1 + x_3^2)$$

$$T_5 = y_1^2(3k^2y_1^2 + 8kx_3y_1 + 6x_3^2)/24$$

$$T_6 = y_1(0.25k^3y_1^3 + k^2x_3y_1^2 + 1.5kx_3^2y_1 + x_3^3)/3$$

$$A = D_x + 2c^2D_1 + 4c^2D_{xy} + c^4D_y$$

$$B = s^2(D_1 + c^2D_y)$$

$$E = sc(D_1 + c^2D_y + 2D_{xy})$$

$$F = s^4D_y$$

$$G = s^3cD_y$$

$$H = s^2(c^2D_y + D_{xy})$$

$$c = \cos\alpha / \sin\alpha$$

$$s = 1 / \sin\alpha$$

$$k = (x_4 - x_3)/ y_1$$

Note: D_x, D_y, D_1, and D_{xy} are given in Eq. (2.29)

FIG. 7, Continued

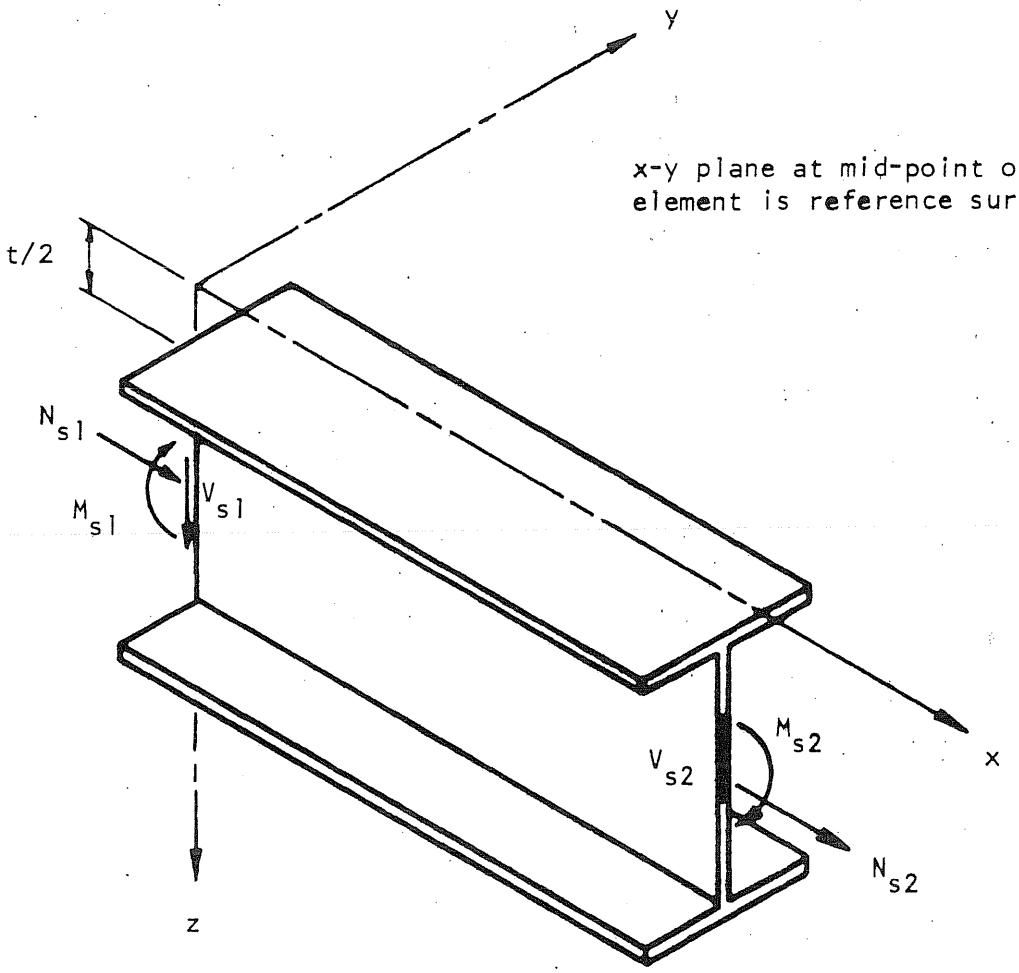

FIG. 8 ECCENTRIC STIFFENER ELEMENT

$$\begin{bmatrix} 0 & 0 & 1 & 0 & 0 & 0 \\ 0 & 0 & 0 & 1 & 0 & 0 \\ 1 & 0 & 0 & 0 & 0 & 0 \\ 0 & 0 & 1 & L & L^2 & L^3 \\ 0 & 0 & 0 & 1 & 2L & 3L^2 \\ 1 & L & 0 & 0 & 0 & 0 \end{bmatrix}$$

(a) C_s Matrix

$$\begin{bmatrix} 0 & 0 & 1 & 0 & 0 & 0 \\ 0 & 0 & -1/L & 0 & 0 & 1/L \\ 1 & 0 & 0 & 0 & 0 & 0 \\ 0 & 1 & 0 & 0 & 0 & 0 \\ -3/L^2 & -2/L & 0 & 3/L^2 & -1/L & 0 \\ 2/L^3 & 1/L^2 & 0 & -2/L^3 & 1/L^2 & 0 \end{bmatrix}$$

(b) C_s^{-1} Matrix

FIG. 9 C_s AND C_s^{-1} MATRICES

$$
\begin{bmatrix} V_{s1} \\ M_{s1} \\ T_{s1} \\ N_{s1} \\ V_{s2} \\ M_{s2} \\ T_{s2} \\ N_{s2} \end{bmatrix}
=
\begin{bmatrix}
\frac{12E_sI_x}{L^3} & \frac{6E_sI_x}{L^2} & 0 & 0 & \frac{-12E_sI_x}{L^3} & \frac{6E_sI_x}{L^2} & 0 & 0 \\
 & \frac{4E_sI_x}{L} & 0 & \frac{-E_sI_x}{L} & \frac{-6E_sI_x}{L^2} & \frac{2E_sI_x}{L} & 0 & \frac{E_sS_x}{L} \\
 & & \frac{JG}{L} & 0 & 0 & 0 & \frac{-JG}{L} & 0 \\
 & & & \frac{E_sA_s}{L} & 0 & \frac{E_sS_x}{L} & 0 & \frac{-E_sA_s}{L} \\
 & \text{Symmetric} & & & \frac{12E_sI_x}{L^3} & \frac{-6E_sI_x}{L^2} & 0 & 0 \\
 & F_s = \bar{K}_s\ u_s & & & & \frac{4E_sI_x}{L} & 0 & \frac{-E_sS_x}{L} \\
 & & & & & & \frac{JG}{L} & 0 \\
 & & & & & & & \frac{E_sA_s}{L}
\end{bmatrix}
\begin{bmatrix} w_1 \\ \theta_{y1} \\ \theta_{x1} \\ u_1 \\ w_2 \\ \theta_{y2} \\ \theta_{x2} \\ u_2 \end{bmatrix}
$$

FIG. 10 $\bar{K}_s$ MATRIX

$$
\begin{bmatrix}
T_1 & T_2 & T_3 & T_4 & T_5 & T_6 & T_7 & T_8 & T_9 & T_{10} & T_{11} & T_{12} \\
 & T_4 & T_5 & T_7 & T_8 & T_9 & T_{13} & T_{11} & T_{14} & T_{12} & T_{15} & T_{16} \\
 & & T_6 & T_8 & T_9 & T_{10} & T_{11} & T_{14} & T_{12} & T_{17} & T_{18} & T_{19} \\
 & & & T_{13} & T_{11} & T_{14} & T_{20} & T_{15} & T_{18} & T_{16} & T_{21} & T_{22} \\
 & & & & T_{14} & T_{12} & T_{15} & T_{18} & T_{16} & T_{19} & T_{23} & T_{24} \\
 & & & & & T_{17} & T_{18} & T_{16} & T_{19} & T_{25} & T_{22} & T_{26} \\
 & & & & & & T_{27} & T_{21} & T_{23} & T_{22} & T_{28} & T_{29} \\
 & & & & & & & T_{23} & T_{22} & T_{24} & T_{30} & T_{31} \\
 & & & & & & & & T_{24} & T_{26} & T_{29} & T_{32} \\
 & & & & & & & & & T_{33} & T_{31} & T_{34} \\
 & & & & & & & & & & T_{35} & T_{36} \\
 & & & & & & & & & & & T_{37}
\end{bmatrix}
$$

Symmetric

(Figure continued on next page)

FIG. 11 $\int_0^{\overline{y}_1 \sin \alpha} \int_0^{ky+x_3} Z_f^T Z_f \, dx \, dy$

$$T_1 = y_1(0.5ky_1 + x_3)$$

$$T_2 = 0.5y_1(k^2y_1^2/3 + kx_3y_1 + x_3^2)$$

$$T_3 = y_1^2(ky_1/3 + 0.5x_3)$$

$$T_4 = y_1(k^3y_1^3 + 4k^2x_3y_1^2 + 6kx_3^2y_1 + 4x_3^3)/12$$

$$T_5 = y_1^2(3k^2y_1^2 + 8kx_3y_1 + 6x_3^2)/24$$

$$T_6 = y_1^3(3ky_1 + 4x_3)/12$$

$$T_7 = y_1(0.2k^4y_1^4 + k^3x_3y_1^3 + 2k^2x_3^2y_1^2 + 2kx_3^3y_1 + x_3^4)/4$$

$$T_8 = y_1^2(0.8k^3y_1^3 + 3k^2x_3y_1^2 + 4kx_3^2y_1 + 2x_3^3)/12$$

$$T_9 = y_1^3(1.2k^2y_1^2 + 3kx_3y_1 + 2x_3^2)/12$$

$$T_{10} = y_1^4(4ky_1 + 5x_3)/20$$

$$T_{11} = y_1^2(k^4y_1^4 + 4.8k^3x_3y_1^3 + 9k^2x_3^2y_1^2 + 8kx_3^3y_1 + 3x_3^4)/24$$

$$T_{12} = y_1^4(2k^2y_1^2 + 4.8kx_3y_1 + 3x_3^2)/24$$

$$T_{13} = y_1(k^5y_1^5 + 6k^4x_3y_1^4 + 15k^3x_3^2y_1^3 + 20k^2x_3^3y_1^2 + 15kx_3^4y_1 + 6x_3^5)/30$$

$$T_{14} = y_1^3(2k^3y_1^3 + 7.2k^2x_3y_1^2 + 9kx_3^2y_1 + 4x_3^3)/36$$

$$T_{15} = y_1^2(6k^5y_1^5/7 + 5k^4x_3y_1^4 + 12k^3x_3^2y_1^3 + 15k^2x_3^3y_1^2 + 10kx_3^4y_1 + 3x_3^5)/30$$

$$T_{16} = y_1^4(20k^3y_1^3/7 + 10k^2x_3y_1^2 + 12kx_3^2y_1 + 5x_3^3)/60$$

FIG. 11, Continued

$$T_{17} = y_1^5(5ky_1 + 6x_3)/30$$

$$T_{18} = y_1^3(3k^4y_1^4/7 + 2k^3x_3y_1^3 + 3.6k^2x_3^2y_1^2 + 3kx_3^3y_1 + x_3^4)/12$$

$$T_{19} = y_1^5(3k^2y_1^2 + 7kx_3y_1 + 4.2x_3^2)/42$$

$$T_{20} = y_1(k^6y_1^6/7 + k^5x_3y_1^5 + 3k^4x_3^2y_1^4 + 5k^3x_3^3y_1^3 + 5k^2x_3^4y_1^2 + 3kx_3^5y_1 + x_3^6)/6$$

$$T_{21} = y_1^2(k^6y_1^6 + 48k^5x_3y_1^5/7 + 20k^4x_3^2y_1^4 + 32k^3x_3^3y_1^3 + 30k^2x_3^4y_1^2 + 16kx_3^5y_1 + 4x_3^6)/48$$

$$T_{22} = y_1^4(k^4y_1^4 + 32k^3x_3y_1^3/7 + 8k^2x_3^2y_1^2 + 6.4kx_3^3y_1 + 2x_3^4)/32$$

$$T_{23} = y_1^3(0.3k^5y_1^5 + 12k^4x_3y_1^4/7 + 4k^3x_3^2y_1^3 + 4.8k^2x_3^3y_1^2 + 3kx_3^4y_1 + 0.8x_3^5)/12$$

$$T_{24} = y_1^5(k^3y_1^3 + 24k^2x_3y_1^2/7 + 4kx_3^2y_1 + 1.6x_3^3)/24$$

$$T_{25} = y_1^6(ky_1/7 + x_3/6)$$

$$T_{26} = y_1^6(3k^2y_1^2 + 48kx_3y_1/7 + 4x_3^2)/48$$

$$T_{27} = y_1(k^7y_1^7 + 8k^6x_3y_1^6 + 28k^5x_3^2y_1^5 + 56k^4x_3^3y_1^4 + 70k^3x_3^4y_1^3 + 56k^2x_3^5y_1^2 + 28kx_3^6y_1 + 8x_3^7)/56$$

$$T_{28} = y_1^2(k^7y_1^7 + 63k^6x_3y_1^6/8 + 27k^5x_3^2y_1^5 + 52.5k^4x_3^3y_1^4 + 63k^3x_3^4y_1^3 + 189k^2x_3^5y_1^2/4 + 21kx_3^6y_1 + 4.5x_3^7)/63$$

FIG. 11, Continued

$$T_{29} = y_1^4(4k^5y_1^5/9 + 2.5k^4x_3y_1^4 + 40k^3x_3^2y_1^3/7 + 20k^2x_3^3y_1^2/3 + 4kx_3^4y_1 + x_3^5)/20$$

$$T_{30} = y_1^3(k^6y_1^6 + 6.75k^5x_3y_1^5 + 135k^4x_3^2y_1^4/7 + 30k^3x_3^3y_1^3 + 27k^2x_3^4y_1^2 + 13.5kx_3^5y_1 + 3x_3^6)/54$$

$$T_{31} = y_1^5(k^4y_1^4 + 4.5k^3x_3y_1^3 + 18k^2x_3^2y_1^2/7 + 6kx_3^3y_1 + 1.8x_3^4)/36$$

$$T_{32} = y_1^6(k^3y_1^3/27 + k^2x_3y_1^2/8 + kx_3^2y_1/7 + x_3^3/18)$$

$$T_{33} = y_1^7(ky_1/8 + x_3/7)$$

$$T_{34} = y_1^7(7k^2y_1^2 + 15.75kx_3y_1 + 9x_3^2)/126$$

$$T_{35} = y_1^3(3k^7y_1^7 + 70k^6x_3y_1^6/3 + 105k^5x_3^2y_1^5/4 + 150k^4x_3^3y_1^4 + 175k^3x_3^4y_1^3 + 126k^2x_3^5y_1^2 + 52.5kx_3^6y_1 + 10x_3^7)/210$$

$$T_{36} = y_1^5(k^5y_1^5 + 50k^4x_3y_1^4/9 + 12.5k^3x_3^2y_1^3 + 100k^2x_3^3y_1^2/7 + 25kx_3^4y_1/3 + 2x_3^5)/50$$

$$T_{37} = y_1^7(k^3y_1^3/30 + k^2x_3y_1^2/9 + kx_3^2y_1/8 + x_3^3/21)$$

$$k = (x_4 - x_3)/\bar{y}_1$$

$$y_1 = \bar{y}_1 \sin \alpha$$

FIG. 11, Continued

$$
\begin{bmatrix}
6xy(1 - x/L)/L^2 & 0 & 1 - 3(x/L)^2 + 2(x/L)^3 \\
y(-1 + 4x/L - 3(x/L)^2) & 0 & x(1 - 2x/L + (x/L)^2) \\
0 & y(x/L - 1) & z(x/L - 1) \\
1 - x/L & 0 & 0 \\
6xy(x/L - 1)/L^2 & 0 & (3 - 2x/L)(x/L)^2 \\
xy(2 - 3x/L)/L & 0 & x^2(x/L - 1)/L \\
0 & -xy/L & -xz/L \\
x/L & 0 & 0
\end{bmatrix}
$$

FIG. 12 Z_m^T

$$\rho AL \begin{bmatrix}
\frac{1}{3} & 0 & 0 & 0 & \frac{1}{6} & 0 & 0 & 0 \\
 & \frac{13}{35} + \frac{6I_z}{5AL^2} & 0 & \frac{11L}{210} + \frac{I_z}{10AL} & 0 & \frac{9}{70} - \frac{6I_z}{5AL^2} & 0 & \frac{-13L}{420} + \frac{I_z}{10AL} \\
 & & \frac{J}{3A} & 0 & 0 & 0 & \frac{J}{6A} & 0 \\
 & & & \frac{L^2}{105} + \frac{2I_z}{15A} & 0 & \frac{13L}{420} - \frac{I_z}{10AL} & 0 & \frac{-L^2}{140} - \frac{I_z}{30A} \\
 & \text{Symmetric} & & & \frac{1}{3} & 0 & 0 & 0 \\
 & & & & & \frac{13}{35} + \frac{6I_z}{5AL^2} & 0 & \frac{-11L}{210} - \frac{I_z}{10AL} \\
 & & & & & & \frac{J}{3A} & 0 \\
 & & & & & & & \frac{L^2}{105} + \frac{2I_z}{15A}
\end{bmatrix}$$

FIG. 13 $\bar{M}_s$

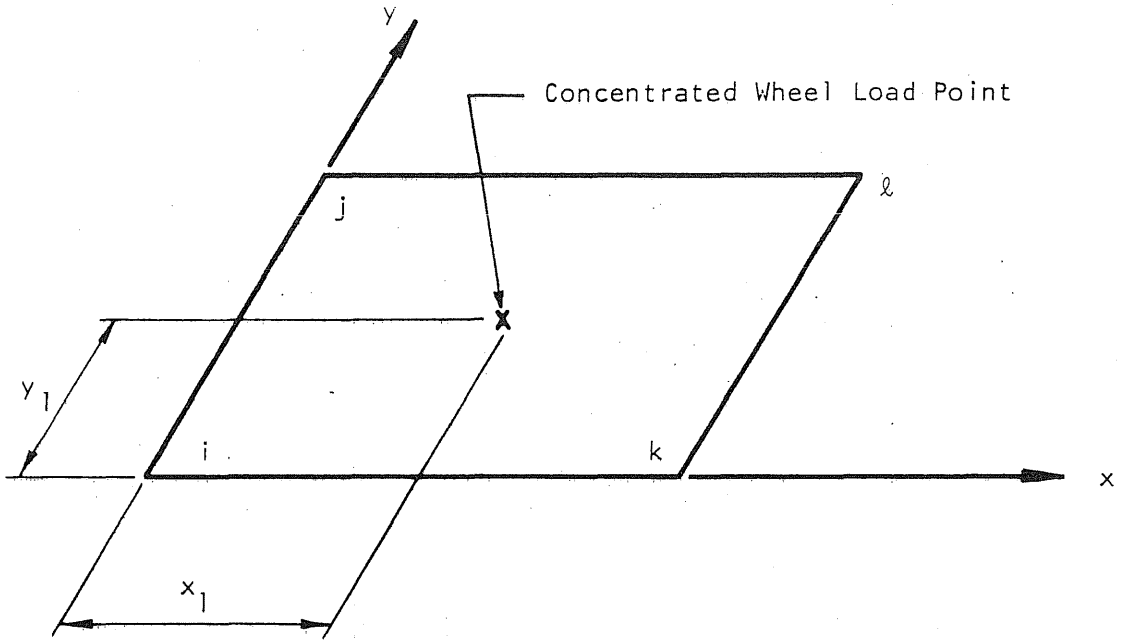

FIG. 14 LOCATION OF CONCENTRATED WHEEL LOADS

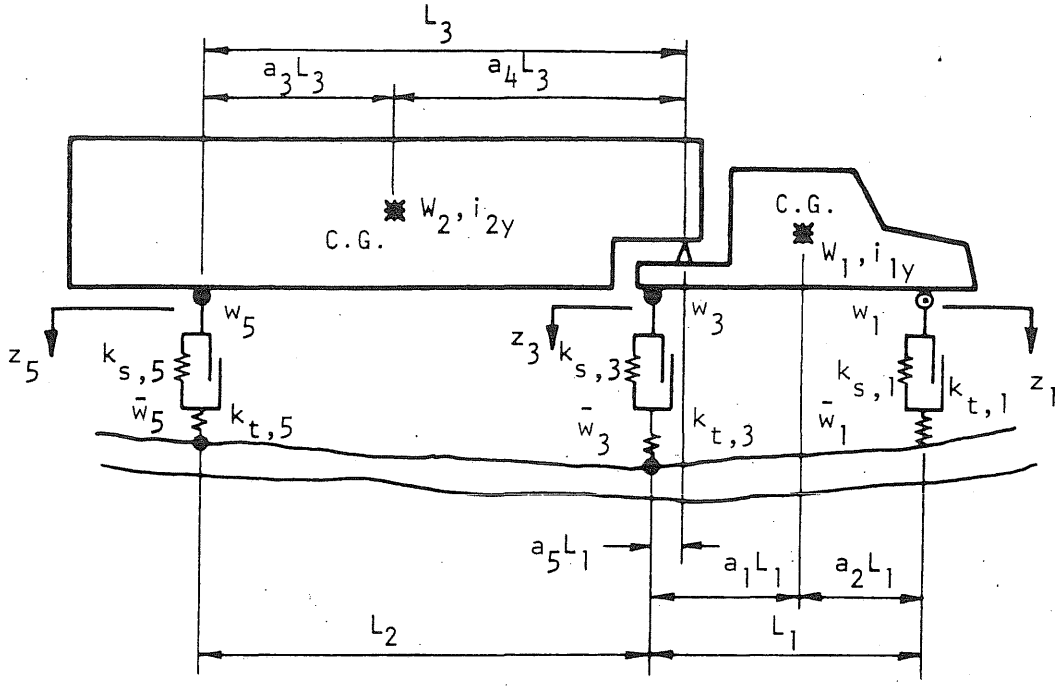

(a) Side View

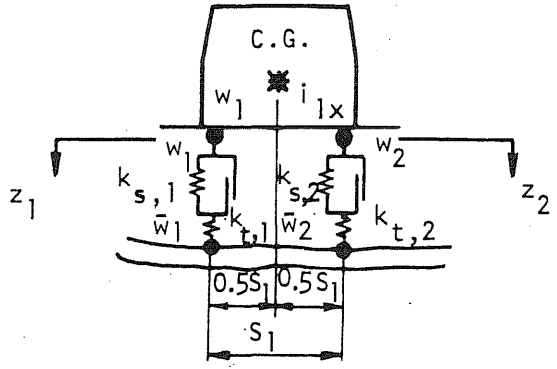

(b) Front View

FIG. 15 TRACTOR-TRAILER VEHICLE MODEL

$$
\begin{bmatrix}
T_1 & T_2 & T_3 & -T_4 & -T_5 & -T_5 \\
 & T_6 & T_7 & T_4 & T_8 & T_8 \\
 & & T_9 & T_4 & T_{10} & T_{10} \\
\text{Symmetric} & & & & & \\
 & & & -T_4 & 0 & 0 \\
 & & & & T_{11} & T_{12} \\
 & & & & & T_{13}
\end{bmatrix}
$$

FIG. 16 [m] MATRIX (Continued on next page)

$$T_1 = ((a_1-a_2)(a_1-a_2+i_{1x}) + 4a_1a_2i_{1y})\frac{W_1}{4g} + a_3(1-2a_5)^2\ (a_3+a_4i_{2y})\frac{W_2}{4g} + \frac{w_1}{g}$$

$$T_2 = (a_1-a_2-i_{1x})\frac{W_1}{4g} - a_3(1-2a_5)(a_3+a_4i_{2y})\frac{W_2}{4g}$$

$$T_3 = a_2(a_1(1-2i_{1y})-a_2)\frac{W_1}{2g} - a_3(1-a_5)(1-2a_5)(a_3+a_4i_{2y})\frac{W_2}{2g}$$

$$T_4 = \frac{w_4}{g}$$

$$T_5 = a_3a_4(1-2a_5)(1-i_{2y})\frac{W_2}{4g}$$

$$T_6 = (1+i_{1x})\frac{W_1}{4g} + a_3(a_3+a_4i_{2y})\frac{W_2}{4g} + \frac{w_2}{g}$$

$$T_7 = a_2\frac{W_1}{2g} + a_3(1-a_5)(a_3+a_4i_{2y})\frac{W_2}{2g}$$

$$T_8 = a_3a_4(1-i_{2y})\frac{W_2}{4g}$$

$$T_9 = a_2(a_2+a_1i_{1y})\frac{W_1}{g} + a_3(1-a_5)^2\ (a_3+a_4i_{2y})\frac{W_2}{g} + \frac{w_3}{g}$$

$$T_{10} = a_3a_4(1-a_5)(1-i_{2y})\frac{W_2}{2g}$$

$$T_{11} = (a_4+i_{2x}-a_3a_4(1-i_{2y}))\frac{W_2}{4g} + \frac{w_5}{g}$$

$$T_{12} = (a_4-i_{2x}-a_3a_4(1-i_{2y}))\frac{W_2}{4g}$$

$$T_{13} = (a_4+i_{2x}-a_3a_4(1-i_{2y}))\frac{W_2}{4g} + \frac{w_6}{g}$$

FIG. 16, Continued

$$
\begin{bmatrix}
k_1 & 0 & 0 & -k_4 & 0 & 0 \\
0 & k_2 & 0 & k_4 & 0 & 0 \\
0 & 0 & k_3 & k_4 & 0 & 0 \\
-k_4 & k_4 & k_4 & -k_4 & 0 & 0 \\
0 & 0 & 0 & 0 & k_5 & 0 \\
0 & 0 & 0 & 0 & 0 & k_6
\end{bmatrix}
$$

FIG. 17 k_v MATRIX

$$\begin{bmatrix} 1 & 0 & 0 & -1 & 0 & 0 \\ 0 & 1 & 0 & 1 & 0 & 0 \\ 0 & 0 & 1 & 1 & 0 & 0 \\ 0 & 0 & 0 & 0 & 0 & 0 \\ 0 & 0 & 0 & 0 & 1 & 0 \\ 0 & 0 & 0 & 0 & 0 & 1 \end{bmatrix}$$

FIG. 18 h MATRIX

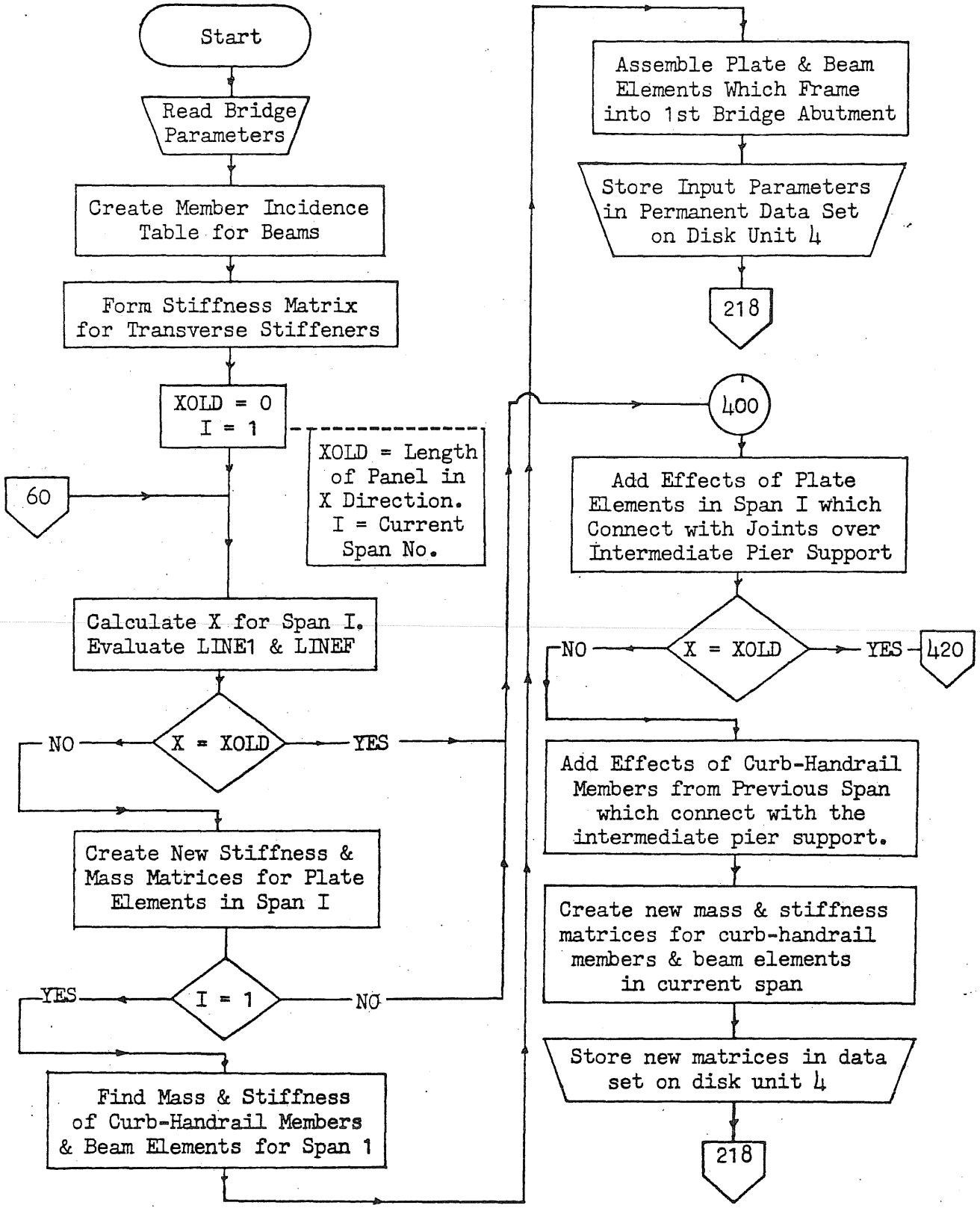

FIG. 19 GENERAL FLOW CHART FOR PROGRAM 1

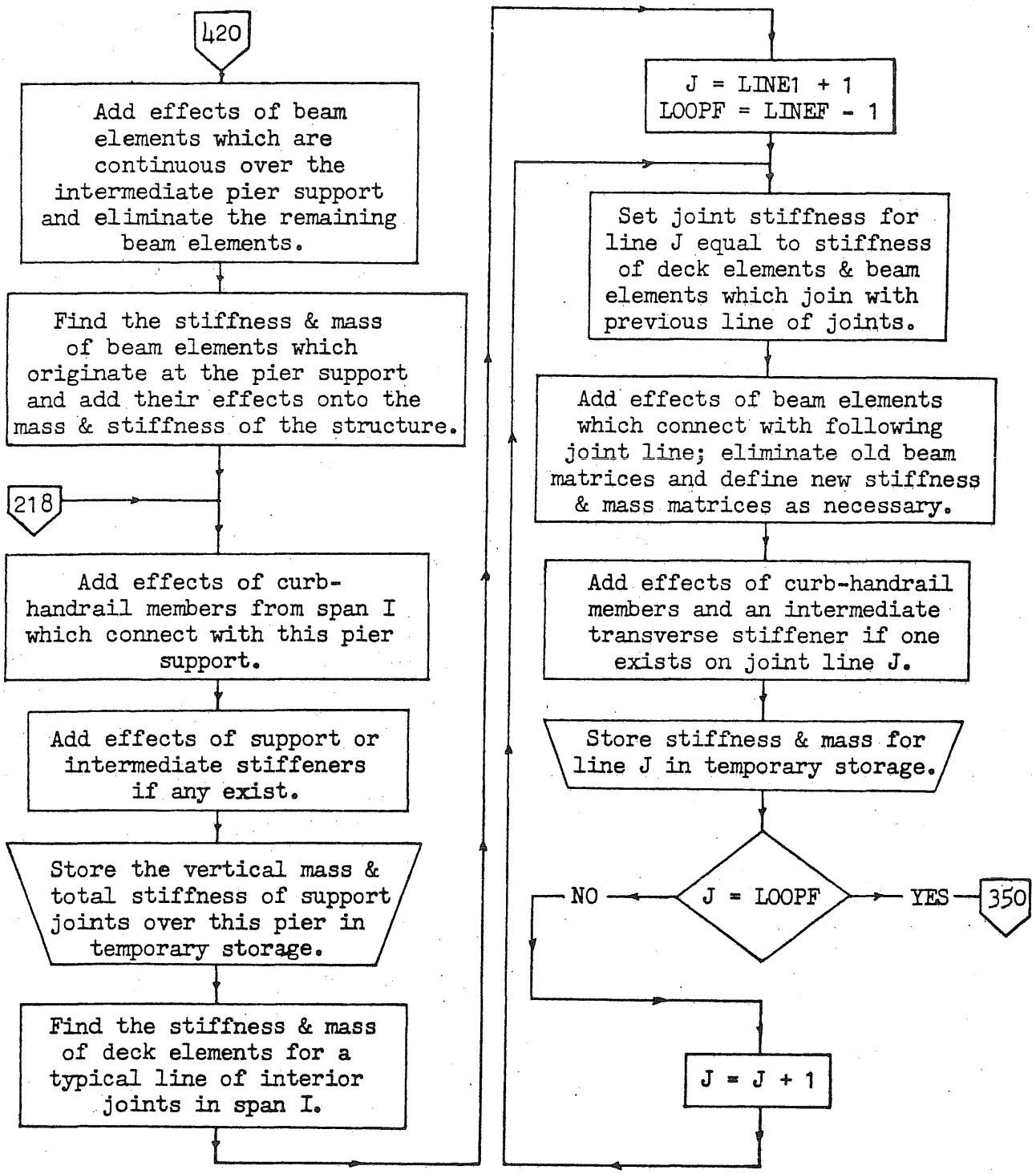

FIG. 19, Continued

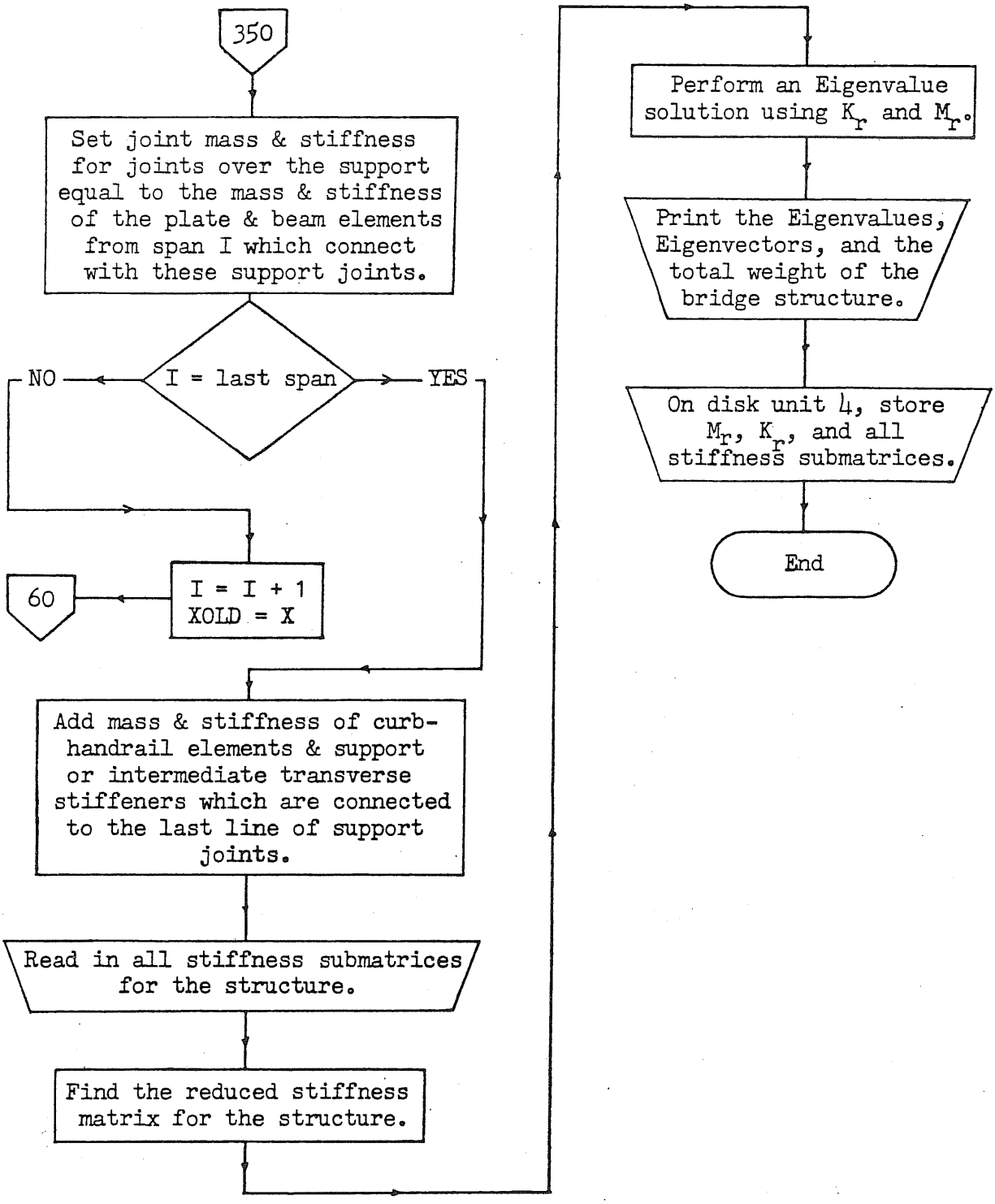

FIG. 19, Continued

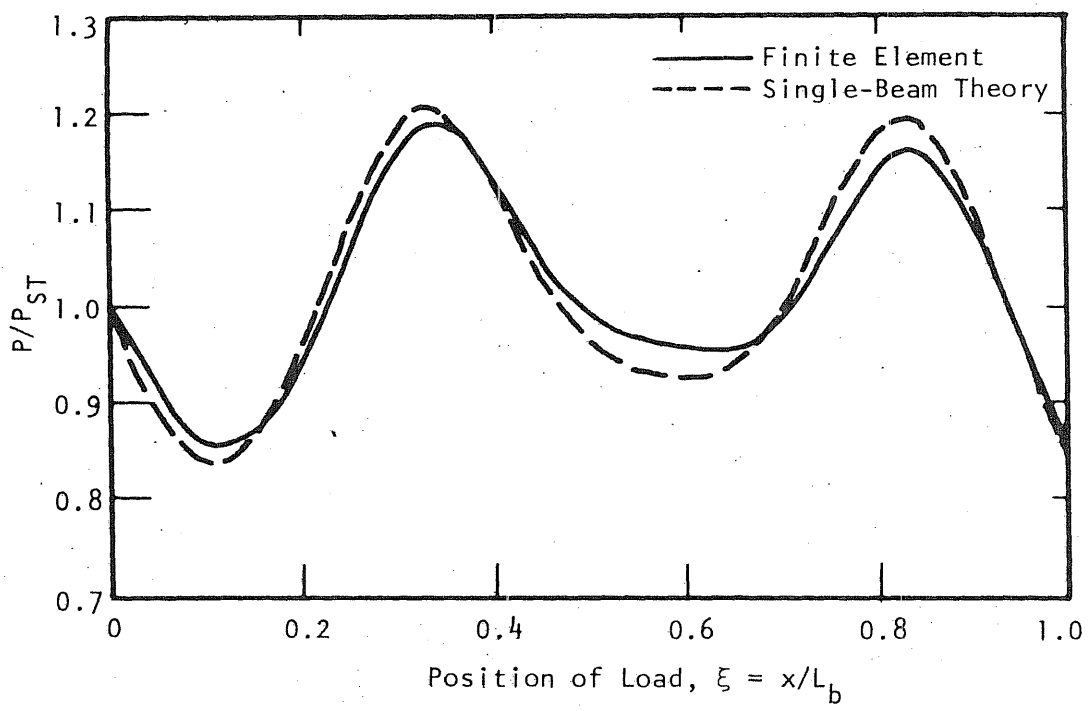

FIG. 20 INTERACTING FORCE, SOLUTION 6, TABLE 1

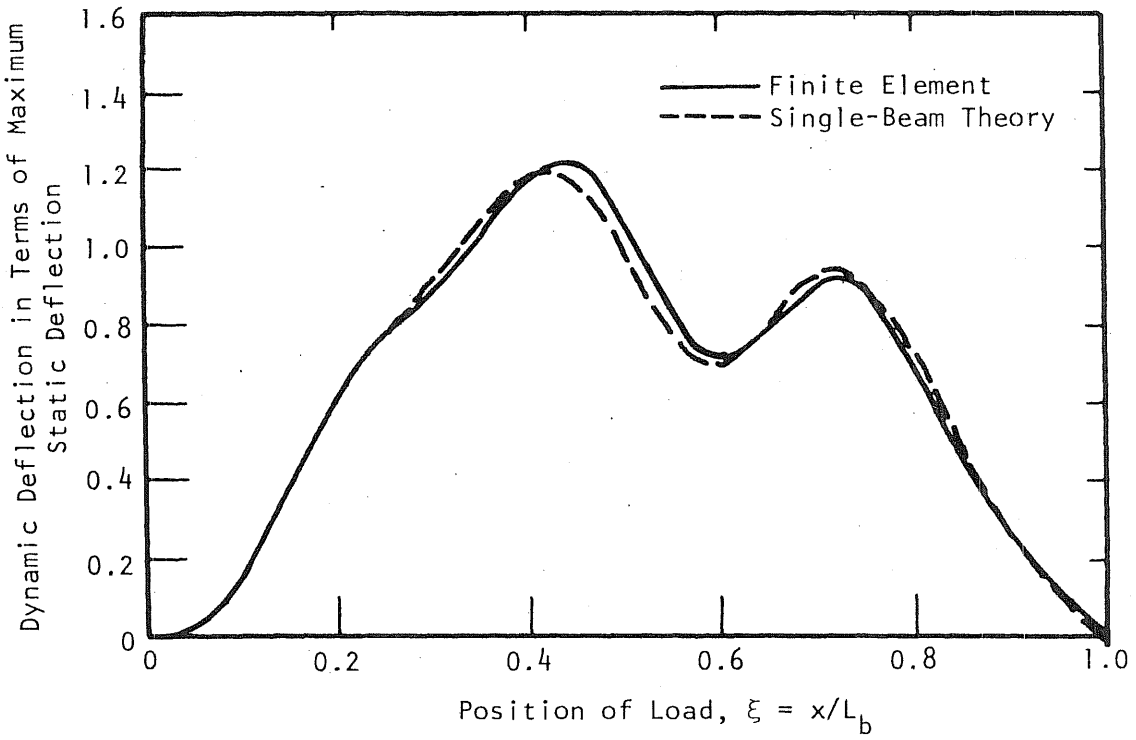

FIG. 21 DYNAMIC DEFLECTION AT MIDSPAN, SOLUTION 6, TABLE 1

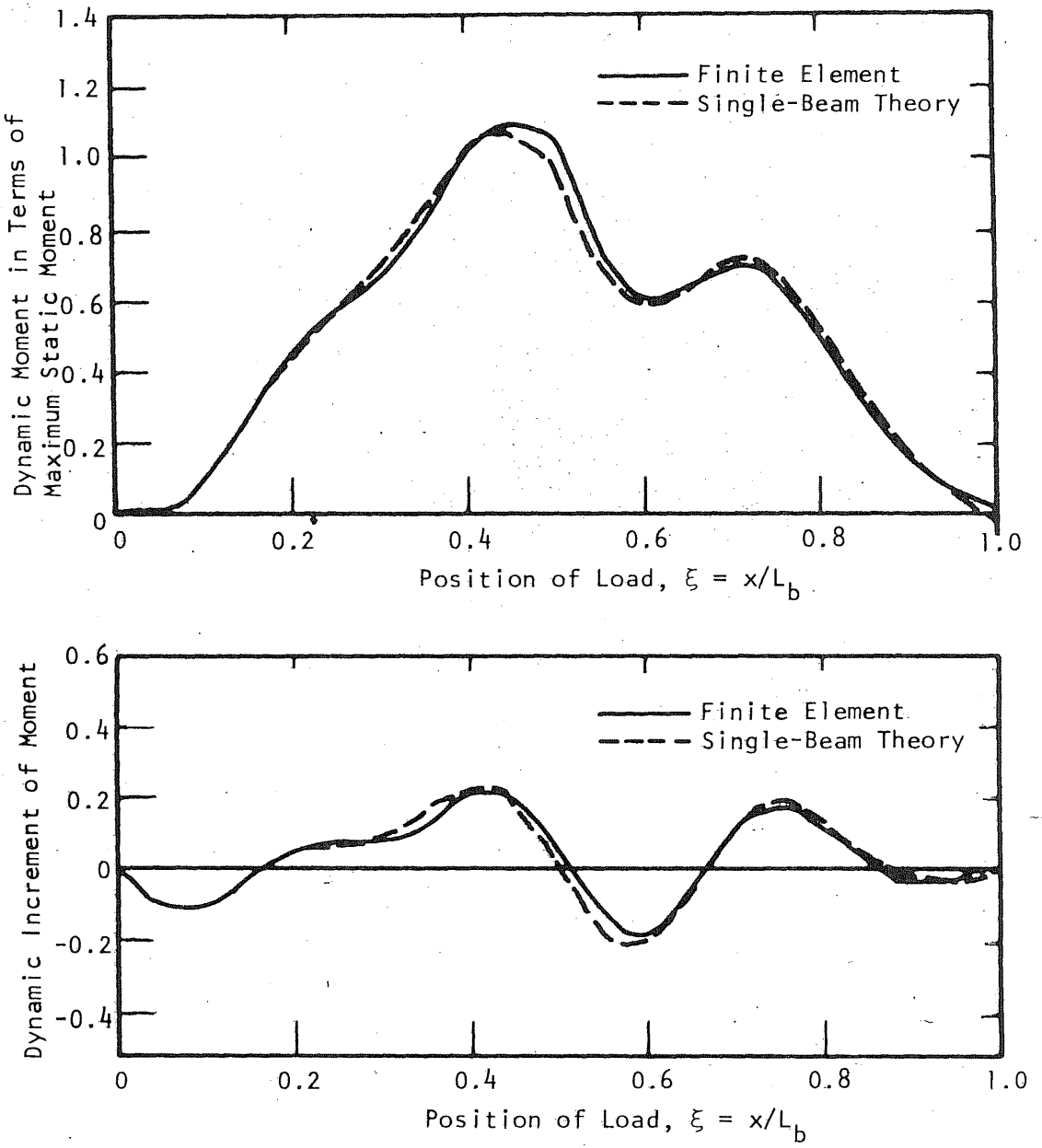

FIG. 22 DYNAMIC MOMENT AT MIDSPAN, SOLUTION 6, TABLE 1

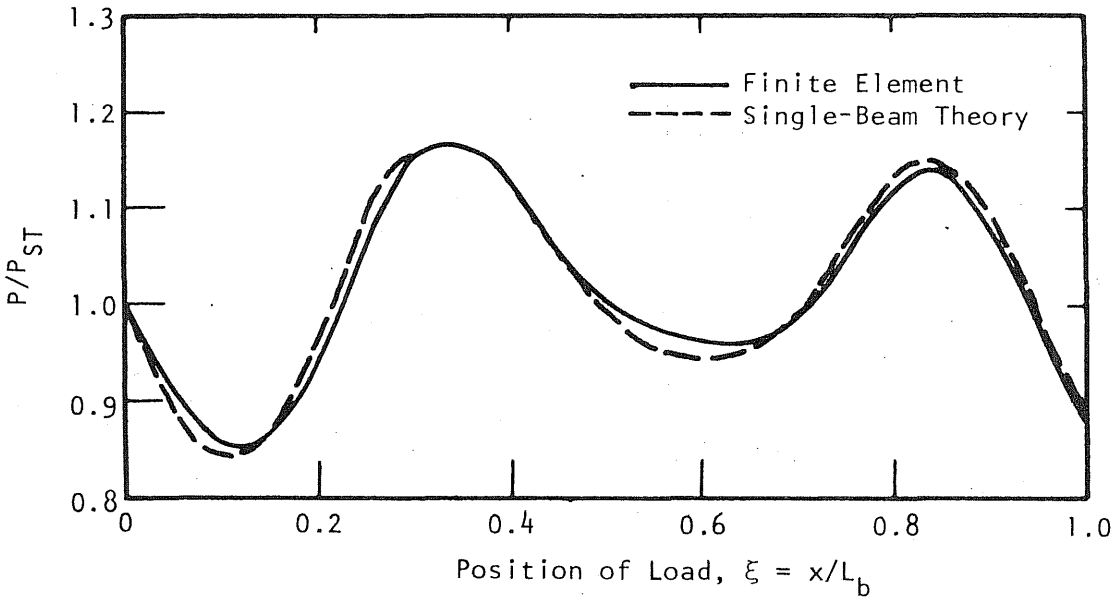

FIG. 23 INTERACTING FORCE, SOLUTION 9, TABLE 1

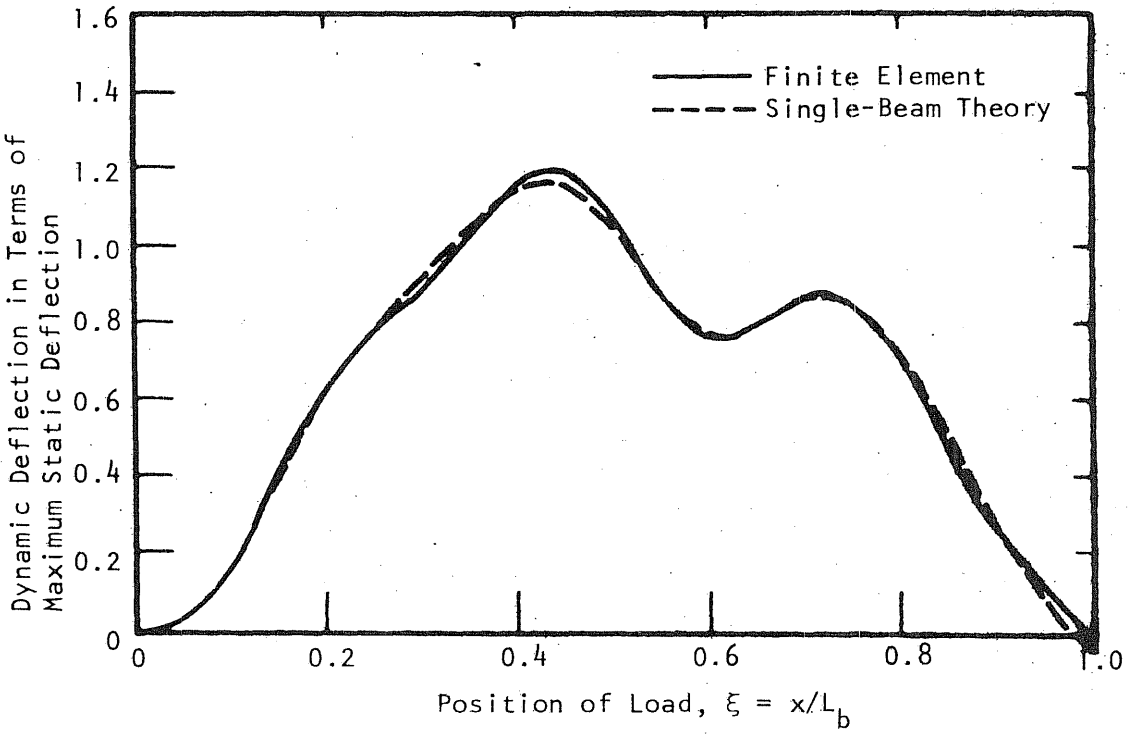

FIG. 24 DYNAMIC DEFLECTION AT MIDSPAN, SOLUTION 9, TABLE 1

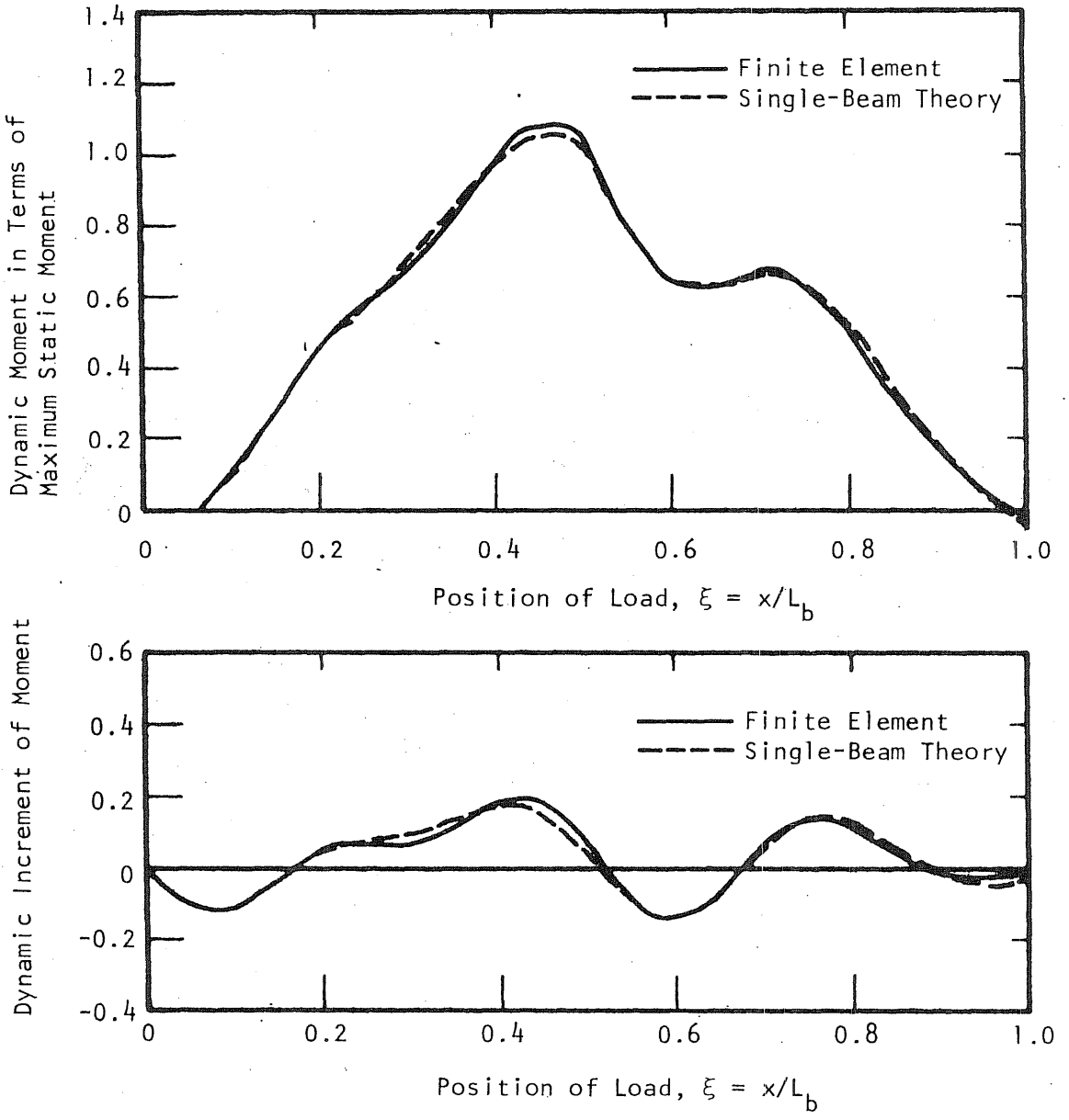

FIG. 25 DYNAMIC MOMENT AT MIDSPAN, SOLUTION 9, TABLE 1

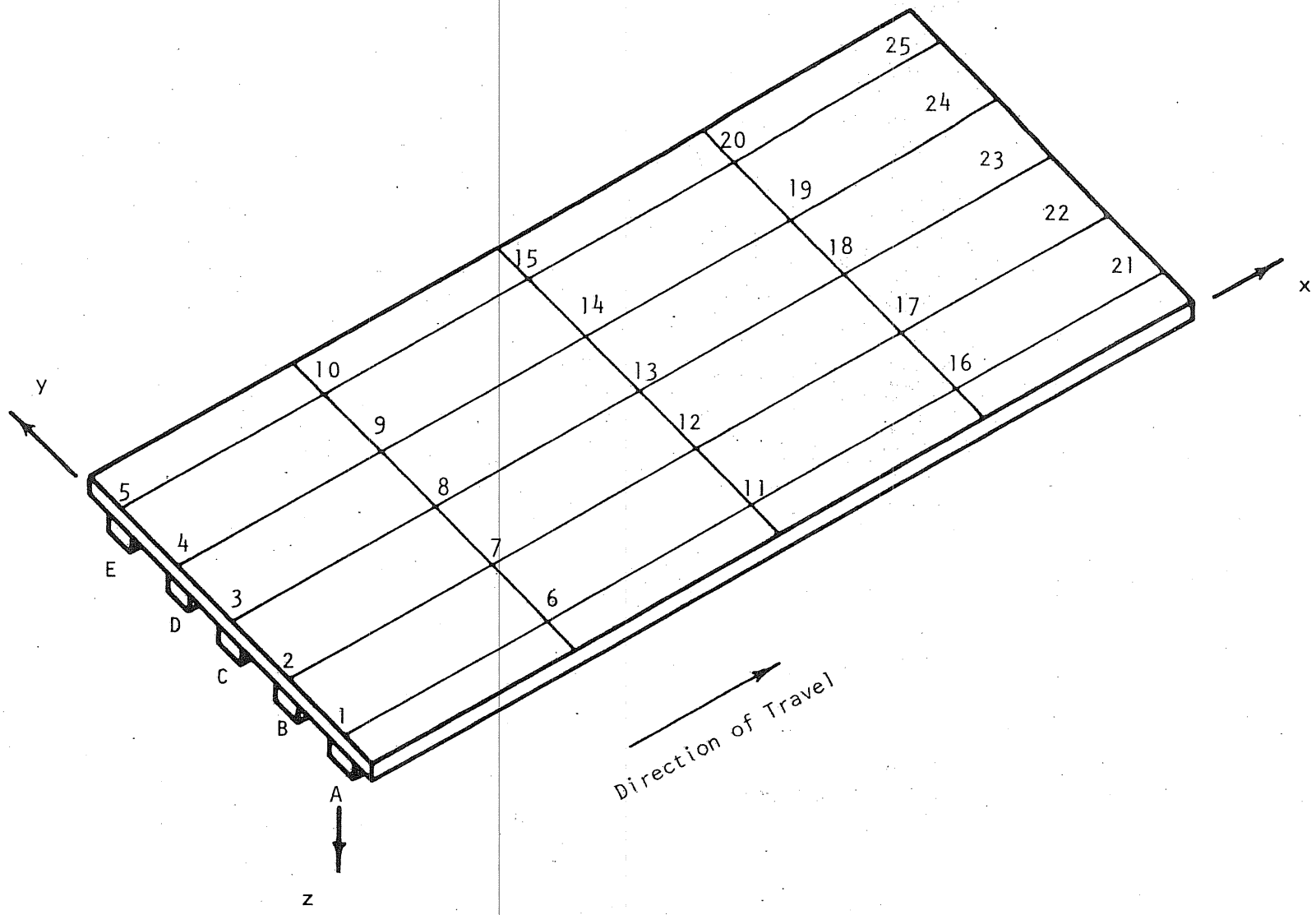

FIG. 26 SINGLE-SPAN, FIVE-GIRDER ALUMINUM BRIDGE MODEL

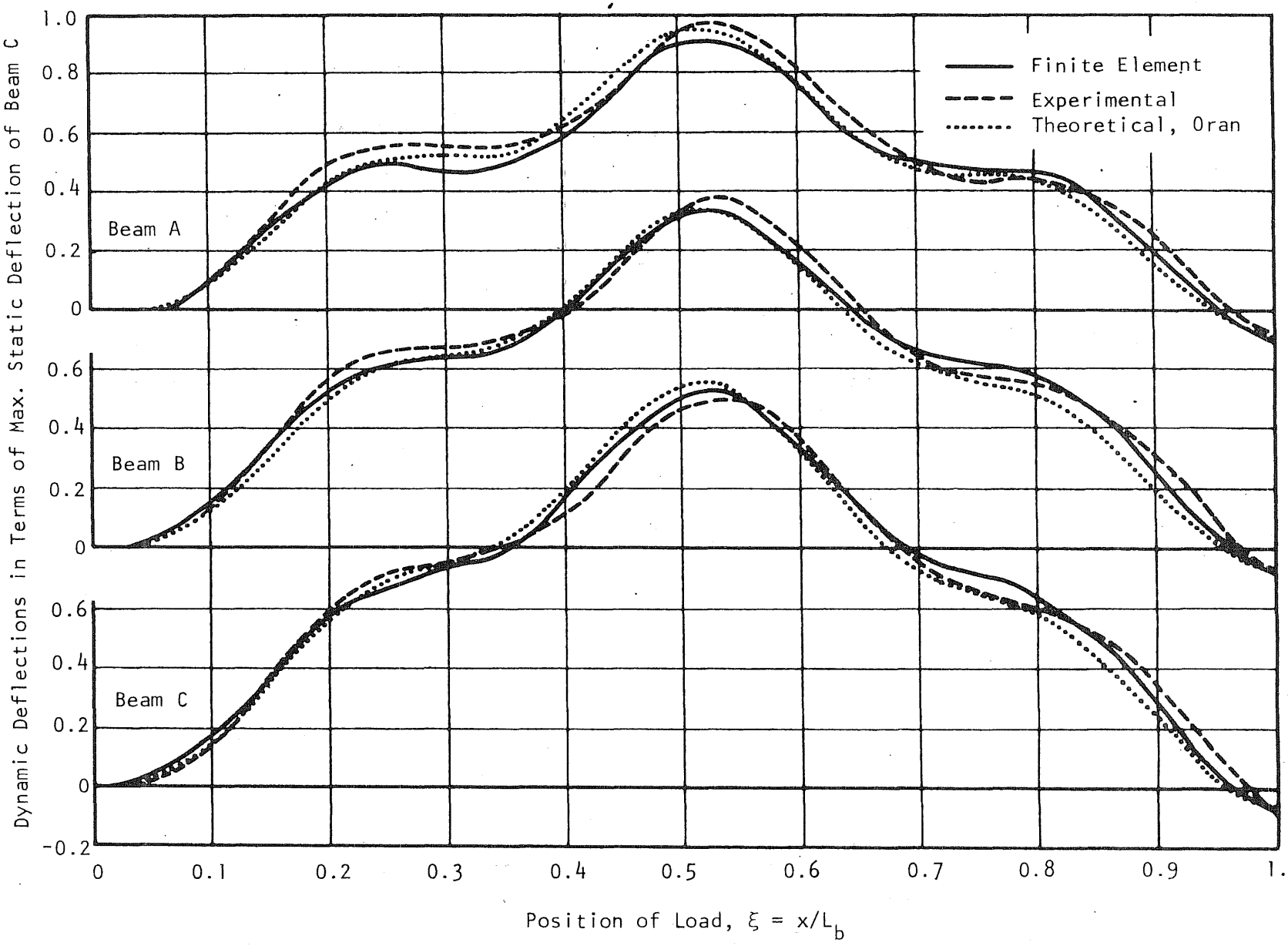

FIG. 27 COMPARISON OF THEORETICAL AND EXPERIMENTAL DEFLECTION CURVES, LOAD OVER BEAM C

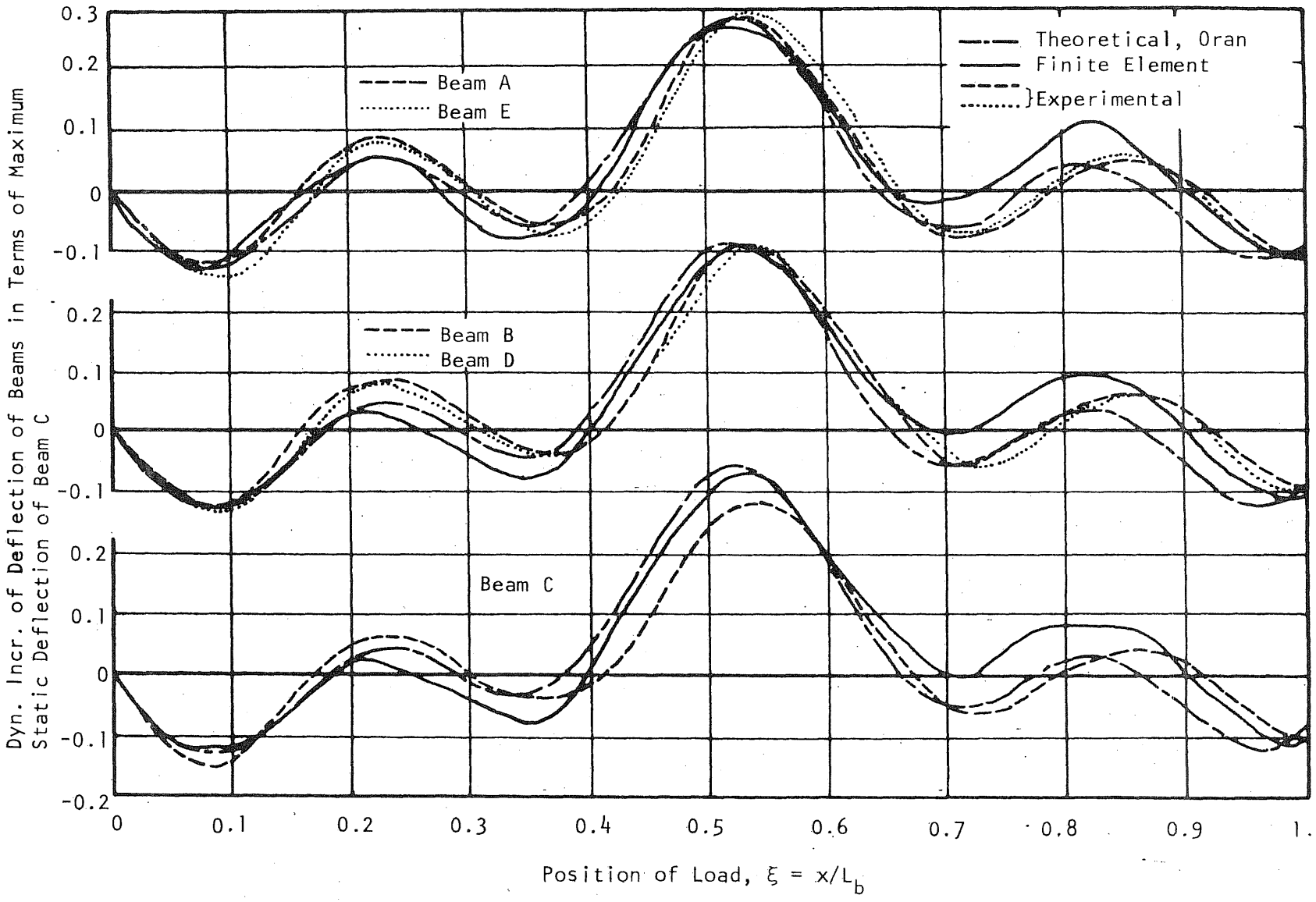

FIG. 28 COMPARISON OF THEORETICAL AND EXPERIMENTAL CURVES FOR DYNAMIC INCREMENT OF DEFLECTION, LOAD OVER BEAM C

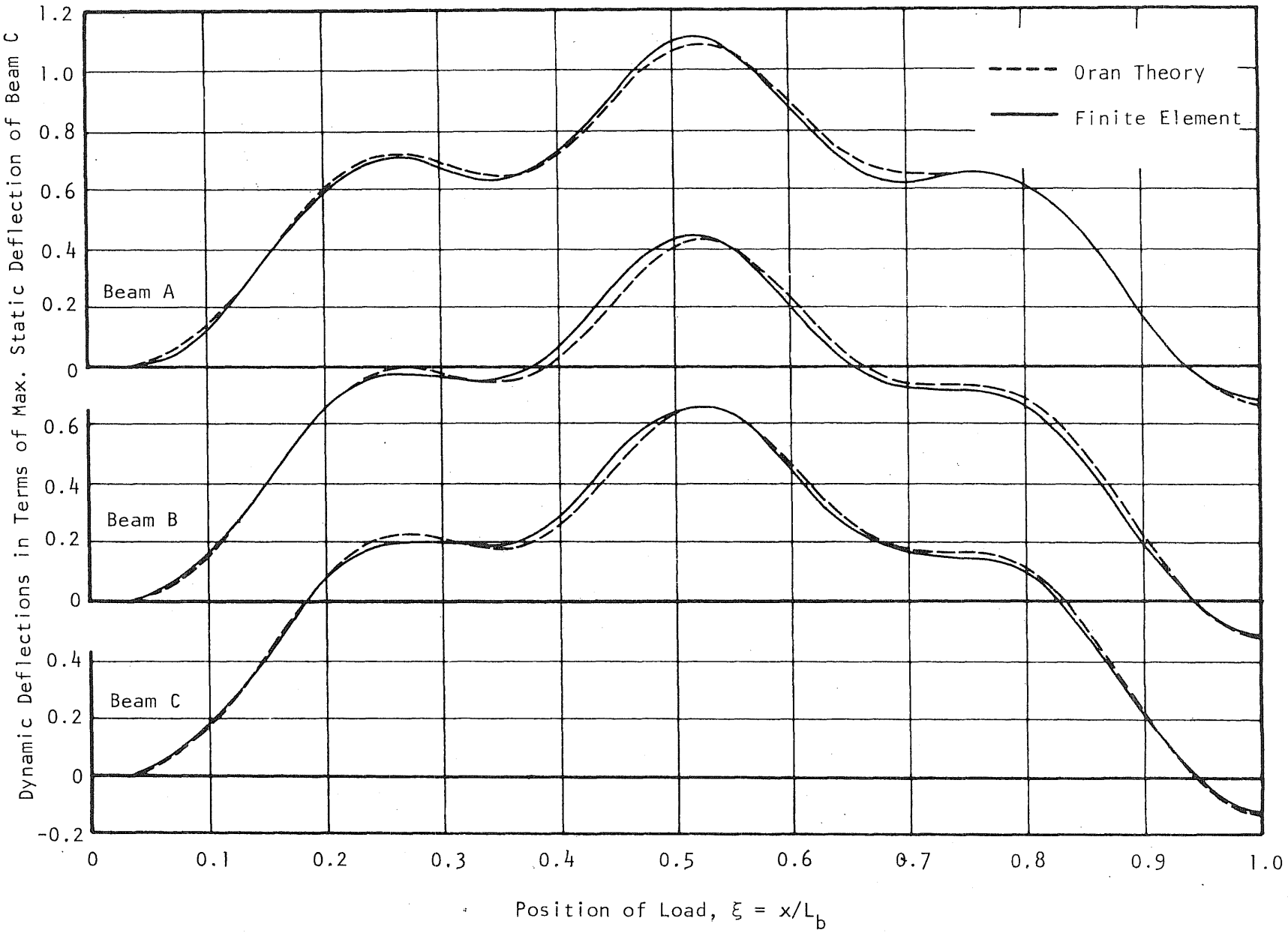

FIG. 29 COMPARISON OF THEORETICAL DEFLECTION CURVES, LOAD OVER BEAM C;
No Torsion, Composite Action, or Camber

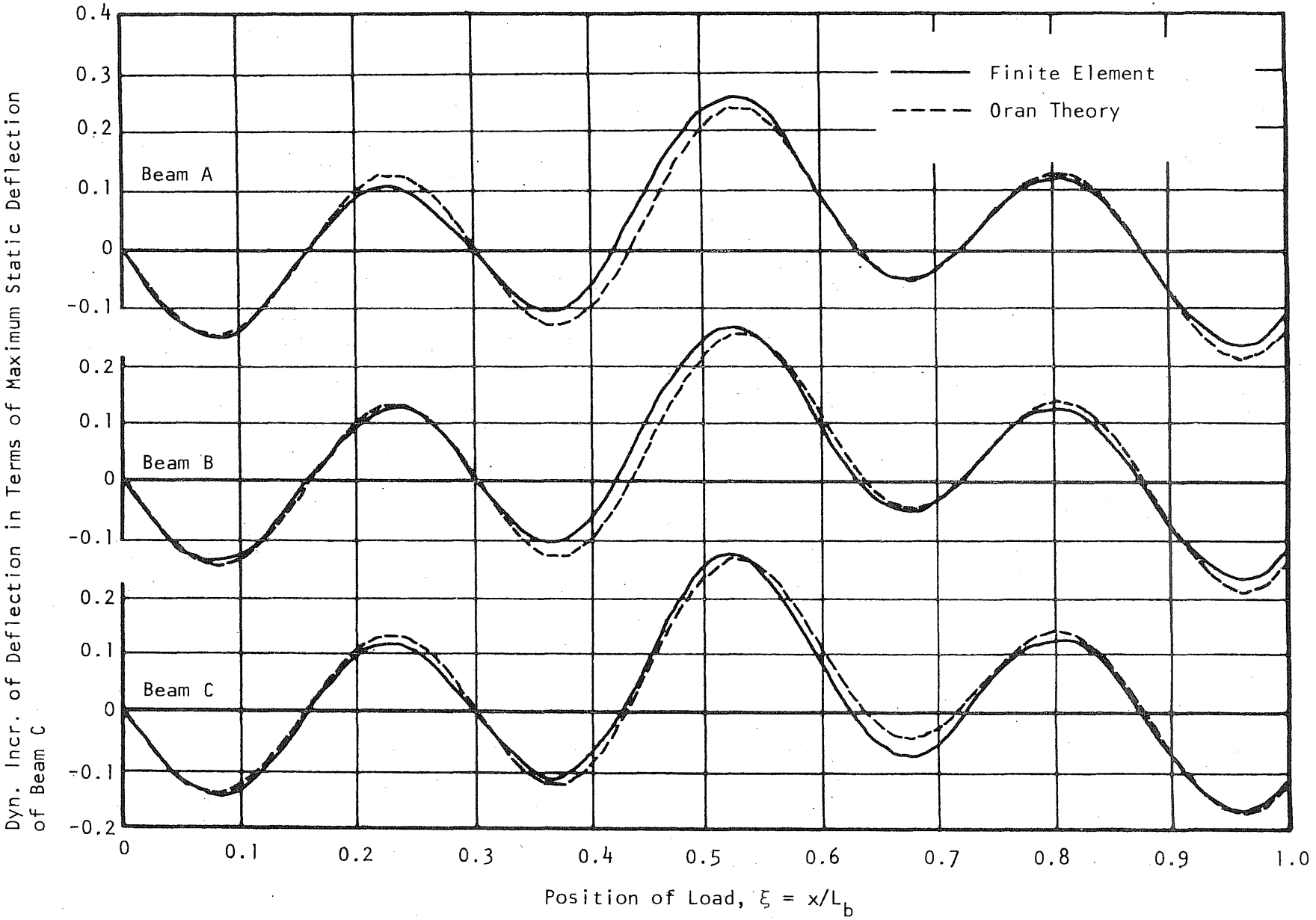

FIG. 30 COMPARISON OF THEORETICAL CURVES FOR DYNAMIC INCREMENT OF DEFLECTION, LOAD OVER BEAM C; No Torsion, Composite Action, or Camber

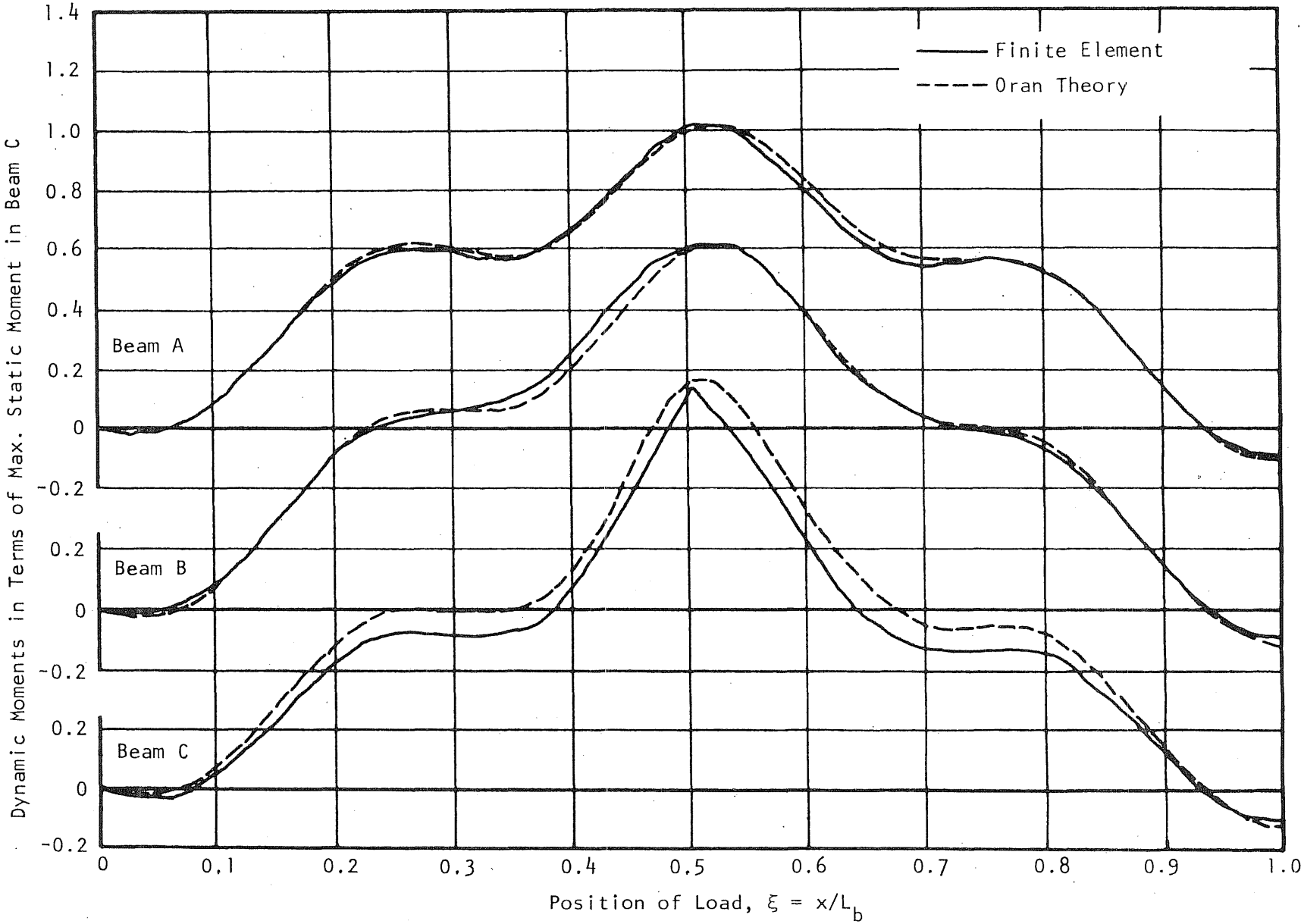

FIG. 31 COMPARISON OF THEORETICAL CURVES FOR DYNAMIC MOMENT, LOAD OVER BEAM C; No Torsion, Composite Action, or Camber

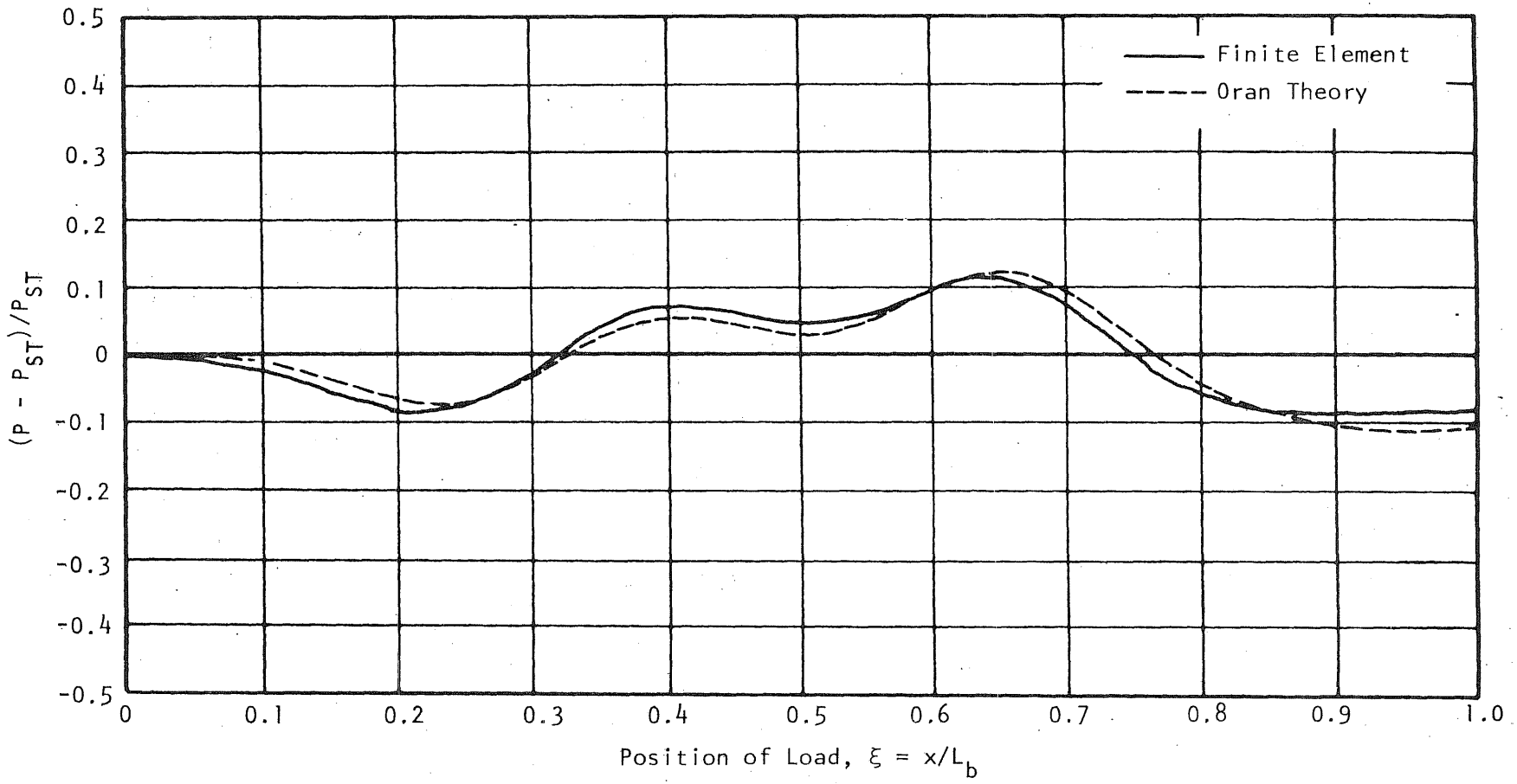

FIG. 32 COMPARISON OF THEORETICAL CURVES FOR INTERACTING FORCE; No Torsion, Composite Action, or Camber

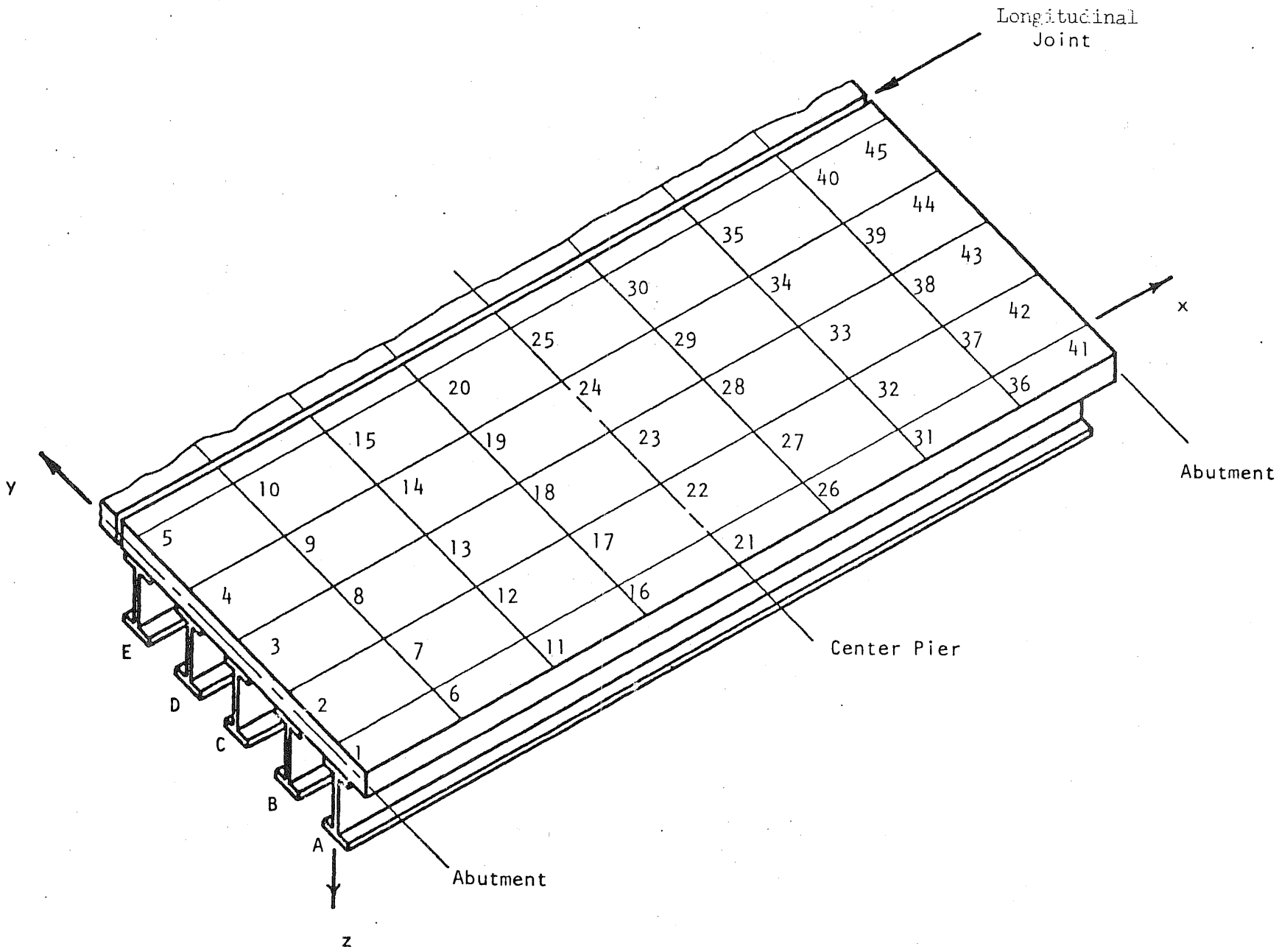

FIG. 33 SHAFFER CREEK FIVE-BEAM BRIDGE MODEL

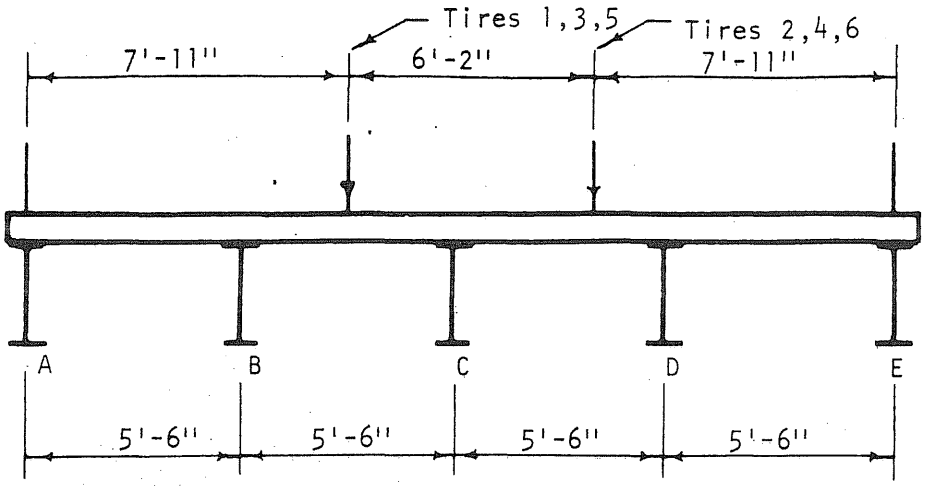

Transverse Position of Wheel Paths

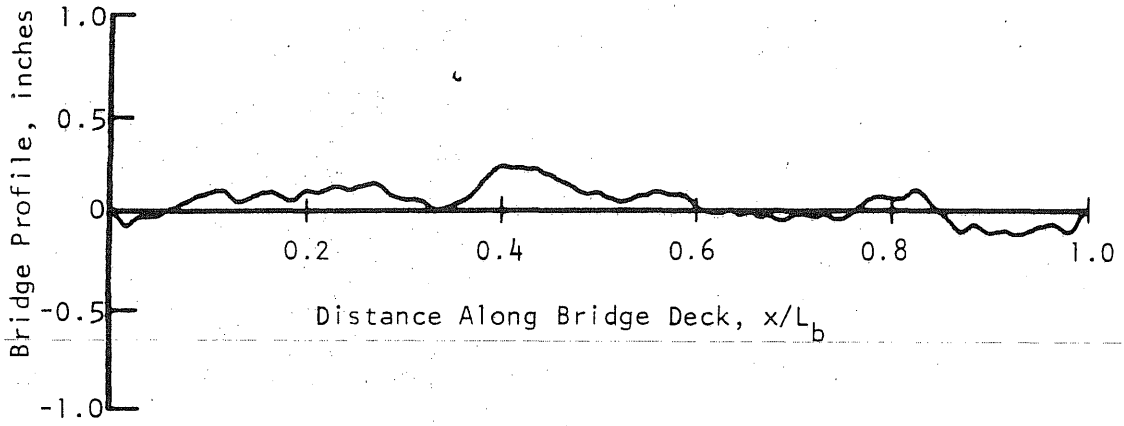

Bridge Profile for Tires 1, 3, and 5

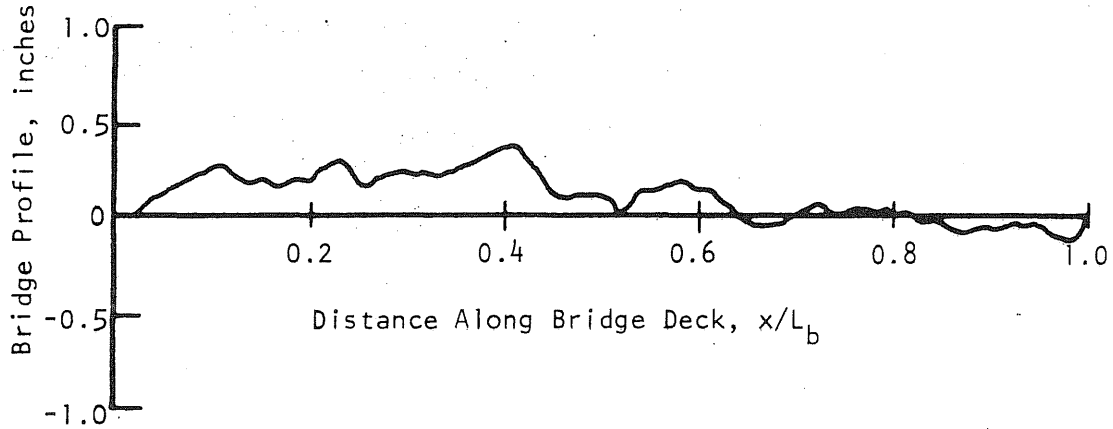

Bridge Profile for Tires 2, 4, and 6

FIG. 34 WHEEL PATH LOCATIONS AND BRIDGE PROFILES FOR SHAFFER CREEK BRIDGE SOLUTIONS

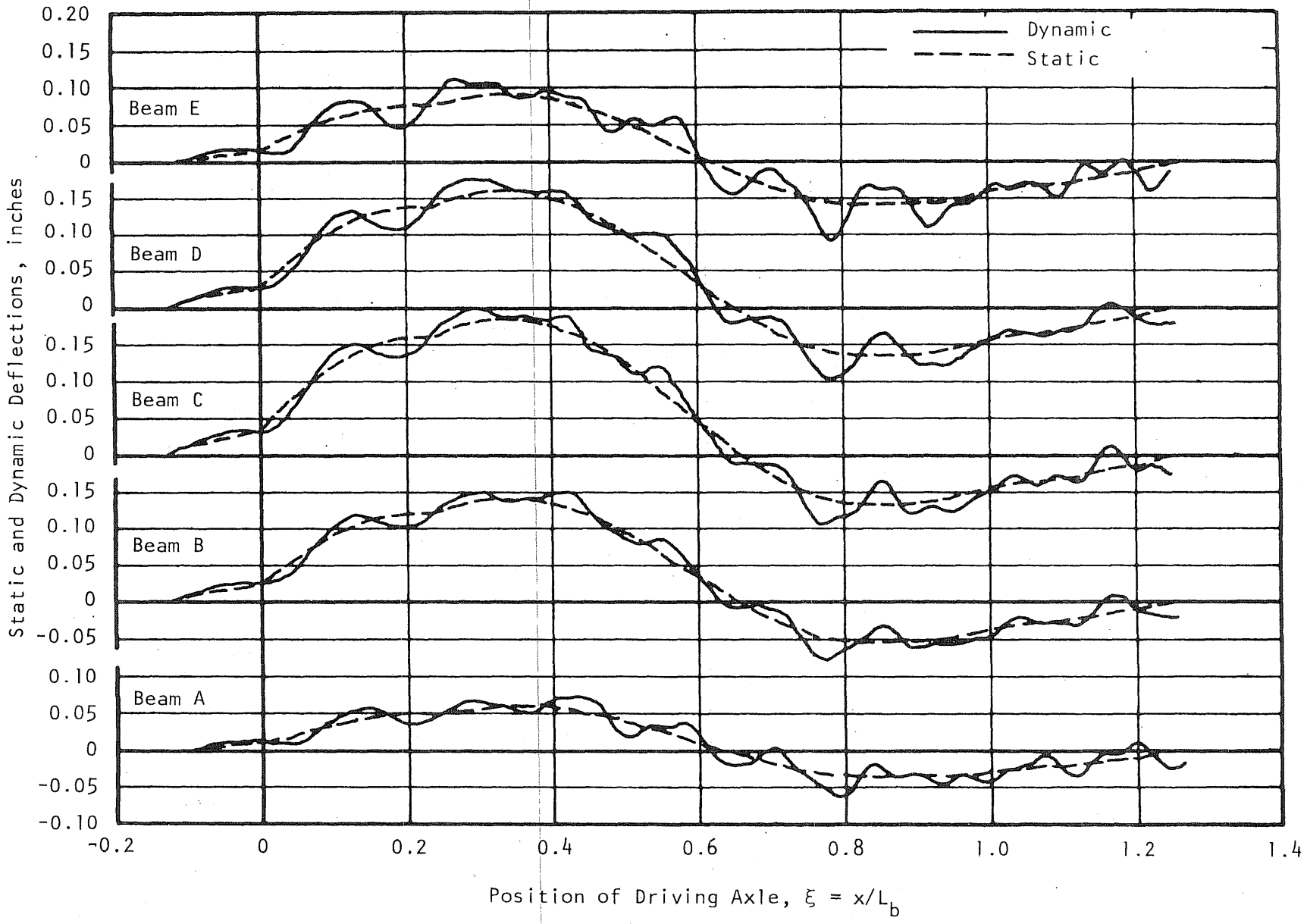

FIG. 35 THEORETICAL DEFLECTIONS AT MIDSPAN OF WEST SPAN

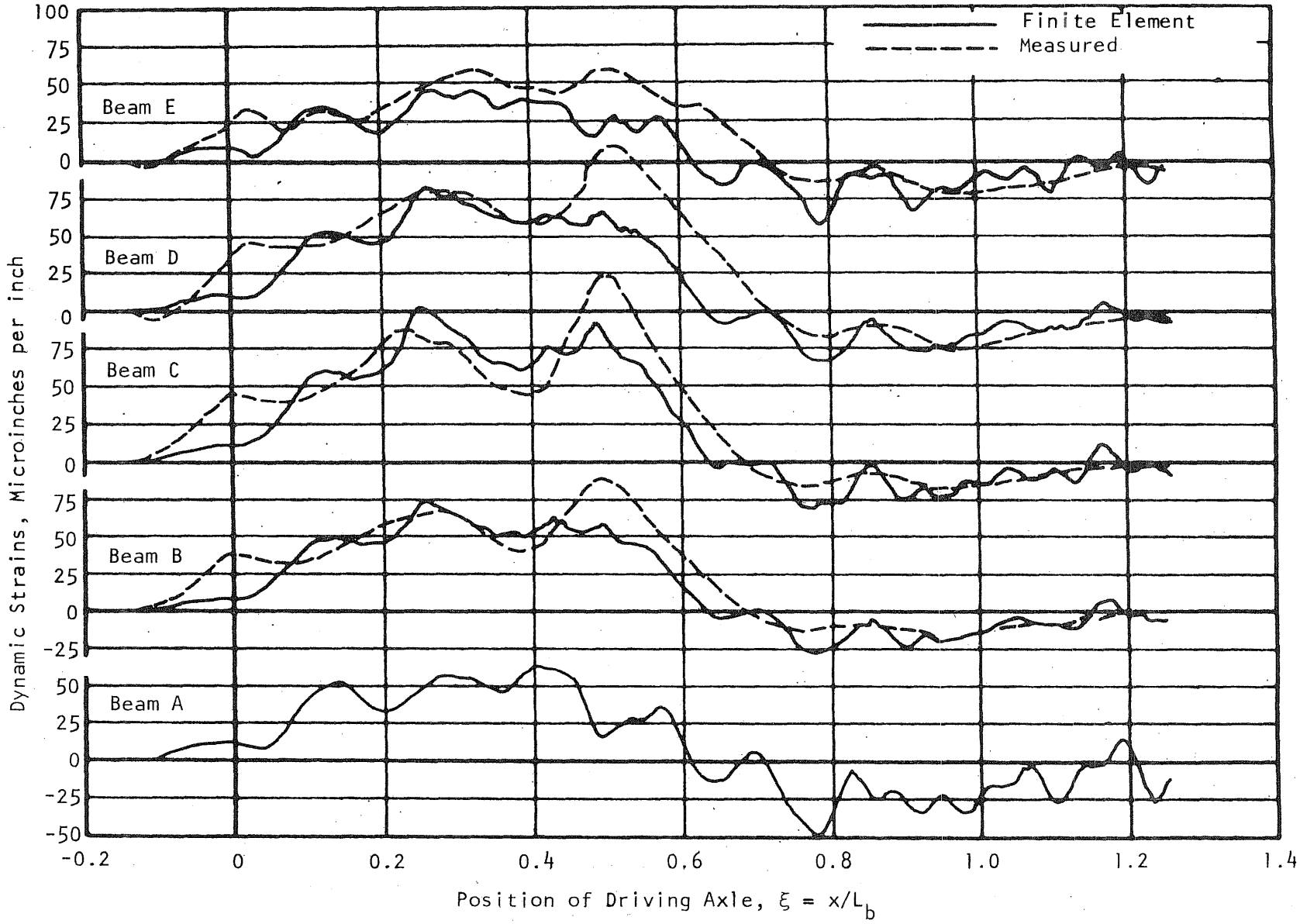

FIG. 36 COMPARISON OF THEORETICAL AND MEASURED DYNAMIC STRAINS IN BOTTOM FLANGE OF BRIDGE GIRDERS AT MIDSPAN OF WEST SPAN

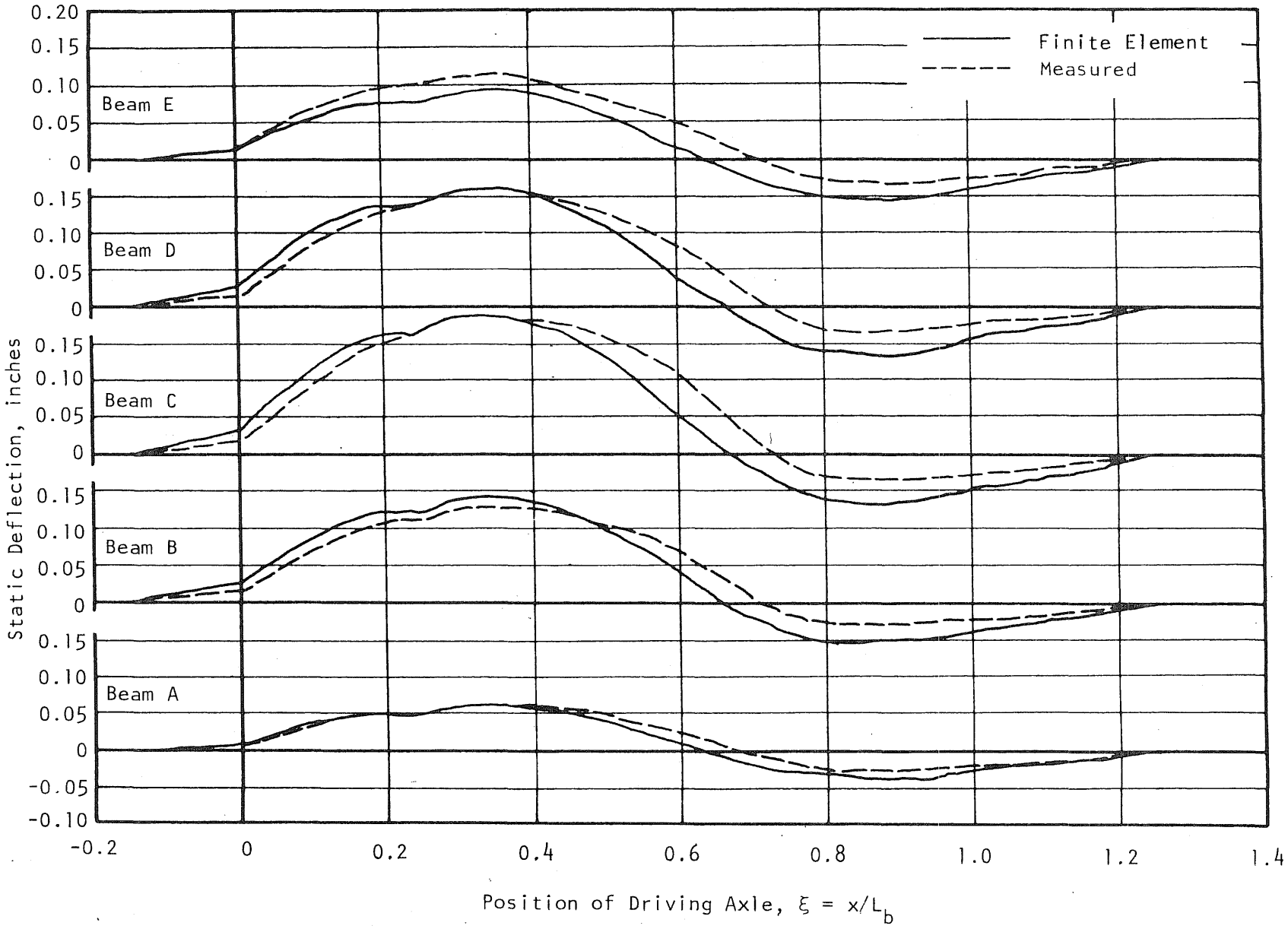

FIG. 37 COMPARISON OF THEORETICAL AND MEASURED STATIC DEFLECTIONS AT MIDSPAN OF WEST SPAN

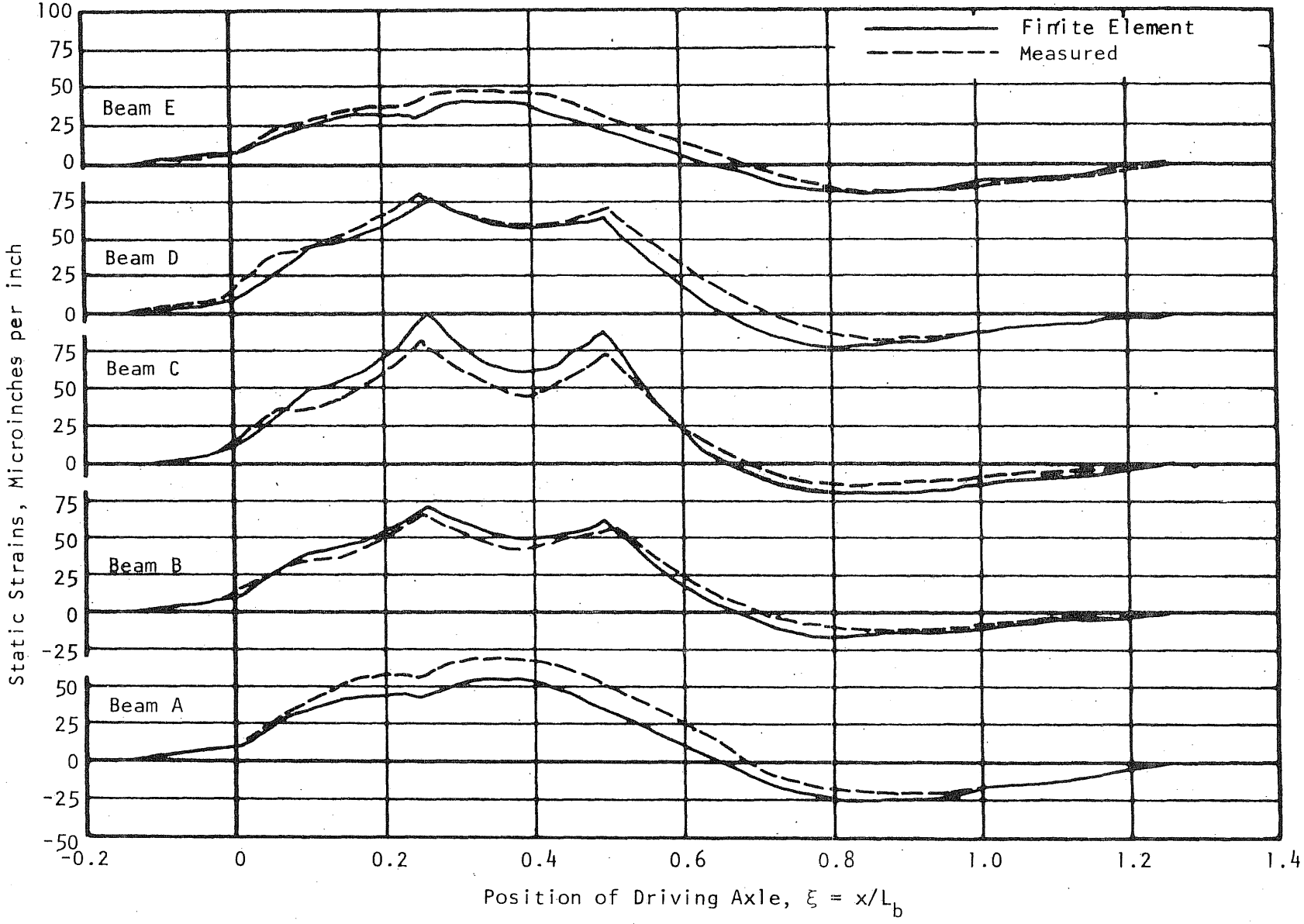

FIG. 38 COMPARISON OF THEORETICAL AND MEASURED STATIC STRAINS IN BOTTOM FLANGE OF BRIDGE GIRDERS AT MIDSPAN OF WEST SPAN

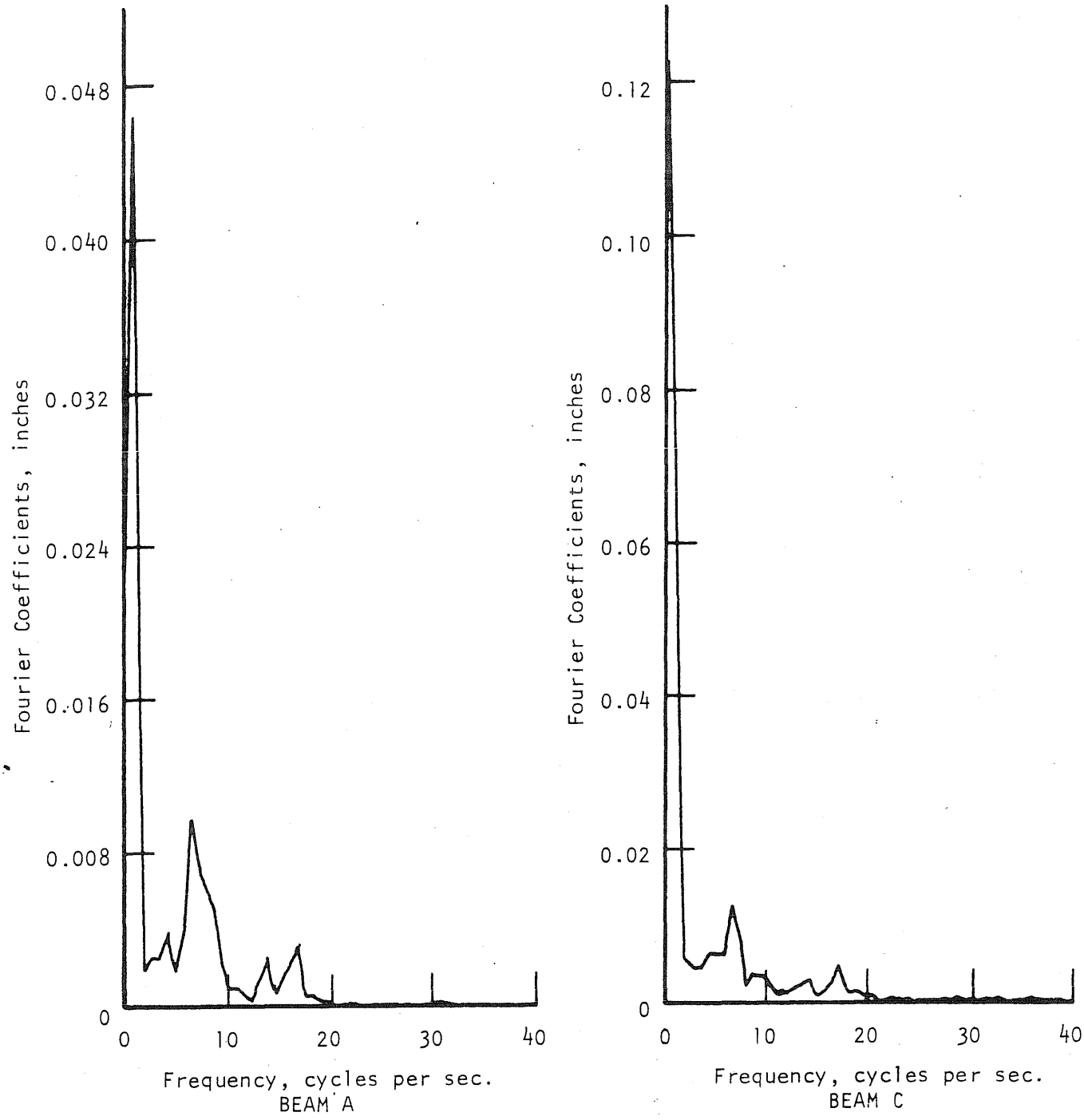

FIG. 39 FOURIER COEFFICIENTS FOR DYNAMIC DEFLECTIONS OF BEAM A AND BEAM C AT MIDSPAN OF WEST SPAN

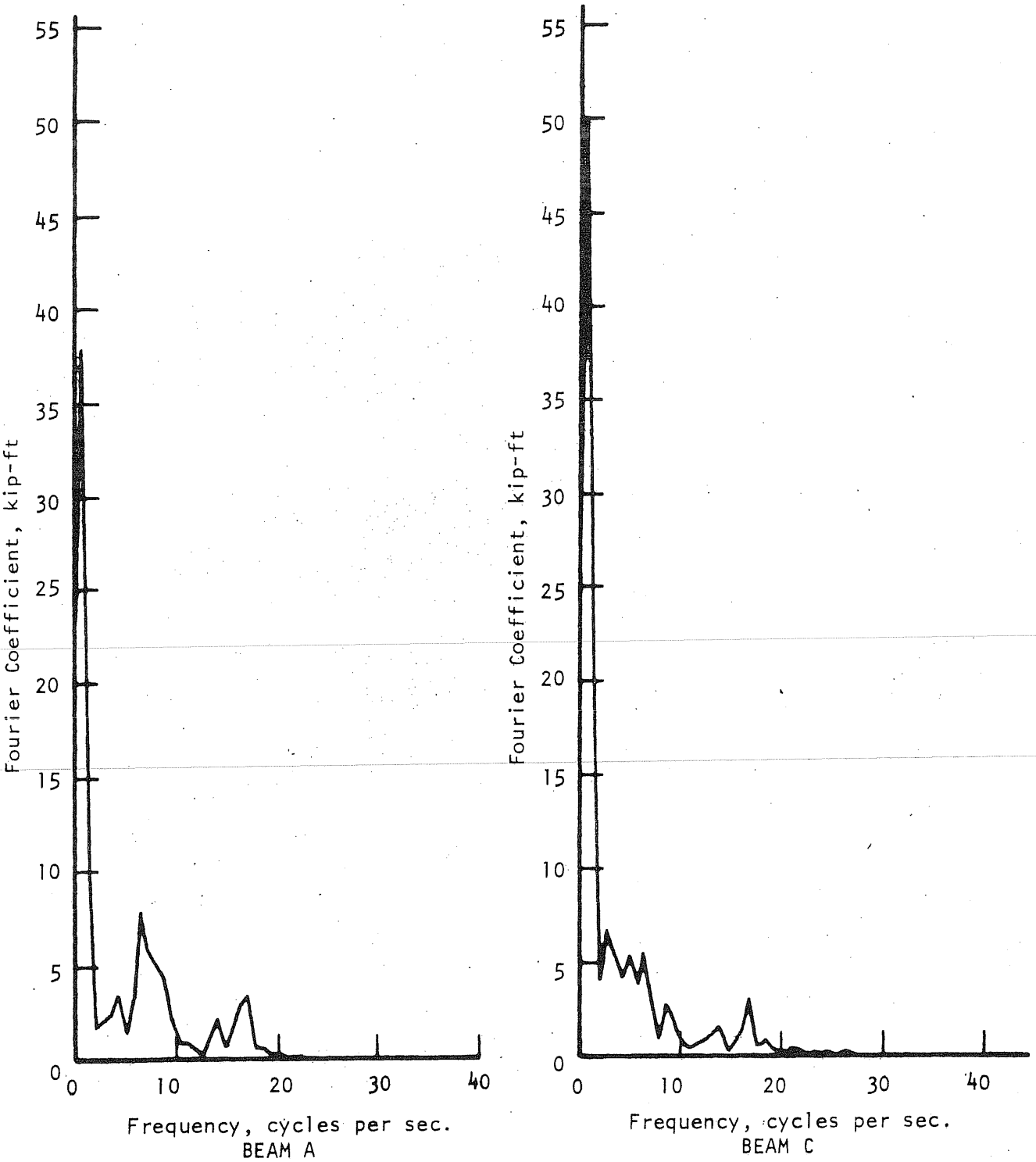

FIG. 40 FOURIER COEFFICIENTS FOR DYNAMIC MOMENTS IN BEAM A AND BEAM C AT MIDSPAN OF WEST SPAN

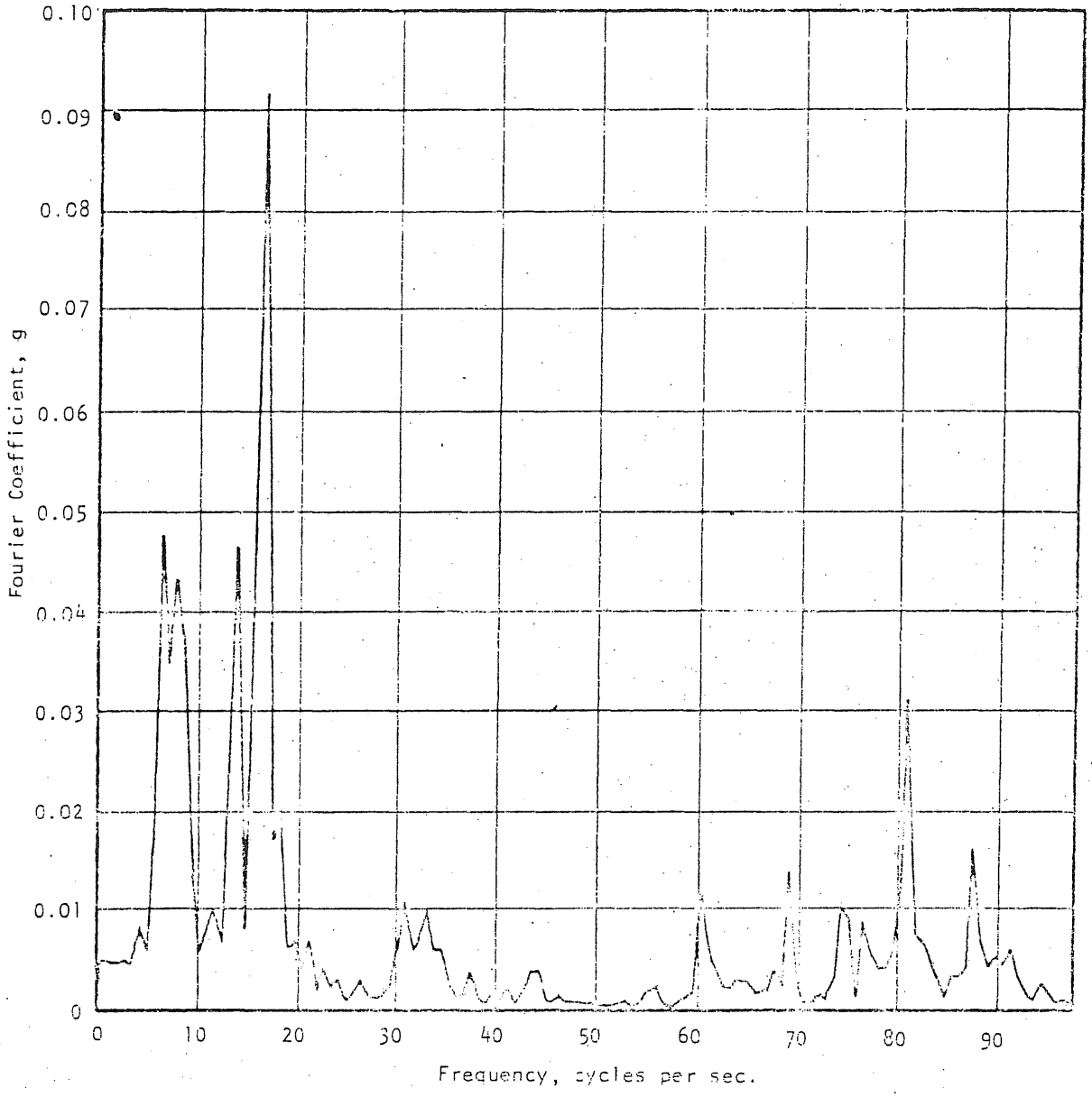

FIG. 41 FOURIER COEFFICIENTS FOR ACCELERATIONS OF BEAM A AT MIDSPAN OF WEST SPAN

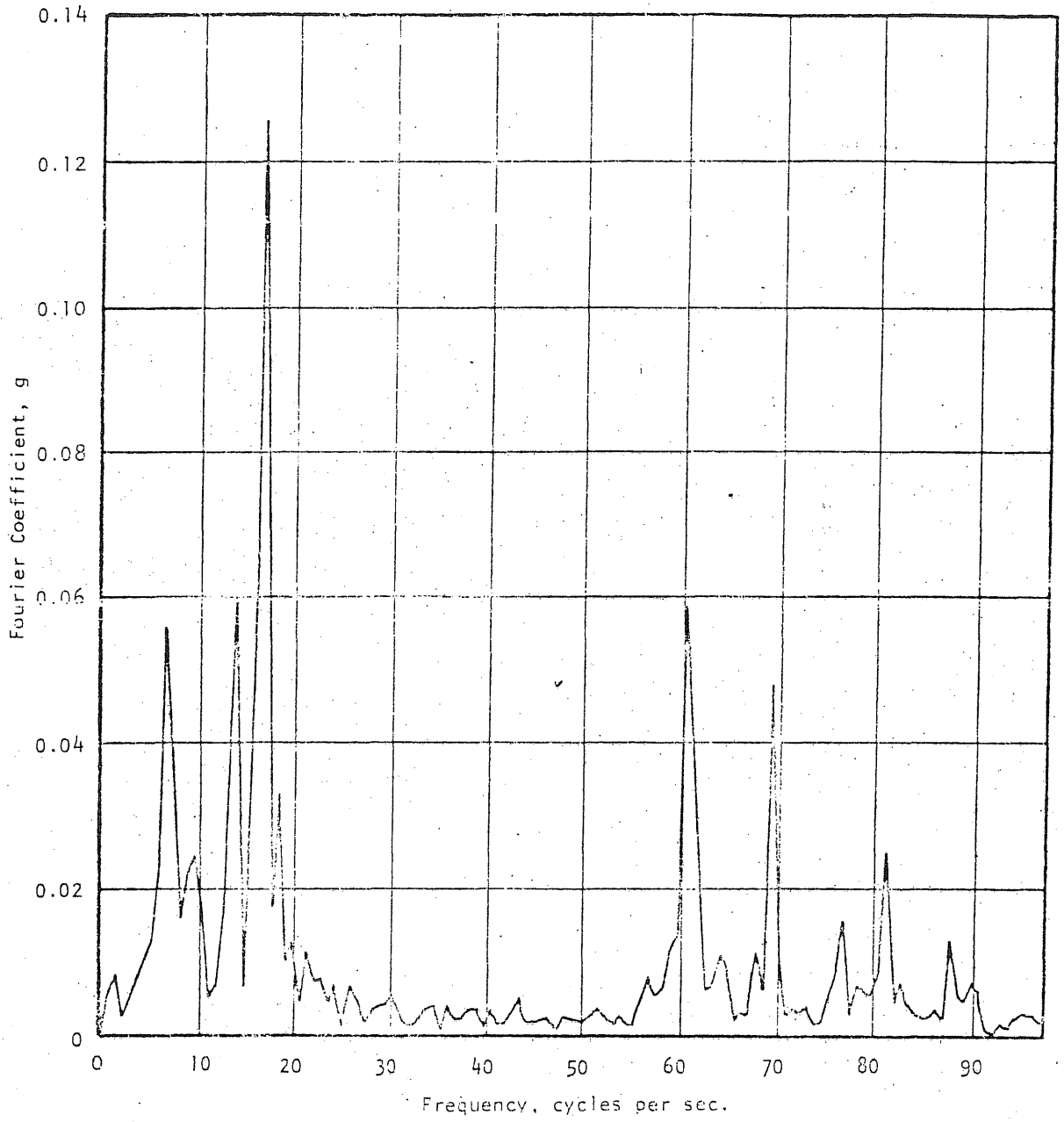

FIG. 42 FOURIER COEFFICIENTS FOR ACCELERATIONS OF BEAM C AT MIDSPAN OF WEST SPAN

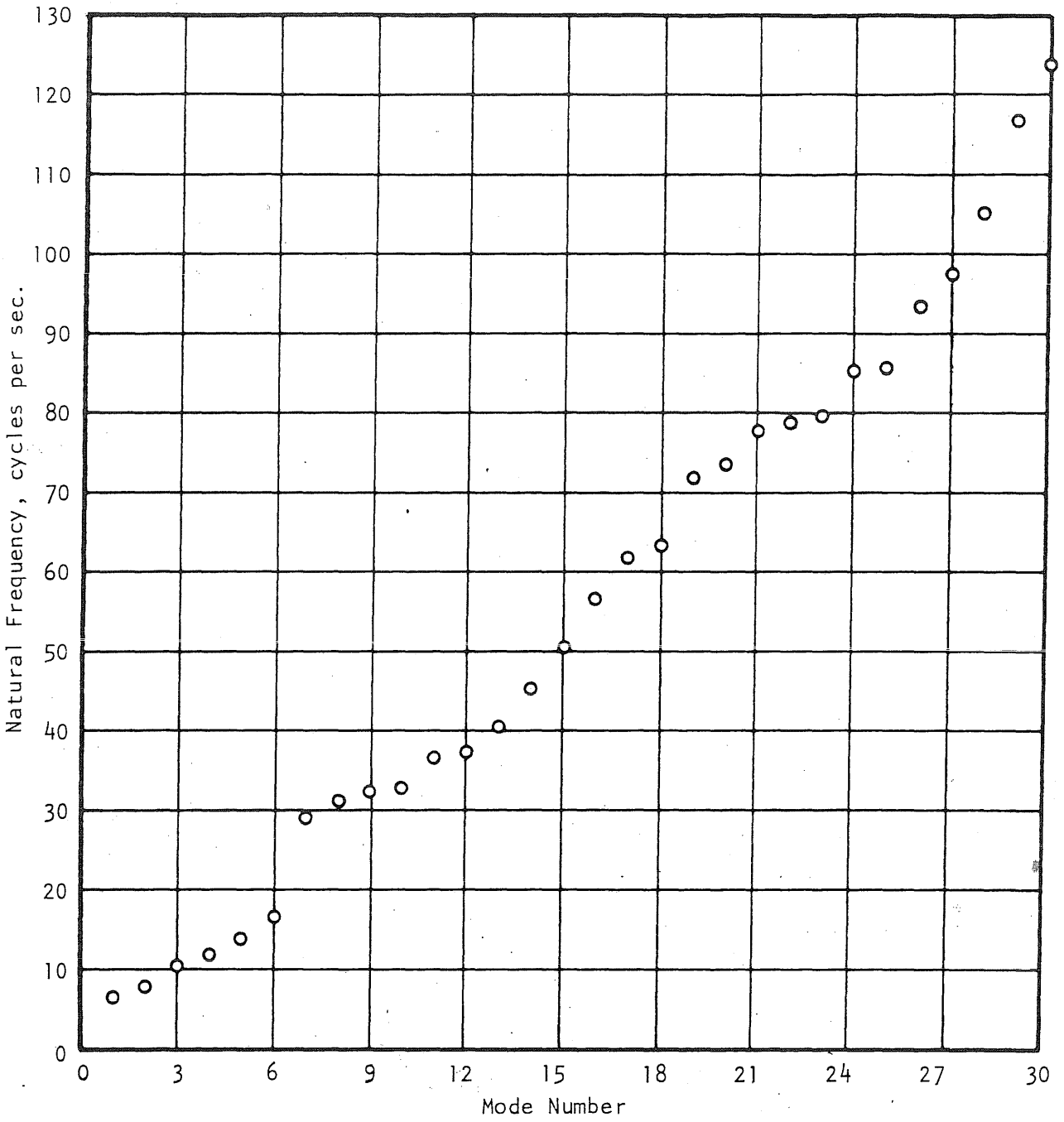

FIG. 43 NATURAL FREQUENCIES FOR THE 30 DEGREE-OF-FREEDOM SHAFFER CREEK BRIDGE MODEL

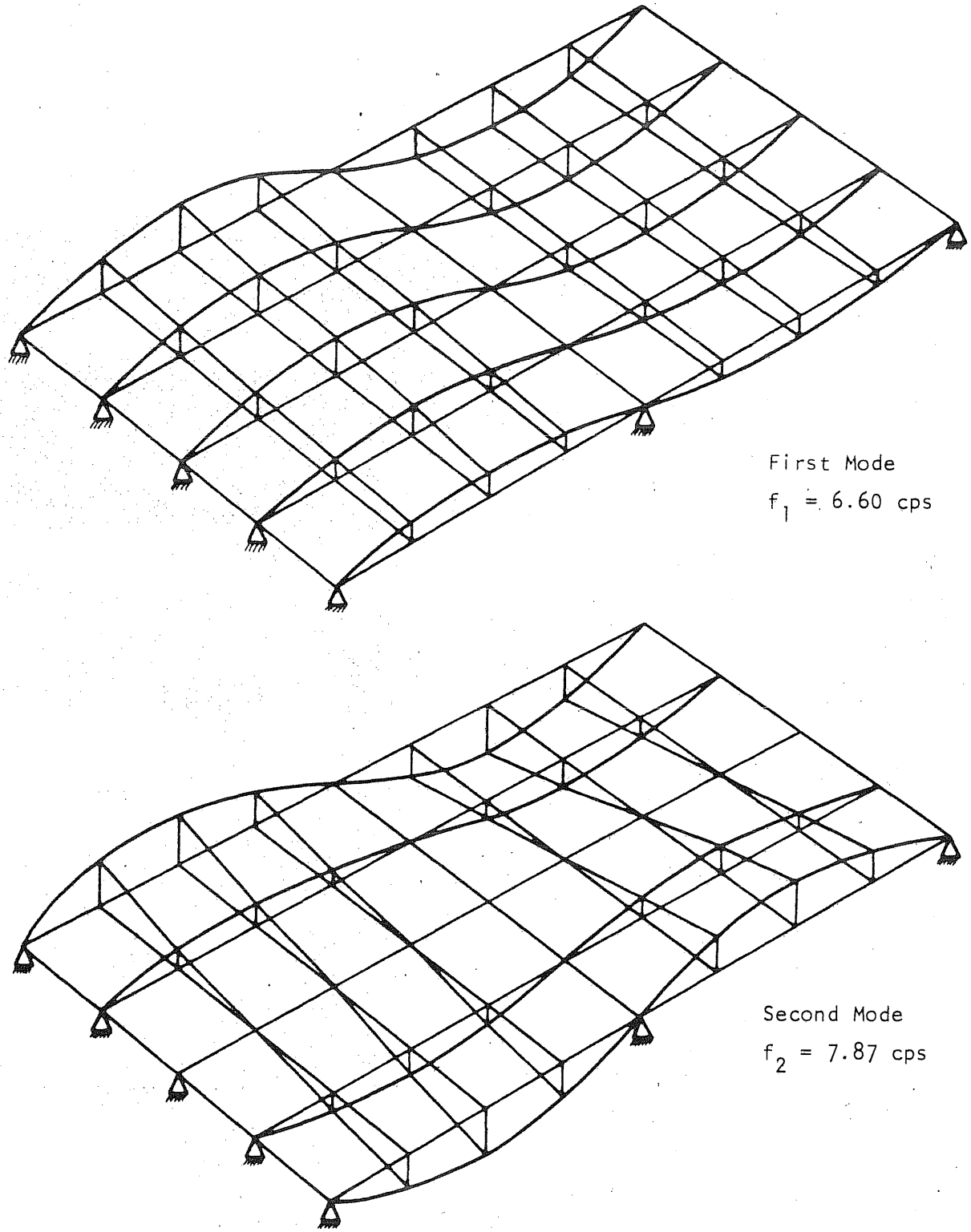

FIG. 44 FIRST AND SECOND MODE SHAPES FOR SHAFFER CREEK BRIDGE

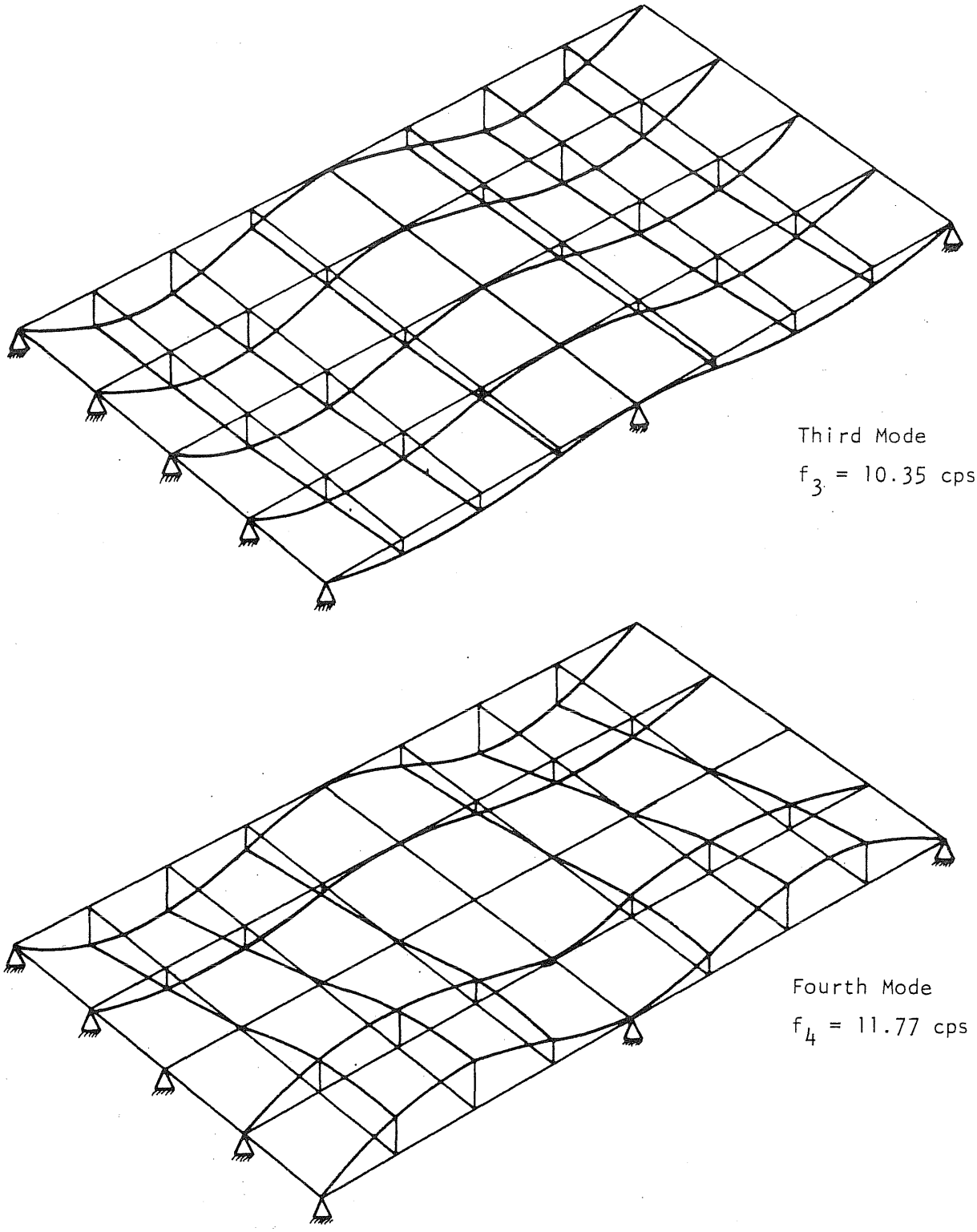

FIG. 45 THIRD AND FOURTH MODE SHAPES FOR SHAFFER CREEK BRIDGE

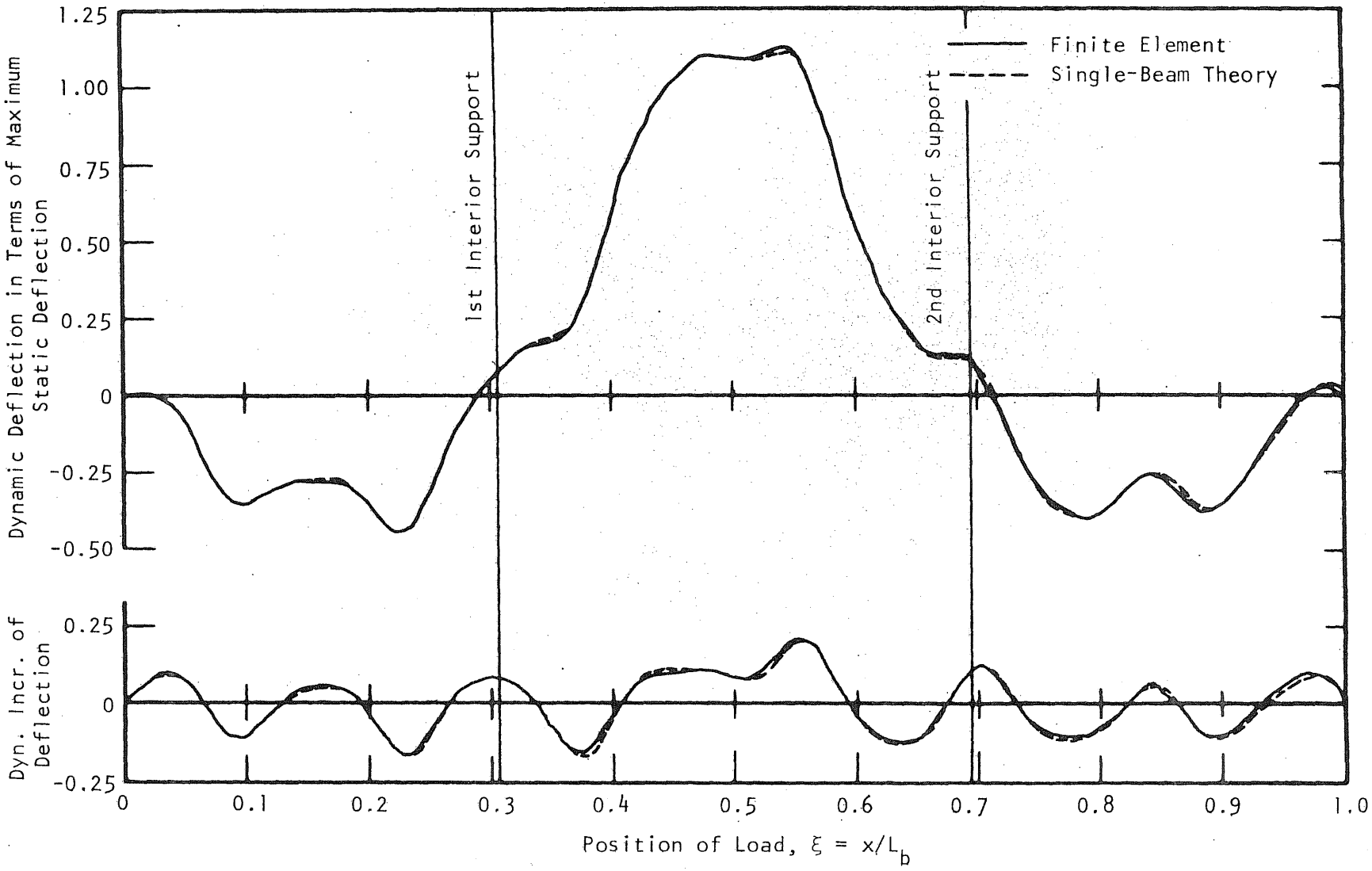

FIG. 46 DYNAMIC DEFLECTION AT MIDPOINT OF CENTER SPAN, CASE A

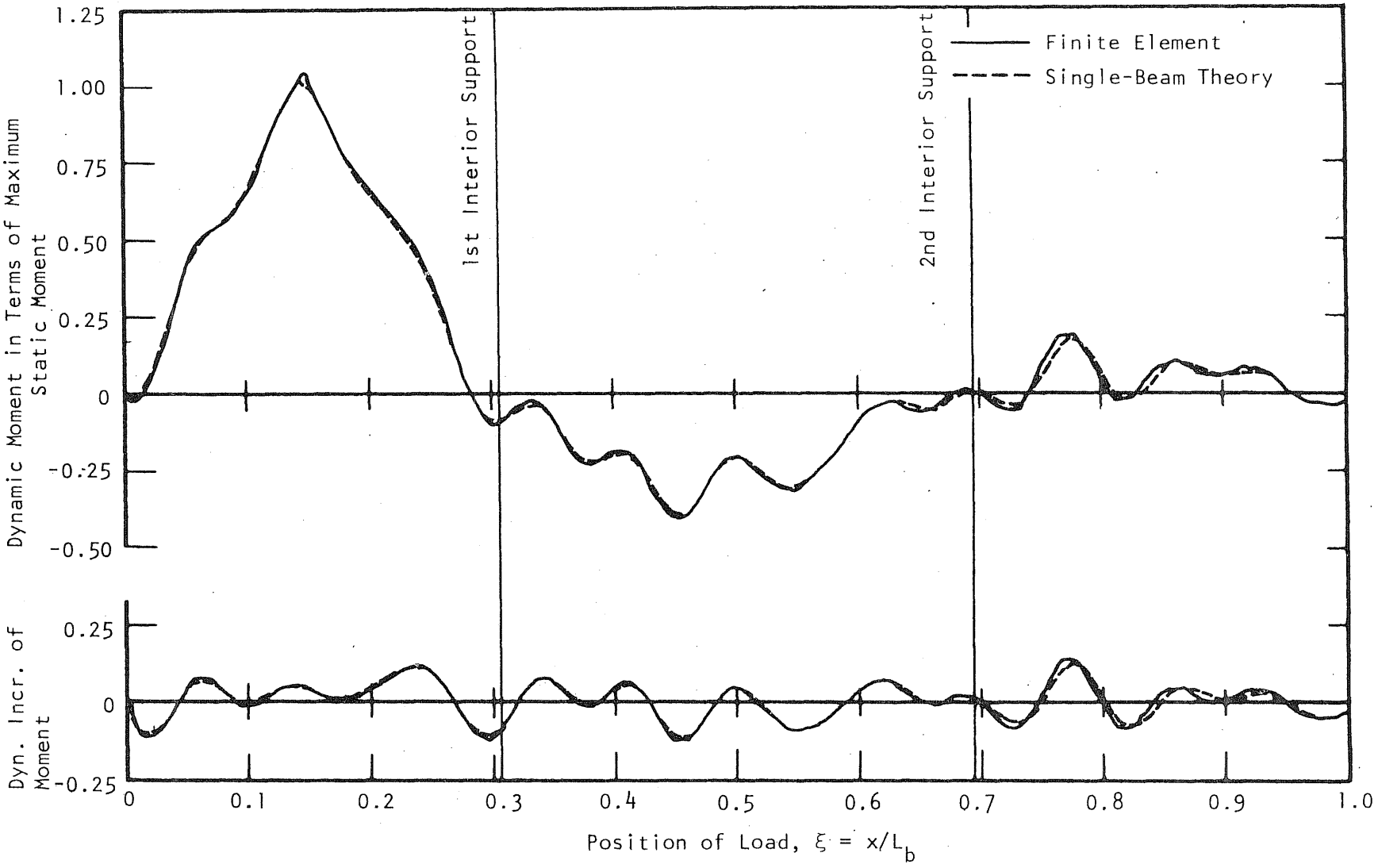

FIG. 47 DYNAMIC MOMENT AT MIDPOINT OF LEFT SPAN, CASE A

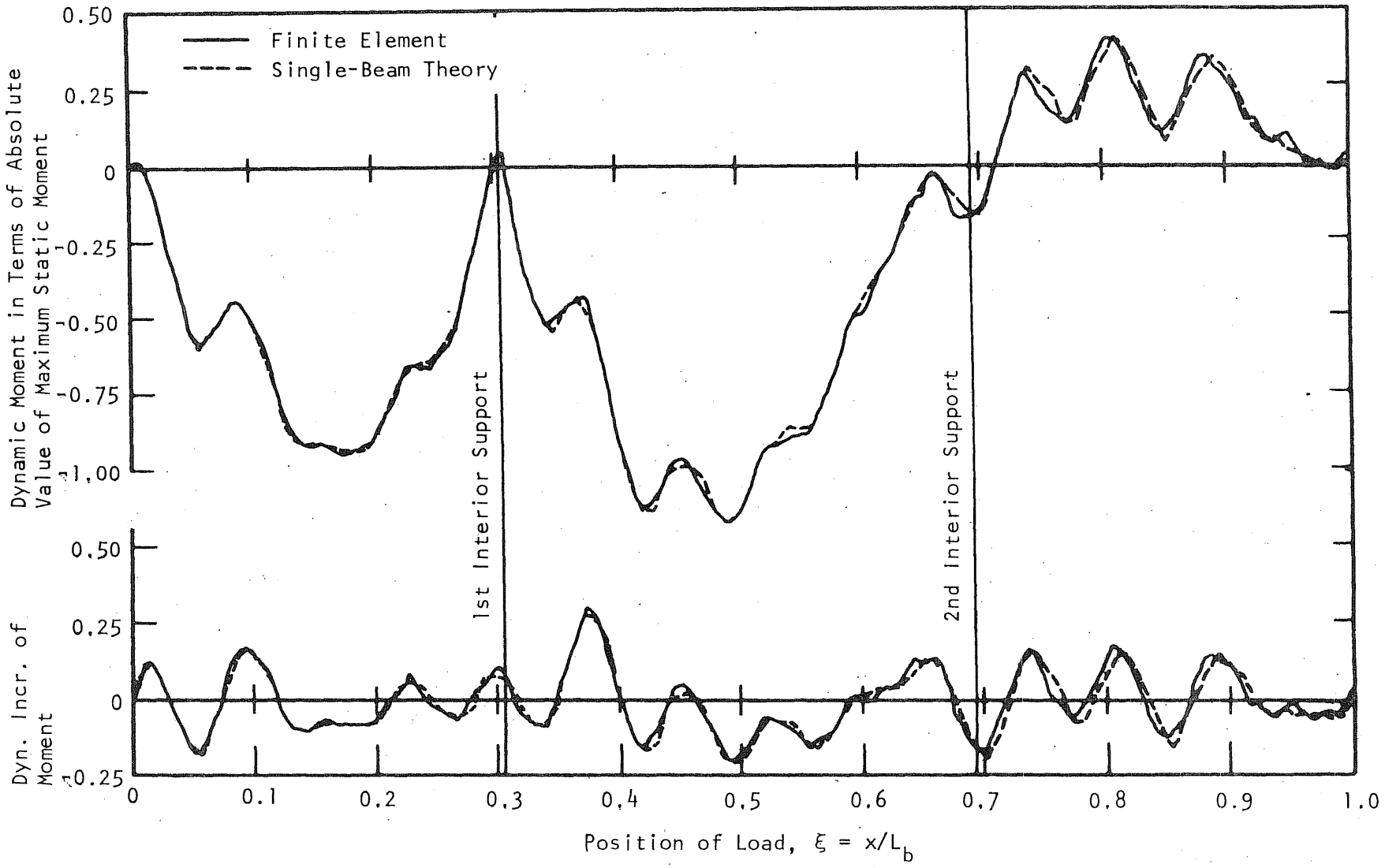

FIG. 48 DYNAMIC MOMENT AT FIRST INTERIOR SUPPORT, CASE A

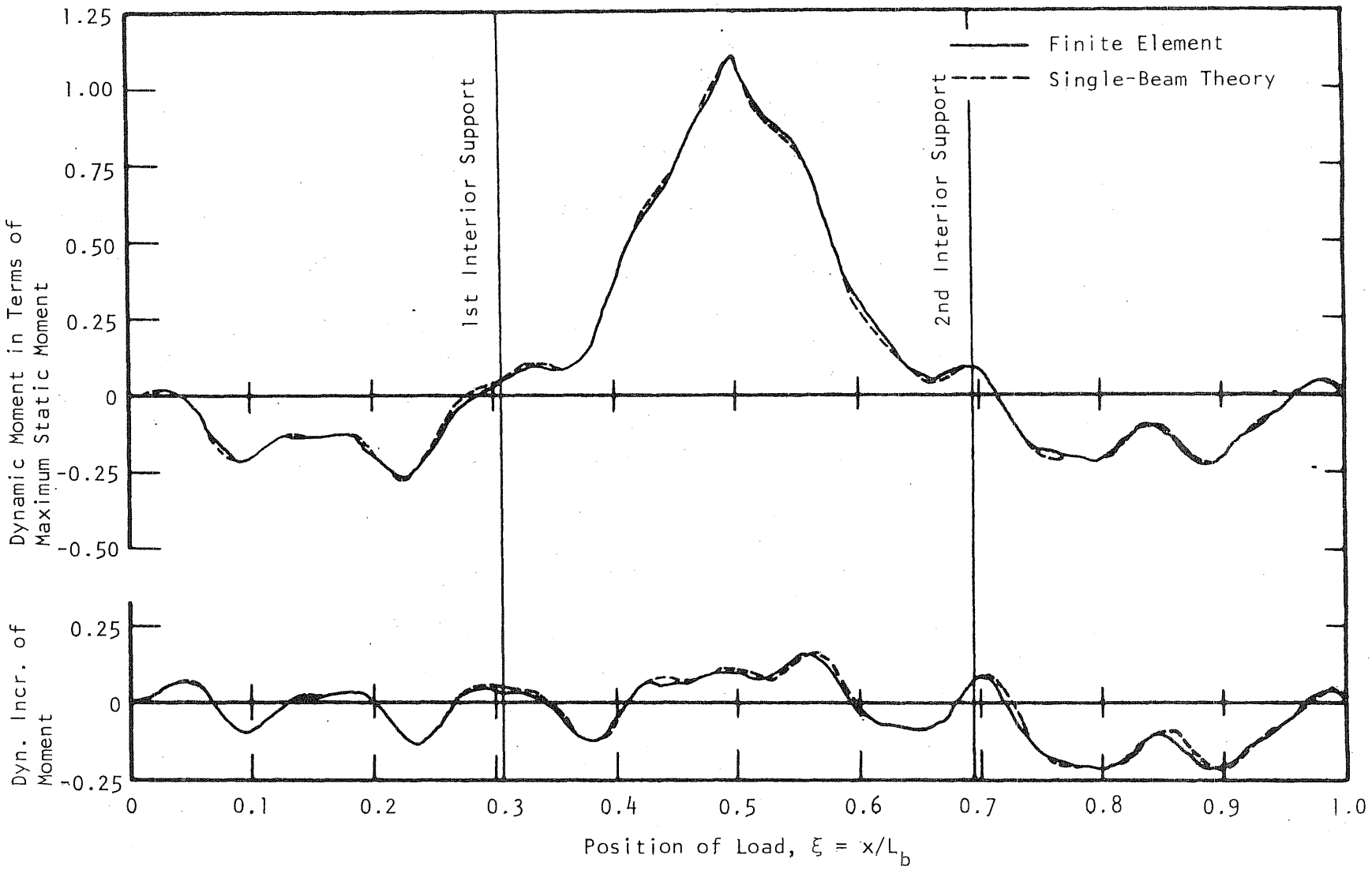

FIG. 49 DYNAMIC MOMENT AT MIDPOINT OF CENTER SPAN, CASE A

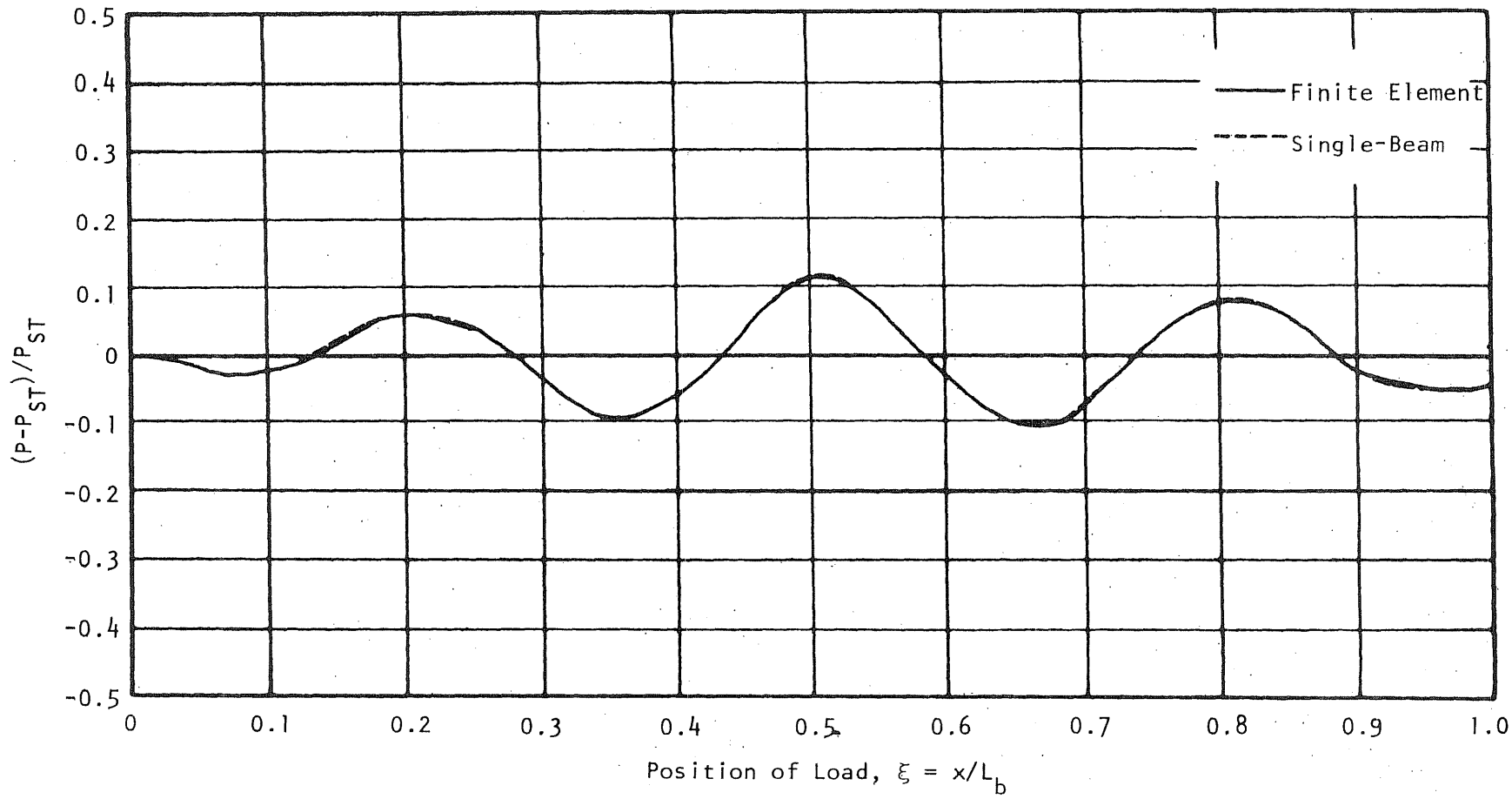

FIG. 50 COMPARISON OF THEORETICAL INTERACTING FORCES FOR THREE-SPAN, SINGLE-BEAM SOLUTION, CASE A

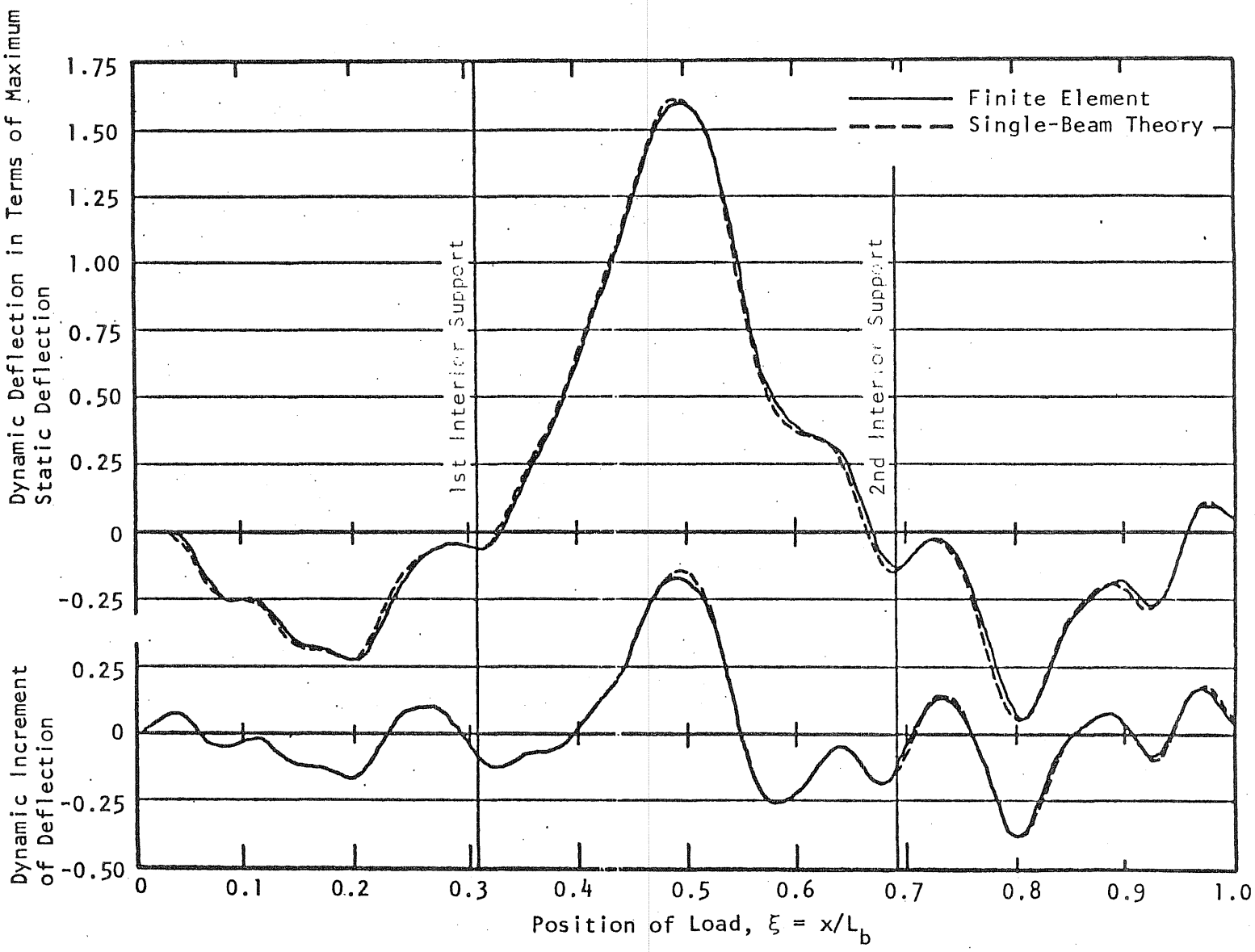

FIG. 51 DYNAMIC DEFLECTION AT MIDPOINT CENTER SPAN, CASE B

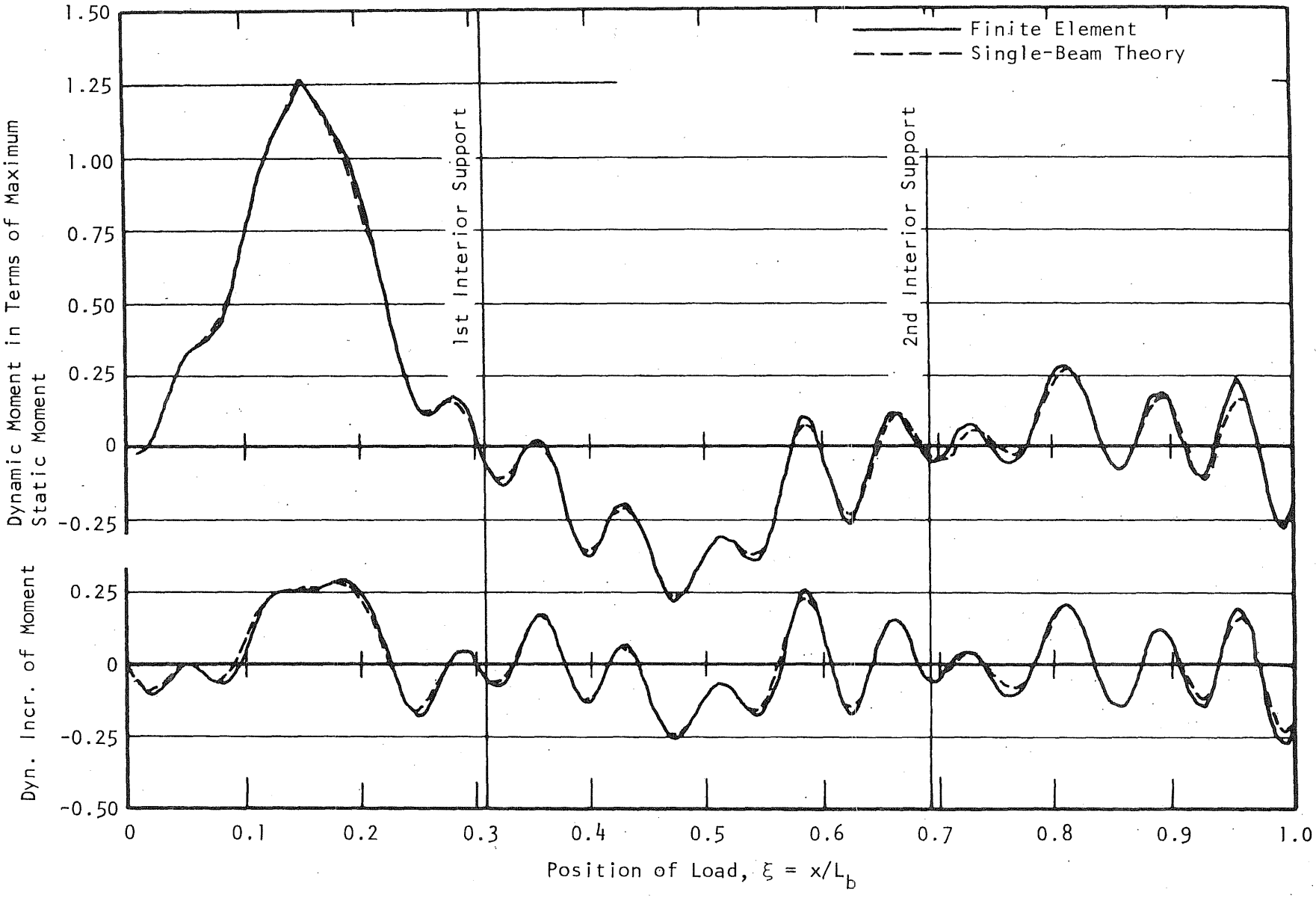

FIG. 52 DYNAMIC MOMENT AT MIDPOINT OF LEFT SPAN, CASE B

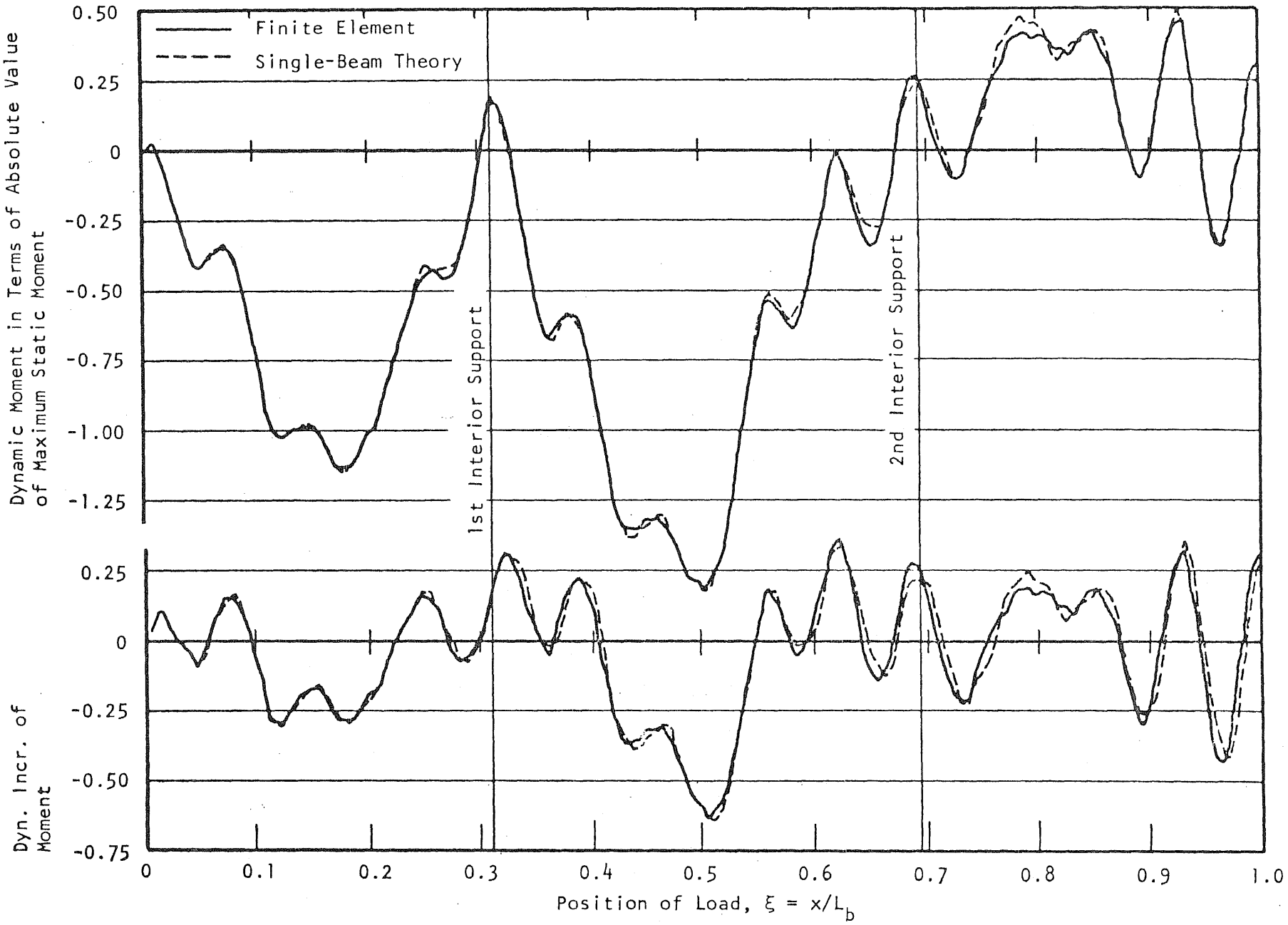

FIG. 53 DYNAMIC MOMENT AT FIRST INTERIOR SUPPORT, CASE B

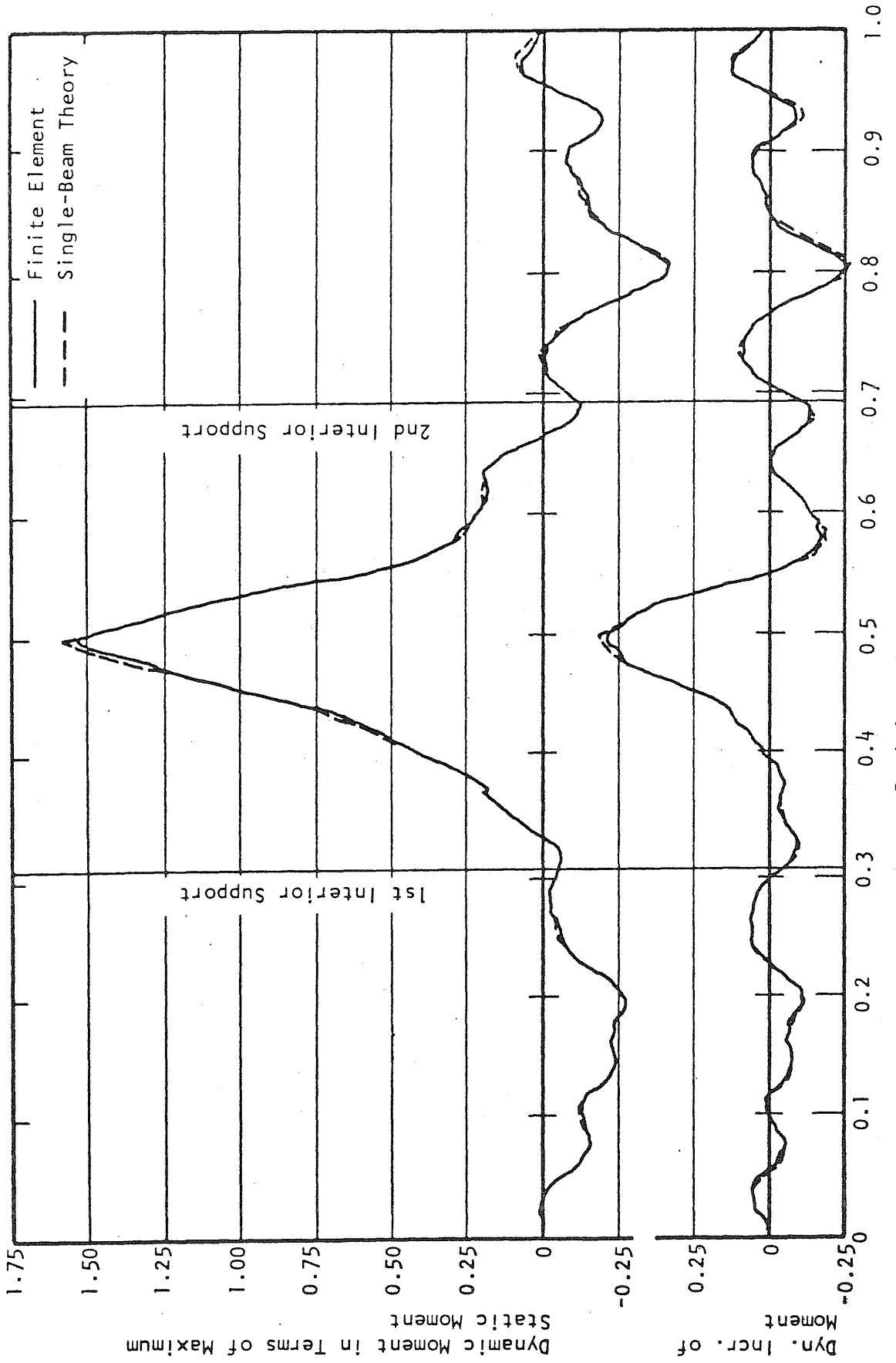

FIG. 54 DYNAMIC MOMENT AT MIDPOINT OF CENTER SPAN, CASE B

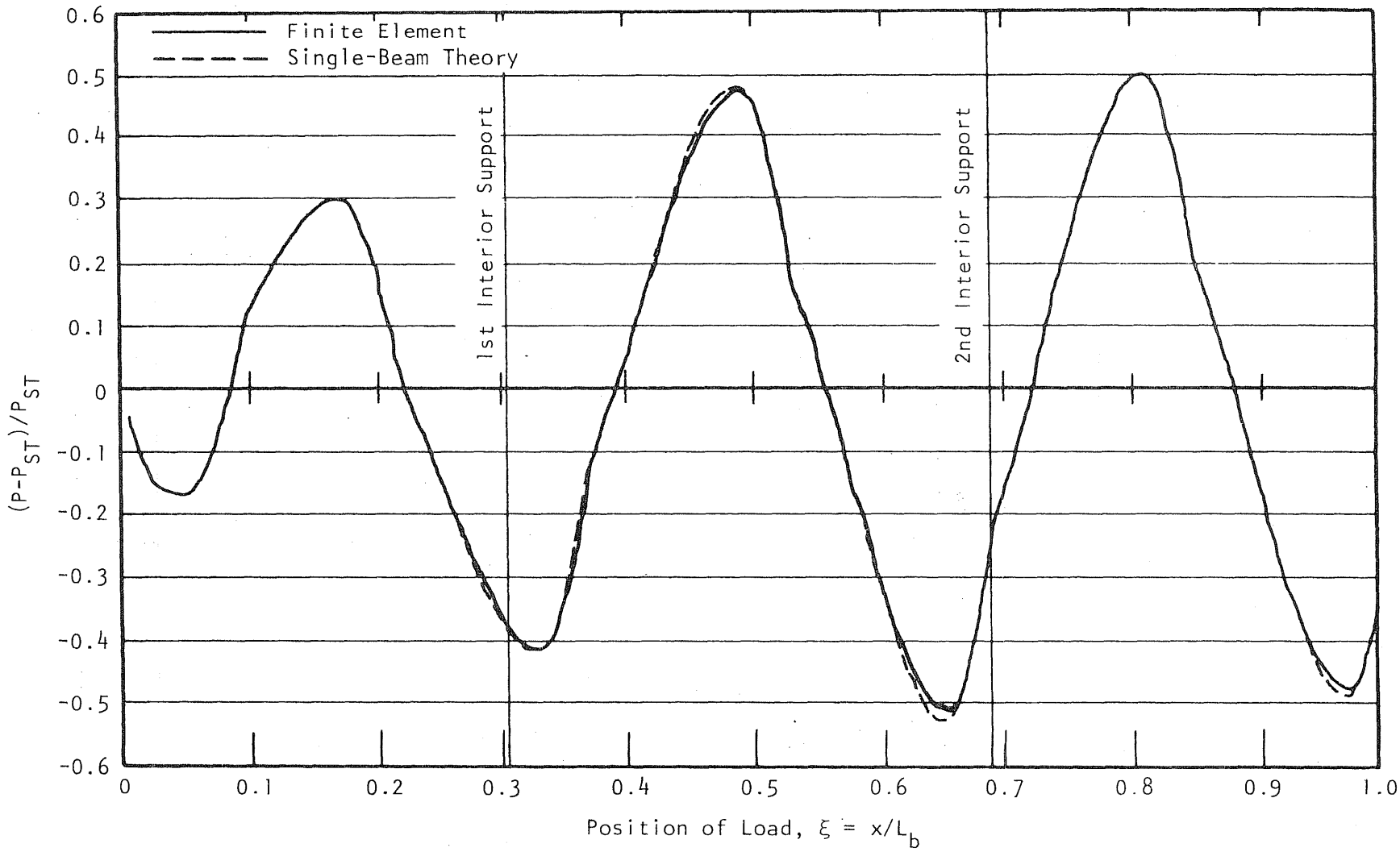

FIG. 55 COMPARISON OF THEORETICAL INTERACTING FORCES FOR THREE-SPAN. SINGLE-BEAM SOLUTION, CASE B

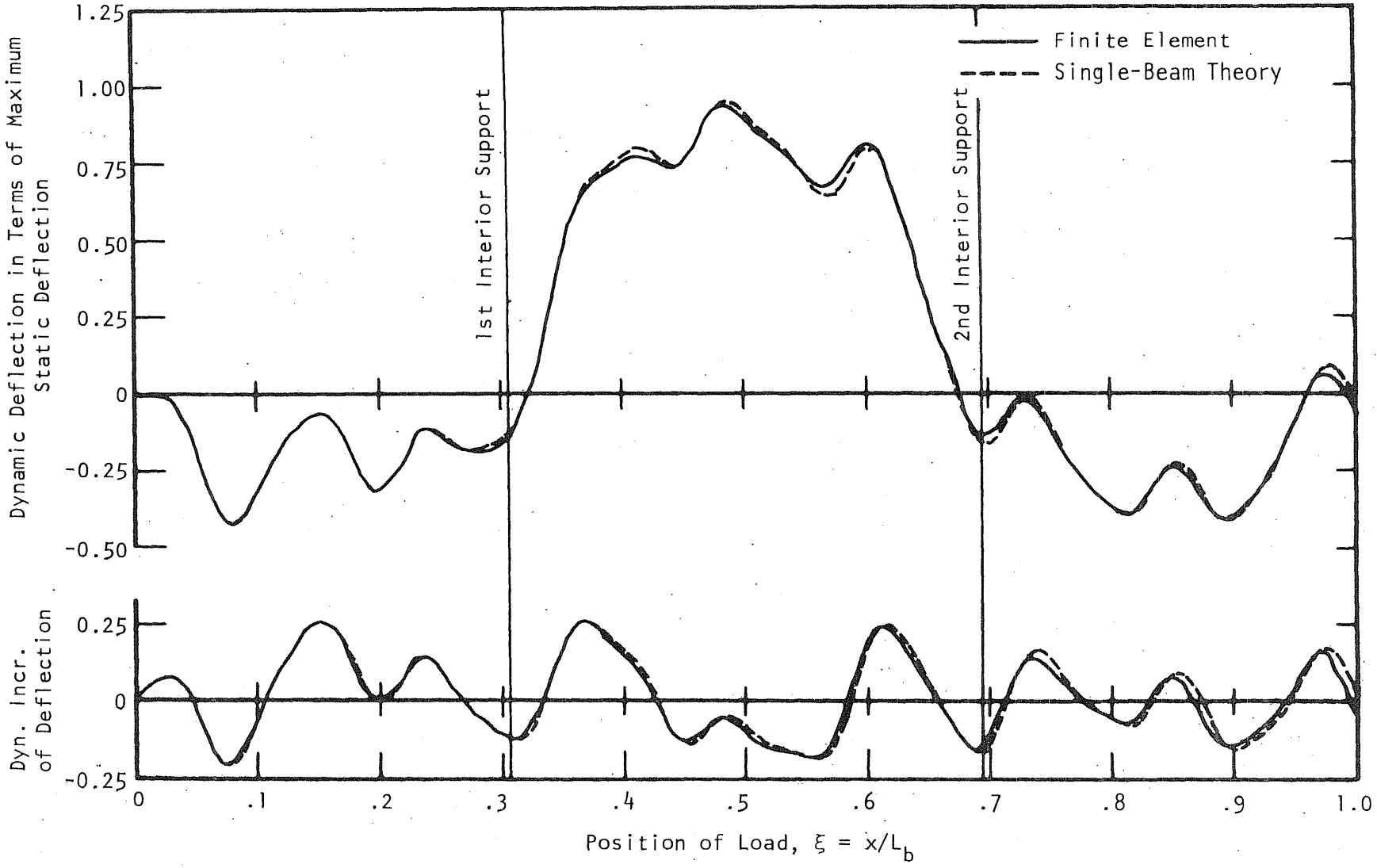

FIG. 56 DYNAMIC DEFLECTION AT MIDPOINT OF CENTER SPAN, CASE C

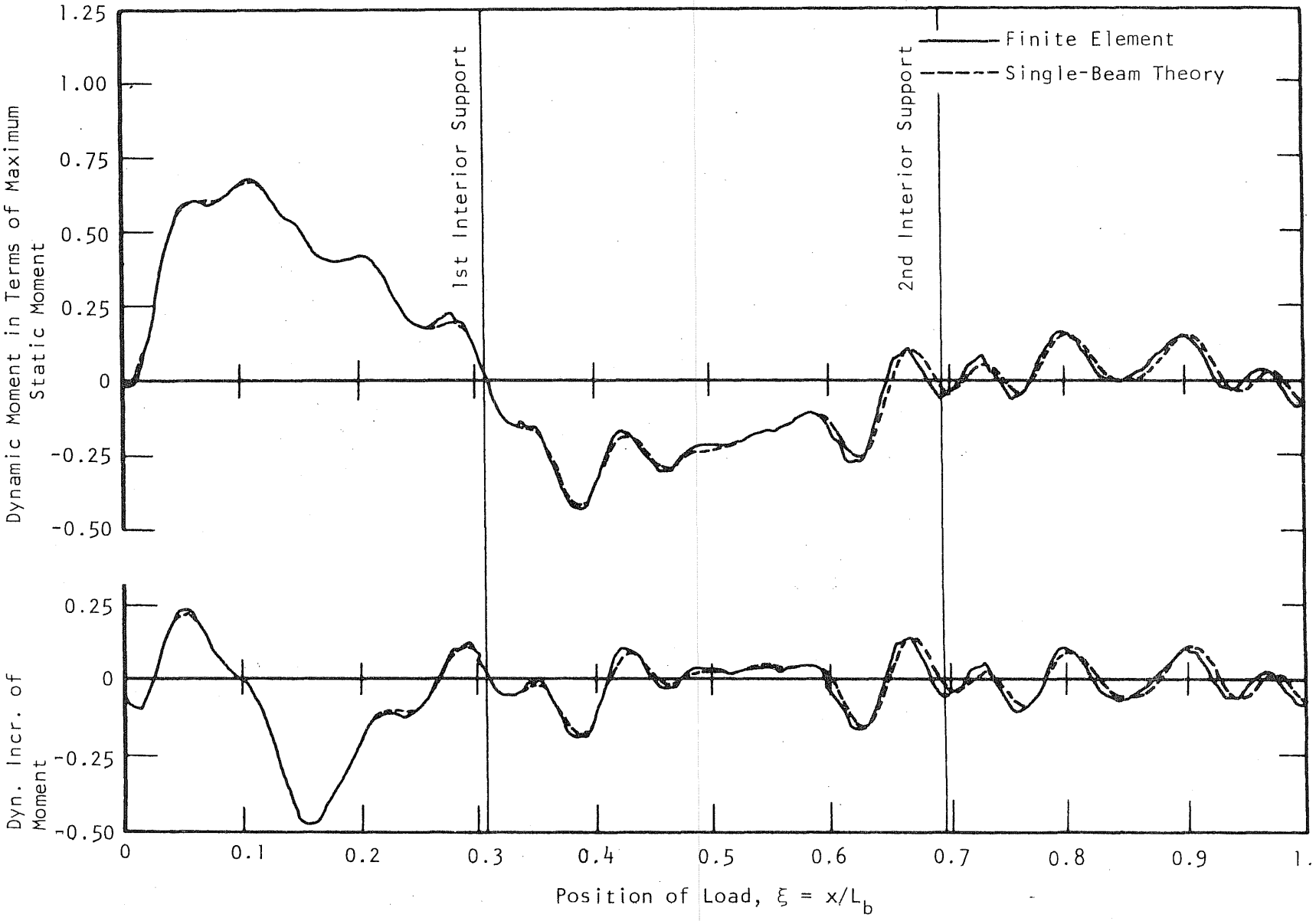

FIG. 57 DYNAMIC MOMENT AT MIDPOINT OF LEFT SPAN, CASE C

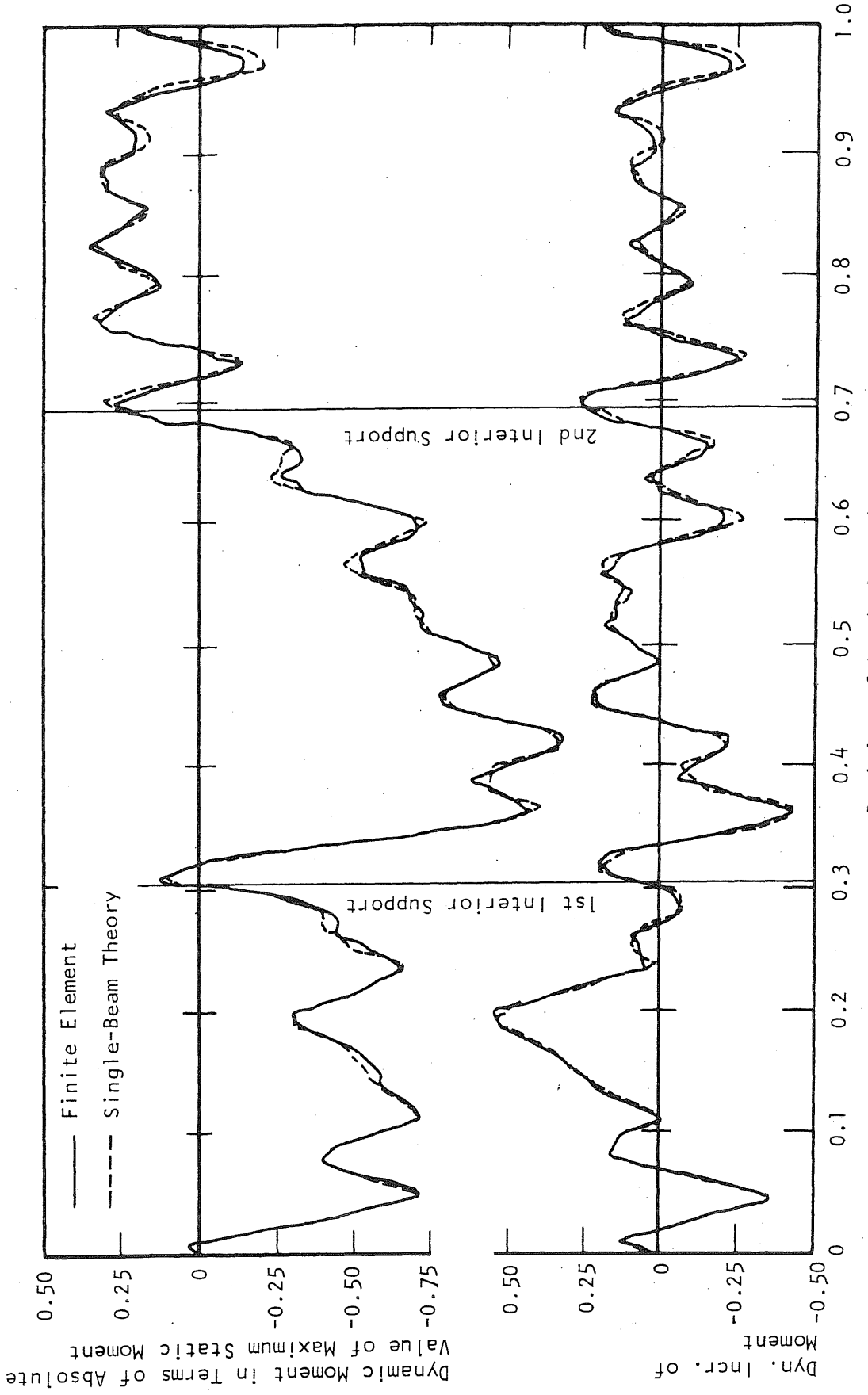

FIG. 58 DYNAMIC MOMENT AT FIRST INTERIOR SUPPORT, CASE C

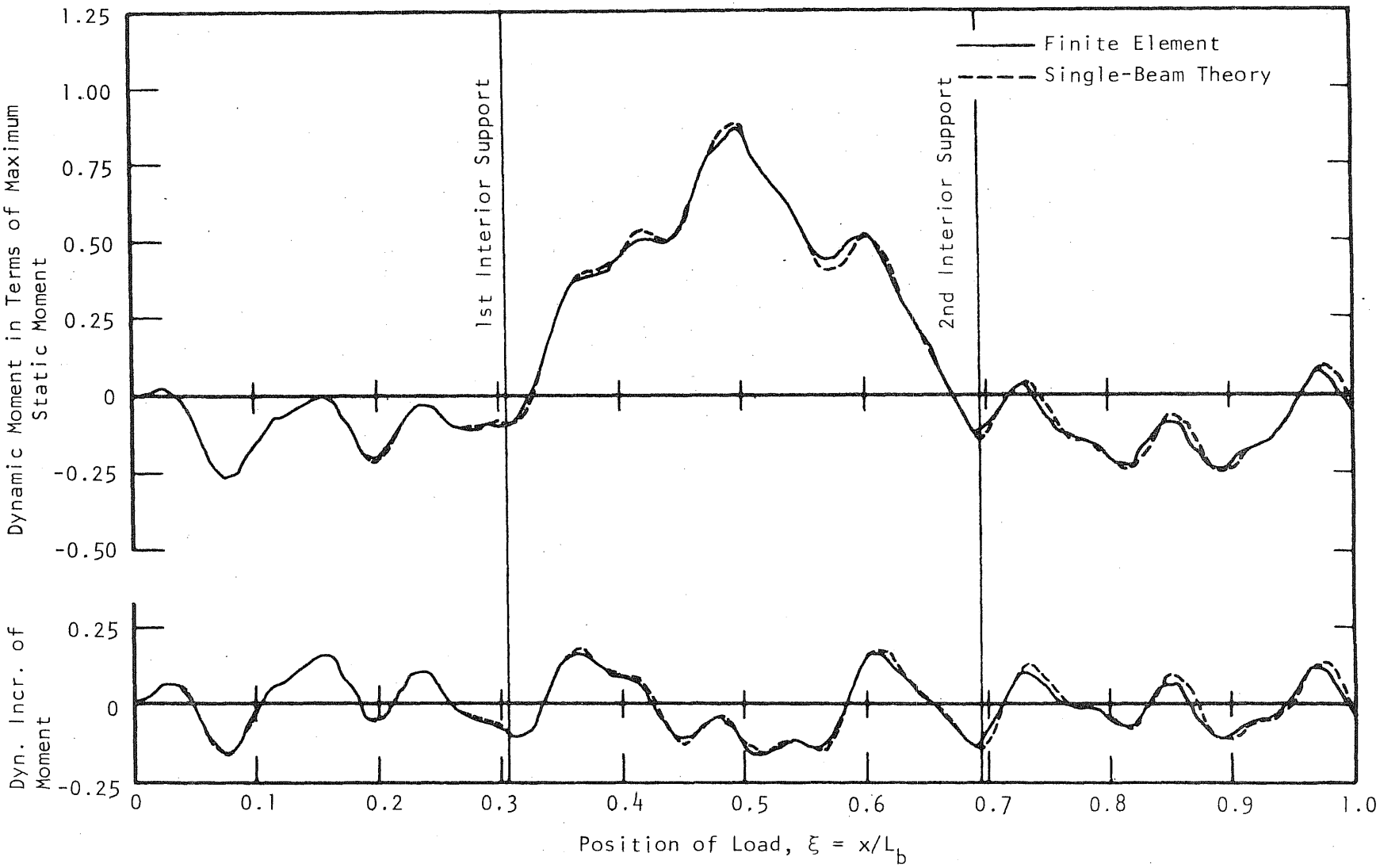

FIG. 59 DYNAMIC MOMENT AT MIDPOINT OF CENTER SPAN, CASE C

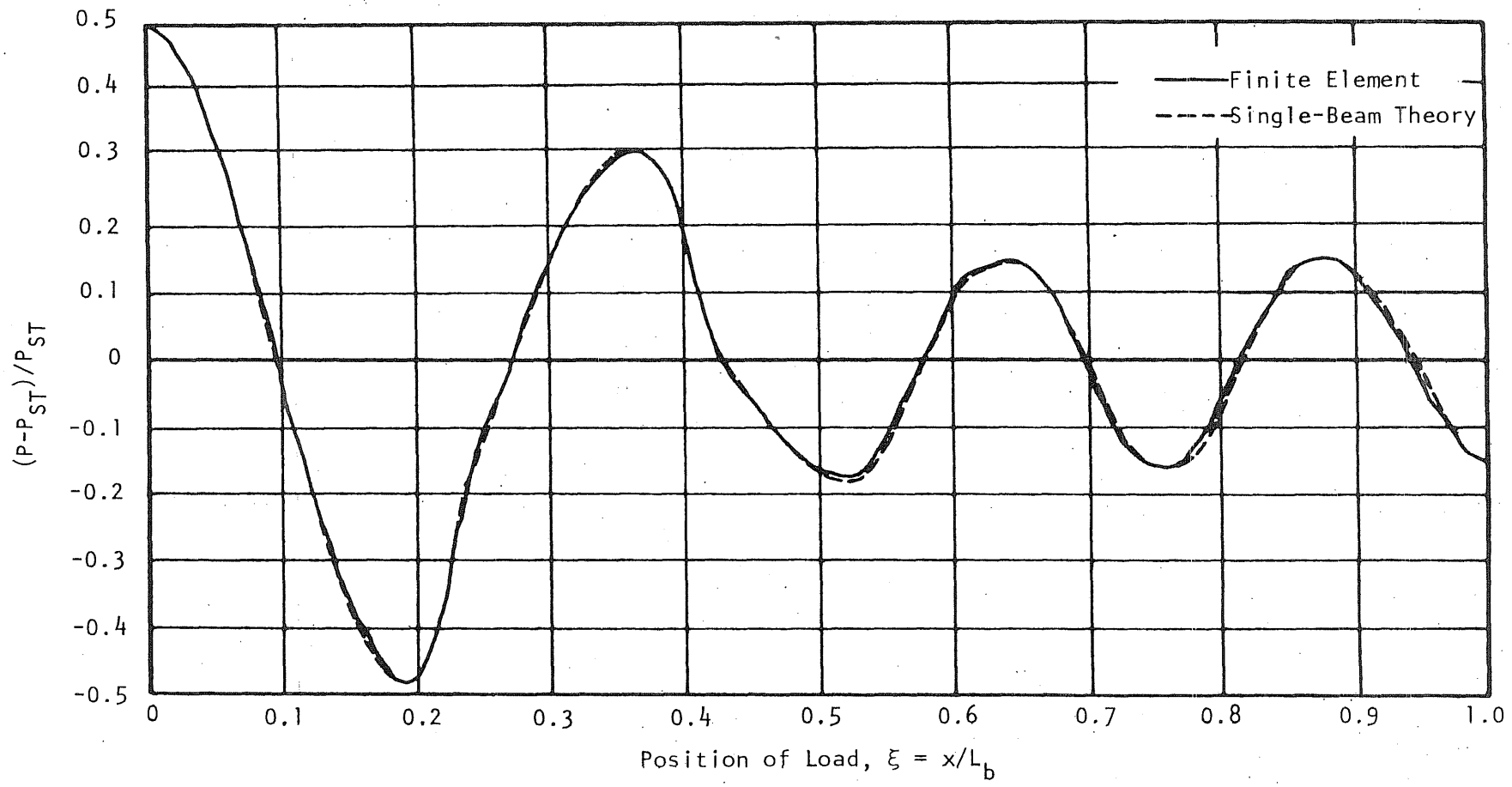

FIG. 60 COMPARISON OF THEORETICAL INTERACTING FORCES FOR THREE-SPAN, SINGLE-BEAM SOLUTION, CASE C

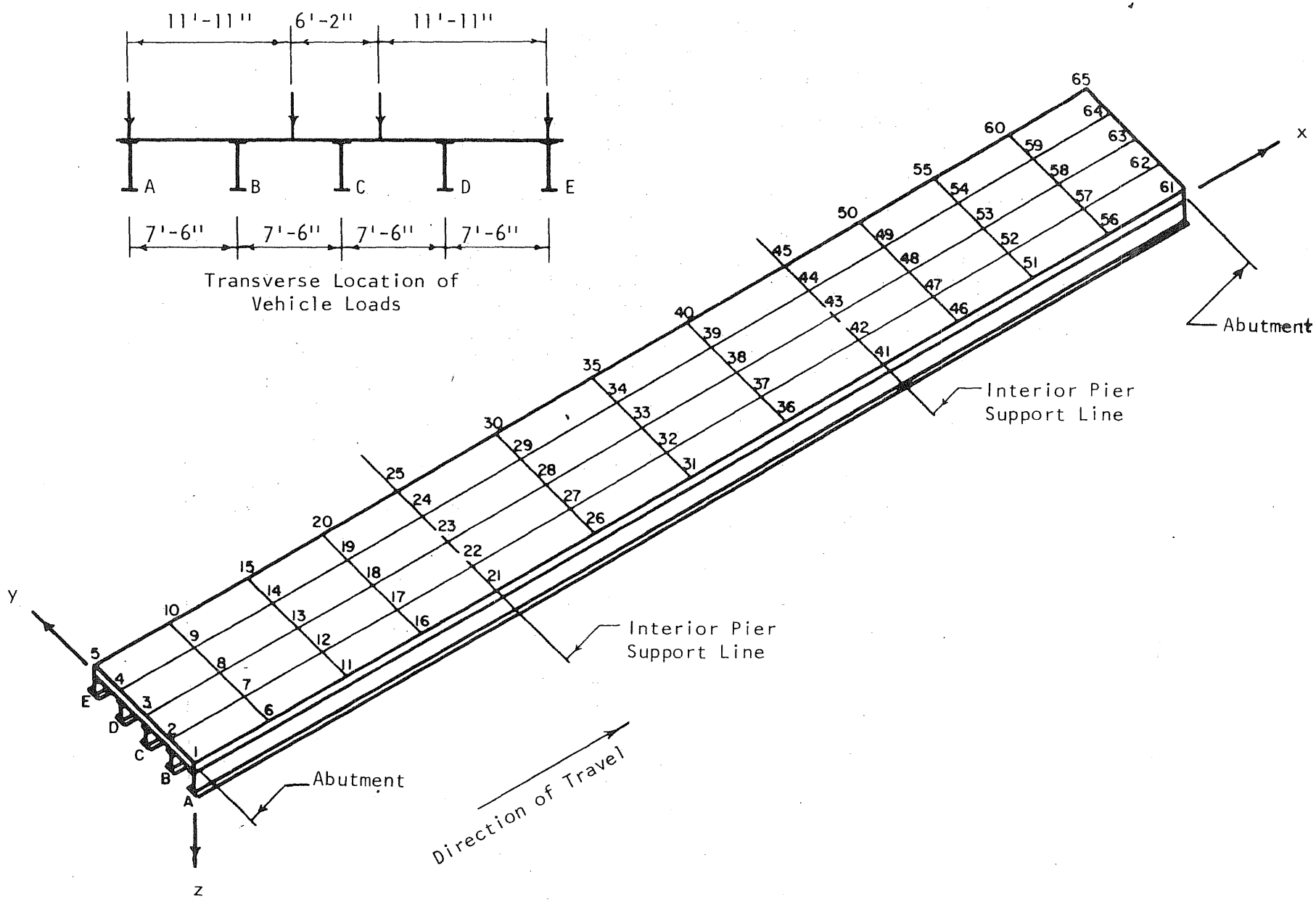

FIG. 61 SALT FORK RIVER BRIDGE MODEL

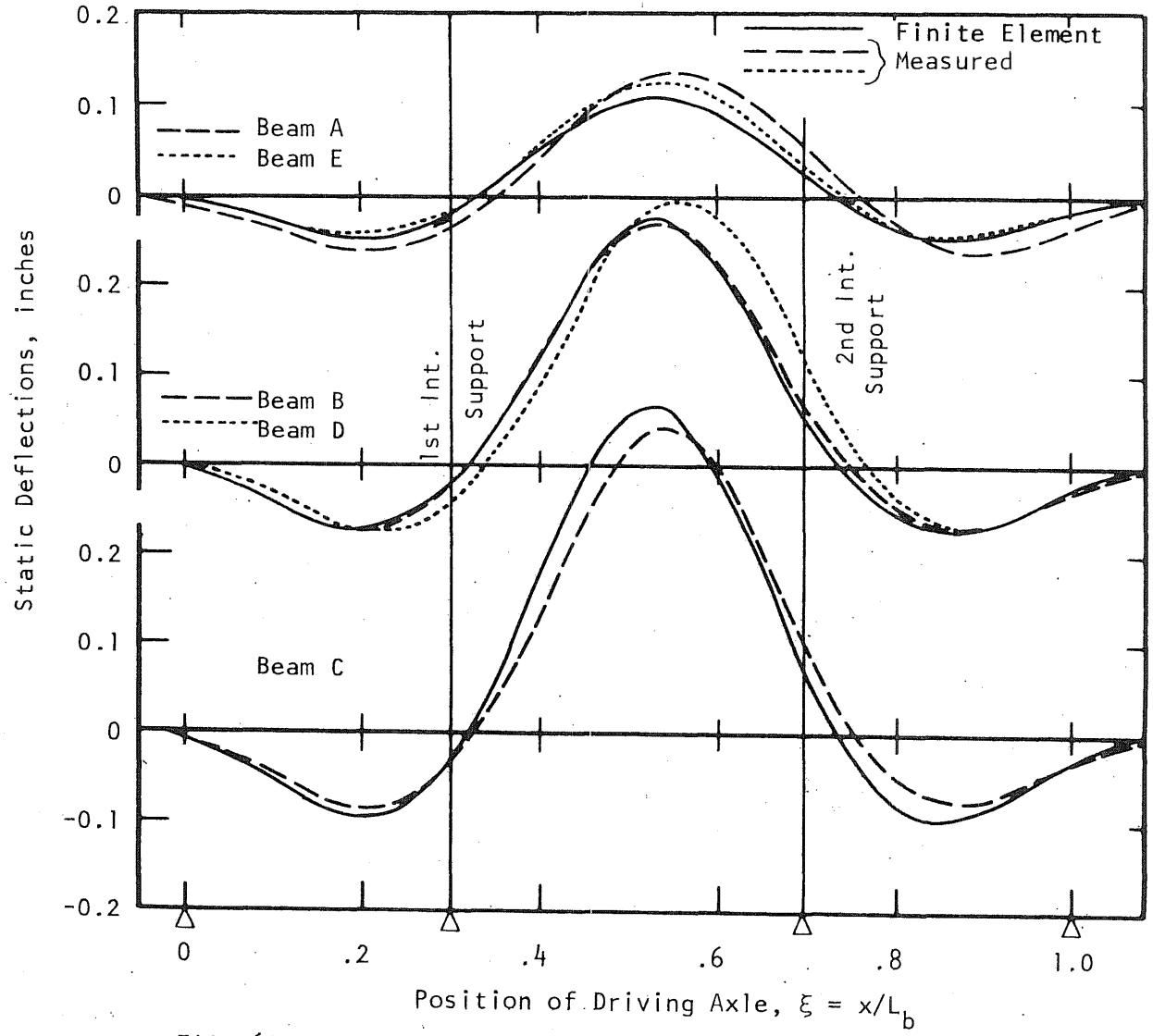

FIG. 62 COMPARISON OF THEORETICAL AND MEASURED DEFLECTIONS AT MIDPOINT OF CENTER SPAN

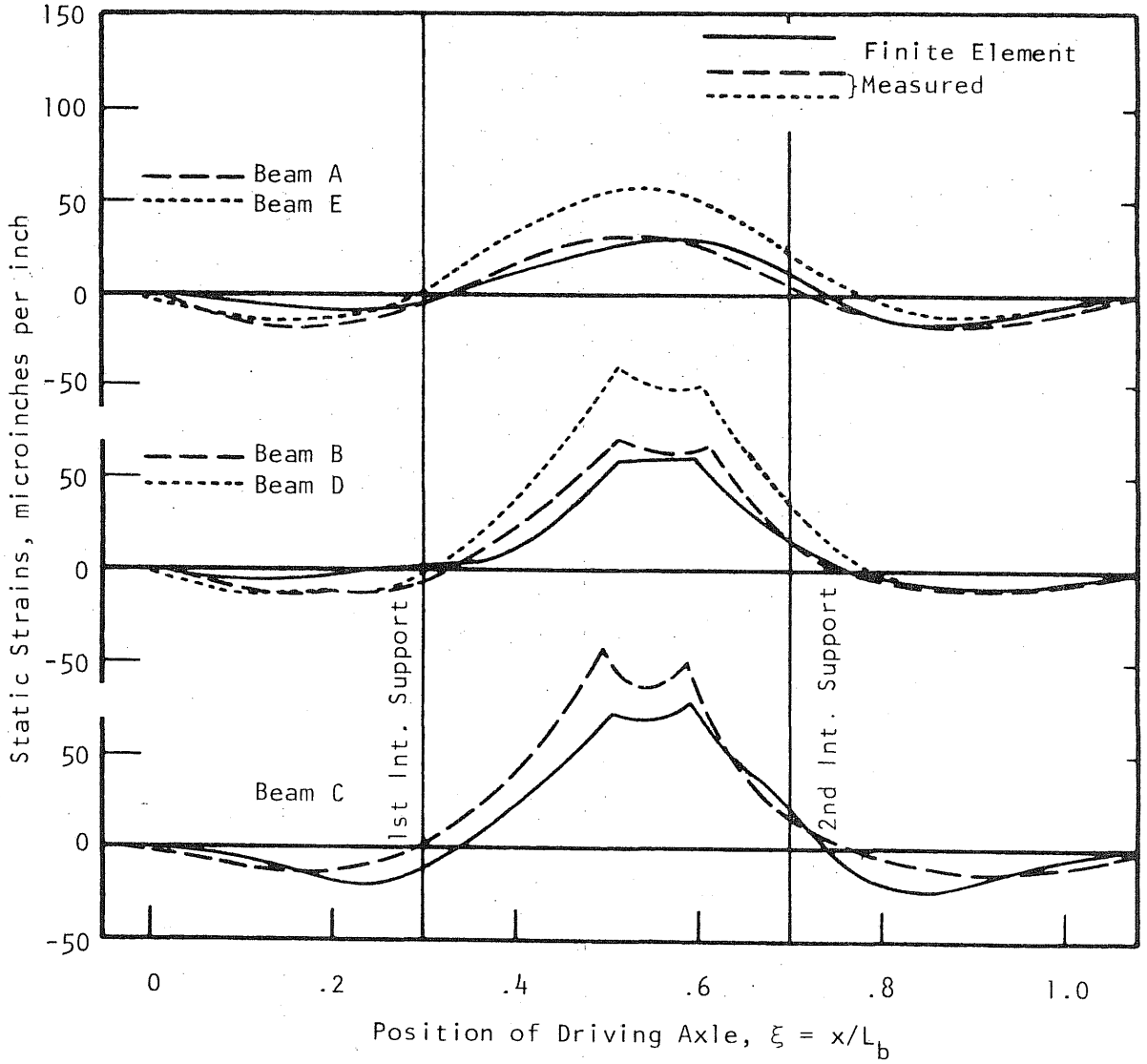

FIG. 63 COMPARISON OF THEORETICAL AND MEASURED STRAINS AT MIDPOINT OF CENTER SPAN

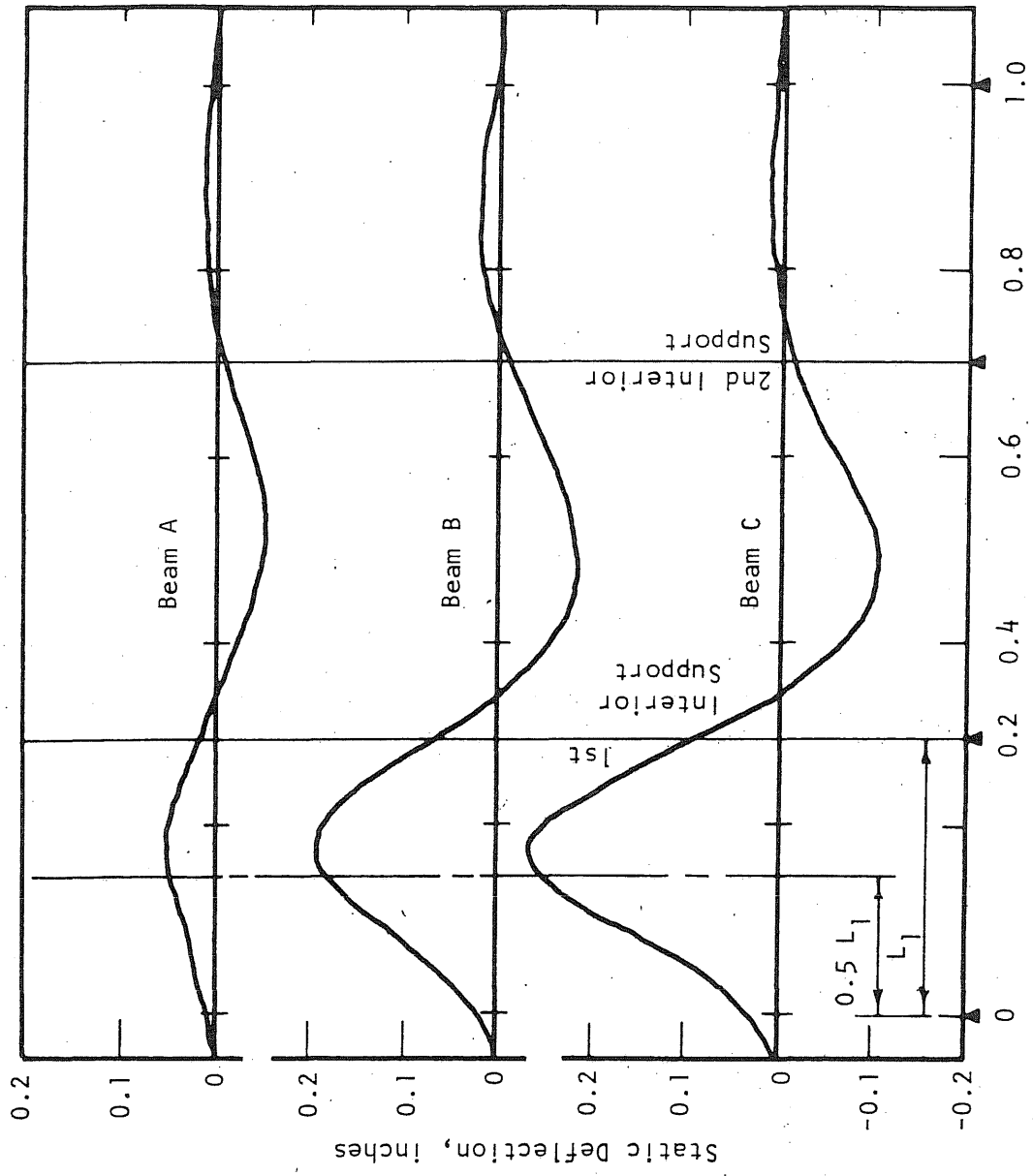

FIG. 64 THEORETICAL DEFLECTIONS AT MIDPOINT OF SPAN 1

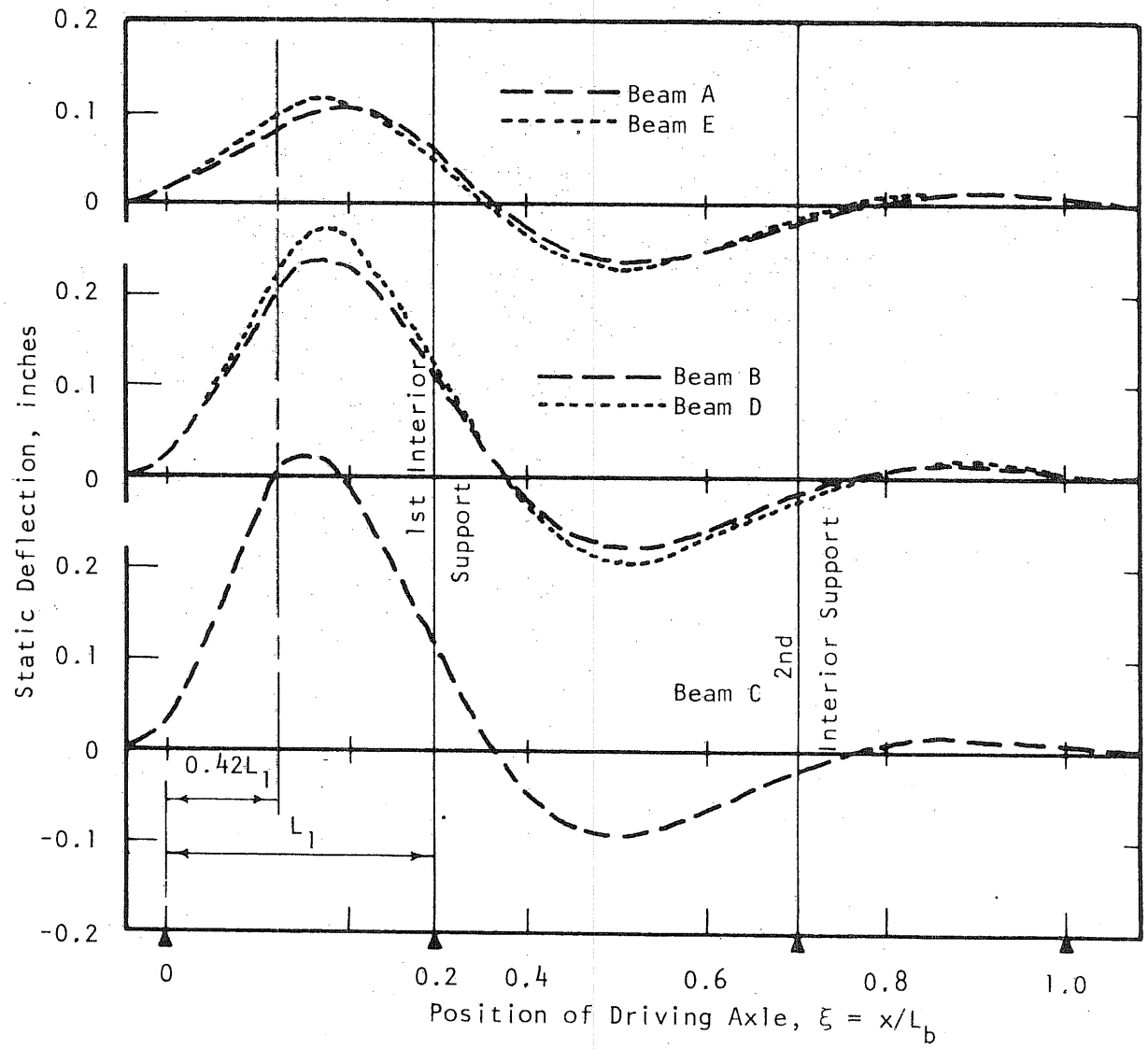

FIG. 65 EXPERIMENTAL DEFLECTIONS AT 0.42 L_1

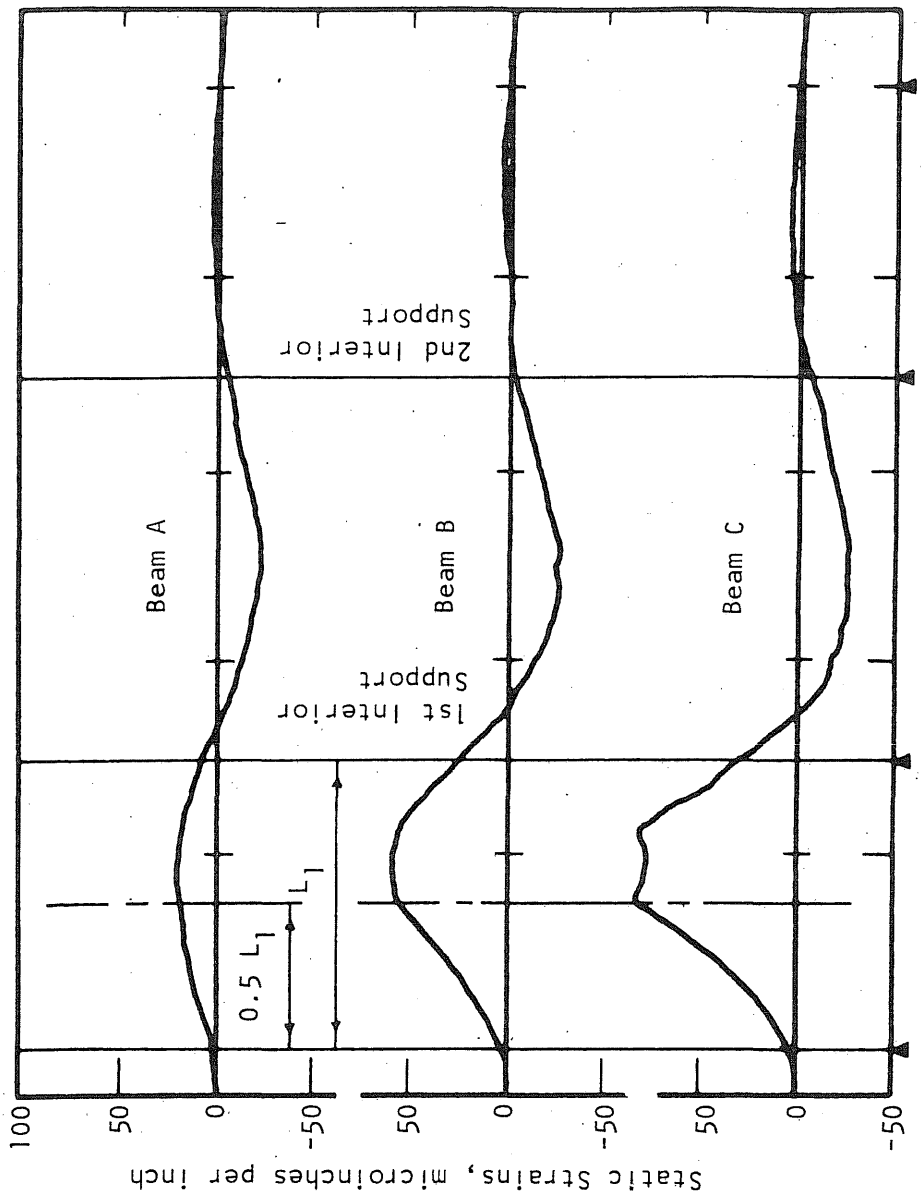

FIG. 66 THEORETICAL STRAINS AT MIDPOINT OF SPAN 1

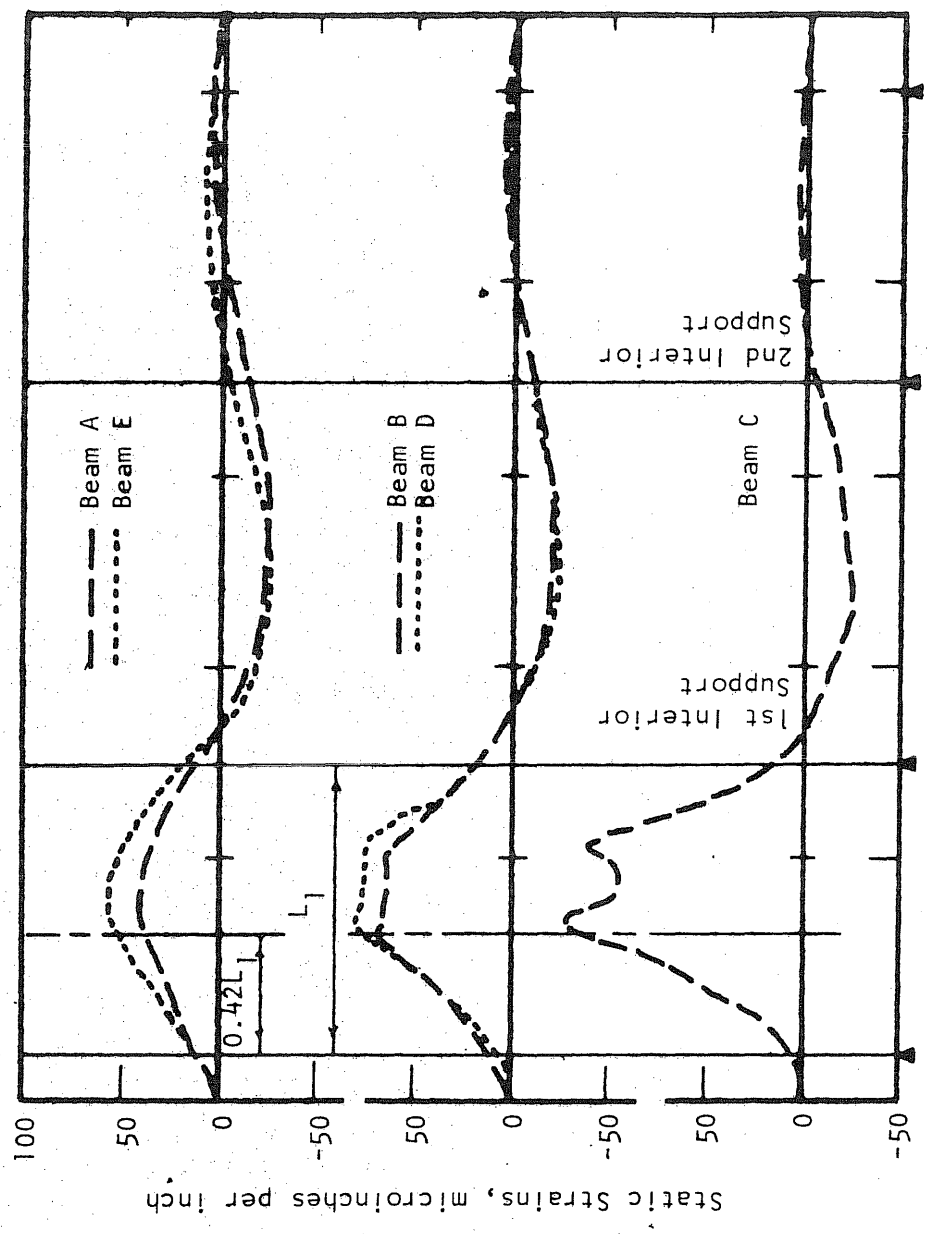

FIG. 67 EXPERIMENTAL STRAINS AT 0.42 L_1

APPENDIX A

A METHOD OF ASSEMBLING THE STIFFNESS MATRIX OF A STRUCTURE

A structural mechanics problem may be solved statically by generating and satisfying the following equation:

$$\{p\} = [K] \{w\} \qquad (A.1)$$

In the K matrix, the submatrix $K_{i,j}$ will be used to represent the coefficients which determine the force subvector that is developed at the ith node of the structure as a result of a unit displacement vector which is imposed on the jth node of the structure. The submatrix $K_{i,j}$ may be generated by summing all member stiffness terms which relate the ith force vector to the jth displacement vector. The stiffness matrix for a single plate element can be written as follows:

$$\left\{\begin{array}{c} F_{fi} \\ F_{pi} \\ \hline F_{fj} \\ F_{pj} \\ \hline F_{fk} \\ F_{pk} \\ \hline F_{fl} \\ F_{pl} \end{array}\right\} = \left[\begin{array}{cc|cc|cc|cc} K_{fii} & 0 & K_{fij} & 0 & K_{fik} & 0 & K_{fil} & 0 \\ & K_{pii} & 0 & K_{pij} & 0 & K_{pik} & 0 & K_{pil} \\ \hline & & K_{fjj} & 0 & K_{fjk} & 0 & K_{fjl} & 0 \\ & & & K_{pjj} & 0 & K_{pjk} & 0 & K_{pjl} \\ \hline & & & & K_{fkk} & 0 & K_{fkl} & 0 \\ & & & & & K_{pkk} & 0 & K_{pkl} \\ \hline & & & & & & K_{fll} & 0 \\ & & & & & & & K_{pll} \end{array}\right] \left\{\begin{array}{c} u_{fi} \\ u_{pi} \\ \hline u_{fj} \\ u_{pj} \\ \hline u_{fk} \\ u_{pk} \\ \hline u_{fl} \\ u_{pl} \end{array}\right\} \qquad (A.2)$$

(Symmetric)

Each K_f term is a 3X3 submatrix of the 12 X 12 stiffness matrix for a given plate element in flexure, and each K_p term is a 2x2 submatrix

of the 8x8 stiffness matrix for a given plain-stress plate element. The subvectors F_{fi} and F_{pi} together form the force vector for the ith node of the plate element. Similarly, K_{fij} and K_{pij} combine to form a 5x5 submatrix which determines the forces that develop at the ith node of the element as a result of a unit displacement vector imposed on the jth node of the element.

Fig. A.1 shows part of a structure that is to be analyzed. In order to illustrate the procedure used in this study, the operations required to form the submatrix which relates the forces at node 12 to the displacements at node 13 will be demonstrated. In order to clarify the procedure, the stiffness matrix which represents the whole structure and includes the stiffness of both plate and beam elements will be referred to as the "global" stiffness matrix. First, the element stiffness matrices for beam element 22 and plate elements 6 and 10 must be developed since these elements are all incident to both node 12 and node 13 as shown in Fig. A.1.

When setting up Eq. (A.2) for plate element 6, the subscripts i, j, k, and l represent nodes 7, 8, 12, and 13, respectively. Therefore, the submatrices K_{fkl} and K_{pkl} in Eq. (A.2) determine the magnitude of the forces at node 12 as a result of the stiffness of plate element 6 when node 13 undergoes some given deformation. Similarly, the subscripts i, j, k, and l represent nodes 12, 13, 17, and 18 when the stiffness matrix in Eq. (A.2) is being developed for plate element 10. The submatrices K_{fij} and K_{pij} represent that part of the stiffness of plate element 10 which determines the relationship between the forces at node 12 and the displacements at node 13.

The stiffness equation for a typical beam element may be written as follows:

$$\begin{Bmatrix} F_{si} \\ \hline F_{sj} \end{Bmatrix} = \left[\begin{array}{c|c} K_{sii} & K_{sij} \\ \hline K_{sji} & K_{sjj} \end{array}\right] \begin{Bmatrix} u_{si} \\ \hline u_{sj} \end{Bmatrix} \qquad \text{(A.3)}$$

The subvector F_{si} includes the shear in the vertical direction, the bending moment, the torsion, the axial force, and the shear in the horizontal direction at the ith node. The subvector u_{si} contains the vertical displacement, the bending, rotation, the torsional rotation, the axial deformation, and the horizontal displacement of the member at the ith node. The horizontal component of shear will be zero except for the case in which a skewed structure is analyzed. If the stiffness matrix in Eq. (A.3) is generated for beam element 22, the term K_{ij} would relate the forces at node 12 to the displacements at node 13. The global stiffness submatrix $K_{g12,13}$ is found to be the sum of the submatrices K_{fkl} and K_{pkl} from plate element 6, K_{fij} and K_{pij} from plate element 10, and K_{sij} from beam element 22.

The above process can be performed according to information contained in the member incidence table for the structure. However, for larger problems an alternate approach becomes more advantageous. If the global stiffness matrix is generated directly from information contained in the member incidence table, the procedure is best performed by considering one member at a time. However, when analyzing larger problems, it is more efficient to form the K_g matrix joint by joint rather than member by member. This can be accomplished simply by scanning the member incidence table and creating a joint incidence

table; a joint incidence table is one which lists the elements which connect with each joint. In general, each joint will have a maximum of four plate elements and four beam elements connected to it. The table might be arranged as follows for joints 11 and 12 in Fig. A.1:

	plate elements				beam elements			
Jt. No.					x dir.		y dir.	
	i	j	k	l	i	j	i	j
11	9	0	5	0	9	5	21	0
12	10	9	6	5	10	6	22	21

The global stiffness matrix may now be created five rows at a time; each of the five rows will correspond to one of the five degrees of freedom at the joint currently under consideration. Only those elements in each row which fall within the band width of the matrix must be considered. All elements outside the band width are null and, therefore, not considered in the procedure. The band width for the structure shown in Fig. A.1 includes fifteen joints. Since each joint has five degrees of freedom, the size of the portion of the K_g matrix which is generated at any one time is 5 rows deep by 75 columns wide. This 5x75 element potion of the K_g matrix can be subdivided into fifteen 5x5 submatrices. For simplicity, each 5x5 submatrix will hereafter be treated as if it were a single term in the K_g matrix. Therefore, a 5x75 element portion of K_g will now be considered to be one row in depth and fifteen columns wide. Dotted lines show how the stiffness matrix in Eq. (A.2) can also be divided into 5x5 submatrices. Hence, this stiffness matrix will now be treated as if it were a 4x4 matrix in this discussion. Similarly, K_s in Eq. (A.3) will be treated as a 2x2 matrix.

As shown in the joint incidence table, four plate elements and four beam elements affect the stiffness coefficients in the twelfth row of K_g. For plate element 10, the subscripts i, j, k, and l in Eq. (A.2) represent joints 12, 13, 17, and 18, respectively. Hence, the first row corresponds to the twelfth row of K_g, and the four terms in the first row are placed in columns 12, 13, 17, and 18, respectively, in K_g. Similarly, the four terms in the second row of the element stiffness matrix for plate element 9 are placed in columns 11, 12, 16, and 17, respectively, in K_g. When the twelfth row of K_g is completed, there will be non-zero terms in columns 6, 7, 8, 11, 12, 13, 16, 17, and 18. All 15 terms within the band width are then placed in secondary storage, and the process is repeated for the thirteenth row K_g. The terms in columns 9, 10, 14, 15, 19, and 20 in the twelfth row are stored in secondary storage even though they are all equal to zero simply because it reduces the amount of "bookkeeping" to be done.

The process discussed above is quite satisfactory since only eight element stiffness matrices and one row of K_g has to be in primary storage at any one time. The amount of storage required can be further reduced if symmetry is taken into account.

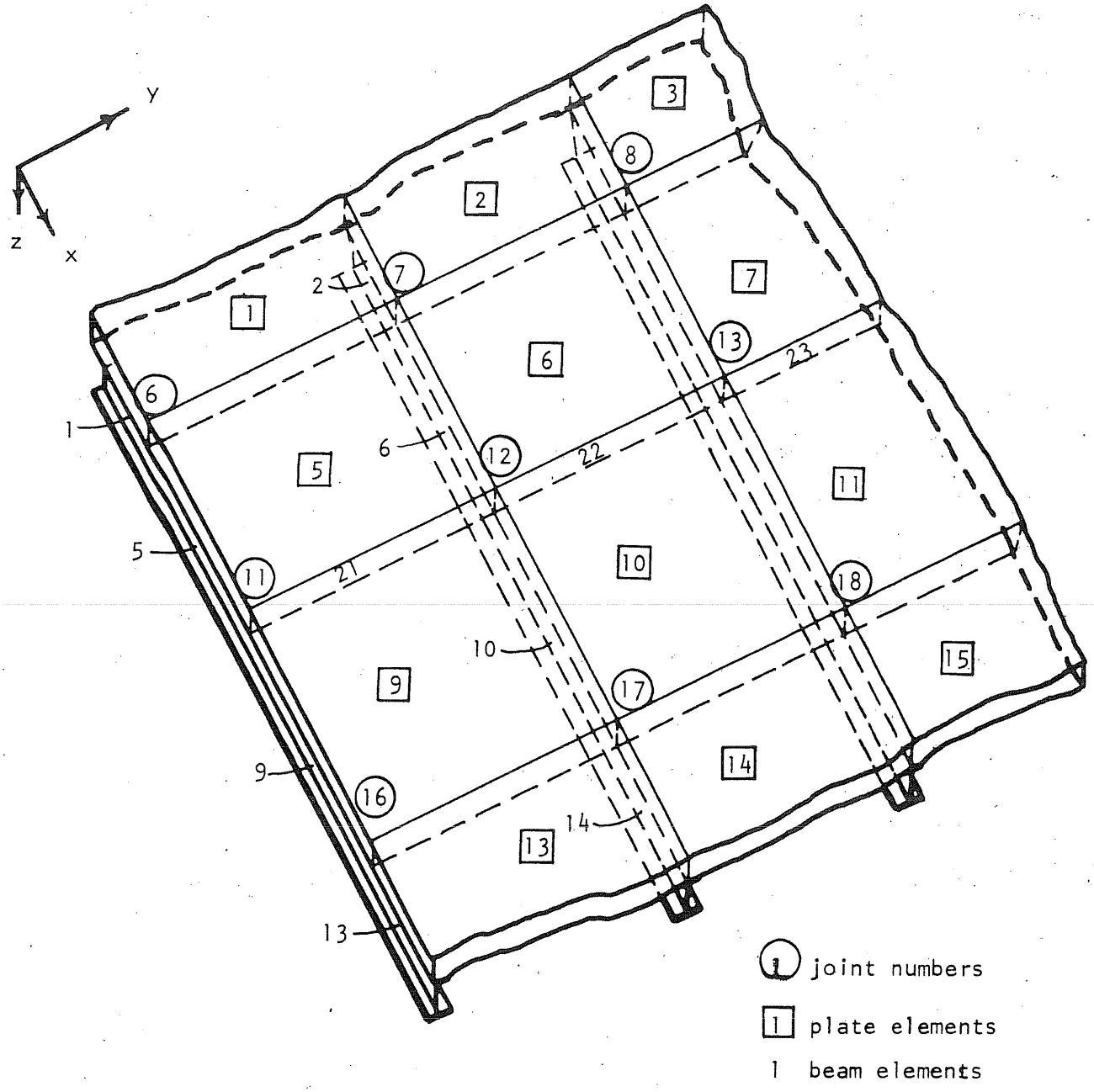

FIG. A.1 - SECTION FROM A TYPICAL BRIDGE MODEL

APPENDIX B

DERIVATION OF THE EQUATIONS OF MOTION FOR THE VEHICLE

B.1 Notation

In addition to the symbols used in the text, the following notation is introduced:

F_{ta1}, F_{ta2} = vertical inertia forces of W_1 and W_2, respectively

f_{tai} = vertical inertia force of w_i

P_{di} = disturbing force at the ith support point of the vehicle mass

T_{taix}, T_{taiy} = inertial torques of W_i about the x and y axes, respectively

R_v = the difference between the dynamic and static components of the vertical interacting forces at the "fifth wheel pivot"

I_{1x}, I_{1y}, I_{2x}, I_{2y} = rotary moments of inertia of W_1 and W_2 about the x and y axes. These quantities are given by the equations

$$\frac{I_{1x}}{S_1^2} = \frac{i_{1x}^2 W_1}{4g} \qquad \frac{I_{1y}}{L_1^2} = a_1 a_2 i_{1y}^2 \frac{W_1}{g}$$

$$\frac{I_{2x}}{S_3^2} = \frac{i_{2x}^2 W_2}{4g} \qquad \frac{I_{2y}}{L_3^2} = a_3 a_4 i_{2y}^2 \frac{W_2}{g}$$

B.2 Derivation of Equations

In the derivation which follows, it has been assumed that S_1 is equal to S_2. The quantities S_1 and S_2 are shown in Fig. B.1. First, a free body of the trailer is taken as shown in Fig. B.1a. The

elevation of the "fifth wheel pivot" is

$$E_5 = 1/2\ (a_5(z_1 + z_2) + (1-a_5)(z_3 + z_4)) + \text{a constant}$$

The elevation of the center of gravity of W_2 is

$$E_2 = 1/2\ a_4\ (z_5 + z_6) + a_3(E_5) + \text{a constant}$$

$$= 1/2(a_3a_3(z_1 + z_2) + a_3(1-a_5)(z_3 + z_4) + a_4(z_5 + z_6)) + \text{a constant}$$

The angular rotations of W_2 about the x and y axes are

$$\theta_{ta2x} = (z_6 - z_5) / S_3 + \text{a constant}$$

and

$$\theta_{ta2y} = (E_5 - 1/2\ (z_5 + z_6)) / L_3 + \text{a constant}$$

$$= (a_5(z_1 + z_2) + (1-a_5)(z_3 + z_4) - z_5 - z_6) / (2L_3) + \text{a constant}$$

The vertical inertia forces are

$$F_{ta2} = W_2(a_3a_5(\ddot{z}_1 + \ddot{z}_2) + a_3(1-a_5)(\ddot{z}_3 + \ddot{z}_4) + a_4(\ddot{z}_5 + \ddot{z}_6))/(2g) \quad (B.1)$$

$$f_{ta5} = w_5\ \ddot{z}_5 / g \quad (B.2)$$

$$f_{ta6} = w_6\ \ddot{z}_6 / g \quad (B.3)$$

The inertial torques are

$$T_{ta2x} = I_{2x}\ (\ddot{z}_6 - \ddot{z}_5) / S_3 \quad (B.4)$$

and

$$T_{ta2y} = I_{2y}(a_5(\ddot{z}_1 + \ddot{z}_2) + (1-a_5)(\ddot{z}_3 + \ddot{z}_4) - \ddot{z}_5 - \ddot{z}_6)/(2L_3) \quad (B.5)$$

Taking moments about an axis through points c and d, one obtains the equation

$$R_v + a_3 F_{ta2} + T_{ta2y} / L_3 = 0. \tag{B.6}$$

By substituting Eqs. (B.1) and (B.5), Eq. (B.6) becomes

$$R_v = -a_5(a_3^2 + a_3 a_4 i_{2y}) \frac{W_2}{2g} (\ddot{z}_1 + \ddot{z}_2) - (1-a_5)(a_3^2 + a_3 a_4 i_{2y}) \frac{W_2}{2g} (z_3 + z_4)$$
$$-a_3 a_4 (1 - i_{2y}) \frac{W_2}{g} (\ddot{z}_5 + \ddot{z}_6) \tag{B.7}$$

Taking moments about an axis parallel to the x axis through point c, one obtains

$$1/2\ F_{ta2} + f_{ta6} + T_{ta2x} / S_3 + 1/2\ R_v + P_{d6} = 0. \tag{B.8}$$

Substitution of Eqs. (B.1), (B.3), (B.4), and (B.7) yields

$$a_3 a_4 a_5 (1-i_{2y}) \frac{W_2}{4g} (\ddot{z}_1 + \ddot{z}_2) + a_3 a_4 (1-a_5)(1-i_{2y}) \frac{W_2}{4g} (\ddot{z}_3 + \ddot{z}_4)$$
$$+(a_4 - i_{2x} - a_3 a_4 (1-i_{2y})) \frac{W_2}{4g} \ddot{z}_5 + \left[(a_4 + i_{2x} - a_3 a_4 (1-i_{2y})) \frac{W_2}{4g} + \frac{W_6}{g} \right] \ddot{z}_6$$
$$+ P_{d6} = 0. \tag{B.9}$$

Taking moments about an axis parallel to the x axis through point d, one obtains the equation

$$1/2\ F_{ta2} + f_{ta5} - T_{ta2x} / S_3 + 1/2\ R_v + P_{d5} = 0. \tag{B.10}$$

After substituting Eqs. (B.1), (B.2), (B.4), and (B.7), Eq. (B.10) becomes

$$a_3 a_4 a_5 (1-i_{2y}) \frac{W_2}{4g} (\ddot{z}_1 + \ddot{z}_2) + a_3 a_4 (1-a_5) (1-i_{2y}) \frac{W_2}{4g} (\ddot{z}_3 + \ddot{z}_4)$$
$$+ \left[(a_4 + i_{2x} - a_3 a_4 (1-i_{2y}) \frac{W_2}{4g} + \frac{W_5}{g} \right] \ddot{z}_5 + (a_4 - i_{2x} - a_3 a_4 (1-i_{2y})) \frac{W_2}{4g} \ddot{z}_6$$
$$+ P_{d5} = 0. \qquad \text{(B.11)}$$

Next, a free body of the tractor is taken as shown in Fig. B.1b. The elevation of the center of gravity of W_1 is

$$E_1 = 1/2 \, (a_1 (z_1 + z_2) + a_2 (z_3 + z_4)) + \text{a constant}$$

The angular rotations of W_1 about the x and y axes are

$$\theta_{ta1x} = (a_1 (z_2 - z_1) + a_2 (z_4 - z_3)) / S_1$$

and

$$\theta_{ta1y} = 1/2 \, (z_1 + z_2 - z_3 - z_4) / L_1$$

The vertical inertia forces are

$$F_{ta1} = W_1 (a_1 (\ddot{z}_1 + \ddot{z}_2) + a_2 (\ddot{z}_3 + \ddot{z}_4)) / (2g) \qquad \text{(B.12)}$$

$$f_{ta1} = w_1 \ddot{z}_1 / g \qquad \text{(B.13)}$$

$$f_{ta2} = w_2 \ddot{z}_2 / g \qquad \text{(B.14)}$$

$$f_{ta3} = w_3 \ddot{z}_3 / g \qquad \text{(B.15)}$$

$$f_{ta4} = w_4 \ddot{z}_4 / g \qquad \text{(B.16)}$$

The inertial torques are

$$T_{ta1x} = I_{1x}(a_1(\ddot{z}_2 - \ddot{z}_1) + a_2(\ddot{z}_4 - \ddot{z}_3)) / S_1 \qquad (B.17)$$

and

$$T_{ta1y} = I_{1y}(z_1 + z_2 - z_3 - z_4) / (2L_1) \qquad (B.18)$$

Taking moments about an axis which is parallel to the y axis through point b, one obtains the equation

$$a_1 F_{ta1} - a_5 R_v + T_{ta1y} / L_1 + f_{ta1} + f_{ta2} + P_{d1} + P_{d2} = 0 \qquad (B.19)$$

The substitution of Eqs. (B.7), (B.12), (B.13), (B.14), and (B.18) into Eq. (B.19) yields the following:

$$\begin{aligned}
&(a_1(a_1 + a_2 i_{1y}) \frac{W_1}{2g} + a_3 a_5 (a_3 + a_4 i_{2y}) \frac{W_2}{2g})(\ddot{z}_1 + \ddot{z}_2) + \frac{W_1}{g}\ddot{z}_1 + \frac{W_2}{g}\ddot{z}_2 \\
&+ (a_1 a_2 (1-i_{1y}) \frac{W_1}{2g} + a_3 a_5 (1-a_5)(a_3 + a_4 i_{2y}) \frac{W_2}{2g})(\ddot{z}_3 + \ddot{z}_4) \\
&+ a_3 a_4 a_5 (1-i_{2y}) \frac{W_2}{2g}(z_5 + z_6) + P_{d1} + P_{d2} = 0. \qquad (B.20)
\end{aligned}$$

By taking moments about an axis which is parallel to the x axis through point a, the following equation is obtained:

$$1/2\, F_{ta1} - 1/2\, R_v + T_{ta1x} / S_1 + f_{ta2} + f_{ta4} + P_{d2} + P_{d4} = 0. \qquad (B.21)$$

Eqs. (B.7), (B.12), (B.14), (B.16), and (B.17) are now substituted into Eq. (B.21) with the following result:

$$\left(a_1(1-i_{1x})\frac{W_1}{4g} + a_3a_5(a_3 + a_4i_{2y})\frac{W_2}{4g}\right)\ddot{z}_1$$

$$+ \left(a_1(1+i_{1x})\frac{W_1}{4g} + a_3a_5(a_3 + a_4i_{2y})\frac{W_2}{4g} + \frac{w_2}{g}\right)\ddot{z}_2$$

$$+ \left(a_2(1-i_{1x})\frac{W_1}{4g} + a_3(1-a_5)(a_3 + a_4i_{2y})\frac{W_2}{4g}\right)\ddot{z}_3$$

$$+ \left(a_2(1+i_{1x})\frac{W_1}{4g} + a_3(1-a_5)(a_3 + a_4i_{2y})\frac{W_2}{4g} + \frac{w_4}{g}\right)\ddot{z}_4$$

$$+ a_3a_4(1-i_{2y})\frac{W_2}{4g}(\ddot{z}_5 + \ddot{z}_6) + P_{d2} + P_{d4} = 0. \qquad (B.22)$$

Next, moments are summed about an axis through point a parallel to the y axis with the following result:

$$a_2F_{ta1} - (1-a_5)R_v - T_{ta1y}/L_1 + f_{ta3} + f_{ta4} + P_{d3} + P_{d4} = 0. \qquad (B.23)$$

Through the use of Eqs. (B.7), (B.12), (B.15), (B.16), and (B.18), Eq. (B.23) is modified as follows:

$$\left(a_1a_2(1-i_{1y})\frac{W_1}{2g} + a_3a_5(1-a_5)(a_3 + a_4i_{2y})\frac{W_2}{2g}\right)(\ddot{z}_1 + \ddot{z}_2)$$

$$+ \left(a_2(a_2 + a_1i_{1y})\frac{W_1}{2g} + a_3(1-a_5)^2(a_3 + a_4i_{2y})\frac{W_2}{2g}\right)(z_3 + z_4) + \frac{w_3}{g}\ddot{z}_3 + \frac{w_4}{g}\ddot{z}_4$$

$$+ a_3a_4(1-a_5)(1-i_{2y})\frac{W_2}{2g}(\ddot{z}_5 + \ddot{z}_6) + P_{d3} + P_{d4} = 0. \qquad (B.24)$$

Eq. (B.20) is now modified by subtracting Eq. (B.22) from it as follows:

$$\left(a_1\left(a_1 - a_2(1-2i_{1y}) + i_{1x}\right)\frac{W_1}{4g} - a_3a_5(1-2a_5)(a_3 + a_4 i_{2y})\frac{W_2}{4g} + \frac{w_1}{g}\right)\ddot{z}_1$$

$$+ \left(a_1\left(a_1 - a_2(1-2i_{1y}) - i_{1x}\right)\frac{W_1}{4g} - a_3a_5(1-2a_5)(a_3 + a_4 i_{2y})\frac{W_2}{4g}\right)\ddot{z}_2$$

$$+ \left(a_2\left(a_1(1-2i_{1y}) - a_2 + i_{1x}\right)\frac{W_1}{4g} - a_3(1-a_5)(1-2a_5)(a_3 + a_4 i_{2y})\frac{W_2}{4g}\right)\ddot{z}_3$$

$$+ \left(a_2\left(a_1(1-2i_{1y}) - a_2 - i_{1x}\right)\frac{W_1}{4g} - a_3(1-a_5)(1-2a_5)(a_3 + a_4 i_{2y})\frac{W_2}{4g} - \frac{w_4}{g}\right)\ddot{z}_4$$

$$- a_3a_4(1-2a_5)(1-i_{2y})\frac{W_2}{4g}(\ddot{z}_5 + \ddot{z}_6) + P_{d1} - P_{d4} = 0. \qquad \text{(B.25)}$$

The vehicle model used in this study is one degree indeterminate. Therefore, one condition of compatibility is required in order to provide one additional independent equation. Since the tractor body is assumed to be a rigid mass, it can be shown geometrically that the following relationship must be true:

$$z_4 = z_2 + z_3 - z_1 \qquad \text{(B.26)}$$

If Eq. (B.26) is differentiated twice with respect to time, the result is as follows:

$$\ddot{z}_4 = \ddot{z}_2 + \ddot{z}_3 - \ddot{z}_1 \qquad \text{(B.27)}$$

At this point it becomes advantageous to define P_{di}, the disturbing force at the ith support point of the vehicle mass, mathematically as follows:

$$P_{di} = k_i z_i - P_{wi} \tag{B.28}$$

where k_i is the stiffness of the tire-suspension spring assembly that acts at the ith support point of the vehicle mass. The quantity P_{wi} denotes that part of the total disturbing force which cannot be expressed as a function of the vehicle displacement coordinate z_i; P_{wi} is instead a function of the configuration of the surface on which the vehicle is traveling.

Eqs. (B.27) and (B.28) are now substituted into Eqs. (B.25), (B.22), and (B.24) as follows:

$$\left[((a_1 - a_2)(a_1 - a_2 + i_{1x}) + 4a_1a_2i_{1y})\frac{W_1}{4g} + a_3(1-2a_5)^2(a_3 + a_4 i_{2y})\frac{W_2}{4g} + \frac{w_1}{g}\right]\ddot{z}_1$$
$$+ \left[(a_1 - a_2 - i_{1x})\frac{W_1}{4g} - a_3(1-2a_5)(a_3 + a_4 i_{2y})\frac{W_2}{4g}\right]\ddot{z}_2$$
$$+ \left[a_2(a_1(1-2i_{1y}) - a_2)\frac{W_1}{2g} - a_3(1-a_5)(1-2a_5)(a_3 + a_4 i_{2y})\frac{W_2}{2g}\right]\ddot{z}_3 - \frac{w_4}{g}\ddot{z}_4$$
$$- a_3a_4(1-2a_5)(1-i_{2y})\frac{W_2}{4g}(\ddot{z}_5 + \ddot{z}_6) + k_1z_1 - P_{w1} - k_4z_4 + P_{w4} = 0. \tag{B.29}$$

$$\left[(a_1 - a_2 - i_{1x})\frac{W_1}{4g} - a_3(1-2a_5)(a_3 + a_4 i_{2y})\frac{W_2}{4g}\right]\ddot{z}_1$$
$$+ \left[(1+i_{1x})\frac{W_1}{4g} + a_3(a_3 + a_4 i_{2y})\frac{W_2}{4g} + \frac{w_2}{g}\right]\ddot{z}_2$$
$$+ \left[a_2\frac{W_1}{2g} + a_3(1-a_5)(a_3 + a_4 i_{2y})\frac{W_2}{2g}\right]\ddot{z}_3 + \frac{w_4}{g}\ddot{z}_4$$
$$+ \left[a_3a_4(1-i_{2y})\frac{W_2}{4g}\right](\ddot{z}_5 + \ddot{z}_6) + k_2z_2 - P_{w2} + k_4z_4 - P_{w4} = 0. \tag{B.30}$$

$$\left[a_2(a_1(1-2i_{1y})-a_2)\frac{W_1}{2g} - a_3(1-a_5)(1-2a_5)(a_3 + a_4 i_{2y})\frac{W_2}{2g} \right] \ddot{z}_1$$

$$+ \left[a_2\frac{W_1}{2g} + a_3(1-a_5)(a_3 + a_4 i_{2y})\frac{W_2}{2g} \right] \ddot{z}_2$$

$$+ \left[a_2(a_2 + a_1 i_{1y})\frac{W_1}{g} + a_3(1-a_5)^2(a_3 + a_4 i_{2y})\frac{W_2}{g} + \frac{W_3}{g} \right] \ddot{z}_3 + \frac{W_4}{g} \ddot{z}_4$$

$$+ \left[a_3 a_4(1-a_5)(1-i_{2y})\frac{W_2}{2g} \right] (\ddot{z}_5 + \ddot{z}_6) + k_3 z_3 - P_{w3} + k_4 z_4 - P_{w4} = 0. \quad (B.31)$$

Next, Eq. (B.26) is multiplied by k_4 and added to Eq. (B.27) multiplied by w_4 / g to yield the following modified compatibility equation:

$$\frac{w_4}{g}(-\ddot{z}_1 + \ddot{z}_2 + \ddot{z}_3 - \ddot{z}_4) + k_4(-z_1 + z_2 + z_3 - z_4) = 0. \quad (B.32)$$

Eqs. (B.27) and (B.28) are also substituted into Eqs. (B.11) and (B.9) as follows:

$$-a_3 a_4(1-2a_5)(1-i_{2y})\frac{W_2}{4g} \ddot{z}_1 + a_3 a_4(1-i_{2y})\frac{W_2}{4g} \ddot{z}_2$$

$$+ a_3 a_4(1-a_5)(1-i_{2y})\frac{W_2}{2g} \ddot{z}_3$$

$$+ \left[(a_4 + i_{2x} - a_3 a_4(1-i_{2y}))\frac{W_2}{4g} + \frac{w_5}{g} \right] \ddot{z}_5$$

$$+ (a_4 - i_{2x} - a_3 a_4(1-i_{2y}))\frac{W_2}{4g} \ddot{z}_6 + k_5 z_5 - P_{w5} = 0. \quad (B.33)$$

and

$$-a_3a_4(1-2a_5)\,(1-i_{2y})\,\frac{W_2}{4g}\,\ddot{z}_1 + a_3a_4(1-i_{2y})\,\frac{W_2}{4g}\,\ddot{z}_2$$

$$+ \quad a_3a_4(1-a_5)\,(1-i_{2y})\,\frac{W_2}{2g}\,\ddot{z}_3 + (a_4 - i_{2x} - a_3a_4(1-i_{2y}))\,\frac{W_2}{4g}\,\ddot{z}_5$$

$$+ \left[(a_4 + i_{2x} - a_3a_4(1-i_{2y}))\,\frac{W_2}{4g} + \frac{w_6}{g}\right]\ddot{z}_6 + k_6z_6 - P_{w6} = 0. \qquad \text{(B.34)}$$

Finally, the equations of motion for the vehicle model can be written in matrix form as follows:

$$[m]\,\{\ddot{z}\} + [k_v]\,\{z\} = [h]\,\{P_w\} \qquad \text{(B.35)}$$

Eqs. (B.29) through (B.34) form rows 1 through 6, respectively, in the above matrix expression. The 6x6 matrices m, k_v, and h are given explicitly in the text.

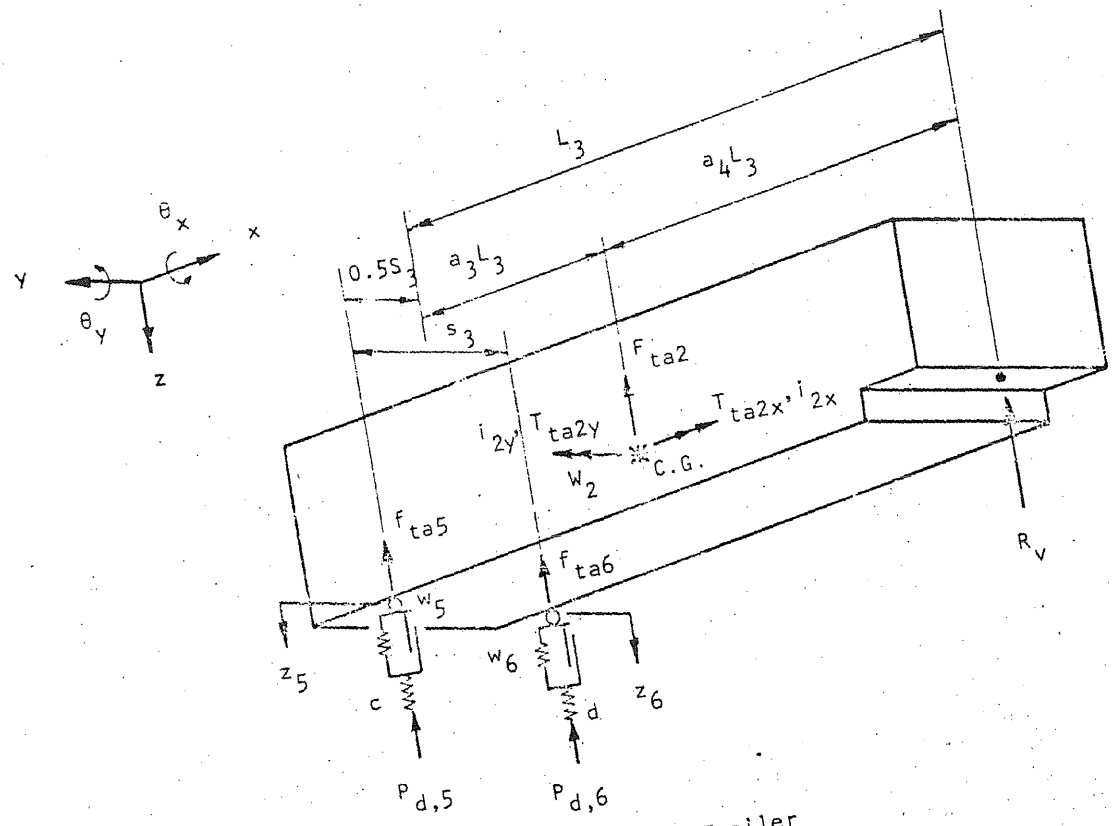

a. Free Body Diagram of Trailer

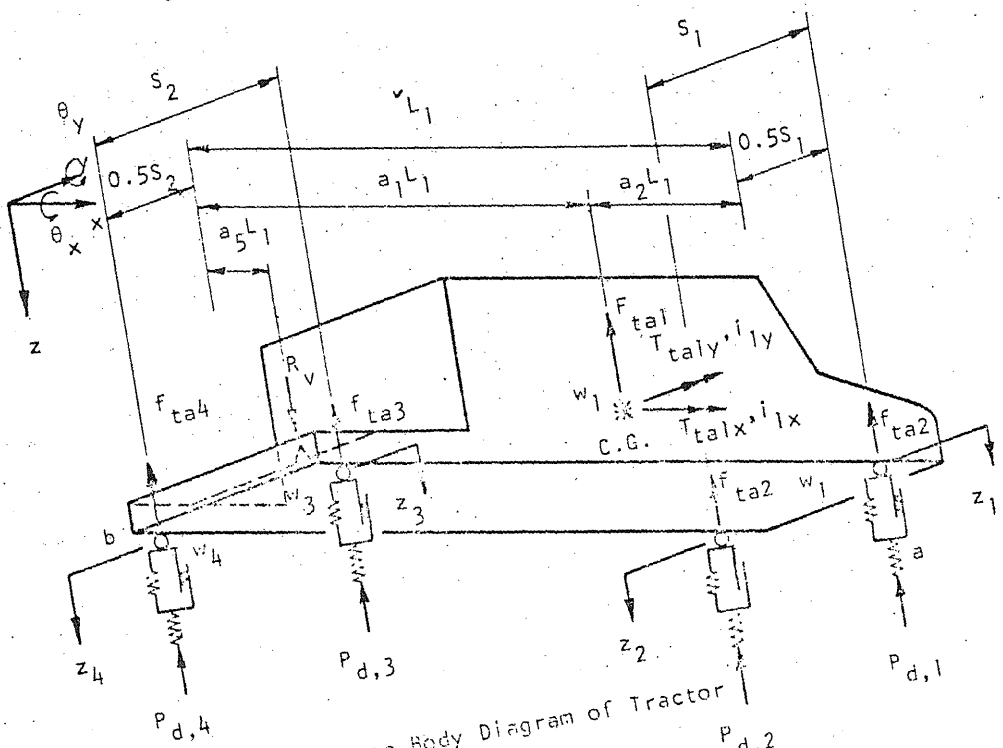

b. Free Body Diagram of Tractor

FIG. B.1 FREE BODY DIAGRAMS OF VEHICLE MODEL

APPENDIX C

INPUT PARAMETERS FOR FINITE ELEMENT SOLUTIONS

Input parameters for the single-span, multibeam, the two-span, multibeam, the three-span, single-beam, and the three-span, multibeam solutions are presented in Tables C.1 through C.8. In each table, two quantities are required to define the initial y coordinates for the vehicle wheels. The first quantity defines the y coordinate for tires 1, 3, and 5; the second defines the y coordinate for tires 2, 4, and 6. The first four plot parameters define the Y scale for accelerations, deflections, moments, and reactions, respectively. The fifth parameter defines the X scale for all plots. All other plot parameters are generated in the computer programs as needed.

For problems involving the three-axle vehicle model, parameters describing the properties of the axles will be followed by three numbers which from left to right are assigned to axles one, two, and three, respectively. Numbers following the parameter "Sprung Vehicle Load" represent the weight of the tractor and trailer bodies, respectively.

TABLE C.1

SINGLE-SPAN, MULTIBEAM BRIDGE SOLUTION PARAMETERS

Number of Spans	1
Span Length (ft.)	6.0
Bridge Width (ft.)	2.15
No. of Transverse Elements	4
Interval Between Supports	1
No. of Longitudinal Elements per Span	4

	AREA (in^2)	TORSION IX (in^4)	BENDING IY (in^4)	DEPTH (in.)	WEIGHT (lbs.)
Beam Properties	.44325	.03096	.0129	0.409	0.5356
Left Curb Prop.	.2935	0.00	.0002025	-0.091	0.3542
Right Curb Prop.	.2935	0.00	.0002025	-0.091	0.3542

Deck Thickness (in.)	0.091
Poisson's Ratio for Deck Material	0.33
Composite Action Factor (Percent)	100
Unit Weight of Deck Material ($kips/ft.^3$)	0.1738
Elastic Modulus for Beams (KSI)	10300
Poisson's Ratio for Beams	0.33
Elastic Modulus for Deck (KSI)	10300
Static Wheel Loads (kips)	0.00583
Initial X Coordinate for Axles (in.)	0.0
Initial Y Coordinate for Wheels (in.)	12.9 12.9
No. of Steps Required to Cross Bridge	220
Total No. of Steps	220
Print Interval	2
Initial Oscillation	0.0
Initial Friction Force In Suspension System	0.0
Problem Description	SINGLE-SPAN ALUMINUM BRIDGE
No. of Axles	1
Roughness Amplitude / Dead Load Deflection	1.0
No. of Half Sine Waves of Bridge Roughness	1
Sprung Axle Loads (kips)	0.00583
Unsprung Load (kips)	0.00057
Limiting Friction Force in Suspension System (kips)	1000
Vehicle Damping Factor (Percent of Critical)	6.5
Tire Frequencies (cyc./sec.)	5.5
Frequency of Tire-Suspension System (cyc./sec.)	N.A.
Speed Parameter, Alpha	0.16
Integration Constant, Beta	0.1667
Frequency of Fundamental Bridge Mode (cyc./sec.)	10.61
Frequency of Highest Mode (cyc./sec.)	191.8
Bridge Damping Factor (Percent of Critical)	0.6
Plot Parameters	1.0 3.0 3.0 0.035 0.125

TABLE C.2

SHAFFER CREEK BRIDGE

Number of Spans	2
Span Length (ft.)	43.00
Total Length (ft.)	86.00
Bridge Width (ft.)	22.00
No. of Transverse Elements	4
Interval Between Supports	1
No. of Longitudinal Elements per Span	4

	AREA (in^2)	TORSION IX (in^4)	BENDING IY (in^4)	DEPTH (in.)	WEIGHT (kips)
Beam Properties	29.43	5.24	2987.30	24.50	0.10
Left Curb Prop.	105.00	950.00	428.75	-7.00	0.11
Right Curb Prop.	439.00	10000.00	13292.00	5.50	0.45

Deck Thickness (in.)			7.000
Poisson's Ratio for Deck Material			0.25
Composite Action Factor (Percent)			50.0
Unit Weight of Deck Material ($kips/ft.^3$)			0.150
Elastic Modulus for Beams (KSI)			29000
Poisson's Ratio for Beams			0.30
N. Ratio (E_b/E_d)			8.5
Static Wheel Loads (kips)	4.940000	16.029999	15.929999
Initial X Coordinates for Axles (in.)	0.0	-156.0000	-400.8000
Initial Y Coordinates for Wheels (in.)		95.0000	169.0000
Vehicle Velocity (in./sec.)			1056
No. of Steps Required to Cross Bridge			644
Total No. of Steps			644
Print Interval			2
Minimum No. of Steps Required for Conversion			645
Initial Oscillation			0.0
Initial Phase Angle			0.0
Initial Friction Force in Suspension System			0.0
Problem Description			SHAFFER CREEK-LANE 1
No. of Axles			3
No. of Bridge Rough Coef. per Wheel Path			259
No. of Half Sine Waves of Bridge Roughness			0.0
Roughness Amplitude / Dead Load Deflection			0.0
Roughness Amplitude (in.)			0.0
Sprung Vehicle Load (kips)		7.663600	28.635391
Sprung Axle Load (kips)	1.108199	1.712299	1.612300
Unsprung Load (kips)	0.0	0.0	0.0
Max. Force in Suspension System / P_{st}	0.075000	0.200000	0.200000
Dynamic Indeces for Sprung Mass	1.0000	1.0000	1.0000
Vehicle Damping Factor (Percent of Critical)			0.0
Tire Frequencies (cyc./sec.)	3.5000	3.5000	3.5000
Frequency of Tire-Susp. Sys. (cyc./sec)	1.6000	2.0000	2.0000
Integration Constant, Beta			0.166667
Frequency of Fundamental Bridge Mode (cyc./sec.)			6.458300
Frequency of Highest Mode (cyc./sec.)			123.619995
Bridge Damping Factor (Percent of Critical)			1.0000

TABLE C.3

PARAMETERS FOR THREE-SPAN, SINGLE-BEAM BRIDGE

Number of Spans			3
Span Length (ft.)	48.00	60.00	48.00
Bridge Width (ft.)			1.00
No. of Transverse Elements			1
Interval Between Supports			1
No. of Longitudinal Elements per Span	4	6	4
No. of Beam Property Cards			1

	AREA (in^2)	TORSION IX (in^4)	BENDING IY (in^4)	DEPTH (in.)	WEIGHT (kips)
Beam Properties	40.00	3.00	90000.0	-7.00	1.42

Deck Thickness (in.)	7.000
Poisson's Ratio for Deck Material	0.33
Composite Action Factor (Percent)	0.0
Unit Weight of Deck Material ($kips/ft.^3$)	0.150
Elastic Modulus for Beams (KSI)	10300
Poisson's Ratio for Beams	0.33
Elastic Modulus for Deck (KSI)	3500

TABLE C.4

THREE-SPAN, SINGLE-BEAM SOLUTION PARAMETERS, CASE A

Static Wheel Loads (kips)	17.565
Initial X Coordinate for Axles (in.)	0.0
Initial Y Coordinate for Wheels (in.)	0.0 12.0
No. of Steps Required to Cross Bridge	300
Total No. of Steps	300
Print Interval	2
Initial Oscillation	0.0
Initial Friction Force in Suspension System	0.0
Problem Description	THREE-SPAN, SINGLE-BEAM - CASE A
No. of Axles	1
No. of Half Sine Waves of Bridge Roughness	0.0
Roughness Amplitude / Dead Load Deflection	0.0
Roughness Amplitude (in.)	0.0
Sprung Axle Loads (kips)	17.565
Unsprung Loads (kips)	0.0
Limiting Friction Force in Suspension System (kips)	10000
Vehicle Damping Factor (Percent of Critical)	0.0
Tire Frequencies (cyc./sec.)	3.255
Frequency of Tire-Suspension System (cyc./sec.)	N.A.
Speed Parameters, Alpha	0.175
Integration Constant, Beta	0.16667
Frequency of Fundamental Bridge Mode (cyc./sec.)	6.51
Frequency of Highest Mode (cyc./sec.)	111.06
Bridge Damping Factor (Percent of Critical)	0.0
Plot Parameters	2.0 3.0 3.0 0.035 0.125

TABLE C.5

THREE-SPAN, SINGLE-BEAM SOLUTION PARAMETERS, CASE B

Static Wheel Loads (kips)					15.37
Initial X Coordinate for Axles (in.)					0.0
Initial Y Coordinate for Wheels (in.)			0.0		12.0
No. of Steps Required to Cross Bridge					300
Total No. of Steps					300
Print Interval					2
Initial Oscillation					0.0
Initial Phase Angle (degrees)					0.0
Initial Friction Force in Suspension System					0.0
Problem Description	CASE B - 48 FT. WAVE LENGTH, 0.3 IN. AMPLITUDE				
Length of Span 1 / Length of Half Sine Wave					2
Roughness Amplitude (in.)					-0.3
Sprung Axle Load (kips)					15.37
Unsprung Load (kips)					0.0
Max. Force in Suspension System / P_{st}					0.15
Vehicle Damping Factor (Percent of Critical)					0.0
Tire Frequencies (cyc./sec.)					3.255
Frequency of Tire-Suspension System (cyc./sec.)					1.953
Speed Parameter, Alpha					0.15
Integration Constant, Beta					0.16667
Frequency of Fundamental Bridge Mode (cyc./sec.)					6.51
Frequency of Highest Mode (cyc./sec.)					111.06
Bridge Damping Factor (Percent of Critical)					0.0
Plot Parameters	0.5	3.0	3.0	0.035	0.125

TABLE C.6

THREE-SPAN, SINGLE-BEAM SOLUTION PARAMETERS, CASE C

Static Wheel Loads (kips)	15.37
Initial X Coordinate for Axles (in.)	0.0
Initial Y Coordinate for Wheels (in.)	0.0 12.0
No. of Steps Required to Cross Bridge	300
Total No. of Steps	300
Print Interval	2
Initial Oscillation / P_{st}	0.5
Initial Phase Angle	0.0
Initial Friction Force in Suspension System	-0.15
Problem Description	CASE C - INITIAL OSCILLATION
No. of Axles	1
No. of Half Sine Waves of Bridge Roughness	0.0
Roughness Amplitude / Dead Load Deflection	0.0
Roughness Amplitude (in.)	0.0
Sprung Axle Loads (kips)	15.37
Unsprung Loads (kips)	0.0
Max. Force in Suspension System / P_{st}	0.15
Vehicle Damping Factor (Percent of Critical	0.0
Tire Frequencies (cyc./sec.)	3.255
Frequency of Tire-Suspension System (cyc./sec.)	1.953
Speed Parameters, Alpha	0.15
Integration Constant, Beta	0.16667
Frequency of Fundamental Bridge Mode (cyc./sec.)	6.51
Frequency of Highest Mode (cyc./sec.)	111.06
Bridge Damping Factor (Percent of Critical)	0.0
Plot Parameters	0.5 3.0 3.0 0.035 0.125

TABLE C.7

BRIDGE PARAMETERS FOR SALT FORK RIVER BRIDGE

Number of Spans			3
Span Length (ft.)	75.08	96.50	75.08
Bridge Width (ft.)			30.00
No. of Transverse Elements			4
Interval Between Supports			1
No. of Longitudinal Elements per Span	4	4	4
No. of Beam Property Cards			1

	AREA (in^2)	TORSION IX (in^4)	BENDING IY (in^4)	DEPTH (in.)	WEIGHT (kips)
Beam Properties	49.98	16.03	10470.0	43.91	0.17
Left Curb Prop.	432.00	5375.00	2618.0	0.0	0.45
Right Curb Prop.	432.00	5375.00	2618.0	0.0	0.45
Tran. Supt. Stiff.	10.59		541.0	24.10	
Tran. Stiffener	10.59		446.3	38.38	

Deck Thickness (in.)	7.000
Deck Strength (KSI)	3.5
Poisson's Ratio For Deck Material	0.25
Composite Action Factor (Percent)	100
Unit Weight of Deck Material ($kips/ft.^3$)	0.15
Elastic Modulus for Beams (KSI)	30000
Poisson's Ratio for Beams	0.30

TABLE C.8

PARAMETERS FOR SALT FORK RIVER BRIDGE CRAWL-CURVE ANALYSIS

Static Wheel Loads (kips)	4.700	17.345	15.795
Initial X Coordinate for Axles (in.)	0.0	-156.0	-400.8
Initial Y Coordinate for Wheels (in.)		143.0	217.0
Solution Code (crawl curve or constant force)			0.0
Vehicle Velocity (MPH)			0.1
No. of Steps Required to Cross Bridge			150
Total No. of Steps			150
Print Interval			1
No. of Axles			3
Problem Description	SALT FORK CRAWL CURVE ANALYSIS		
Plot Parameters	1.2	2400	0.2